The Pennsylvania State University
The Graduate School
The Eberly College of Science

CORRELATIONS IN QUANTUM GRAVITY AND COSMOLOGY

A Dissertation in
Physics
by
Bekir Baytas

Submitted in Partial Fulfillment
of the Requirements
for the Degree of

Doctor of Philosophy

August 2018

The dissertation of Bekir Baytas was reviewed and approved* by the following:

Sarah Shandera
Assistant Professor of Physics
Dissertation Advisor, Chair of Committee

Eugenio Bianchi
Assistant Professor of Physics

Martin Bojowald
Professor of Physics

Donghui Jeong
Assistant Professor of Astronomy and Astrophysics

Nitin Samarth
Professor of Physics
Head of the Department of Physics

*Signatures are on file in the Graduate School.

Abstract

We study what kind of implications and inferences one can deduce by studying correlations which are realized in various physical systems. In particular, this thesis focuses on specific correlations in systems that are considered in quantum gravity (loop quantum gravity) and cosmology.

In loop quantum gravity, a spin-network basis state, nodes of the graph describe un-entangled quantum regions of space, quantum polyhedra. We introduce Bell-network states and study correlations of quantum polyhedra in a dipole, a pentagram and a generic graph. We find that vector geometries, structures with neighboring polyhedra having adjacent faces glued back-to-back, arise from Bell-network states. The results present show clearly the role that entanglement plays in the gluing of neighboring quantum regions of space.

We introduce a discrete quantum spin system in which canonical effective methods for background independent theories of quantum gravity can be tested with promising results. In particular, features of interacting dynamics are analyzed with an emphasis on homogeneous configurations and the dynamical building-up and stability of long-range correlations. We conclude that an analysis of the building-up of long-range correlations in discrete systems requires non-perturbative solutions of the dynamical equations.

For the early universe cosmology part of the thesis, we present examples of non-Gaussian statistics that can induce bispectra matching local and non-local (including equilateral) templates in biased sub-volumes. We find cases where the biasing from coupling to long wavelength modes affects only the power spectrum, only the bispectrum or both.

Table of Contents

List of Figures viii

List of Tables xii

Acknowledgments xiii

Chapter 1
Perspectives 1

Chapter 2
Fundamentals of correlations in quantum systems 4
2.1 Introduction . . . 4
2.2 Building blocks of quantum mechanics . . . 5
2.2.1 States and Dynamics . . . 6
2.2.2 Observables and Measurement . . . 9
2.2.3 Qubit and spin-$\frac{1}{2}$ . . . 10
2.3 Quantum bipartite systems and quantum correlations . . . 11
2.3.1 Quantum entanglement . . . 12
2.3.2 Quantum mutual information and correlations . . . 14
2.3.3 Two-qubit system and entanglement . . . 15
2.4 Quantum spin chains . . . 17
2.4.1 Heisenberg (XXX) spin chain . . . 17
2.5 Quantum geometry of space . . . 20
2.5.1 Quantum tetrahedron . . . 21
2.6 Quantum fields in Minkowski spacetime . . . 25
2.6.1 Free scalar fields in Minkowski vacuum . . . 25

Chapter 3
Gluing polyhedra with entanglement in loop quantum gravity 29
3.1 Introduction . . . 30

3.2 Classical geometries on a graph Γ . . . 35
3.2.1 Hierarchy of discrete geometries . . . 35
3.2.2 Twisted geometries . . . 37
3.2.3 Vector geometries . . . 38
3.2.4 Regge geometries . . . 40
3.3 Quantum polyhedron and Heisenberg uncertainty relations . . . 41
3.4 Quantum geometries on a graph Γ . . . 44
3.4.1 Quantum twisted geometries . . . 45
3.4.2 Quantum vector geometries . . . 47
3.4.3 Quantum shape-matching conditions . . . 54
3.4.4 Bell states on the dipole graph . . . 57
3.4.4.1 Bell states on Γ_2 . . . 58
3.4.4.2 Bell states at fixed spins j_ℓ on Γ_2 . . . 61
3.4.5 Bell states on the pentagram . . . 63

Chapter 4
Minisuperspace models of quantum spin systems **75**
4.1 Introduction . . . 76
4.2 Canonical effective methods . . . 77
4.3 The quantum spin chain model . . . 79
4.4 Minisuperspace models . . . 84
4.4.1 A minimal minisuperspace model . . . 84
4.4.2 A condensate model . . . 85
4.4.3 Two interacting minisuperspace models . . . 86
4.4.4 Effective equations and potentials . . . 90
4.4.4.1 Minimal minisuperspace model . . . 91
4.4.4.2 Interacting minisuperspace models . . . 93
4.4.4.3 Condensate model . . . 94
4.5 Continuum theories . . . 95
4.5.1 Continuum models . . . 96
4.5.1.1 Minimal model . . . 96
4.5.1.2 Interacting minisuperspace models . . . 97
4.6 Effective analysis of the discrete theory . . . 99
4.6.1 Effective dynamics . . . 99
4.6.2 Dynamical stability for small number of nodes . . . 102
4.6.2.1 Single-node graph . . . 103
4.6.2.2 Two-node graph and beyond . . . 106
4.7 Possible implications for quantum cosmology . . . 109

Chapter 5
Super cosmic variance from non-Gaussian statistics **111**
5.1 Introduction . . . 111
5.2 Super cosmic variance . . . 113
5.3 Primordial non-Gaussianity . . . 114
5.4 Super cosmic variance from general type non-Gaussian fields . . . 116
5.4.1 The model . . . 117
5.4.2 Quadratic Terms . . . 120
5.4.2.1 Recovering the standard bispectral templates . . . 122
5.4.2.2 The long-short wavelength split . . . 124
5.4.2.3 The field observed in biased sub-volumes . . . 125
5.4.3 Cubic Terms . . . 129
5.4.3.1 Generation of cubic terms . . . 129
5.4.3.2 Constraints on cubic terms from their contributions to the power spectrum . . . 130
5.4.3.3 The field observed in biased sub-volumes . . . 131
5.4.3.4 Families of cubic terms from the super cosmic variance point of view . . . 134
5.5 Space of non-Gaussian fields with single-clock bispectra . . . 138
5.5.1 Introduction . . . 138
5.5.2 Generating super cosmic variance free models . . . 140
5.5.3 Constructing a non-Gaussian field with an equilateral bispectrum . . . 140
5.5.4 Obtaining the single-clock orthogonal template . . . 143
5.5.5 Comparison with previous work . . . 148

Chapter 6
Summary and Outlook **150**
6.1 Entanglement and quantum spacetimes . . . 150
6.2 Discrete spin systems and canonical quantum gravity . . . 154
6.3 Non-local bispectra from super cosmic variance . . . 156
6.4 Shapes for super cosmic variance free from non-Gaussianities . . . 158

Appendix A
Vector geometry for equal spins $j_{ab} = j$ **160**

Appendix B
Entanglement entropy at fixed total area J **162**

Appendix C
Derivation of the Bell states on a pentagram graph **164**

Appendix D
Hessian of the action for $15j$-symbol **167**

Appendix E
Shape-matched configurations for a 4-simplex in $\mathbb{R}^3$ **171**
E.1 Pachner move: **1-4** 172
E.2 Pachner move: **2-3** 174

Appendix F
Cubic terms and the cubic kernel **176**
F.1 Quadratic terms induced by a cubic term in biased sub-volumes . . 178
F.2 Power spectrum from the cubic field Φ_3 179
F.3 Special cubic kernels and its corresponding trispectra 180

Appendix G
Basis functions for bispectra **182**

Bibliography **185**

List of Figures

2.1 Graphical representation of a one dimensional isotropic Heisenberg (XXX) chain of spin-1/2 particles s_i with N sites connected by N-1 links. 18
2.2 A picture for a spin-network graph consisting of 31 nodes [1]. 20
2.3 A description for a 3-valent node and its dual two-dimensional surface. 21
2.4 Tetrahedron formed by the edge-vectors $\mathbf{e}_i$. Thenormal $\mathbf{n}_3 = \frac{1}{2A_3}\mathbf{e}_1 \times \mathbf{e}_2$ is the normal, outward-pointing vector normalized to the area of the associated face. 23

3.1 Dipole graph. A pair of nodes connected by l links coloured by spins j_ℓ. 34
3.2 A local patch of a vector geometry. The glued faces have the same areas: $A_a = A_{a'}$, $A_b = A_{b'}$, $A_c = A_{c'}$, and their normals are anti-parallel $\mathbf{n}_a = -\mathbf{n}_{a'}$, $\mathbf{n}_b = -\mathbf{n}_{b'}$, $\mathbf{n}_c = -\mathbf{n}_{c'}$. The lengths of edges in juxtaposed triangles are not necessarily matched in a vector geometry. 39
3.3 Geometric meaning of the shape-matching conditions (3.12): The internal angle α^a_{bc} in the shaded triangle can be expressed in terms of the dihedral angles associated with the thick edges of either tetrahedra. 41
3.4 The set of L links. Each oriented link corresponds to an ordered pair $\ell = (s, t)$, where $s(\ell)$ and $t(\ell)$ are the source and target nodes at link l, respectively. The spin at the link ℓ is j_ℓ. 49
3.5 Dipole graph Γ_2. The source (s) and target (t) nodes are connected by four links $\ell = 1, \ldots, 4$. The graph is dual to the triangulation of the 3-sphere formed by two tetrahedra glued along their boundaries. A spin-network state is labelled by spins j_ℓ and intertwiners i_s, i_t. . 58

3.6 Pentagram graph Γ_5. The graph is dual to a triangulation of the three-sphere with five tetrahedra. A spin-network state on Γ_5 is labeled by five intertwiners i_{k_n} and ten spins j_ℓ attached to the nodes and links of the graph, respectively. The links are oriented according to $t(\ell) < s(\ell)$. 63
3.7 Pachner move 1-4. A single tetrahedron is divided into a gluing of four tetrahedra by the introduction of a new vertex i in its interior. 69
3.8 Graphical representation of a 1-4 vector geometry in a 3d box generated by using maximal tree method. Each colored point labels different node of the pentagram. The set of normals at each node satisfy the closure condition (3.96). Dashed black arrows stand for the anti-aligned normals which connect neighbor nodes: $\mathbf{n}_{a(a+1)} = -\mathbf{n}_{(a+1)a}$, $a = 1, \cdots, 4$. Dashed colored arrows stand for the remaining normals such that $\mathbf{n}_{ab} = -\mathbf{n}_{ba}$ with $\big\{(a,b) = 1, \cdots, 5 \;\big|\; a < b \wedge a \neq b-1\big\}$. . 70
3.9 Sampling of exact relative magnitudes $(|\mathrm{det}H_0|^{1/2}_{1-4})/(|\mathrm{det}H|^{1/2}_{1-4})$ in terms of the cosine of the gauge-invariant 3d dihedral angles $\phi_{ab,db}$ and$\phi_{cd,bd}$. The relative magnitude reaches its maximum at the shape-matched configuration (SM-1) with $\mathbf{n}_{ab} \cdot \mathbf{n}_{db} = \mathbf{n}_{cd} \cdot \mathbf{n}_{bd} = 1/2$. 73

4.1 The inhomogeneous one-dimensional graph Γ with N nodes and $2N+1$ links. The Hamiltonian (4.8) is invariant under a mapping of spins that corresponds to a reflection of the graph in a horizontal direction. If the orientation of a link, indicated by an arrow, changes under this reflection, the corresponding mapped spin has a negative sign. 80
4.2 A re-arranged representation of the discrete spin model. As before, lines with a given orientation stand for the spin operators. There are now five different spins meeting at a given node j, among which only the two triplets $(\hat{\mathbf{J}}_{\mathrm{h1},j}, \hat{\mathbf{J}}_{\mathrm{v1},j}, \hat{\mathbf{J}}_{\mathrm{h2},j})$ and $(\hat{\mathbf{J}}_{\mathrm{h2},j}, \hat{\mathbf{J}}_{\mathrm{v2},j}, \hat{\mathbf{J}}_{\mathrm{h1},j+1})$ are interacting as indicated by wavy lines with different wave lengths. The spin $\hat{\mathbf{J}}_{\mathrm{h2},j}$ appears in both triplets, and is therefore doubled in the diagrammatic visualization. Also the constraints relate only the spins that occur together in a triplet. 87
4.3 Correlations between the farthest spin sets for $\hat{\mathbf{J}}_1$ and $\hat{\mathbf{J}}_{2N+1}$ after solving the equations M times iteratively for a graph with N nodes for $2M \leq N+1$. The semi-circles represent non-zero covariances $\Delta(J^a_1 J^b_{2M+1})$ and $\Delta(J^a_{2N+1} J^b_{2N+1-2M})$. 102

4.4 Correlations between the farthest spin sets for $\hat{\mathbf{J}}_1$ and $\hat{\mathbf{J}}_{2N+1}$ after solving the equations M times iteratively for a graph with N nodes for $N < 2M$. The semi-circles represent non-zero covariances $\Delta(J_1^a J_{2M+1}^b)$ and $\Delta(J_{2N+1}^a J_{2N+1-2M}^b)$. 103

5.1 Momentum-space polygons formed by the N momenta $\mathbf{k}_i$ such that $\sum_{i=1}^{N} \mathbf{k}_i = 0$. 116

5.2 Graph of the RMS amplitude of long-wavelength super cosmic variance terms from non-local bispectra, $\frac{1}{k_*}\langle(\partial\phi_l)^2\rangle^{1/2}$ and $\frac{1}{k_*^2}\langle(\partial^2\phi_l)^2\rangle^{1/2}$. This plot assumes that the power spectrum on scales larger than $k_* = 0.05\,\mathrm{Mpc}^{-1}$ remains consistent with *Planck* satellite observations: $\Delta_\Phi^2(k) = 3.98772 \times 10^{-9}(k/k_*)^{n_s-1}$ with $n_s = 0.9619$ [2]. Notice that the plotted quantities are not sensitive to more than about an e-fold of inflation and remain $\mathcal{O}(10^{-5})$ so, as expected, only the local bispectrum can generate a significant super cosmic variance contribution to the power spectrum. 128

5.3 Assuming that a single sub-volume measurement of $f_{\rm NL}^{\rm equil} = 10$, this plot shows the probability distribution for the value of $f_{\rm NL}^{\rm equil}$ that could be present in the (mean statistics of the) parent volume. Both curves assume the parent volume has a power spectrum consistent with *Planck* satellite observations and $g_{\rm NL}^{\rm equil} = 5 \times 10^3$ (where $g_{\rm NL}^{\rm equil}$ is defined as the amplitude of the non-local cubic term specified in Eq.(5.55)). If there are no further SCV effects from higher order terms, any sub-volume will have the same power spectrum and $g_{\rm NL}^{\rm equil}$ as the parent volume. The solid (blue) curve considers a parent volume larger than the sub-volume by a factor of 50 extra e-folds. The dotted (black) curve show a parent volume larger by a factor of 100 extra e-folds. For the best fit *Planck* power spectrum and $N_e = 50$, 100, the RMS variance of the long wavelength modes is $\sqrt{\langle\phi_l^2\rangle} \approx 0.0008$ and 0.0022 respectively. 137

5.4 This is the 3D plot of the flat-only shape $S_{flat-only}(x_2, x_3)$ proportional to $(k_1k_2k_3)^2 B_{flat-only}(k_1, k_2, k_3)$ 148

5.5 Contour plot of the flat-only shape. 148

E.1 This is a description of a 1-4 move to construct five glued tetrahedra by placing a fifth vertex i, origin of the coordinates, in the center point of the tetrahedra $pqrs$ labeled by τ_f. 172

E.2 Pachner move 2-3. Two tetrahedra glued back to back are transformed into three tetrahedra with the inclusion of a new edge from the vertex s to the vertex i. 174

List of Tables

5.1 The overlap between the shapes associated with the four linearly independent kernels with the single-clock squeezed limit. 147

E.1 A table for solutions for gluing five copies of a tetrahedron for a 4-simplex with a fixed spin configuration 171

G.1 The set of terms in the real space field expansion, $\Phi_2(x)$ that correspond to each polynomial $\mathcal{K}_n$ (see Eq.(G.1)) appearing in the shape of the bispectrum. The different $\Phi_2(x)$ terms on a given horizontal line result in redundant terms in the shape of the bispectrum but contribute differently to the lowest order non-Gaussian (loop) contribution to the power spectrum. The conditions of a well-behaved loop correction in general introduce constraints among terms corresponding to different from $\mathcal{K}_n$. However, some $\Phi_2(x)$ terms are truly redundant even once loops are considered (eg, they come with unconstrained coefficients) and so are not needed. The last column lists the labels a_i we used in the main text, where $\times$ indicates the term was redundant for our purposes and so was not included. . . 183

Acknowledgments

I express all my gratefulness to my committee members. In the first place, I thank my adviser, *Sarah Shandera*, for helping me to specify the relevant questions for my research interests, to solve the problems on my own and for teaching me how to write coherently my first two projects [3,4]. For my project [5], I am very thankful to *Martin Bojowald* for being not hesitated to conduct research with me on a specific problem in which I was interested. He was really helpful for me to be able to see the important physical implications and details behind our work. For my project [6], I am very grateful to *Eugenio Bianchi* for being extremely helpful when I faced difficulties during conducting the project. He showed me explicitly fundamental key points to understand underlying physical and mathematical aspects of the work. I should also add that I learned from him to sustain and develop ideas even they are at fundamental level.

My graduate research has been particularly fruitful when I had discussions about mathematical and physical background with my collaborators in Penn State. I particularly wish to thank *Nelson Yokomizo* for helping me to build rigorous mathematical or physical statements that were essential for our work and he was really patient to answer all my questions in detail. Of course, I should express my gratitudes to my friends *Elliot Nelson, Aruna Kesavan, Soyhun Park, Sean Crowe* and all others in IGC for their help in my research.

The research, which I conducted during my doctorate degree, has been supported by the National Science Foundation under the NSF grants: PHY-1417385, PHY-0748336, PHY-1417385, PHY-1607414 and PHY-1417385 with supports by the Duncan and Downsbrough Fellowship.

I would not have been able to be successful in all these projects without all possible supports of my ***father****, my* ***mother****, my* ***brother*** *and my* ***aunt****. But I must say that I found my invaluable supports from my lovely* ***wife*** *during my last two years.*

To all people who have passionate curiosity.

Chapter 1
Perspectives

Correlation is an overarching notion in statistics. Correlations play a prominent role in the study of the classical and the quantum behavior of various different systems, from condensed matter physics to cosmology. Heuristically, if one considers a system consisting of two or more parts, correlations allow us to quantify how much one can predict about a subsystem, given our knowledge of the surrounding system.

In classical mechanics, there are statistical systems such as many clusters in the universe or a collection of particles in a box where one can investigate about the features of that system (temperature of the box or number of particles in one half of the system after the measurement). If one divides the system after into subparts, then the knowledge of the part of the system which can provide certain inferences about the other part of the system will depend on how these subparts are correlated.

In contrast to classical mechanics, all quantum mechanical systems are "statistical" systems and we can ask equivalent sets of questions for the quantum system as for the classical one. But, there are degrees of correlations in quantum mechanics which cannot appear if one models the system with classical mechanics. Here, quantum correlations scope all possible classifications of correlations in quantum states of compound systems (not only quantum entanglement).

In many interesting physical phenomena at either quantum or classical level, observing correlations for various complex systems is intensely connected to the amount of information that is shared between subparts of the relevant physical system. Thus, providing an information-theoretic framework of physical systems can help to understand correlations between physical observables. Moreover, according

to a phenomenological point of view, studying particular correlations such as thermal fluctuations on cosmic microwave background radiation are one of the possible paths to explore fundamental principles of inflationary mechanisms. Furthermore, one can find the importance of the role by correlations in other areas such as many-body physics and information technology.

This work aimed to study special sets of correlations in physical systems at both quantum and classical level and to investigate how correlations are linked to fundamental concepts of the theory that is considered. In particular, the contents which are presented in this thesis, consist of contributions to quantum gravity and cosmology communities. Along my research line, I benefited from fruitful collaborations with scholars and colleagues in my institute.

The thesis is organized in chapters and their subparts. Each chapter has its own introductory part specifying the relevant information about the field of study. The content of each chapter is the following:

- **Chapter 2** introduces correlations in simple quantum systems. In the first place, there is a review on the postulates and tools of quantum mechanics. In the second place, I present an understanding of quantum entanglement in quantum subsystems including the formulation of quantum mechanical correlation function, quantum mutual information. Then, I consider several simple quantum systems where correlations are shown explicitly between relevant observable of the system.

- **Chapter 3** is about how quantum entanglement can be seen as a guiding tool to understand the structure of the quantum spacetime. In particular, we develop a class of highly entangled states of the quantum geometry on a fixed graph in loop quantum gravity describes a superposition of discrete spaces that optimally approximates vector and Regge geometries.

- **Chapter 4** presents a discrete quantum spin system in which canonical quantum gravity methods are tested with promising results. In particular, we analyze certain properties of interacting dynamics on homogeneous configurations, the dynamical building-up and stability of long-range correlations. It is concluded that an analysis of the building-up of long-range correlations in discrete systems requires non-perturbative solutions of the dynamical equations.

- **Chapter 5** discusses examples of non-Gaussian statistics that can induce bispectra matching local and non-local templates in biased sub-volumes. Our results suggest that ruling out multi-field scenarios is quite difficult: some measurements of the scalar correlations, including the shape of the bispectrum, can be consistent with single-clock predictions even when cosmic variance from super-horizon modes is at work. Moreover, we develop a mathematical construction of non-Gaussian fields whose bispectra satisfy the single-clock inflation consistency relation. Our findings add support for the idea that both theory and data driven considerations will be best served if next generation non-Gaussianity constraints are made in a basis that uses the degree of coupling between long and short wavelength modes as an organizing principle.

- Finally, in **Chapter 6**, I summarize all the contributions of the thesis and provide possible outlook and future lines in quantum gravity and cosmology.

The most of the materials presented here has been reported in the following papers:

1. **B. Baytas, E. Bianchi and N. Yokomizo:** *Gluing polyhedra with entanglement in loop quantum gravity*, arXiv:1805.05856 [gr-qc], submitted to Phys. Rev. D [6]

2. **B. Baytas and M. Bojowald:** *Minisuperspace models of discrete systems*, Phys. Rev. D 95, 086007, (2017) [5].

3. **B. Baytas, A. Kesavan, E. Nelson, S. Park and S. Shandera:** *Non-local bispectra from super cosmic variance*, Phys. Rev. D 91, 083518, (2015) [3].

4. **B. Baytas and S. Shandera:** *Space of non-Gaussian fields with single-clock bispectra*, Phys. Rev. D 94, 043510, (2016) [4].

Chapter 2
Fundamentals of correlations in quantum systems

2.1 Introduction

The analysis of natural and spontaneous fluctuations in nature is performed by the theory of statistical physics. The presence of these fluctuations is mainly based on the level of the complexity of the physical system on which we perform measurements [7]. Statistical systems are complex systems where we can completely know their macroscopic structures that are needed to characterize such systems. However, not knowing all the information needed to characterize the system does not prevent us to develop a theory of the system. We try to understand the properties of complex systems without knowing all the information of the system.

The basic characteristics of classical statistics are derived from the following assumptions: distinguishability of fundamental and composite particles and no restrictions on placing more than one particle in any given state accessible to the system. As a consequence of these assumptions, it is possible to track any particle in the system and find its position, energy and history of interaction. If one exchanges positions of two classical particles, one counts it as a different state. A possible complete description of a classical system is given by the points in the phase space (q, p) and the Hamiltonian equations of motion $dq/dt = \partial H/\partial p$, $dp/dt = -\partial H/\partial q$. The solution to the equations of motion defines a trajectory in the phase space where we apply statistical methods in order to describe the macroscopic state of the microscopic information.

In contrast to classical statistics, quantum particles are treated fundamentally indistinguishable in quantum statistics. Therefore, one cannot label particles and distinguish them by following their trajectory so that the concept of a phase trajectory becomes meaningless in a quantum mechanical system. Even though the state of the system may be completely known in the same special cases, the result of a measurement can be predicted probabilistically since any measurement distorts the system. This lack of knowledge manifests itself in the statistical interpretation of a wave function ψ and in the uncertainty relations between q and p, which cannot be sharply measured at the same time.

Quantum particles are divided into two classes on the basis of the symmetry of the system. The spin-statistics theorem, was first formulated in 1939 by Markus Fierz [8] and rederived in a systematic way by Wolfgang Pauli in 1940 [9], explains two kinds of combinatorial symmetry with two kinds of spin symmetry. Technically, the theorem states that the wave function of a system of identical integer (half-integer) spin particles has the same (opposite signed) value when the positions of any two particles are interchanged. These particles with wave functions symmetric (antisymmetric) under exchange are called bosons (fermions).

The concepts and methods used in statistical physics overlap with their applications in many other fields of science, engineering and mathematics: ensembles, entropy, Monte Carlo, correlations. In particular, we intend to think of statistical physics only describing the average behavior of an ensemble of systems. But, we can also describe the entire distribution of behaviors, the fluctuations and the evolution in space-time of the system using correlation functions [10]. Based on this canonical framework of statistical physics at both quantum and classical level, our primary focus will be a set of various realizations of correlations in different systems and models, in particular quantum gravitational and cosmological settings. As quantum mechanics allows for the full range of correlations between events, we start first introducing the building blocks of quantum mechanics.

2.2 Building blocks of quantum mechanics

Quantum mechanics is a mathematical setup of axioms and principles for developing possible descriptions of physical world and building fundamental cornerstones of the spectrum of physical theories. By itself, quantum mechanics is not a theory

consisting of particular laws and models which describe the relevant physical systems in nature. Instead, it exits as a conceptual framework for the development of these relevant physical theories. So far, there are various theories[1] based on quantum theoretical postulates, which are the most successful and accurate descriptions of the physical world that we are observing.

Historically, the birth of quantum mechanics can be traced back to the discoveries and explorations of failures of classical physics in the contexts of heat capacities of molecular gas and solid, and the ultraviolet catastrophe in black-body radiation [11]. But, mathematically rigorous foundations of quantum mechanics were essentially developed by Paul Dirac [12], David Hilbert [13], John Von Neumann [14] and various other brilliant collaborators [15–18] in the time period of 1920-30s.

Based on the mathematical apparatus of the linear algebra, we can move forward to how quantum mechanics formulates the physical world as a collection of systems which are interacting with each other. Physical systems belong to our observable universe and interact with other portions of a larger system referring as environment. They are characterized by physical variables and interactions where the possible sets of interactions depend on the value taken by their variables. Based on how much we know about the values taken by the variables and their interactions, we can perform predictions about the system. Classically, physical systems consist of a collection of possible states known as *phase space* and transformation rules among the states known as *time evolution*. Similarly, quantum mechanics is playing the role of describing physical system in terms of its complete information (variables and interactions). The postulates [19] are precisely addressing to the fundamental ingredients for the possible description of a physical system: *state* 2.2.1 (with a prescription of its *dynamics*) and *observable* 2.2.2 (with a prescription of a *measurement*).

2.2.1 States and Dynamics

The mathematical background of quantum mechanics lies on the tools from the linear algebra as linear operations on vectors spaces. As a brief introduction, a vector space is an algebra with operations of additions of vectors to other vectors and ordinary multiplications over scalar complex numbers on vectors. The mostly

[1] In principle, one can also include theories based on the principles of classical physics which can be derived from quantum mechanics as an approximation valid at macroscopic scale.

interested vector space in quantum mechanics is $\mathbb{C}^n$ which is the space of all n-tuples of complex numbers. The standard quantum mechanical (Dirac) notation is adapted to the fundamental concepts of vector spaces such as the quantum vector and its dual: *ket* vector $|\psi\rangle \in V$, where ψ is a label for the vector, and *bra* vector $\langle\psi| \in V^*$ is dual to the vector $|\psi\rangle$. The dual space V^* consists of continuous linear functionals from V to C such that $\langle\psi| : V \to \mathbb{C}$. There exists an isomorphism between a vector space and its dual which is called as *Hermitian conjugate*:

$$\dagger : |\psi\rangle \to |\psi\rangle^\dagger = |\psi\rangle^{*t} = \langle\psi| \,. \tag{2.1}$$

In this respect, we can represent $|\psi\rangle$ as a column vector

$$\begin{pmatrix} \psi_1 \\ \vdots \\ \psi_{d_V} \end{pmatrix} \tag{2.2}$$

and $\langle\psi|$ as a row vector $\left(\psi_1^*, \cdots, \psi_{d_V}^*\right)$, where d_V is the dimension of the vector space V.

The first postulate of quantum mechanics is about defining the configuration space in which different possible ways of a physical system can be realized: *state space*. The states associated to any isolated system are living in a complex vector space known as *Hilbert space* $\mathcal{H}$ equipped with a inner product [19]. The inner product $\langle\,,\rangle$ maps an ordered pair of vectors (ϕ, ψ) to $\mathbb{C}$:

$$\langle\phi|\psi\rangle = \psi_1\phi_1^* + \cdots + \psi_{d_\mathcal{H}}\phi_{d_\mathcal{H}}^* \tag{2.3}$$

which satisfy the following properties:

i. Linearity: $\langle\phi|\big(a|\psi_1\rangle + b|\psi_2\rangle\big) = a\langle\phi|\psi_1\rangle + b\langle\phi|\psi_2\rangle$.

ii. Positivity: $\langle\psi|\psi\rangle \geq 0$ with equality if and only if $|\psi\rangle = 0$.

iii. Skew-Symmetry: $\langle\phi|\psi\rangle = \langle\psi|\phi\rangle^*$,

and it is complete in the norm $||\psi|| = \langle\psi|\psi\rangle^{1/2}$.

There is also an important inequality called *Cauchy-Schwarz* which reveals geometric features of Hilbert spaces. It states that for any two vectors $|v\rangle$ and $|w\rangle$,

we have the following relation

$$|\langle v|w\rangle|^2 \leq \langle v|v\rangle\langle w|w\rangle\,, \tag{2.4}$$

where the equality appears if and only if the two vectors $|v\rangle$ and $|w\rangle$ are linearly related by some complex scalar.

The postulate about the time evolution of a quantum system[2] is characterized by a special class of linear operations: *unitary* transformation. The state $|\psi(t)\rangle$ of a quantum system is related to another state $|\psi'\rangle$ by a unitary operator $U(t_1, t_2)$ ($U^\dagger = U^{-1}$) within a finite time interval (t_1, t_2):

$$|\psi'\rangle \equiv |\psi(t_2)\rangle = U(t_1, t_2)|\psi(t_1)\rangle\,. \tag{2.5}$$

There is an equivalent statement of this formulation which can be described by Schrödinger equation [20] for a quantum system in continuous time t:

$$i\hbar\frac{d|\psi\rangle}{dt} = H|\psi\rangle\,, \tag{2.6}$$

where $\hbar$ is the Planck constant and H is the *Hamiltonian* of the quantum system. Hermitian operators have spectral decomposition in a Hilbert space $\mathcal{H}$ such that their eigenstates form a complete orthonormal basis in $\mathcal{H}$. As the Hamiltonian operator H is a Hermitian operator, it can be expressed as

$$H = \sum_{\varepsilon} \varepsilon|\varepsilon\rangle\langle\varepsilon| \tag{2.7}$$

in terms of orthonormal basis $|\varepsilon\rangle$ with its corresponding eigenvalue ε. Conventionally, the states $|\varepsilon\rangle$ are called as *energy* states and ε is the energy of that state $|\varepsilon\rangle$. The lowest energy is called as *ground state* energy for the system with its corresponding ground state.

[2]The postulate for the time evolution is valid if the quantum system is closed. In a realistic case, all systems are interacting with each other such that they cannot be seen as closed systems. But, in principle every open system can be described as part of a larger closed system which is undergoing unitary evolution.

2.2.2 Observables and Measurement

Observables reflect the properties of a physical system such that they can be measured and provide the physical variables which take their values in nature. In quantum mechanics, an observable occurs as a Hermitian operator on the state space of the system being observed.

An observable $\mathcal{O}$ has a spectral decomposition as

$$\mathcal{O} = \sum_m m P_m \,, \tag{2.8}$$

where P_m is the orthogonal projector, called as *projective* or *von Neumann* measurement operator, onto the space of eigenvectors $\mathcal{O}$ with eigenvalue m which is the numerical outcome of the measurement. The orthogonal projectors satisfy $P_m P_n = \delta_{m,n} P_n$ and $P_m^\dagger = P_m$.

The *expectation value* of an ensemble of identical systems are computed as one the favored statistical key properties of complex systems. It is rigorously defined as a result of measuring an observable $\mathcal{O}$ on large ensemble prepared in the state ψ. For the projective measurements, the expectation value is defined by

$$\langle \mathcal{O} \rangle := \sum_m m \, \langle \psi | P_m | \psi \rangle = \langle \psi | \big(\sum_m m P_m \big) | \psi \rangle = \langle \psi | \mathcal{O} | \psi \rangle \,. \tag{2.9}$$

If we pick an orthonormal basis $|m\rangle$ of $\mathcal{H}$, the expectation value can be expressed in terms of the trace of $\mathcal{O}P_\psi$:

$$\langle \psi | \mathcal{O} | \psi \rangle = \sum_m \langle m | \mathcal{O} | \psi \rangle \langle \psi | | m \rangle = \mathrm{Tr}[\mathcal{O} | \psi \rangle \langle \psi |] = \mathrm{Tr}[\mathcal{O} P_\psi] \,. \tag{2.10}$$

The other key ingredient in statistics is to have a formula for the *variance* (*fluctuations*) of the consecutive measurements of the observable $\mathcal{O}$:

$$\Delta(\mathcal{O})^2 \equiv \langle \big(\mathcal{O} - \langle \mathcal{O} \rangle \big)^2 \rangle = \langle \mathcal{O}^2 \rangle - \langle \mathcal{O} \rangle^2 \,. \tag{2.11}$$

According to classical physics, the variables describing a physical system always determine a precise point in the phase space. Practically, any physical system lies in a finite region of phase space which can be made arbitrary small. On the other hand, quantum theory states that the allowed values of the physical variables cannot

be made smaller than $2\pi\hbar$ per each degree of freedom of the system. This fact does restrict the possible configurations in which the observables can be realized. *Heisenberg uncertainty principle* [21] formulates this underlying fact of quantum mechanics.

For two observables $\mathcal{O}_1$ and $\mathcal{O}_2$, the Heisenberg uncertainty principle states that

$$\Delta(\mathcal{O}_1)^2\Delta(\mathcal{O}_2)^2 \geq \frac{|\langle[\mathcal{O}_1, \mathcal{O}_2]\rangle|^2}{4}\,. \tag{2.12}$$

This relation can be interpreted in a setting of measuring $\mathcal{O}_1$ on some set of identically prepared system at state-level and $\mathcal{O}_2$ on other set of systems in the ensemble. As an example, the canonically conjugate operators $[\hat{q}, \hat{p}] = i\hbar$ have the following relation in terms of their fluctuations:

$$\Delta(\hat{q})\Delta(\hat{p}) \geq \frac{\hbar}{2}\,. \tag{2.13}$$

2.2.3 Qubit and spin-$\frac{1}{2}$

The simplest quantum mechanical system is the unit of quantum information known as *qubit*. It has a non-trivial two dimensional Hilbert space. We usually denote a set of orthonormal basis for a two dimensional vector space as $\{|0\rangle, |1\rangle\}$. Then, an arbitrary normalized state $|\psi\rangle$ can be expressed as

$$|\psi(a, b)\rangle = a|0\rangle + b|1\rangle\,, \tag{2.14}$$

where a and b are complex scalars and $|a|^2 + |b|^2 = 1$ from the normalization condition for the state vectors. There are two measurement operators on a single qubit (2.14) with two outcomes $\{0, 1\}$: $P_0 = |0\rangle\langle 0|$ and $P_1 = |1\rangle\langle 1|$ which are both Hermitian and satisfy completeness relation. The probabilities of measuring the two outcomes for 0 and 1 are $|a|^2$ and $|b|^2$ respectively.

The state $|\psi\rangle$ can be naturally used to describe the state of an quantum object with spin-$\frac{1}{2}$. We can assign the orthonormal basis vectors $|0\rangle$ and $|1\rangle$ to spin up $|+\rangle$ and spin down $|-\rangle$ respectively along the z-axis in the three dimensional Euclidean space $\mathbb{R}^3$. Due to the overall phase-independence and the normalization condition, only two real numbers of a and b characterize the qubit as a description of the orientation of the spin (polar angle θ and azimuthal angle ϕ) in $\mathbb{R}^3$. The

transition between states of a qubit system is performed by an arbitrary unitary transformation which acts as a rotation of the spin along z-axis to an arbitrary direction $\mathbf{n}$:

$$U(\mathbf{n},\theta) = \exp\Big(-\frac{i}{2}\theta(\mathbf{n}\cdot\boldsymbol{\sigma})\Big) = \mathbb{1}\cos\frac{\theta}{2} - i(\mathbf{n}\cdot\boldsymbol{\sigma})\sin\frac{\theta}{2}\,, \tag{2.15}$$

which is the general 2×2 unitary matrix with unit determinant. The spatial components of $\boldsymbol{\sigma}$

$$\sigma^x = \begin{pmatrix} 0 & 1 \\ 1 & 0 \end{pmatrix} \quad \sigma^y = \begin{pmatrix} 0 & -i \\ i & 0 \end{pmatrix} \quad \sigma^z = \begin{pmatrix} 1 & 0 \\ 0 & -1 \end{pmatrix} \tag{2.16}$$

are called *Pauli matrices*. They satisfy the following commutation relations:

$$[\sigma_i, \sigma_j] = 2i\epsilon_{ijk}\sigma^k\,, \tag{2.17}$$

where the repeated index k is summed over the spatial components $k = \{x, y, z\}$. The state pointing the direction $\mathbf{n} = (\sin\theta\cos\phi, \sin\theta\sin\phi, \cos\theta)$ can be obtained by applying a rotation θ about the axis $(-\sin\phi, \cos\phi, 0)$ to the state $|+\rangle$, which is an eigenstate of σ_z. As a conclusion, we obtain a state that can be interpreted as a spin pointing in the (θ,ϕ) direction by assigning $a \equiv e^{-i\phi/2}\cos\frac{\theta}{2}$ and $b \equiv e^{i\phi/2}\sin\frac{\theta}{2}$.

2.3 Quantum bipartite systems and quantum correlations

Actual measurements and observables are mostly associated to subsystems which are parts of a composite system. This fact motivates us to describe state space of composite systems. The space of states in a composite system is the tensor product of the the state space of the composite system: $|\psi_1\rangle \otimes |\psi_2\rangle \otimes \cdots \otimes |\psi_n\rangle$ where ith subsystem is prepared to a state $|\psi_i\rangle$.

For composite systems, one usually prefers to use the language of *density operator* instead of state vectors. It serves as a convenient tool for describing the quantum systems when states are not completely known, and the subsystems of a composite system. All the postulates of quantum mechanics can be consistently reformulated in terms of the density operator language. Suppose a quantum system

is in one of a number of states $|\psi_i\rangle$ with probability p_i.

The density operator for the system is defined by

$$\rho \equiv \sum_i p_i |\psi_i\rangle\langle\psi_i| \,. \tag{2.18}$$

An operator ρ is the density operator associated to some ensemble $\{p_i, |\psi_i\rangle\}$ if and only if ρ satisfies: $\mathrm{Tr}\rho = 1$ and $\rho \geq 0$. A quantum system, whose state $|\psi\rangle$ is known exactly, is said to be in a *pure* state where density operator is simply $\rho = |\psi\rangle\langle\psi|$, otherwise ρ is in a *mixed* state. In particular, for $\mathrm{Tr}\rho^2 = 1$ we have pure states and $\mathrm{Tr}\rho^2 < 1$ we have mixed states.

2.3.1 Quantum entanglement

There is a prominent selection for classifying states of composite systems, related to a fundamental quantum phenomenon observed in nature. The quantum phenomenon, known as *entanglement*, was first recognized through a "counterintuitive" feature of quantum mechanics by Einstein, Podolsky, Rosen and Schrödinger [**?**, 22]. This feature simply demonstrates that there is a finite set of states of a composite system which cannot be expressed as a product of the states of subsystems. Interestingly, Einstein, Podolsky and Rosen used quantum entanglement to show that quantum mechanics can be a "complete" theory by assigning values to the physical quantities prior to measurement with effects of not exceeding some universal limit (local realism). But, in fact Bell showed, combined with experimental testing, that quantum mechanics cannot satisfy both the principle of locality and counterfactual definiteness [23].

A state ρ_{AB} on $\mathcal{H}_A \otimes \mathcal{H}_B$ is called *separable/non-entangled* if and only if there exist density operators $\rho_A^{(j)}, \rho_B^{(j)}$ and $0 \leq p_j \leq 1$ with $\sum_j p_j = 1$ such that

$$\rho_{AB} = \sum_j p_j \rho_A^{(j)} \otimes \rho_B^{(j)} \,. \tag{2.19}$$

Quantum entanglement is not necessarily connected to the space of "*correlated*" states in general since the general definition of quantum entanglement exists as a counterpart of the separability of states. The space of separable states consists the

hierarchy of correlated bipartite states except the space of entangled states[3].

Entanglement is a genuine quantum aspect of a state, i.e. correlations between parts of composite systems which cannot be described within a classical picture and cannot be provided locally. It reveals non-local quantum "spookiness" in quantum mechanics. After the promising contributions of John Bell, the existence of entangled states can be tested experimentally [25]. Until present, all performed experiments verify the principles of quantum mechanics thus providing the physical being of quantum entanglement [26]. In general, it is used for a synonym of *quantum correlations* [23] but we should remark that this statement is valid only for pure states. Entanglement is not sufficient to violate Bell inequalities for mixed states where there is a class of quantum correlations which is more general than entanglement [27–29]. An entangled state describes a composite system where subsystems are not in definite states.

As we formulate the general definition of entanglement, we can provide how the quantification of entanglement can be established. This can be done by the von Neumann (entanglement) entropy [14]. Let ρ be an arbitrary density operator, then the von Neumann entropy is defined as

$$S(\rho) = -\mathrm{Tr}\rho \log \rho \tag{2.20}$$

which satisfy the following properties: $0 \leq S(\rho) \leq \log d_{\mathcal{H}}$ for pure states ρ such that $S(\rho) = \log d_{\mathcal{H}}$ is maximal if and only if $\rho = \mathbb{1}/d_{\mathcal{H}}$. In a bipartite system $\mathcal{H}_A \otimes \mathcal{H}_B$ if ρ_A, ρ_B are density operators on $\mathcal{H}_A, \mathcal{H}_B, d_{\mathcal{H}_A} \leq d_{\mathcal{H}_B}$ then the entanglement entropy on the bipartite system is $S(\rho_A \otimes \rho_B) = S(\rho_A) + S(\rho_B)$. For a pure state $\rho_{AB} = |\psi_{AB}\rangle\langle\psi_{AB}|$, the entanglement entropy on subsystem A can be listed as a consequence of the general features of $S(\rho)$:

1. $S(\rho_A) = 0 \Longleftrightarrow |\psi_{AB}\rangle$ is separable and $S(\rho_A) > 0 \Longleftrightarrow |\psi_{AB}\rangle$ is entangled.

2. $S(\rho_A) = \log(\mathrm{dim}\mathcal{H}_A) \Longleftrightarrow |\psi_{AB}\rangle$ is maximally entangled.

[3]There is a distinct set of states in the space of separable states called as "uncorrelated" in the form of $\rho^A \otimes \rho^B$ since the expectation value of joint measurements on both A and B factorizes: $\langle A \otimes B\rangle = \mathrm{Tr}\rho A \otimes B = \big(\mathrm{Tr}\rho^A A\big)\big(\mathrm{Tr}\rho^B B\big)$ [24]. In this case, the measurements performed by the subsystems and their evolution can be treated independently.

2.3.2 Quantum mutual information and correlations

The development of *quantum information* science designates the interests to quantum entanglement viewed as a resource in quantum processing. The role of entanglement in quantum information encourages to conduct research on its qualitative and quantitative aspects [19].

In classical (Shannon) information theory [30] information is associated to randomness shared by two physical ensembles. The quantitative picture of information is provided by a probability framework which describes the information that we have on some set of events. For a random variable X taking values $\{x_i\}$ with probability $\{p_i\}$, the associated Shannon entropy $H(X)$ is defined as the classical analogue of the von Neumann entropy (2.20) where the density operators are replaced by probability distributions. It is a measure of uncertainty on a variable along the stochastic event and it also quantifies the information of the variable X [31]. The statistical correlations between two random variables X and Y represent the information shared by these two variables and are measured by the mutual information I defined as

$$I(X|Y) := H(X) + H(Y) - H(X,Y)\,, \tag{2.21}$$

where $H(X,Y)$ is the joint entropy of X and Y. For independent observables and variables, the mutual information vanishes identically, $I(X|Y) = 0$.

In quantum scenario the information is stored in the quantum states of a physical system. Qubits as the fundamental unit of quantum information theory can exist in quantum superpositions which are completely unknown to classical theory. They can be physically implemented by a spin-1/2 object as in (2.14). The random variables in classical information theory are replaced by the observables and their possible values by the eigenvalues of the observables in the quantum information theory.

The standard definition of quantum mutual information for a information-theoretic description of a bipartite quantum system AB is the quantum version of (2.21):

$$I(A|B) = S(\rho_A) + S(\rho_B) - S(\rho_{AB})\,. \tag{2.22}$$

The quantum mutual information, which can be applied to pure as well as mixed states, quantifies the amount of total (classical and quantum) correlations between

two subsystems. In particular, it is maximized for a maximally entangled pure state: $I(A|B) = 2\log 2$, where $S(\rho_A) = S(\rho_B) = \log 2$ and $S(\rho_{AB}) = 0$.

It is stated multiple times in this work that quantum systems are characterized by the observable correlations they exhibit. A known example is that the correlation function between two spins in a typical spin chain may decay exponentially as a function of the distance separating them and results in a phase transition of the system [32]. A *connected equal-time correlation* $C(\mathcal{O}_A, \mathcal{O}_B)$ between two observables $\mathcal{O}_A$ and $\mathcal{O}_B$ in subsystems (or regions) A and B is defined by

$$C(\mathcal{O}_A, \mathcal{O}_B) := \langle\psi|\mathcal{O}_A \otimes \mathcal{O}_B|\psi\rangle - \langle\psi|\mathcal{O}_A|\psi\rangle\langle\psi|\mathcal{O}_B|\psi\rangle\,. \tag{2.23}$$

This definition of the connected correlation vanishes for any product state $\otimes_i|\psi_i\rangle$ which directly implies that the non-zero correlations can only realized from entanglement in the pure state $|\psi\rangle \neq \otimes_i|\psi_i\rangle$. Therefore, the relevant features of quantum entanglement can be made transparent by studying correlations functions for a product of an arbitrary number of observables on a given state.

The two concepts, *connected correlations* (2.23) and *quantum mutual information* (2.22), can be related by considering the mutual information as a relative entropy and by using the norm bound on $S(\rho_A|\rho_B)$ [33]:

$$I(A|B) \geq \frac{C(\mathcal{O}_A, \mathcal{O}_B)^2}{2||\mathcal{O}_A||^2||\mathcal{O}_B||^2}\,, \tag{2.24}$$

where $||\mathcal{O}||$ is the operator norm: $||\mathcal{O}|\psi\rangle|| \leq c\,|||\psi\rangle||$ with a real number c for all states $|\psi\rangle$. The lower bound on the quantum mutual information simply implies that while connected correlation functions may be all arbitrary small, the state itself can be still highly correlated [34].

2.3.3 Two-qubit system and entanglement

Consider a quantum bipartite system $A \otimes B$ where A and B are the subsystems. An arbitrary normalized pure state of the Hilbert space $\mathcal{H}_A \otimes \mathcal{H}_B$ can be expanded as

$$\rho = |\psi_{AB}\rangle\langle\psi_{AB}|\,, \tag{2.25}$$

where $\psi_{AB} = \sum_{i,j} a_{ij}|i\rangle_A \otimes |j\rangle_B$ written in terms of the orthonormal basis $|i\rangle_A$ and $|j\rangle_B$ for $\mathcal{H}_A$ and $\mathcal{H}_B$ respectively.

An observable acting only on subsystem A can be expressed as $\mathcal{O}_A \otimes \mathbb{1}_B$, where $\mathcal{O}_A$ is a Hermitian operator on A and $\mathbb{1}_B$ is the identity operator on B. The expectation value of $\mathcal{O}_A \otimes \mathbb{1}_B$ in the state ρ_{AB} is

$$\langle \mathcal{O}_A \rangle = \mathrm{Tr}\big(\mathcal{O}_A \rho_A\big) \tag{2.26}$$

by using (2.10). ρ_A is called *reduced density operator* for the subsystem A, $\rho_A = \mathrm{Tr}_B\big(|\psi_{AB}\rangle\langle\psi_{AB}|\big)$ which is obtained by tracing ρ_{AB} over the subsystem B.

In particular, the Hilbert space $\mathcal{C}^2 \otimes \mathcal{C}^2$ consisting of two qubits is spanned by the four orthonormal maximally entangled pure state known as *Bell states*:

$$|\psi^{\pm}\rangle = \frac{1}{\sqrt{2}}\big(|0\rangle|1\rangle \pm |1\rangle|0\rangle\big) \tag{2.27}$$

$$|\phi^{\pm}\rangle = \frac{1}{\sqrt{2}}\big(|0\rangle|0\rangle \pm |1\rangle|1\rangle\big) \tag{2.28}$$

In particular, the state $|\psi^-\rangle$ is called *EPR* state, or *singlet* state. Bell states have interesting features that if one measures only the observables in one of the subsystems then the probability of its outcome is equal in both state $|0\rangle$ or $|1\rangle$ and the outcomes of the measurements for both subsystems are perfectly correlated. Another feature is these four Bell states are unitarily equivalent such that a unitary operation on a subsystem can transform one of the Bell states to the other ones. Bell states are in fact a special case of bipartite maximally entangled states on $\mathcal{C}^d \otimes \mathcal{C}^d$ given by [29]

$$|\Phi_d^+\rangle = \frac{1}{\sqrt{d}} \sum_{i=1}^{d} |i\rangle|i\rangle\,, \tag{2.29}$$

which is also equivalent to a singlet state up to local unitary transformations. The explicit form of the density operator for EPR state is

$$\rho_{12} = \frac{1}{2}\big(|0\rangle|0\rangle\langle 0|\langle 0| + |1\rangle|1\rangle\langle 0|\langle 0| + |0\rangle|0\rangle\langle 1|\langle 1| + |1\rangle|1\rangle\langle 1|\langle 1|\big)\,. \tag{2.30}$$

Tracing out the second qubit, we obtain the reduced density operator of the first

qubit:

$$\rho_1 := \mathrm{Tr}\,\rho_{12} = \frac{1}{2}\big(|0\rangle|0\rangle + |1\rangle\langle 1| = \frac{\mathbb{1}}{2}\,, \tag{2.31}$$

which is mixed state, since $\mathrm{Tr}\,\rho_1 < 1$. This result implies that the state of the two-qubit system is known exactly, but the first qubit is in a mixed state that is we do not have maximal knowledge in that state. Now we can move forward to a set canonical quantum systems in which all these fundamentals of quantum correlations and more will be studied.

2.4 Quantum spin chains

There are fundamental models in theoretical physics such as quantum harmonic oscillators or Heisenberg quantum spin chains which are used to approximate real systems. The Heisenberg quantum spin chain [35] is simply formulated and describes systems which are experimentally accessible [36]. In particular, one-dimensional spin-1/2 Heisenberg model with coupling between nearest-neighbor sites has an exact analytical solution [37]. This modeling is extended to the studies of integrable quantum many-body systems [38]. There are various field of studies where Heisenberg models play the central role [35, 39–42]. Specifically, they are used for quantum computers in quantum information and each spin-1/2 represents a qubit in the analysis of quantum entanglement [19, 43].

2.4.1 Heisenberg (XXX) spin chain

Heisenberg quantum spin chain simply consists of N *sites* connected by N-1 *links* where each site i is associated to a spin-1/2 particle s_i (see Fig.2.1). For N spin-1/2 particles, the Hilbert space of the whole chain is $\mathcal{H}_{\text{chain}} = \bigotimes_{\text{N}} \mathbb{C}^2$. At each site i, a basis for the observables consists of identity matrix $\mathbb{1}_i$ and spin operators $\mathbf{S}_i \equiv (\hbar/2)\boldsymbol{\sigma_i}$ (2.16).

Spin operators $\mathbf{S}_i$ acting on each site i satisfy following commutation relations as in (2.17):

$$[S_i^a, S_j^b] = i\hbar\,\delta_{ij}\,\epsilon_{abc}\,S_i^c\,, \tag{2.32}$$

where $a, b = \{x, y, z\}$. The quantum state of each spin-1/2 particle can be represented by the qubit state given in (2.14) of which the basis vectors correspond to

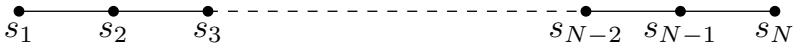

Figure 2.1. Graphical representation of a one dimensional isotropic Heisenberg (XXX) chain of spin-1/2 particles s_i with N sites connected by N-1 links.

the eigenstates of S_i^z with eigenvalues $+\hbar/2$ for spin up and $-\hbar/2$ for spin down states. The standard Hamiltonian for a closed chain describing nearest neighbor spin-spin interaction is defined by

$$H_N = \alpha \sum_{i=1}^{N} \mathbf{S}_i \cdot \mathbf{S}_{i+1} - \alpha \frac{\hbar^2 N}{2}, \quad \mathbf{S}_{N+1} = \mathbf{S}_1 \,, \tag{2.33}$$

where α ($\alpha > 0$) is the coupling strength, which is limited to nearest neighbor spins. This Hamiltonian generates the following Heisenberg equation of motion:

$$\frac{d}{dt} S_i^a := \frac{i}{\hbar}[H, S_i^a] = \alpha \epsilon_{abc} \big(S_{i-1}^b + S_{i+1}^b \big) S_i^c \,. \tag{2.34}$$

The equation of motions for each spin observable depend on its neighbor spins and they are highly non-linear even at the expectation value level of the relevant observables. We will consider later the detailed analysis of the dynamical behaviors of expectation value and higher correlations under an effective approach. Furthermore, for large values of N, the diagonalization of the Hamiltonian (2.33) is computationally harder since it is a $2^N \times 2^N$ matrix. Here we will only consider the case where N = 2.

The two-site Heisenberg spin chain consisting of two spin-1/2 particles connected by a single link has the following simple Hamiltonian:

$$H_2 = \alpha \big(\mathbf{S}_1 \cdot \mathbf{S}_2 - \hbar^2 \big) = \frac{\alpha}{2} \big(\mathbf{S}^2 - \mathbf{S}_1^2 - \mathbf{S}_2^2 - 2\hbar^2 \big) \,, \tag{2.35}$$

which is expressed in terms of the total spin operator $\mathbf{S} \equiv \mathbf{S}_1 + \mathbf{S}_2$ in the second equality. We should notice that the total spin operator $\mathbf{S}$ commutes with the Hamiltonian (2.35), $[\mathbf{S}, H_2] = 0$. This feature allows to select states that diagonalize

both the total spin operator $\mathbf{S}^2|S,S^z\rangle = \hbar^2 s(s+1)|S,S^z\rangle$ and the Hamiltonian:

$$H_2|S,S^z\rangle = \frac{\alpha}{2}\big(\hbar^2 s(s+1) - 2\hbar^2\big)|S,S^z\rangle \quad \text{for} \quad s=0,1 \tag{2.36}$$

In particular, for $s=1$ the energy is $E=0$ and for $s=1$ the energy is $E=-\hbar^2\alpha$. For a positive coupling strength $\alpha>0$ (antiferromagnetic), then the ground state energy is $-\hbar^2\alpha$ which corresponds to the singlet state (EPR) $|\psi^-\rangle$ given in (2.27):

$$|\psi^-\rangle = \frac{1}{\sqrt{2}}\big(|+\rangle|-\rangle - |-\rangle|+\rangle\big)\,. \tag{2.37}$$

In the first place we can shortly discuss how two spin observables are correlated in this state and bounded from the information that they shared. We know that the quantum mutual information $I(s_1|s_2)$ sets an upper bound on the correlation functions for the spins $\mathbf{S}_1, \mathbf{S}_2$ at opposite ends of the link (2.24). The spin-spin correlation of the $|\psi^-\rangle$ pair is obtained by using the definition (2.23):

$$\langle\psi^-|S_1^a \otimes S_2^b|\psi^-\rangle = -\frac{\hbar^2}{4}\delta^{ab}\,, \tag{2.38}$$

$$\langle\psi^-|\mathbf{S}_1|\psi^-\rangle = -\langle\psi^-|\mathbf{S}_2|\psi^-\rangle = 0\,, \tag{2.39}$$

which simply leads to

$$\frac{C(S_1^a, S_2^b)^2}{2||S_1^a||^2||S_2^b||^2} = \frac{1}{2}\delta^{ab}\,, \tag{2.40}$$

where the norm $||S_1^a|| = ||S_2^b|| = \hbar/2$. This result can be tested by using the upper bound on correlations by the quantum mutual information, which is for a pure state $S(s_{12})=0$ reduces to:

$$I(s_1|s_2) = S(s_1) + S(s_2) = 2\log 2 > \frac{1}{2}\,. \tag{2.41}$$

Tracing out the degrees of freedom of one of the spin, we find that the reduced density matrix is proportional to the identity operator and entanglement entropy of each spin is the maximal entropy. For a general graph with N-1 links, the state is then the superposition of tensor products of states in $\otimes(\mathcal{C}^2 \otimes \mathcal{C}^2)$. We should note that the state $|\psi^-\rangle$ is not the only state maximizing the quantum mutual information. It is possible to introduce an element $g \in \mathrm{SU}(2)$ which allows singlet

states, for which the spins at endpoints of a link are to be rotated with respect to each other while remaining perfectly correlated.

2.5 Quantum geometry of space

The fundamental roles and relations of spins are not only restricted to the quantum mechanical framework. They serve interestingly to construct a bridge between quantum mechanics and the general relativity, in particular, in the very fundamentals of spinfoam gravity [44, 45]. This relation can be summarized as the convergence of the asymptotic limit (large spins $j_i \gg 1$) of the Wigner $6j$-symbol [46] to the action of general relativity in three dimensional space [47]. The asymptotic formula is realized such that the action [48] can be evaluated at a region where the induced geometry is the one of a flat Euclidean tetrahedron.

The quantization of the geometry of physical space is well-built in loop quantum gravity (LQG) [49, 50]. The basis states of the kinematical Hilbert space of LQG are called *spin-networks*.

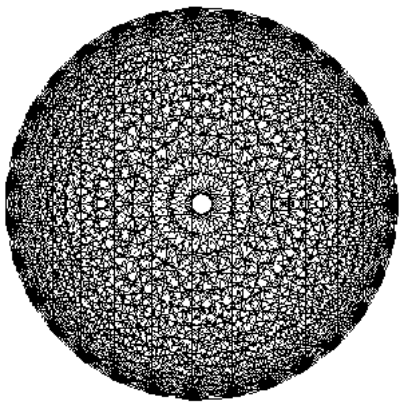

Figure 2.2. A picture for a spin-network graph consisting of 31 nodes [1].

The spectrum of the operators corresponding to the relevant geometrical degrees of freedom is based on two sets of quantum numbers in a spin network: $SU(2)$ spins label the links and $SU(2)$-invariant tensors (*intertwiners*) label the nodes. Each spin is associated to the area of a surface intersected by each link, while each intertwiner is associated with the volume of spatial regions that contain the node and to the angles formed by intersection of surfaces [51]. The elementary

spin-network state is a four-valent node dual to a tetrahedra where links are also dual to two-dimensional surfaces (see Fig.4.4), respectively.

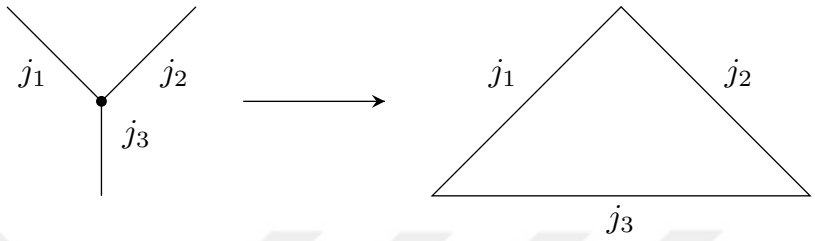

Figure 2.3. A description for a 3-valent node and its dual two-dimensional surface.

In what follows, we briefly summarize a quantization scheme that establishes the relation between the *quantum geometry* of an "atom of space" and the classical geometry of a tetrahedron.

2.5.1 Quantum tetrahedron

An atom of physical space can be seen as a *quantum tetrahedron* where areas fix the spins at each link and volume determines the intertwiner. Hilbert space describing a single quantum tetrahedron is obtained by a formal quantization of the degrees of freedom of the classical geometry of a tetrahedron [52,53], without even referring to the full quantization of general relativity. For a four-valent node, we will consider four irreducible representations $\{j_1, \cdots, j_4\}$ of $SU(2)$ with their corresponding Hilbert space, $\mathcal{H}_{j_i}$. Based on the global rotation symmetry of a tetrahedra, the $SU(2)$-invariant component of the tensor product of $\mathcal{H}_{j_i}$ can be expressed as

$$\mathcal{K}_{j_1,\cdots,j_4} := \mathrm{Inv}\left[\bigotimes_{i=1}^{4} \mathcal{H}_{j_i}\right]. \tag{2.42}$$

The degrees of freedom of the quantum geometry of a tetrahedron are then described by the Hilbert space: $\bigoplus_{j_i} \mathcal{K}_{j_1,\cdots,j_4}$. For convenience, we will consider fixed spins as some set of configurations of $\{j_i\}$ for all links.

For a possible quantization scheme, we should provide the degrees of freedom which completely determine the classical geometry of a tetrahedron, modulo rotations and translations. We start by introducing a convenient representation of the

geometry of a tetrahedron in $\mathbb{R}^3$ [54]. The geometry of the flat tetrahedron can be encoded in a triad of edge-vectors $\mathbf{e}_i$, $i = 1, 2, 3$, parallel to a specified set of edges, with norms given by the corresponding lengths. All geometric properties of the tetrahedron can be expressed in terms of such edge-vectors. An alternative set of redundant variables is provided by the normal vectors $\mathbf{n}_a$, $a = 1, \ldots, 4$, where the index a labels the faces of the tetrahedron, and a normal $\mathbf{n}_a$ is defined as the outward-pointing vector normal to the face a with area A_a (Fig. 2.4). The normal vectors satisfy the closure condition:

$$\mathbf{C} := \sum_{a=1}^{4} A_a \mathbf{n}_a = 0\,. \tag{2.43}$$

We can label the faces so that edge-length and normal vectors are related by:

$$\mathbf{n}_i = \frac{1}{4A_i} \epsilon_i{}^{jk} \mathbf{e}_j \times \mathbf{e}_k\,, \qquad i = 1, 2, 3\,, \tag{2.44}$$

with $\mathbf{n}_4$ fixed by Eq. (2.43). The vectors $(\mathbf{n}_1, \mathbf{n}_2, \mathbf{n}_3)$ are assumed to form a positively oriented set, and we raise and lower indices with the Kronecker delta δ^j_i. The dihedral angle θ_{ab} for any pair of faces in the tetrahedron is

$$\mathbf{n}_a \cdot \mathbf{n}_b = \cos\theta_{ab}, \qquad a \neq b\,. \tag{2.45}$$

The length $l_i = \sqrt{\mathbf{e}_i \cdot \mathbf{e}_i}$ of an edge $\mathbf{e}_i$ and the angles between the edge-vectors are given by:

$$\mathbf{e}_i \cdot \mathbf{e}_j = \epsilon_i{}^{pq} \epsilon_j{}^{rs} \frac{(A_p \mathbf{n}_p \cdot A_r \mathbf{n}_r)(A_q \mathbf{n}_q \cdot A_s \mathbf{n}_s)}{A_1 \mathbf{n}_1 \cdot (A_2 \mathbf{n}_2 \times A_3 \mathbf{n}_3)}\,. \tag{2.46}$$

This completes the description of the tetrahedron in terms of the normals $\mathbf{n}_a$ with areas A_a.

There is one set of six parameters for a complete description, but also for a convenient comparison with the quantum theory: four areas and two dihedral angles (two opposite angles) between the faces[4]. Overall, if we fix the areas of the triangular faces, then the classical geometry of a tetrahedron is completely

[4]In principle, one can also consider six edge-lengths to completely describe a tetrahedron but they become difficult at the operator level for computational purposes.

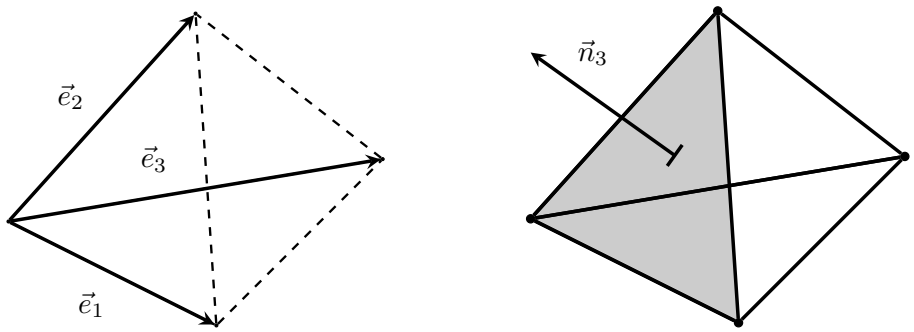

Figure 2.4. Tetrahedron formed by the edge-vectors $\mathbf{e}_i$. Thenormal $\mathbf{n}_3 = \frac{1}{2A_3}\mathbf{e}_1 \times \mathbf{e}_2$ is the normal, outward-pointing vector normalized to the area of the associated face.

determined only by two opposite angles, for instance θ_{12}, θ_{13}.

The quantization of these geometric quantities is performed by identifying the generators of $SU(2)$ as quantum operators corresponding to $A_i\mathbf{n}_i$ [52, 53] with satisfying the closure constraint at quantum level:

$$A_i\mathbf{n}_i \Longrightarrow \mathbf{J}_i\,, \quad \sum_{i=1}^{4}\mathbf{J}_i = 0\,, \tag{2.47}$$

where the Planck length is taken as $l_{\mathrm{P}} = 1$ for simplicity so that the Casimir operator $\mathbf{J}_i^2$ of $SU(2)$ representation directly determines the area of the ith triangle:$\sqrt{j_i(j_i+1)}$. As a consequence, a quantum state of a tetrahedron with fixed spins are in the direct product of $\mathcal{H}_{j_i}$ and since the state is invariant under global rotations by imposed closure constraints, the state itself will be a singlet state in $\mathcal{H}_{j=0} \equiv \mathbb{C}$ [55]:

$$|j\rangle_{12} = \sum_m \frac{(-1)^{j-m}}{\sqrt{2j+1}}|j,m\rangle_{12}|j,-m\rangle_{34}\,. \tag{2.48}$$

This class of basis singlet states is obtained by coupling the two spins j_1 and j_2, $\mathbf{J}_{12} := \mathbf{J}_1 + \mathbf{J}_2$ and also the spins j_3 and j_4, $\mathbf{J}_{13} := \mathbf{J}_1 + \mathbf{J}_3$. Four areas and dihedral angle θ_{12} are diagonalized by this basis $|j\rangle_{12}$ which is the eigenvector of $\mathbf{J}_{12}$. Analogously, we can construct the basis of singlet states $|j'\rangle_{13}$ which are the eigenvectors of $\mathbf{J}_{13}$. These basis vectors are related by the Winger $6j$-symbol, $\{6j\}$, using $SU(2)$ recoupling theory:$|j'\rangle_{13} = \sum_j \left((-1)^{\sum_i j_i}\sqrt{d_j d_{j'}}\{6j\}\right)|j\rangle_{12}$ with

$d_j = 2j + 1$.

The quantum geometry of a tetrahedron is then encoded in the operators of $\mathbf{J}_i^2, \mathbf{J}_{ij}^2$ and the commutator $[\mathbf{J}_1 \cdot \mathbf{J}_2, \mathbf{J}_1 \cdot \mathbf{J}_3]$ which is related to the relevant dihedral angle operators $\widehat{\theta_{ij}}$:

$$\cos\widehat{\theta}_{ij} := \frac{\mathbf{J}_i \cdot \mathbf{J}_j}{\sqrt{j_i(j_i+1)j_j(j_j+1)}} = \frac{1}{2\sqrt{j_i(j_i+1)j_j(j_j+1)}}\big(\mathbf{J}_{ij}^2 - \mathbf{J}_i^2 - \mathbf{J}_j^2\big) \quad (2.49)$$

A significant property of the these operators is that not all of them are commuting:

$$[\mathbf{J}_1 \cdot \mathbf{J}_2, \mathbf{J}_1 \cdot \mathbf{J}_3] = \frac{1}{4}[\mathbf{J}_{12}^2, \mathbf{J}_{13}^2] \neq 0\,, \quad (2.50)$$

at the same time we know that $[\mathbf{J}_m^2, \mathbf{J}_i \cdot \mathbf{J}_j] = 0$. Therefore, a complete set of commuting operators can be given by the operators either $\{\mathbf{J}_i^2, \mathbf{J}_{12}^2\}$ or $\{\mathbf{J}_i^2, \mathbf{J}_{13}^2\}$. As we conclude that the basis states $|j\rangle_{12}$ are eigenvectors of the five commuting operators $\{\mathbf{J}_i^2, \mathbf{J}_{12}^2\}$ so that the average value of the sixth variable J_{13}^2 is maximally spread. This explains the intrinsic *fuzziness* property of the quantum tetrahedron where one cannot measure all the operators that completely determine the geometry. This leads to obtain superpositions of the states in order to provide the *semiclassical* limit of the quantum geometry. One of the conventional way to obtain coherent states is to minimize the Heisenberg uncertainty relations (2.12) between non-commuting observables:

$$\Delta(\mathbf{J}_{12}^2)\Delta(\mathbf{J}_{13}^2) \geq \frac{1}{2}|\langle\big[\mathbf{J}_{12}^2, \mathbf{J}_{13}^2\big]\rangle|\,. \quad (2.51)$$

On the other hand, it is possible to construct a class of semiclassical states not requiring the minimization of the uncertainty relations, rather vanishing all the relative dispersions such as $\langle\Delta\widehat{\theta_{ij}}\rangle/\langle\widehat{\theta_{ij}}\rangle \to 0$ in the large spin limit $j_i \gg 1$, while the areas are taken fixed sharp values. For instance, there is a family of good semiclassical states $|\psi\rangle := \sum_j c_j|j\rangle_{12} \in \mathcal{K}_{j_1,\cdots,j_4}$ in [56] such that the coefficients c_j are chosen so that the expectation values of the geometric operators are peaked around classical values with vanishing relative dispersions in the large spin limit. In this work, we will introduce a particular class of semiclassical states that is describing geometries dual to more general graphs.

2.6 Quantum fields in Minkowski spacetime

Quantum harmonic oscillators are building blocks for *quantum fields* which are the central mathematical tools of quantum field theories. Standard quantum field theory is a set of notions and principles that combine classical fields, special relativity and quantum mechanics [57]. Currently, quantum field theory is seen as effective field theory, low energy approximation to more fundamental theories due to its consecutive failures of quantizing general relativity (for higher than linear expansion of the metric). "Particles" called as *field quanta* correspond to the direct excitation states of the underlying field and the quantum interactions between the field quanta are described by the interaction terms among the corresponding quantum fields.

A classical field is described by a function $\phi(\mathbf{x}, t)$, where $\mathbf{x}$ is three dimensional coordinate in space and t is time. At every point, $\phi(\mathbf{x}, t)$ takes real numbers in some finite-dimensional configuration space and the field itself can be a scalar, vector or tensor. Quantum fields are conserving the functional properties of classical fields defined over space and time, but they also comprise the axioms and observations of quantum mechanics. Mathematically, quantum fields are obtained by promoting classical oscillators representing modes of classical fields to quantum harmonic oscillators which are realized as operator-valued functions or distributions [58]. In what follows we will only concentrate on the relevant features of a simplest quantum field: free scalar field in Minkowski vacuum.

2.6.1 Free scalar fields in Minkowski vacuum

Free scalar quantum fields can be constructed by quantizing an infinite set of decoupled harmonic oscillators. Therefore, we introduce a description of an action with N decoupled harmonic oscillators:

$$S[q] = \frac{1}{2} \int dt \sum_{i=1}^{N} \left(\dot{q}_i^2 - q_i^2 \right), \tag{2.52}$$

where q_i are the generalized coordinates and the corresponding frequencies are taken to be unity $w_i = 1$. The canonically conjugate variables to the generalized coordinates q_i are the generalized momenta p_a such that they satisfy canonical commutation relations [46] $\{q_i, p_j\} = \delta_{ij}$. The canonical quantization scheme

is performed by quantization this classical phase space to the Hilbert space on which the fundamental operators $\hat{q}_i(t), \hat{p}_j(t)$ are acting. They satisfy the standard equal-time commutation relations:

$$[\hat{q}_i, \hat{p}_j] = i\delta_{ij}, \quad [\hat{q}_i, \hat{q}_j] = [\hat{p}_i, \hat{p}_j] = 0\,, \tag{2.53}$$

where we take the Planck constant $\hbar = 1$. The (time-independent) creation $a_i^\dagger$ and annihilation operators a_i for the harmonic oscillators are defined as

$$a_i^\dagger := \sqrt{\frac{1}{2}}\Big(\hat{q}_i - i\hat{p}_i\Big) \tag{2.54}$$

$$a_i := \sqrt{\frac{1}{2}}\Big(\hat{q}_i + i\hat{p}_i\Big)\,, \tag{2.55}$$

where they also satisfy the commutations relations: $[a_i, a_j^\dagger] = \delta_{ij}$.

The Hilbert space $\mathcal{H}_{\rm osc}^{(N)}$ for a system of $i = 1, \cdots, N$ quantum oscillators is built with the set of $\{a_i, a_i^\dagger\}$ operators. The ground state (vacuum) $|0\rangle \equiv \otimes_i |0\rangle_i$ is defined uniquely by annihilations operators a_i:

$$a_i|0\rangle = 0 \quad \text{for} \quad i = 1, \cdots, N\,. \tag{2.56}$$

The general state $|\{n_i\}\rangle$, that spans $\mathcal{H}_{\rm osc}^{(N)}$, with all possible occupation numbers n_i is defined by

$$|\{n_i\}\rangle := \left[\prod_{i=1}^{N} \frac{\big(a_i^\dagger\big)^{n_i}}{\sqrt{n_i!}}\right]|0\rangle\,. \tag{2.57}$$

Now we treat a classical field $\phi(\mathbf{x}, t)$ as an infinite collection of oscillators attached to each point $\mathbf{x}$ and we replace the discrete sums over the indices of oscillators i by the integrals over the continuous $\mathbf{x}$ in the action (2.52) such that it must be realized in the following Lagrangian $\mathcal{L}$ form:

$$S[\phi] = \int d^3\mathbf{x}\,\mathcal{L} = \frac{1}{2}\int d^3\mathbf{x}\,dt\Big[- \eta^{\mu\nu}\big(\partial_\mu\phi\big)\big(\partial_\nu\phi\big) - m^2\phi^2\Big]\,, \tag{2.58}$$

where the Minkowski metric $\eta_{\mu\nu} = \text{diag}(-1, 1, 1, 1)$ and $(t, \mathbf{x}) \equiv (x^0, x^1, x^2, x^3)$. The

oscillators can be seen decoupled in the Fourier transform of the field itself:

$$\phi(\mathbf{x},t) := \int \frac{d^3\mathbf{k}}{(2\pi)^3} e^{i\mathbf{k}\cdot\mathbf{x}} \phi(\mathbf{k},t) \tag{2.59}$$

and the action:

$$S[\phi] = \frac{1}{2}\int d^3\mathbf{k}, dt \bigg(\dot{\phi}(\mathbf{k},t)\dot{\phi}(-\mathbf{k},t) - (k^2+m^2)\phi(\mathbf{k},t)\phi(-\mathbf{k},t) \bigg), \tag{2.60}$$

where the frequencies for each oscillator restrict $\sqrt{k^2+m^2} = 1$. We will continue the field quantization with the reformulation of the theory in the Hamiltonian formalism through defining the conjugate variable to the field: $\pi(\mathbf{x},t) \equiv \delta\mathcal{L}/\delta\dot{\phi}(\mathbf{x},t) = \dot{\phi}(\mathbf{x},t)$. Then the classical Hamiltonian is given by

$$H = \int d^3\mathbf{x} \bigg(\pi(\mathbf{x},t)\dot{\phi}(\mathbf{x},t) - \mathcal{L} \bigg) = \frac{1}{2}\int d^3\mathbf{x} \bigg(\pi^2 + (\nabla\phi)^2 + m^2\phi^2 \bigg). \tag{2.61}$$

The canonical quantization of the field and the momentum in the momentum representation satisfy following commutation relations:

$$\big[\phi(\mathbf{k},t), \pi(\mathbf{k}',t)\big] = i\delta(\mathbf{k}+\mathbf{k}') \tag{2.62}$$

and the corresponding creation $a^\dagger(\mathbf{k})$ and annihilation $a(\mathbf{k})$ operators are then defined based on (2.54) by replacing $q_i \to \phi(\mathbf{k})$ and $p_i \to \pi(\mathbf{k})$. The vacuum state $|0\rangle$ exists as in (2.56): $a(\mathbf{k})\,|0\rangle = 0$ for all momenta $\mathbf{k}$ and the Hamiltonian (2.61) can be expressed in terms of $a(\mathbf{k})$ and $a^\dagger(\mathbf{k})$ in the normal ordered form:

$$H = \int d^3\mathbf{k} \big(a^\dagger(\mathbf{k})a(\mathbf{k}) + \frac{1}{2}\delta^3(0) \big), \tag{2.63}$$

which simply implies Heisenberg equation of motions for the time-dependent creation and annihilation operators: $\dot{a}(\mathbf{k},t) = -ia(\mathbf{k},t)$ and $\dot{a}^\dagger(\mathbf{k},t) = ia^\dagger(\mathbf{k},t)$. Based on this set of equation of motion, we can obtain the mode expansion of the quantum field $\phi(\mathbf{x},t)$:

$$\phi(\mathbf{x},t) = \int \frac{d^3\mathbf{k}}{\sqrt{2}(2\pi)^3} \big[a(\mathbf{k})e^{i\mathbf{k}\cdot\mathbf{x}-it} + a^\dagger(\mathbf{k})e^{-i\mathbf{k}\cdot\mathbf{x}+it} \big] \tag{2.64}$$

As we established a setup for the states and operators in Minkowski background,

we can simply compute first the ground state energy. From the Hamiltonian (2.63), the total energy of the free scalar field in the vacuum state $|0\rangle$ is

$$E_0 = \langle 0|H|0\rangle = \frac{1}{2}\delta^3(0)\int d^3\mathbf{k}\,. \tag{2.65}$$

The ground state energy diverges due to the delta function $\delta^3(0)$ in the infinite volume of space and also the divergence in the integral over $\mathbf{k}$. This can be avoided simply by subtracting the ground state energy E_0 from the Hamiltonian in the absence of the curvature in Minkowski (flat) background [59] so that the vacumm state is then become an eigenstate of H with zero eigenvalue. More importantly, the modification of the Hamiltonian by subtracting the ground state energy does not cause to cancel the vacuum fluctuations of quantum fields. Vacuum fluctuations can be obtained by computing the correlation function between two points in space based on (2.64):

$$C_\phi(|\mathbf{x}-\mathbf{y}|) := \langle 0|\phi(\mathbf{x},t)\phi(\mathbf{y},t)|0\rangle = \frac{1}{4\pi^2}\int dk\, k^2\left(\frac{\sin(k|\mathbf{x}-\mathbf{y}|)}{k|\mathbf{x}-\mathbf{y}|}\right), \tag{2.66}$$

which only depends on the modulus of the relative distances in space because of the Poincaré invariance of the background geometry. For a finite region of space with a volume of L^3, the typical amplitude of vacuum fluctuations then decays as $L^{3/2}$ on scales $L \sim 1/k$ [59].

Chapter 3
Gluing polyhedra with entanglement in loop quantum gravity

In section 2.5 we introduce a self-consistent scheme for a quantization of the geometry of space based on loop quantum gravity. The elementary building block of the quantum geometry is considered as constructing the quantization of a classical tetrahedron. In summary, one first quantize the phase space of four face-normal vectors $A_i\mathbf{n}_i$ to each face of the tetrahedron by promoting these vectors to operators $\mathbf{J}_i$ associated to the four copies of $SU(2)$ with eigenvalues squared to $j_i(j_i+1)$. Then one imposes the closure constraint $\sum_i \mathbf{J}_i = 0$ at the operational level. The Hilbert space for this quantization is the space of 4-valent intertwiners, space of $SU(2)$ invariant vectors. A basis for this space, we specify the invariant states $|j_i, i_{12}\rangle \equiv |j_{12}\rangle$ (2.48) diagonalizing the operator $(\mathbf{J}_1 + \mathbf{J}_2)^2$ with eigenvalues $i_{12}(i_{12}+1)$ and labelled by a intertwiner label which is also a spin.

This quantization scheme is extended to obtain a quantization procedure of a collection of geometric structures in $\mathbb{R}^3$ through which spin-network states of loop quantum gravity are understood. It is possible now to ask how the collection of these geometric structures will be configured at the quantum level. We will claim that imposing correlations between geometric quantities will be a possible recipe to understand how to build approximate recognizable geometries in the relevant semiclassical regime.

3.1 Introduction

In a background independent theory of quantum gravity, the geometry of spacetime is completely encoded in the quantum state $|\psi\rangle$ of the gravitational field, which lives in a Hilbert space $\mathcal{H}$ defined without any reference to an external geometry g_{ab}. In the semiclassical regime, geometric structures must then emerge from the properties of the state $|\psi\rangle$ alone. Indications that entanglement in fluctuations of the gravitational field play a crucial role for the emergence of classical spacetimes have surfaced in various approaches to nonperturbative quantum gravity [60–67]. At the topological level, the connectivity of space itself is argued to be related to the presence of entanglement among degrees of freedom in distinct regions of space via holographic arguments [60, 61]. Quantum correlations also reflect metric properties of space in semiclassical gravity, as shown by the generic validity of an area law for the entanglement entropy of quantum fields in curved spaces, a property thus expected to hold for semiclassical states in any theory of quantum gravity [62]. Procedures for measuring distances and curvature from the network of quantum correlations have also been recently discussed in varied emergent geometry scenarios [66, 68, 69]. In this work we explore the relation of entanglement and geometry in loop quantum gravity and discuss conditions on the fluctuations of the quantum geometry associated with the emergence of continuous spatial metrics in the semiclassical regime of the theory.

Loop quantum gravity (LQG) is a canonical nonperturbative approach to quantum gravity based on the quantization of the gravitation field in Ashtekar variables [70–72]. In LQG, any state of the quantum geometry is a superposition of spin network states $|\Gamma, i_n, j_\ell\rangle$ labeled by a graph Γ, half-integer spins j_ℓ at the links, and $SU(2)$ intertwiners i_n at the nodes of the graph [73, 74]. The geometry of a spin network state can be interpreted in terms of twisted geometries [75–77], a generalization of Regge calculus [78, 79] that allows for the presence of metric discontinuities across two-dimensional faces of a $3d$ triangulation. On a graph Γ, the geometry of spin networks describes an assembly of quantum polyhedra, as discussed in [80]. Each node of valence $|n|$ represents a quantum polyhedron obtained by the quantization of the space of shapes of a flat $|n|$-faced polyhedron with fixed areas in $\mathbb{R}^3$, and the state of the quantum polyhedron is described by the intertwiner i_n. For $|n| = 4$, the node describes a quantum tetrahedron [81, 82]. The full state is

obtained by gluing these building blocks together according to the combinatorics of the graph. The resulting geometry describes a generic superposition of twisted geometries.

The relation between classical polyhedral complexes and twisted geometries is encoded in a set of *gluing (or matching) conditions* that express either the continuity of the metric across faces or the existence of normals oriented in opposite directions on glued faces. In a twisted geometry, a given face displays no mismatches for observations of its total area, but it can have distinct normals or shapes as observed from opposite sides. The metric discontinuities at faces correspond precisely to such mismatches of shapes. A geometry is normal-matched if there exist a set of rotations such that the normals on the identified faces of the rotated polyhedra are oriented in opposite directions. This allows one to isometrically embed its polyhedra in $\mathbf{R}^3$ in a manner that normals of identified faces are always antiparallel, so that directions of links are well defined on the 1-skeleton of the dual graph. We call this class of geometries *vector geometries* [83–85]. A geometry is shape-matched if all edge lengths or some combinations of internal angles and diagonals in each two-dimensional face have the same values when measured in any of the polyhedra sharing it. These shape-matched geometries correspond to *Regge geometries* [86][1]. Such a hierarchy of discrete geometries and associated gluing conditions played a decisive role for the geometric interpretation of the classical phase space of LQG, and our aim is to extend it to the quantum regime, as a means of providing new tools for the characterization of states of the geometry, specially in the semiclassical regime.

The translation of classical matching conditions to the quantum regime is not straightforward, however, due to ambiguities arising in their quantization and issues related to gauge invariance. Classical shape-matching conditions, for instance, admit distinct but equivalent formulations in terms of observables that do not commute in the quantum theory. We can match angles or lengths, but these choices lead to inequivalent conditions in the quantum theory. As a result, there is no natural, preferred set of quantum shape-matching conditions. For the normal-matching conditions, one faces the problem that they are not formulated as constraints in the

[1]More precisely, shape-matched twisted geometries are piecewise flat continuous geometries. Special examples are given by triangulations, to which Regge calculus applies. We shall use the term Regge geometry to refer to the more general case of piecewise flat continuous geometries built out of polyhedra with arbitrary numbers of faces.

gauge-invariant classical phase space, but as a requirement of existence of gauge transformations with specified properties in the gauge-dependent phase space, a procedure without an obvious translation in the quantum theory. Moreover, for any given constraint, one can choose between implementing it weakly, as a condition on average values, or strongly, as a projector in the Hilbert space of the theory.

In this thesis we show how these difficulties can be overcome. We present an explicit construction of quantum vector geometries and analyze their geometry in detail with a combination of analytical and numerical methods. In addition, we introduce quantum shape-matching conditions of varying strength designed as tests of the continuity of the geometry, and show that they are satisfied by some special quantum vector geometries. Broadly speaking, our overall strategy consists in first rephrasing the gluing conditions for vector geometries as a set of normal-matching constraints $\mathbf{T}_\ell$ in the non-gauge-invariant Hilbert space $\mathcal{H}_{area}$, where they are implemented strongly, and then projecting the solutions to the gauge-invariant space of states $\mathcal{H}_\Gamma$. It turns out that solutions to these constraints are highly entangled states of the geometry. In fact, before the implementation of gauge-invariance, and for given total areas, they maximize the quantum mutual information for subsystems describing observations of the shape of a face from opposite sides of it.

Such an interplay between a condition of continuity for the normals and entanglement can be qualitatively understood as follows. In a matched classical configuration, some information describing the geometry of a boundary surface is shared by the polyhedra meeting at the boundary. Conversely, shape or normal mismatches correspond to information that is not shared by the subsystems, and as such should be assigned to the individual subsystems. Analogously, for some geometric property to be matched at the quantum level, it must be maximally shared by adjacent tetrahedra, to the extent allowed by the Heisenberg uncertainty relations for the quantum geometry. This contributes to increasing the quantum mutual information, so that the state must be highly entangled. For normal-matching, the correlations turn out to be maximal.

Let us illustrate the argument in more concrete terms in the familiar setup of spin-1/2 systems. Consider a singlet state $|\Psi\rangle_{AB}$ of a two-spin-1/2 system AB

(2.27):

$$|\Psi\rangle_{AB} = \frac{1}{\sqrt{2}} \left(|+\rangle_A|-\rangle_B - |-\rangle_A|+\rangle_B\right) , \tag{3.1}$$

where $|\pm\rangle$ denotes the spin-up and spin-down states. For such a state, if the spin of the particle A is measured to be pointing up in a direction $\vec{n}$, a subsequent measurement of the same spin component for the particle B will always give the opposite result, regardless of the chosen direction:

$$\text{Measure}[(\sigma \cdot \mathbf{n})_A] = -\text{Measure}[(\sigma \cdot \mathbf{n})_B] , \quad \forall \mathbf{n} . \tag{3.2}$$

Even though the operators $\sigma \cdot \mathbf{n}$ do not commute for distinct $\mathbf{n}$'s, the results of measurements in A and B are always perfectly correlated. The existence of such perfect correlations can be characterized in terms of the quantum mutual information $I(A|B)$ given (2.22). The quantum mutual information quantifies the amount of information shared by the subsystems in a composite system, and constitutes a measure of the correlations between the subsystems A and B. For the Bell state $|\Psi\rangle_{AB}$, the reduced density matrix for the system A is proportional to the identity operator:

$$\rho_A = \frac{1}{2}\big(|+\rangle_B\langle+|_B + |-\rangle_B\langle-|_B\big) = \frac{\mathbb{1}_A}{2} , \tag{3.3}$$

and similarly for ρ_B. As a result, the entanglement entropy of each subsystem assumes the maximal value and the quantum mutual information is also maximized $I(A|B) = 2\log 2$. This occurs whenever the information in the system A is completely shared with the system B, and $I(A|B)$ vanishes when no information is shared, i.e., in the absence of correlations.

A similar maximization of the quantum mutual information is responsible for matching normals in quantum vector geometries. For concreteness, consider the case of a dipole graph formed by a pair of nodes, called source and target nodes, connected by l links coloured by spins j_ℓ (Fig. 3.1). The intertwiners i_n at a node can be taken to be eigenstates of some local observable O (normals, edge lengths, internal angles of faces, volume, etc), and we call it O_S or O_T according to where the observation was performed. For a quantum vector geometry on the dipole graph, we find that local measurements of the geometry are always perfectly correlated, as

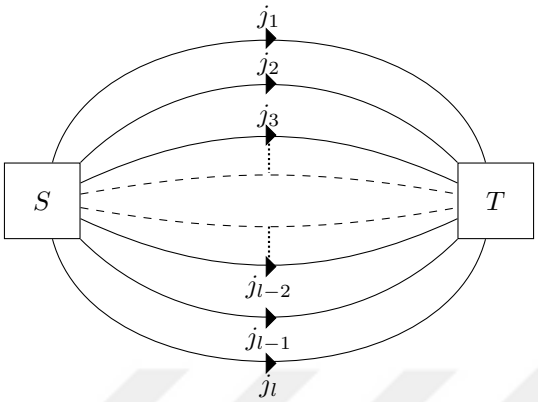

Figure 3.1. Dipole graph. A pair of nodes connected by l links coloured by spins j_ℓ.

in EPR pairs:

$$\text{Measure}[O_S] = \text{Measure}[O_T]\,. \tag{3.4}$$

Before the projection to the Hilbert space of gauge-invariant states, these quantum vector geometries are states in $\mathcal{H}_{area} = L^2[SU(2)^4]$ for which measurements of the components of a normal to a given face at distinct nodes are always antialigned. If we represent the normals by $\mathbf{E}$, we have

$$\text{Measure}[(\mathbf{E}\cdot\mathbf{n})_S] = -\text{Measure}[(\mathbf{E}\cdot\mathbf{n})_T]\,, \quad \forall\mathbf{n}\,, \tag{3.5}$$

in complete analogy with Bell states of a two-qubit system. Moreover, the quantum mutual information for the two nodes is maximized at each link. For general graphs Γ, there are no states with perfect correlations for all observables, but we can still construct states for which normals are always antialigned at each face in $\mathcal{H}_{area}$, the projection of which to the gauge-invariant sector defines quantum vector geometries on Γ. In the coherent state representation, these states are peaked on surfaces formed exclusively by classical vector geometries and average to shape-matched configurations with small mismatch fluctuations in the mesoscopic limit of large spins, so that at large scales they provide good approximations of Regge geometries.

This chapter is organized particularly as follows. We start in Section 3.2 with a discussion of the classical geometries on a fixed graph. In Section 3.3, we review the formalism of quantum polyhedra that provides the geometric interpretation of

spin network states in LQG. We emphasize the fuzziness of the quantum geometry associated with the existence of Heisenberg uncertainty relations for geometric observables, which prevents a straightforward implementation of quantum shape-matching conditions from the well-known classical formulas. In Section 3.4, we introduce quantum versions of the gluing conditions, and describe the full space of quantum vector geometries. In the same section, we present a detailed analysis of solutions to the quantum normal- and shape-matching conditions on the dipole and pentagram graphs. We summarize our results in Section 6 and discuss their relations to the recent literature on entanglement in loop quantum gravity as well as future research directions.

3.2 Classical geometries on a graph Γ

The classical phase space $\mathcal{M}_\Gamma$ of loop quantum gravity (LQG) on a graph Γ is the direct product of $SU(2)$ cotangent bundles $\mathcal{M}_\ell = T^*SU(2)$ over all links ℓ of the graph, $\mathcal{M}_\Gamma = \bigtimes_\ell \mathcal{M}_\ell$. The cotangent bundle $\mathcal{M}_\ell$ is the phase space associated with an $SU(2)$ configuration variable g_ℓ representing the holonomy of the Ashtekar connection A_a^i along the link ℓ. The full classical phase space $\mathcal{M}$ of LQG on a smooth $3d$ manifold M is the direct sum of the phase spaces $\mathcal{M}_\Gamma$ over all embedded graphs Γ in M. The restriction to a fixed graph Γ corresponds to a truncation of the theory to a finite number of degrees of freedom—the holonomies along the links of Γ, and is not sufficient to fully describe the geometry on M. Interestingly, $\mathcal{M}_\Gamma$ can still be interpreted as a space of classical geometries, but these geometries are now discrete, as shown in [75]. The truncated phase space $\mathcal{M}_\Gamma$ describes so-called twisted geometries [75, 76], a generalization of the discrete geometries considered in Regge calculus [78].

3.2.1 Hierarchy of discrete geometries

Twisted geometries are cellular complexes equipped with a metric that is in general discontinuous on two-dimensional faces, i.e., the shape of a $2d$ face can be different as seen from either side of it. In particular gauge-invariant twisted geometries, where the closure conditions are satisfied, define this local flat metric on each polyhedron. As the metric is discontinuous across two-dimensional faces, each face

shared by two polyhedra does not have to be the same shape, which is determined by the variables associated to the two polyhedra, due to the lack of matching conditions on the relevant face.

Before we forward to provide the statements about the hierarchy of the discrete geometries, we introduce the fundamental variables of the space of shapes of polyhedra since it parametrizes the phase space of twisted geometries in general. The space of shapes of (convex) polyhedra are consistently defined by the Minkowski theorem [87] such that given F positive real numbers and unit-vectors, A_a and $\mathbf{n}_a$ respectively, satisfying $\sum_a A_a \mathbf{n}_a = 0$, there always exists a unique convex polyhedron up to rotations $SO(3)$ having A_a and $\mathbf{n}_a$ as areas and normals to its faces. Now we define $\mathbf{E}_a \equiv A_a \mathbf{n}_a$ as face-normal vectors and call $\mathcal{S}_F$ with F faces of given areas A_a:

$$\mathcal{S}_F := \left\{ \mathbf{E}_a \in S^2, a = 1, \cdots, F \,\middle|\, \mathbf{E}_1 + \cdots, \mathbf{E}_F = 0, \big|\big|\mathbf{E}_a\big|\big| = A_a \right\} \Big/ SO(3) \quad (3.6)$$

as the space of shapes of polyhedra. Moreover, $\mathcal{S}_F$ naturally induces the structure of a phase space, knowns as *Kapovich-Millson* [88] phase space where the rotationally-invariant Poisson brackets are obtained from functions of $\mathbf{E}_a$ on $(S^2)^F$. Therefore, $\mathcal{S}_F$ with fixed F areas of faces forms a $2(F-3)$ dimensional phase space [80]. The canonically conjugate of this phase space are given by q_i as the angle between the vectors $\mathbf{p}_i \times \mathbf{E}_{i+1}$ and $\mathbf{p}_i \times \mathbf{E}_{i+2}$ and the conjugate momenta are the norm of the vectors $\mathbf{p}_i \equiv \sum_{a=1}^{i+1} \mathbf{E}_a$, $p_i = ||\mathbf{p}_i||$.

Two subsets of the space $\mathcal{M}_\Gamma$ of twisted geometry on Γ are of particular interest for our purposes: (i) Vector geometries, which naturally arise as boundary states in spinfoam models [83–85]; and (ii) Regge geometries, the subset of continuous twisted geometries that forms the basis of Regge calculus [78]. As we will see, vector geometries are solutions of a set of normal-matching conditions and form a submanifold of $\mathcal{M}_\Gamma$. Since the constraints do not close, this submanifold is not symplectic. Regge geometries are selected by an extra set of shape-matching conditions which determine a smaller submanifold within the space of vector geometries, also without a symplectic structure. That is, we have a hierarchy of discrete geometries on Γ:

$$\text{Regge geometries} \subset \text{Vector geometries} \subset \text{Twisted geometries}\,.$$

In what follows, we briefly review the geometry of twisted geometries and provide a characterization of the submanifolds of vector and Regge geometries in $\mathcal{M}_\Gamma$ in terms of normal-matching and gluing, or shape-matching, conditions. In Section 3.4, we discuss a similar hierarchy of discrete geometries on Γ at the quantum level.

3.2.2 Twisted geometries

Let Γ^* be the cellular decomposition dual to the graph Γ. The topological decomposition Γ^* is equipped with a metric if we colour the two-dimensional faces of all polyhedra with face-normals $\mathbf{E}_a$ satisfying the closure condition (2.43). Such variables fix the local geometry of each polyhedron, and the geometry of Γ^* is the union of these local patches. Instead of working directly with the variables $\mathbf{E}_a$, it is convenient to introduce the following parametrization. Assign an area variable $j_\ell \in \mathbb{R}$ to each link $\ell \in \Gamma$. At each node, assign a unit normal vector $\mathbf{n}_a$ to each link emerging from it. Two normals are thereby attached to any link, sitting at its two endpoints. If j_ℓ is the spin of the link, set $A_a = j_\ell$ at its endpoints. This defines face-normals $\mathbf{E}_a = A_a \mathbf{n}_a$ for all polyhedra, fixing the local geometry everywhere. In general, the resulting global metric on Γ^* will be discontinuous, since faces connected by a dual link have in general distinct shapes.

The variables $\{j_\ell, \mathbf{n}_a\}$ are sufficient to characterize the intrinsic geometry of Γ^* via $\mathbf{E}_a$. A twisted geometry has an extra variable ξ_ℓ at each link that is related to the extrinsic curvature, giving a total of six degrees of freedom per link, namely $\mathbf{n}_{s(\ell)}, \mathbf{n}_{t(\ell)}, j_\ell, \xi_\ell$, where $s(\ell), t(\ell)$ refer to the source and target nodes of the link ℓ. A twisted geometry is thus characterized by $6L$ parameters $\{(\mathbf{n}_{s(\ell)}, \mathbf{n}_{t(\ell)}, j_\ell, \xi_\ell)\}$, where L is the total number of links in Γ. The space of twisted geometries factorizes over links as $\mathcal{P}_\Gamma = \bigtimes_\ell \mathcal{P}_\ell$, where $\mathcal{P}_\ell = S^2 \times S^2 \times T^*S^1$. Let $\mathbf{C}_n$ be the closure constraint at the node n, and $\mathcal{C}$ represent the full set of closure constraints on the graph. As shown in [75], $\mathcal{P}_\Gamma$ is a phase space symplectomorphic to $\mathcal{M}_\Gamma$[2], and the space of gauge invariant configurations is the symplectic reduction $\mathcal{P}_\Gamma//\mathcal{C}$, where the double quotient means imposing the constraint and dividing by its orbits. Moreover, this

[2]More precisely, $\mathcal{P}_\Gamma$ is a presymplectic space with a symplectic quotient obtained by factoring out the subspace of geometries including some $j_\ell = 0$. The statements in the main text refers to this symplectic space.

symplectically reduced space can be parameterized as a Cartesian product of $\mathcal{S}_F$:

$$\mathcal{S}_\Gamma := \mathcal{P}_\Gamma//\mathcal{C} = \bigtimes_l T^*S^1 \bigtimes_n \mathcal{S}_{F(n)}\,, \tag{3.7}$$

where T^*S^1 is the cotangent bundle to a circle, F is the valence of the node n, and $\mathcal{S}_F$ is given in (3.6). We obtain in this way an explicit geometric interpretation of the phase space of gauge-invariant LQG states, $\mathcal{M}_\Gamma//SU(2)^N$, where N is the number of nodes in Γ, as a space of twisted geometries, with a convenient parametrization in terms of quantities with a direct geometric meaning. Each classical holonomy and flux configuration corresponds to unique collection of polyhedra.

3.2.3 Vector geometries

A vector geometry is a twisted geometry in $\mathcal{P}_\Gamma$ that in addition to the closure constraint $\mathcal{C}$ also satisfies so-called normal-matching conditions at each link. In order to describe these conditions, let us denote a link connecting the nodes a and b by $\ell = (a, b)$. The normals at the endpoints of ℓ can then be written as $\mathbf{n}_{ab}$ and $\mathbf{n}_{ba}$, where $\mathbf{n}_{ab}$ is at the node a and $\mathbf{n}_{ba}$ at the node b. We say that a twisted geometry is normal-matched if there exist $SO(3)$ elements R_a at the nodes of Γ such that

$$R_a\mathbf{n}_{ab} = -R_b\mathbf{n}_{ba}\,, \quad \forall a, b\,. \tag{3.8}$$

The rotations R_a can be used to fix a choice of local frame on each polyhedron in Γ^*. After acting with the R_a's as gauge transformations, the normal-matching conditions reduce to the requirement that normals of faces connected by a link of Γ are anti-parallel: the faces have parallel surfaces and can be fitted together (see Figure 3.2). Accordingly, if all polyhedra forming Γ^* are isometrically embedded in $\mathbb{R}^3$, they can be rotated so that identified faces are always parallel with outwards pointing normals oriented in opposite directions. Note that the normal-matching conditions are not a set of constraints in the sense that they are formulated as a condition of existence of R_a's leading to (3.8) rather than as a functional relation between the variables of the twisted geometry.

The conditions (3.8) must be imposed in some chosen gauge, obtained for instance by gauge-fixing via a maximal tree [89], to which the normals $(\mathbf{n}_{ab}, \mathbf{n}_{ba})$ refer. Nonetheless, even though one cannot speak of normal vectors in the gauge-

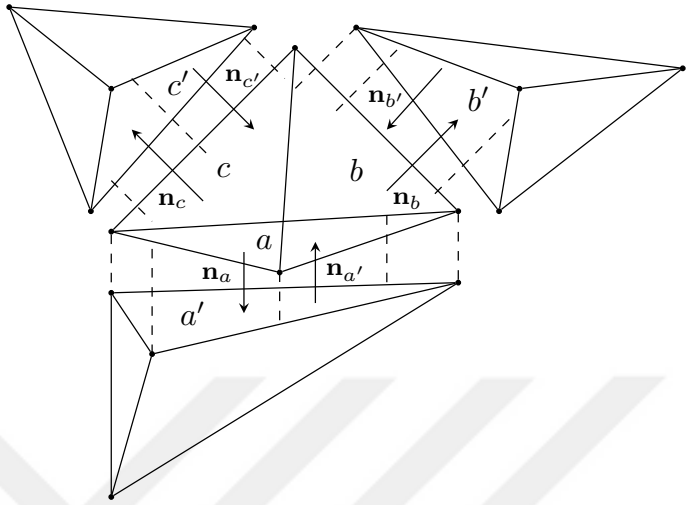

Figure 3.2. A local patch of a vector geometry. The glued faces have the same areas: $A_a = A_{a'}$, $A_b = A_{b'}$, $A_c = A_{c'}$, and their normals are anti-parallel $\mathbf{n}_a = -\mathbf{n}_{a'}$, $\mathbf{n}_b = -\mathbf{n}_{b'}$, $\mathbf{n}_c = -\mathbf{n}_{c'}$. The lengths of edges in juxtaposed triangles are not necessarily matched in a vector geometry.

invariant phase space $\mathcal{P}_\Gamma//\mathcal{C}$, there still is a clear notion of gauge-invariant vector geometries. The key point is that the condition (3.8) defining vector geometries is gauge-invariant: if a set of normals $\{\mathbf{n}_{ab}\}$ forms a vector geometry, then its image $\{U_a\mathbf{n}_{ab}\}$ under gauge transformations $U_a \in SU(2)$ will also form a vector geometry satisfying (3.8) for a new set of R's. Hence, the space of vector geometries is naturally foliated as a union of gauge orbits. Restricting to vector geometries satisfying the closure constraints $\mathcal{C}$, we can construct the space $\mathcal{V}_\Gamma \subset \mathcal{P}_\Gamma//\mathcal{C}$ of gauge-orbits of closed vector geometries, which has a natural interpretation as the space of gauge-invariant vector geometries.

This suggests a procedure for the construction of $\mathcal{V}_\Gamma$. For each link ℓ, we introduce the normal-matching constraint:

$$\mathbf{T}_\ell := \mathbf{n}_{ab} + \mathbf{n}_{ba} = 0\,, \quad \forall\, l = (a,b)\,. \tag{3.9}$$

The solution for this set of constraints is a proper subspace of the phase space P_Γ of twisted geometries characterized by $4L$ parameters. Such a subspace forms a Lagrangian submanifold [90–93] $\mathcal{A}_\Gamma \equiv \mathcal{P}_\Gamma/\mathcal{T}$, where $\mathcal{T}$ is the full set of normal-matching constraints $\mathbf{T}_\ell$. It is clear that any vector geometry satisfies all normal-matching constraints $\mathbf{T}_\ell$ in some gauge. Similarly, let $\mathcal{B}_\Gamma \equiv \mathcal{P}_\Gamma/\mathcal{C}$ be the $(6L -$

$3N$)-dimensional submanifold of P_Γ obtained by imposing the full set of closure constraints $\mathcal{C}$ on $\mathcal{P}_\Gamma$ without dividing by the gauge orbits. The submanifolds $\mathcal{A}_\Gamma$ and $\mathcal{B}_\Gamma$ are not phase spaces, since the constraint algebras are not closed. The intersection $\mathcal{A}_\Gamma \cap \mathcal{B}_\Gamma$ describes simultaneous solutions of both sets of constraints. In this submanifold, the set of oppositely directed normals $(\mathbf{n}_{ab}, -\mathbf{n}_{ab})$ at each link $l = (a, b)$ is selected so that the closure constraints hold at each node. We can now take gauge orbits of points in $\mathcal{A}_\Gamma \cap \mathcal{B}_\Gamma$. The space of such orbits is precisely $\mathcal{V}_\Gamma$.

Vector geometries can be seen as an assembly of polyhera such that any pair of glued faces are parallel. Their shapes can still be different, and in order to obtain a continuous Regge geometry additional conditions must be imposed. We now turn to the description of the conditions that select the proper subspace of Regge geometries within the space of vector geometries.

3.2.4 Regge geometries

When two tetrahedra are glued along a common face, we say that they are shape matched if glued faces have the same intrinsic geometry. In particular, the identified faces have must have the same total area, which corresponds to an area-matching condition. Twisted geometries, and vector geometries in particular, are area-matched by construction. For area-matched configurations, additional *shape-matching conditions*, or *gluing conditions*, correspond to the requirement that the length of edges and the measure of internal angles in glued faces are the same in both tetrahedra.

Conditions on the edge lengths can be imposed using the formula (2.46) for the scalar product of edge vectors. Moreover, the internal angles α^a_{bc} of a face a can be expressed in terms of the dihedral angles as [80, 86]

$$\cos \alpha^a_{bc} = \frac{\cos \theta_{bc} + \cos \theta_{ab} \cos \theta_{ac}}{\sin \theta_{ab} \sin \theta_{ac}} \,. \tag{3.10}$$

In this formula, the faces a, b, c share a vertex and α^a_{bc} is the angle between the edges $a \cap b$ and $a \cap c$ (see Fig. 3.3). In the adjacent tetrahedron, the same angle is

$$\cos \alpha^a_{b'c'} = \frac{\cos \theta_{b'c'} + \cos \theta_{ab'} \cos \theta_{ac'}}{\sin \theta_{ab'} \sin \theta_{ac'}} \,. \tag{3.11}$$

Shape-matching conditions at the face a then correspond to the requirement that

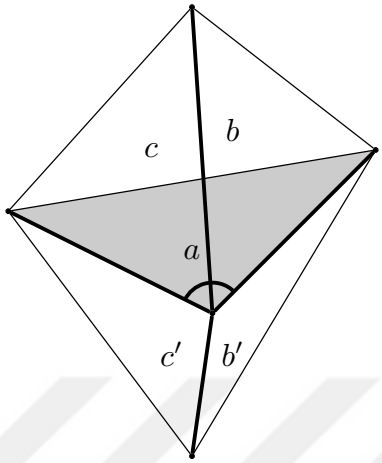

Figure 3.3. Geometric meaning of the shape-matching conditions (3.12): The internal angle α^a_{bc} in the shaded triangle can be expressed in terms of the dihedral angles associated with the thick edges of either tetrahedra.

the relation

$$\cos \alpha^a_{bc} - \cos \alpha^a_{b'c'} = 0 \tag{3.12}$$

is satisfied for any two internal angles of the triangle. These conditions lead to a series of relations among the dihedral angles in both tetrahedra through Eqs. (3.10) and (3.11). In the case where Γ^* is a triangulation, it is sufficient to impose conditions on edge lengths, or on internal angles, for area-matched configurations to be Regge geometries. For general polyhedra, however, both sets of conditions must be imposed, since it is possible to have equiareal faces with edges of the same length but distinct geometries. In constrast, Regge geometries based on triangulations are fully specified by the edge lengths alone.

3.3 Quantum polyhedron and Heisenberg uncertainty relations

For fixed areas A_a, the space of shapes of the polyhedra corresponds to the space of flat polyhedra with the given areas modulo spatial rotations [80] given in (3.6). The quantization of the phase space $\mathcal{S}_F$ was discussed in detail in [80], and provides a picture of the geometry of a quantum polyhedron. Such a description of the

quantum polyhedron agrees exactly with the description of the local geometry at a node in the spin-network representation of loop quantum gravity [54, 80]. The fact that these independent approaches to the quantization of the spatial geometry result in the same mathematical structure is nontrivial, and reinforces the geometrical interpretation of LQG states on a fixed graph Γ as quantum polyhedra. We now review this equivalence as a preparation for the discussion of gluing conditions for quantum polyhedra, in particular we will consider quantum tetrahedra for particular graphs.

Let j_a be a set of nonnegative half-integer spins associated with the faces of the polyhedron. For given spins j_a, the states of the geometry of the quantum polyhedron form the intertwiner space:

$$\mathcal{K}_{j_1\cdots j_F} = \mathrm{Inv}\left[\bigotimes_{a=1}^{F} \mathcal{H}_{j_a}\right] , \tag{3.13}$$

where $\mathcal{H}_{j_a}$ is the irreducible unitary representation of spin j_a of the group $SU(2)$. The face-normals $\mathbf{E}_a$ are quantized as angular momentum operators on the representation $\mathcal{H}_{j_a}$,

$$\mathbf{E}_a = \sigma \mathbf{J}_a \, , \tag{3.14}$$

up to a constant $\sigma > 0$ with units of area that is not fixed by the quantization procedure. The area operator $A_a = (\mathbf{E}_a \cdot \mathbf{E}_a)^{1/2}$ is proportional to the invariant Casimir operator of $SU(2)$, and has discrete eigenvalues labeled by the spins of the representation:

$$A_a = \sigma \sqrt{j_a(j_a+1)} \, . \tag{3.15}$$

The spectrum of the area operator is discrete and gapped, with an area gap of $\sigma\sqrt{3}/2$ for the minimum nontrivial spin $j_a = 1/2$. For large spins, the spectrum is regularly spaced, with steps of σ between consecutive eigenstates. The closure relation (2.43) is promoted to a operator constraint for a quantum polyhedron

$$\mathbf{C} := \sum_{a=1}^{F} \mathbf{J}_a = 0 \, , \tag{3.16}$$

which selects the intertwiner space (3.13) within the tensor product of Hilbert spaces $\mathcal{H}_{j_a}$ associated with the individual faces. All classical observables for the

geometry of the polyhedron can be expressed in terms of the variables $\mathbf{E}_a$, and are quantized by replacing the face-normal vectors in the formula for the given quantity with their corresponding operators (3.14).

Gauge-invariant observables for the intrinsic geometry are in general functions of the Penrose metric operator,

$$g_{ab} = \mathbf{E}_a \cdot \mathbf{E}_b = \sigma^2 \mathbf{J}_a \cdot \mathbf{J}_b \,, \tag{3.17}$$

which measures the dihedral angle θ_{ab} between the faces a and b [94]:

$$\theta_{ab} = \arccos\left[\frac{g_{ab}}{\sqrt{g_{aa}g_{bb}}}\right] . \tag{3.18}$$

Choosing any three faces a, b, c, the corresponding metric operators satisfy the commutation relations:

$$[g_{ab}, g_{ac}] = i\sigma \mathbf{E}_a \cdot (\mathbf{E}_b \times \mathbf{E}_c) \,. \tag{3.19}$$

Since the operators are noncommuting, the fluctuations of the quantum geometry must satisfy Heisenberg uncertainty relations:

$$\Delta g_{ab}\, \Delta g_{ac} \geq \frac{\sigma}{2} \left| \left\langle \mathbf{E}_a \cdot \left(\mathbf{E}_b \times \mathbf{E}_c \right) \right\rangle \right| . \tag{3.20}$$

As a result, if the dihedral angle θ_{ab} formed by the faces a and b is measured precisely, then the dihedral angles formed by a with any other face is completely uncertain. It is impossible to find a state of the quantum polyhedron with definite values for all dihedral angles. The uncertainty relations (3.20) characterize in this precise sense an intrinsic fuzziness of the quantum geometry, which blocks the possibility of interpreting a state of the quantum polyhedron as a simple assignment of quantum amplitudes to classical configurations of the polyhedron. The geometry of the classical polyhedron is recovered only approximately in terms of average values of quantum operators for the geometry, as described by the spin-geometry theorem of Penrose [80, 95, 96].

The Hilbert space of loop quantum gravity on a graph Γ is the space $\mathcal{H}_\Gamma = L^2[SU(2)^L/SU(2)^N]$ of square integrable functions over $SU(2)$ configurations on the graph modulo gauge transformations. A basis of $\mathcal{H}_\Gamma$ is provided by spin-

network states $|\Gamma, j_\ell, \mathrm{i}_n\rangle$ labeled by spins j_ℓ attached to links and intertwiners i_n attached to nodes of Γ. For each F-valent node n, the intertwiners i_n form an orthogonal basis of the intertwiner space $\mathcal{K}_{j_1\cdots j_F}$ where the spins j_ℓ are associated with the links meeting at the node. Taking the tensor product of all intertwiner spaces and summing over the spin configurations we obtain the full space of states, $\mathcal{H}_\Gamma = \bigoplus_{j_\ell} \bigotimes_n \mathcal{K}_{j_1\cdots j_F}$. Now let the graph Γ be dual to a cellular decomposition, so that each node represents a polyhedron, and each link represents a face in the decomposition. Then the Hilbert space of intertwiners at a node is precisely the space of states $\mathcal{K}_{j_1\cdots j_F}$ of the quantum polyhedron. Moreover, the area operator in loop quantum gravity is given by:

$$\mathbf{E}_a = 8\pi l_p^2 \gamma \mathbf{J}_a \,, \tag{3.21}$$

where γ is the Immirzi parameter and $8\pi l_p^2$ is the Planck's area. This formula is identical to Eq. (3.14) with

$$\sigma = 8\pi l_p^2 \gamma \,. \tag{3.22}$$

The observables for the local geometry at a node of a graph Γ dual to a cellular decomposition can then be identified with those for the quantum polyhedron by setting the parameter σ involved in the quantization of the space of shapes $\mathcal{S}$ equal to the factor $8\pi l_p^2\gamma$ which characterizes the discreteness scale in loop quantum gravity [80]. Any observable describing the internal geometry of a single polyhedron can then be constructed in terms of the area normals $\mathbf{E}_a$. Since a single spin j_ℓ is assigned to each link ℓ, and the total area of the corresponding face is completely determined by the spin through Eq. (3.15), the states of the geometry in loop quantum gravity are always area matched.

3.4 Quantum geometries on a graph Γ

The full space of states in loop quantum gravity is the direct sum $\mathcal{H} = \oplus_\Gamma \mathcal{H}_\Gamma$ of Hilbert spaces $\mathcal{H}_\Gamma$ associated to graphs Γ, where the sum runs over all graphs embedded in a smooth $3d$ manifold M. As in the classical theory, it is possible to truncate the theory to a single fixed graph Γ as an approximation for the description of the full quantum geometry. The resulting theory captures only a finite number of degrees of freedom and corresponds to the quantization of the classical phase

space $\mathcal{M}_\Gamma//SU(2)^N$ symplectomorphic to the space $\mathcal{S}_\Gamma \equiv \mathcal{P}_\Gamma//\mathcal{C}$ of gauge-invariant twisted geometries on Γ, as discussed in Section 3.2. In this section we consider the construction of representations of twisted, vector and Regge geometries in the truncated quantum theory on a fixed graph Γ.

3.4.1 Quantum twisted geometries

It is convenient for our purposes to work in the bosonic representation of loop quantum gravity [97–100]. The Hilbert space $\mathcal{H}_\Gamma$ of loop quantum gravity on a graph Γ is a proper subspace of a bosonic Hilbert space $\mathcal{H}_{bos}$ describing $4L$ harmonic oscillators, where L is the number of links in the graph. Explicitly, the bosonic Hilbert space is a tensor product of local Hilbert spaces attached to endpoints of links:

$$\mathcal{H}_{bos} = \bigotimes_{\ell=1}^{L} \left(\mathcal{H}_{s(\ell)} \otimes \mathcal{H}_{t(\ell)}\right) , \tag{3.23}$$

where each space $\mathcal{H}_{s(l)}$ and $\mathcal{H}_{t(\ell)}$ is associated with a pair of harmonic oscillators. As a result, there are four oscillators at each link, which we denote by $a^A_{s(\ell)}, a^B_{t(\ell)}$, $A, B = 0, 1$. We now introduce link and node constraints:

$$\mathcal{L}_\ell := \mathrm{I}_{s(\ell)} - \mathrm{I}_{t(\ell)} \approx 0\,, \qquad \mathrm{I}_i = \frac{1}{2}\delta_{AB}\, a_i^{A\dagger} a_i^B\,, \tag{3.24}$$

$$\mathbf{G}_n := \sum_{i\in n} \mathbf{J}_i \approx 0\,, \qquad \mathbf{J}_i = \frac{1}{2}\sigma_{AB}\, a_i^{A\dagger} a_i^B\,. \tag{3.25}$$

Bosonic states $|s\rangle \in \mathcal{H}_{bos}$ in general do not solve these constraints. The link constraint $\mathcal{L}_\ell$ matches the spins $j_{s(\ell)} = j_{t(\ell)} = j_\ell$ at the source and target of a link $l = (s, t)$, generating $U(1)$ transformations at each link. The node constraint $\mathbf{G}_n$ imposes invariance under $SU(2)$ gauge transformations at the node n. The corresponding projectors P_ℓ and P_n to the space of solutions of the link and node constraints form the projector

$$P_\Gamma = \Big(\prod_{n\in\Gamma} P_n\Big)\Big(\prod_{\ell\in\Gamma} P_\ell\Big) \tag{3.26}$$

to the Hilbert space of loop quantum gravity, $\mathcal{H}_\Gamma = P_\Gamma \mathcal{H}_{bos}$. As is well known, an orthonormal basis of states for $\mathcal{H}_\Gamma$ is provided by spin network states $|\Gamma, j_\ell, i_n\rangle$ labelled by spins j_ℓ at the links and $SU(2)$ intertwiners i_n at the nodes of Γ [70–72],

allowing the projector to be written as

$$P_\Gamma = \sum_{j_\ell} \sum_{i_n} |\Gamma, j_\ell, i_n\rangle\langle\Gamma, j_\ell, i_n| \,. \tag{3.27}$$

Since the spins $j_{s(\ell)} = j_{t(\ell)} = j_\ell$ are eigenstates of area operators in the dual triangulation Γ^*, the link constraints have the geometric interpretation of area-matching constraints for the quantum geometry. Accordingly, we call $\mathcal{H}_{area} = \big(\prod_{\ell\in\Gamma} P_\ell\big)\mathcal{H}_{bos}$ the area-matched subspace of the bosonic representation, which can be written as a tensor product over links:

$$\mathcal{H}_{area} = \bigotimes_{\ell=1}^{L} \mathcal{H}_\ell \subset \mathcal{H}_{bos} \,. \tag{3.28}$$

Each link space $\mathcal{H}_\ell$ is isomorphic to a copy of $L^2[SU(2)]$, and can be decomposed into a sum of tensor products of pairs of finite dimensional subspaces of equal spin j_ℓ:

$$\mathcal{H}_\ell \simeq L^2[SU(2)_\ell] = \oplus_{j_\ell}\big(\mathcal{H}_{j_\ell} \otimes \mathcal{H}_{j_\ell}\big) \,, \tag{3.29}$$

where the two Hilbert spaces $\mathcal{H}_{j_\ell}$ are naturally associated with the two endpoints of the link. The full area-matched space is $\mathcal{H}_{area} \simeq L^2[SU(2)^L]$. This space is the quantization of the classical phase space $\mathcal{M}_\Gamma = \bigtimes_\ell T^*SU(2)$ of LQG before imposing gauge invariance. The gauge invariant Hilbert space is then selected by the projector implementing the node constraints, $\mathcal{H}_\Gamma = \big(\prod_{n\in\Gamma} P_n\big)\mathcal{H}_{area} \simeq L^2[SU(2)^L/SU(2)^N]$, and corresponds to the quantization of the symplectic reduction $\mathcal{M}_\Gamma//SU(2)$ under gauge transformations.

We can now ask how to construct a state in $\mathcal{H}_\Gamma$ representing a given classical twisted geometry. This question has been answered in [101, 102], where coherent states peaked at an arbitrary point of the classical phase space of gauge invariant twisted geometries $\mathcal{S}_\Gamma$ were introduced. Such states are called extrinsic coherent states and are peaked with respect to both the intrinsic and extrinsic geometries. Their construction involves two main steps (we follow the presentation of [101]). One first constructs states $|\{(\mathbf{n}_{\mathbf{s}(\ell)}, \mathbf{n}_{t(\ell)}, j_\ell, \xi_\ell)\}\rangle \in \mathcal{H}_{area} \simeq L^2[SU(2)^L]$ that are peaked on points $\{(\mathbf{n}_{\mathbf{s}(\ell)}, \mathbf{n}_{t(\ell)}, j_\ell, \xi_\ell)\}$ of the classical phase space $\mathcal{P}_\Gamma$ of gauge-dependent twisted geometries. These states are defined as tensor products over the links of Γ of

independent Hall's heat kernel states for the cotangent bundle of $SU(2)$. Projecting them to the gauge-invariant subspace of $\mathcal{H}_{area}$, one obtains LQG coherent states $\big(\prod_{n\in\Gamma} P_n\big)|\{(\mathbf{n}_{\mathbf{s}(\ell)}, \mathbf{n}_{t(\ell)}, j_\ell, \xi_\ell)\}\rangle \in \mathcal{H}_\Gamma$ labeled by points of the gauge-independent classical phase space $\mathcal{S}_\Gamma$. Such states provide a resolution of the identity in $\mathcal{H}_\Gamma$, allowing any state $|\psi\rangle \in \mathcal{H}_\Gamma$ to be expanded in terms of extrinsic coherent states. In this precise sense, generic states of the quantum geometry in LQG correspond to quantum superpositions of gauge-invariant twisted geometries.

3.4.2 Quantum vector geometries

Vector geometries form a subset of the space of twisted geometries. This allows one to use a restricted set of extrinsic coherent states as quantum representations of gauge-invariant vector geometries in $\mathcal{H}_\Gamma$. This can be done, for instance, by reproducing at the quantum level the prescription discussed in Section 3.2 for the construction of classical vector geometries. Imposing the normal-matching constraints $\mathbf{T}_\ell$ defined in Eq. (3.9) as conditions on average values on $\mathcal{H}_{area}$,

$$\langle\{(\mathbf{n}_{\mathbf{s}(\ell)}, \mathbf{n}_{t(\ell)}, j_\ell, \xi_\ell)\}|\big(\mathbf{J}_{s(\ell)} + \mathbf{J}_{t(\ell)}\big)|\{(\mathbf{n}_{\mathbf{s}(\ell)}, \mathbf{n}_{t(\ell)}, j_\ell, \xi_\ell)\}\rangle = 0\,, \quad \forall l\,, \tag{3.30}$$

we obtain a suitable set of coherent states for vector geometries in $\mathcal{H}_{area}$, which can then be projected to the gauge-invariant subspace $\mathcal{H}_\Gamma$. Any point in the space $\mathcal{V}_\Gamma$ of gauge-invariant vector geometries is in this way mapped into a quantum state in $\mathcal{H}_\Gamma$. More explicitly, a vector geometry characterized as a gauge orbit with a representative $\{(\mathbf{n}_{\mathbf{s}(\ell)}, \mathbf{n}_{t(\ell)}, j_\ell, \xi_\ell)\}$ is mapped into the state $\big(\prod_{n\in\Gamma} P_n\big)|\{(\mathbf{n}_{\mathbf{s}(\ell)}, \mathbf{n}_{t(\ell)}, j_\ell, \xi_\ell)\}\rangle \in \mathcal{H}_\Gamma$.

By construction, coherent states $|\{(\mathbf{n}_{\mathbf{s}(\ell)}, \mathbf{n}_{t(\ell)}, j_\ell, \xi_\ell)\}\rangle$ satisfying (3.30) are peaked on a vector geometry. However, the fluctuations of the geometry are in general not normal-matched, as we have not imposed conditions on correlations for degrees of freedom at distinct endpoints of a link. As a result, the normals of glued faces fluctuate independently, and individual measurements of the spin projection along some direction $\mathbf{n}$ are not necessarily anti-aligned,

$$\text{Measure}[\mathbf{J}_{s(\ell)} \cdot \mathbf{n}] = \pm\text{Measure}[\mathbf{J}_{t(\ell)} \cdot \mathbf{n}]\,. \tag{3.31}$$

This means that the fluctuations of the geometry in general do not correspond to

vector geometries. We wish to show now that this limitation can be overcome by imposing a stronger quantum version of the normal-matching constraints. This is done by requiring not only the averages of the normals to be matched, but also that the fluctuations of the geometry take place only over normal-matched configurations.

We call a state $|\Gamma, \psi\rangle \in \mathcal{H}_\Gamma$ a quantum vector geometry if it is the projection to $\mathcal{H}_\Gamma$ of a state $|\psi\rangle \in \mathcal{H}_{area}$ satisfying:

$$\langle\psi|\left[\mathbf{J}_{s(\ell)} + \mathbf{J}_{t(\ell)}\right]^2|\psi\rangle = 0\,, \quad \forall \ell\,. \tag{3.32}$$

This condition implements the normal-matching constraints $\mathbf{T}_\ell$ strongly as constraints on $\mathcal{H}_{area}$. States satisfying (3.32) also satisfy the weaker condition (3.30). At each link ℓ, Eq. (3.32) can be solved independently for each subspace $\mathcal{H}_{j_\ell} \otimes \mathcal{H}_{j_\ell}$ of fixed spin j_ℓ, where it selects the singlet of the two spins living at the link. One can then construct tensor products of arbitrary superposition of such singlets over all spins j_ℓ to obtain the general solution,

$$|\psi\rangle = \bigotimes_\ell \sum_{j_\ell} c_{j_\ell} \sum_{m_\ell} (-1)^{j_\ell - m_\ell} |j_\ell, m_\ell\rangle_{t(\ell)} |j_\ell, -m_\ell\rangle_{s(\ell)}\,. \tag{3.33}$$

The space of solutions of (3.32) form a large class of states in $\mathcal{H}_{area}$. We are interested in exploring special subspaces of solutions formed by states that can be parametrized by quantities with a direct geometric interpretation in terms of classical geometries on Γ. The simplest such states are the extrinsic coherent states discussed above, but no solution of (3.32) can be found within this family. A more general class of semiclassical states is provided by squeezed vacua [65], which are gaussian states of the oscillators a_i^A of the bosonic model. All higher-order correlations functions are fixed by the two-point functions of the oscillators, and in this sense squeezed vacua provide the simplest family of states sufficiently general for the study of states with prescribed correlations. Solutions of (3.32) can already be found, for any graph, in the space of squeezed vacua. We call them Bell states, and their geometric properties are analyzed in detail in the remainder of this chapter.

Let us first briefly review the definition of squeezed vacua [65, 100]. On a graph Γ with L links, a squeezed vacuum $|\gamma\rangle \in \mathcal{H}_{bos}$ is labeled by a squeezing matrix γ^{ij}_{AB}

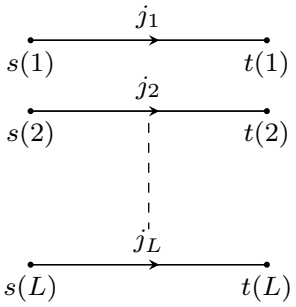

Figure 3.4. The set of L links. Each oriented link corresponds to an ordered pair $\ell = (s, t)$, where $s(\ell)$ and $t(\ell)$ are the source and target nodes at link l, respectively. The spin at the link ℓ is j_ℓ.

in the Siegel disk $\mathcal{D} = \{\gamma \in \mathrm{Mat}(4L, \mathbf{C}) | \gamma = \gamma^t \text{ and } \mathbb{1} - \gamma\gamma^\dagger > 0\}$ and is defined by:

$$|\gamma\rangle = \det\big(\mathbb{1} - \gamma\gamma^\dagger\big)^{1/4} \exp\left(\frac{1}{2}\gamma^{ij}_{AB}\, a_i^{A\dagger} a_j^{B\dagger}\right)|0\rangle\,. \tag{3.34}$$

The indices $i, j = 1, \ldots, 2L$ specify link endpoints, and $A, B = 0, 1$ distinguish between the two oscillators at a given link endpoint. The labeling of link endpoints is represented in Fig. 3.4. Intuitively, a non-zero coefficient γ^{AB}_{ij} of the squeezing matrix introduces correlations between the oscillator A at i and the oscillator B at j. Since we are looking for states with correlations among oscillators within individual links, it is sufficient to consider matrices γ with a block-diagonal form with respect to the links, i.e., such that $\gamma^{AB}_{ij} = 0$ for $i \neq j$. We call these states linkwise squeezed vacua, since they are independently squeezed link by link.

Consider a linkwise squeezing matrix of the form:

$$\gamma^{ij}_{AB} = \begin{cases} \lambda_\ell\, \epsilon_{AB} & , \quad \text{if } i = t(\ell), j = s(\ell)\,, \\ -\lambda_\ell\, \epsilon_{AB} & , \quad \text{if } i = s(\ell), j = t(\ell)\,, \\ 0 & , \quad \text{else}\,. \end{cases} \tag{3.35}$$

where $\lambda_\ell \in \mathbb{C}$, with $|\lambda_\ell| < 1$. We call the corresponding squeezed vacua Bell states, and represent them as $|\mathrm{B}_\gamma\rangle = \otimes_\ell |\mathrm{B}_\gamma\rangle_\ell$. In general, squeezed states do not satisfy the link and node constraints. By construction, however, Bell states satisfy the link constraint $\mathcal{L}_\ell$ that corresponds to the area-matching condition ensuring that the source and target states have exactly the same spin $j_{s(\ell)} = j_{t(\ell)} = j_\ell$, so that

$|\mathrm{B}_\gamma\rangle \in \mathcal{H}_{area} \subset \mathcal{H}_{bos}$.

Since the squeezing matrix γ^{ij}_{AB} in (3.35) does not couple variables at distinct links, the normalized Bell states $|\mathrm{B}_\gamma\rangle$ can be expressed as a tensor product of local states at the links of the graph:

$$|\mathrm{B}_\gamma\rangle = \bigotimes_\ell (1-|\lambda_\ell|^2) \sum_{j_\ell} \lambda_\ell^{2j_\ell} \sum_{m_\ell} (-1)^{j_\ell - m_\ell} |j_\ell, m_\ell\rangle_{t(\ell)} |j_\ell, -m_\ell\rangle_{s(\ell)} \,, \tag{3.36}$$

where the spin states at the link endpoints are represented in the magnetic number basis associated with measurements of the spin along the z-direction, but retains its form in basis associated with measurements of the spin along any direction $\mathbf{n}$. Such states have the form (3.33) and form the full set of solutions of the normal-matching condition (3.32) in the space of squeezed vacua. Let us list the main properties of the states $|\mathrm{B}_\gamma\rangle$ before the projection to the gauge-invariant space.

From the explicit formula (3.36), we see that at each link we have a maximally entangled state on for a decomposition of the link into source and target subsystems:

$$|\psi_l, j_l\rangle := \frac{1}{\sqrt{2j_l+1}} \sum_{m_l=-j_l}^{j_l} (-1)^{j_l - m_l} |j_l, m_l\rangle_{t(l)} |j_l, -m_l\rangle_{s(l)} \,, \tag{3.37}$$

which is annihilated by the following two spin-matching constraints $\mathrm{M}_1^{(l)}$ and $\mathrm{M}_2^{(l)}$, i.e. $\mathrm{M}_1^{(l)}|\psi_l, j_l\rangle = 0$ and $\mathrm{M}^{(l)}{}_2|\psi_l, j_l\rangle = 0$:

$$\mathrm{M}_1^{(l)} := \mathbf{J}^2_{t(l)} - \mathbf{J}^2_{s(l)} \,, \qquad \mathrm{M}^{(l)}{}_2 := \left(\mathbf{J}_{t(l)} + \mathbf{J}_{s(l)}\right)^2 . \tag{3.38}$$

The first constraint $\mathrm{M}_1^{(l)}$ ensures that the source and target states have exactly the same spin $j_{s(l)} = j_{(t)} = j_l$. The second spin-matching constraint $\mathrm{M}_2^{(l)}$ selects particular states for which EPR pairs are generated for spin-1/2 particles and similar perfectly correlated states for larger spins j_l.

We know that the quantum mutual information $I(s|t)$ sets an upper bound on the correlation functions for the spins $\mathbf{J}_{s(l)}, \mathbf{J}_{t(l)}$ at opposite ends of the link (2.24):

$$\frac{C(J^p_{s(l)}, J^r_{t(l)})^2}{2||J^p_{s(l)}||^2 ||J^r_{t(l)}||^2} \leq I(s(l)|t(l)) \,, \tag{3.39}$$

where p, r are the directional components of the spin operator $\mathbf{J}$. The spin-spin

correlation of the $|\psi_l, j_l\rangle$ pair is defined as:

$$C(J^p_{s(l)}, J^r_{t(l)}) := \langle \psi_l, j_l | J^p_{s(l)} \otimes J^r_{t(l)} | \psi_l, j_l \rangle - \langle \psi_l, j_l | J^p_{s(l)} | \psi_l, j_l \rangle \langle \psi_l, j_l | J^r_{t(l)} | \psi_l, j_l \rangle \,. \tag{3.40}$$

As $|\psi_l, j_l\rangle$ solves the spin-matching constraints (3.38), we have the following:

$$\langle \psi_l, j_l | J^p_{s(l)} \otimes J^r_{t(l)} | \psi_l, j_l \rangle = -\frac{j_l(j_l+1)}{3} \delta^{pr} \,, \tag{3.41}$$

$$\langle \psi_l, j_l | \mathbf{J}_{s(l)} | \psi_l, j_l \rangle = -\langle \psi_l, j_l | \mathbf{J}_{t(l)} | \psi_l, j_l \rangle = 0 \,, \tag{3.42}$$

which simply leads to

$$\frac{C(J^p_{s(l)}, J^r_{t(l)})^2}{2||J^p_{s(l)}||^2 ||J^r_{t(l)}||^2} = \frac{1}{18} \frac{(j_l+1)^2}{j_l^2} \delta^{pr} \,, \tag{3.43}$$

where the norm $||J^p_{s(l)}|| = ||J^r_{t(l)}|| = j_l$. This result is bounded by the quantum mutual information, which for a bipartite system reduces to:

$$I(s(l)|t(l)) = S(s(l)) + S(t(l)) \,. \tag{3.44}$$

Tracing out the degrees of freedom of one of the spin, we find that the reduced density matrix is proportional to the identity operator. Therefore, the entanglement entropy of each spin is $S(s(l)) = S(t(l)) = \log(2j + l + 1)$, which is the maximal entropy. We obtain a maximal pairwise mutual information for non-trivial spin-j representation, and we can check that the bound (3.39) is satisfied for correlations of spins:

$$I(s(l)|t(l)) = 2\log(2j_l + 1) \geq \frac{1}{18} \frac{(j_l+1)^2}{j_l^2} \,. \tag{3.45}$$

For a general graph with L links, the state $|\psi_l, j_l\rangle$ is the superposition of tensor products of states in $\otimes_\ell(\mathcal{H}_{j_l} \otimes \mathcal{H}_{j_l})$. For any fixed configuration of spins, the pairwise mutual information $I = \sum_\ell I(s(l)|t(l))$ is maximized by the state $|\psi_l, j_l\rangle$ before the projection of the state to the subspace of gauge-invariant states. Let us note that the state $|\psi_l, j_l\rangle$ is not the only state maximizing the quantum mutual information. It is possible to introduce $g_\ell \in \mathrm{SU}(2)$ which allowing singlet states in Eq. (3.37), for which the spins at the source and target endpoints of a link are to be rotated with respect to each other while remaining perfectly correlated. The

maximally entangled states (3.37) called Bell states are explored in Section 3.4 for the construction of linkwise squeezed states in loop quantum gravity which are highly correlated.

The observation of a spin projection m_ℓ at one endpoint of the link is always accompanied by the observation of a spin projection $-m_\ell$ at the opposite end of the link, as in an EPR pair. It follows that the fluctuations of the spins at both ends of a link are perfectly correlated in arbitrary directions, so that when one measures one of the spins, the remaining spin is immediately known:

$$\text{Measure}[\mathbf{J}_{s(\ell)} \cdot \mathbf{n}] = -\text{Measure}[\mathbf{J}_{t(\ell)} \cdot \mathbf{n}] \,. \tag{3.46}$$

For fixed spins j_ℓ, the quantum mutual information is maximized at each link on the area-matched Hilbert space $\mathcal{H}_{area}$, as discussed shortly above. This means that quantum vector geometries, when projected to subspaces of fixed spins j_ℓ, are maximally entangled states link by link. It is because of this maximization of the correlations that the fluctuations of normals are locked together for glued faces.

The parameters λ_ℓ in the squeezing matrix encode the average values of spins and holonomies at each link. The probability distribution for the spins j_ℓ at a given link is

$$P(j_\ell) = (1 - |\lambda_\ell|^2)^2 (2j_\ell + 1) |\lambda_\ell|^{4j_\ell} \,, \tag{3.47}$$

leading to a mean value

$$\langle j_\ell \rangle = \frac{|\lambda_\ell|^2}{1 - |\lambda_\ell|^2} \,. \tag{3.48}$$

The absolute value of λ_ℓ is thus fixed by the average spin at the link. In addition, the phase θ_ℓ of $\lambda_\ell = |\lambda_\ell| e^{i\theta}$ is fixed by the mean value of the holonomy h_ℓ at ℓ. In the bosonic representation, the holonomy operator is given by [100]:

$$(h_\ell)^A{}_B \equiv (2\mathrm{I}_{t(\ell)} + 1)^{-\frac{1}{2}} \left(\epsilon_{AC}\, a^{C\dagger}_{t(\ell)}\, a^{B\dagger}_{s(\ell)} - \epsilon_{BC}\, a^A_t\, a^C_s \right) (2\mathrm{I}_{s(\ell)} + 1)^{-\frac{1}{2}} \,. \tag{3.49}$$

For the Bell state $|\mathrm{B}_\gamma\rangle$, we can compute the mean value of the trace of the holonomy at a link ℓ:

$$\left\langle (h_\ell)^A{}_A \right\rangle = -2 \cos\theta_\ell \, c(|\lambda_\ell|) \,, \qquad c(|\lambda_\ell|) = (1 - |\lambda_\ell|^2)^2 \sum_{n=1}^{\infty} |\lambda_\ell|^{2n+1} \sqrt{n(n+1)} \,. \tag{3.50}$$

In the limit $|\lambda_\ell| \to 1$ of large spins, $c(|\lambda_\ell|)$ goes to 1, and we have

$$\left\langle (h_\ell)^A{}_A \right\rangle \simeq -2\cos\theta_\ell \,. \tag{3.51}$$

This approximation is quite accurate as soon as one leaves the Planck scale. As an illustration, for a mean spin of order $\langle j_\ell \rangle \simeq 10$, we already have $c(|\lambda_\ell|) \simeq 0.995$. We see that the phase of the squeezing parameter is determined by the mean value of the trace of the holonomy.

In short, a Bell state $|\mathrm{B}_\gamma\rangle \in \mathcal{H}_{area}$ is a state for which the normals of glued faces are perfectly correlated, parametrized by the average spins, $\langle j_\ell \rangle$, and holonomies, $\langle h_\ell \rangle$, at the links ℓ of the graph Γ. A point in the classical phase space $\mathcal{M}_\Gamma$ associated with $\mathcal{H}_{area}$ is characterized by a set of parameters $\{(\mathbf{n}_{\mathbf{s}(\ell)}, \mathbf{n}_{t(\ell)}, j_\ell, \xi_\ell)\}$, and vector geometries form the subspace such that $\mathbf{n}_{\mathbf{s}(\ell)} = -\mathbf{n}_{t(\ell)}$ everywhere. In comparison with the parameters characterizing $|\mathrm{B}_\gamma\rangle$, we have an extra normal vector $\mathbf{n}_{\mathbf{s}(\ell)}$ at each link, provided that we identify $\left\langle (h_\ell)^A{}_A \right\rangle$ with $2\cos\xi_\ell$. A Bell state with squeezing parameters λ_ℓ then corresponds not to a single point in $\mathcal{M}_\Gamma$, but instead to a surface formed by all vector geometries with common spins j_ℓ and holonomies ξ_ℓ. The information on the directions of the normals is partially lost in the symplectic reduction to $\mathcal{M}_\Gamma // SU(2)$ that implements gauge-invariance, but the angles between normals at a single node are gauge-invariant, and Bell states average over all allowed possibilities. (We will see that, in simple regular graphs, this implies that the corresponding quantum tetrahedra are peaked on regular tetrahedra.)

Gauge-invariant quantum vector geometries in $\mathcal{H}_\Gamma$ are obtained by simply projecting (3.36) to the space of physical states:

$$|\Gamma, \mathrm{B}_\gamma\rangle = P_\Gamma \, |\mathrm{B}_\gamma\rangle \in \mathcal{H}_\Gamma \,. \tag{3.52}$$

Let us denote by $|\Gamma, \mathrm{B}_\gamma, j_{ab}\rangle$ the projection of $|\Gamma, \mathrm{B}_\gamma\rangle$ to the subspace of $\mathcal{H}_\Gamma$ with a fixed spin configuration $\{j_{ab}\}$. The full Bell state is the superposition of all its fixed spin components,

$$|\Gamma, \mathrm{B}_\gamma\rangle = \sum_{\{j_{ab}\}} |\Gamma, \mathrm{B}_\gamma, j_{ab}\rangle \,. \tag{3.53}$$

We find that:

$$|\Gamma, \mathrm{B}_\gamma, j_{ab}\rangle = \sum_{i_a} \overline{A_\Gamma(j_{ab}, i_a)} \left(\bigotimes_{c=1}^{N} |i_c\rangle \right), \tag{3.54}$$

where the tensor product runs over all nodes, and the amplitude A_Γ of the graph is defined as

$$A_\Gamma(j_{ab}, i_a) = \sum_{\{m\}} \prod_{a=1}^{N} \big[i_a\big]^{m_{ab}\cdots m_{ae}}, \tag{3.55}$$

the contraction of all intertwiners i_a according to the combinatorics of the graph Γ. The $SU(2)$ invariant amplitude A_Γ can always be expanded in a basis of nj-symbols and corresponds to the spin network evaluation of the graph. Techniques for computing its explicit values for general graphs have been discussed in [103], where a generating function was introduced in a coherent state representation. The asymptotic behaviour for large spins $j_{ab} \to \infty$ has also been recently investigated in [85], and such analysis can be applied to the study of Bell states in the mesoscopic limit of large spins.

3.4.3 Quantum shape-matching conditions

At the classical level, area-matched cellular triangulations are said to satisfy shape-matching conditions when the lengths of two edges or the measures of two internal angles are the same as observed from either side of any given face, as discussed in Section 3.2. Physical states of LQG are area-matched by construction, but there is no immediate quantum analogue of the classical shape-matching conditions that is compatible with the Heisenberg uncertainty relations for the quantum geometry. In fact, the uncertainty relations (3.20) prevent the possibility of simultaneously observing any set of geometric quantities that completely determine the classical geometry of the tetrahedron. Nevertheless, one can still formulate a variety of tests of shape matching at the quantum level in terms of average values and correlations of geometric observables. In this section, we discuss such quantum shape-matching conditions as tools to specify in which precise sense a given state approximates or not a Regge geometry.

Let $|\psi, j_\ell\rangle$ be the projection of a generic state $|\psi\rangle$ to the subspace $\mathcal{H}_{\Gamma,\{j_\ell\}}$ of fixed spins j_ℓ resulting from a measurement of total areas for all faces in Γ^*. For given face areas, classical shape-matching conditions are described by Eq. (3.12). Analogue

conditions could be set at the quantum level by requiring the conditions (3.12) to hold at the level of average values for the corresponding quantum operators:

$$\langle \psi, j_\ell | \mathcal{C}_{SM}(O_\ell) | \psi, j_\ell \rangle = 0 \,, \qquad \mathcal{C}_{SM} := \hat{O}_{s(\ell)} - \hat{O}_{t(\ell)} \,, \tag{3.56}$$

where $\hat{O}_{s(\ell)}, \hat{O}_{t(\ell)}$ represent a generic function O_ℓ of the shape of a two-dimensional face dual to a link $\ell \in \Gamma$ as measured from each side of the face. This notion of shape-matching is problematic, however, since it requires the choice of a preferred set of observables to be matched. For example, one could match the lengths of edges, the measures of internal angles at faces or any set of functions of these quantities sufficient to fix the geometry of a given polyhedron. In general, distinct choices of observables will lead to distinct notions of shape-matching.

In the classical limit, the ambiguity should become irrelevant, and an alternative procedure would be to impose a weaker version of the conditions (3.56) by requiring the mismatches to vanish for all observables in the limit of large spins:

$$\lim_{j_\ell \to \infty} \frac{\langle \psi, j_\ell | \mathcal{C}_{SM}(O_\ell) | \psi, j_\ell \rangle}{\langle \psi, j_\ell | \hat{O}_{s(\ell)} | \psi, j_\ell \rangle} = 0 \,, \qquad \forall O_\ell \,. \tag{3.57}$$

This condition is sufficient to ensure that the mean geometry is a Regge geometry in the mesoscopic limit, and provides a useful test for shape-matching in this limit. Without further conditions, however, it offers limited guidance for the construction of shape-matched states, since the low-spin regime remains completely unconstrained. Note also that, even if the stronger condition (3.56) is satisfied, fluctuations around the average geometry can still display large metric discontinuities.

In order to avoid imposing conditions that involve two-point functions of arbitrary geometric observables, one can alternatively pursue a more abstract strategy and introduce conditions on the mutual information for nearby tetrahedra. Consider the correlation function

$$C\left(\hat{O}_{s(\ell)}, \hat{O}_{t(\ell)}\right) = \left\langle \hat{O}_{s(\ell)} \otimes \hat{O}_{t(\ell)} \right\rangle - \left\langle \hat{O}_{s(\ell)} \right\rangle \left\langle \hat{O}_{t(\ell)} \right\rangle \tag{3.58}$$

for an arbitrary geometric observable O_ℓ at ℓ. In order for the fluctuations of the geometry to be matched, these correlations must be nonzero:

$$C\big(\hat{O}_{s(\ell)}, \hat{O}_{t(\ell)}\big) \neq 0 \,, \tag{3.59}$$

since for vanishing correlations the metric fluctutations at opposite sides of a face are independent. In fact, we wish the correlations to be as strong as possible. Now, a generic bound for the correlation functions can be written in terms of the quantum mutual information between the subsystems [104] as in (3.39):

$$\frac{C\big(\hat{O}_{s(\ell)}, \hat{O}_{t(\ell)}\big)^2}{2\|\hat{O}_{s(\ell)}\|^2 \|\hat{O}_{t(\ell)}\|^2} \leq I(s|t)\,. \tag{3.60}$$

The quantum mutual information is always nonnegative, vanishes for separable states and is maximal for perfectly correlated states. Since shape-matching conditions must be imposed simultaneously for all faces of Γ^*, we also introduce the pairwise mutual information:

$$I = \sum_{\ell} I(s|t)\,, \tag{3.61}$$

where the sum runs over all pairs of nodes connected by a link. This quantity provides a measure of the total amount of information shared by nearest neighbors over the graph. It vanishes if the fluctuations of the geometry in adjacent tetrahedra are independent, and increases in the presence of large correlations, as seen from Eq. (3.60). In order to have the shape fluctuations as correlated as possible, uniformly over the graph, the pairwise mutual information I must be maximized.

The condition of maximal mutual information can be interpreted as a shape-matching condition as follows. In a classical Regge geometry, the information describing the shape of a triangular face is fully shared by the adjacent tetrahedra: owing to the continuity of the metric, the shape of a face is completely determined from observations performed on either side of it. This is not true in a quantum triangulation, where the metric has discontinuities that can be observed by comparing measurements performed at opposite sides of the boundary. The discontinuities encode information that is not shared by the neighboring tetrahedra, and as such are suppressed by the maximization of the mutual information. Ideally, measurements of a geometric property would always agree for observations performed at opposite sides of a common boundary. States of the neighboring tetrahedra would then be perfectly correlated, consistently with a maximal mutual information. Such ideal situation cannot be realized everywhere in a generic graph, however, and the maximization of the pairwise mutual information I offers a compromise where

the metric discontinuities are minimized in a roughly uniform way over the whole graph.

3.4.4 Bell states on the dipole graph

The dipole graph Γ_2 is formed by two nodes $n = s, t$ connected by four links $\ell = 1, 2, 3, 4$, as represented in Fig. 3.5. The graph Γ_2 is dual to a triangulation of the three-sphere formed by two tetrahedra glued along their boundaries. The space of states of loop quantum gravity on Γ_2 is the Hilbert space $\mathcal{H}_{\Gamma_2} = L^2[SU(2)^4/SU(2)^2]$ of gauge-invariant $SU(2)$ states on the graph. An orthonormal basis for $\mathcal{H}_{\Gamma_2}$ is provided by spin-network states $|i_s, i_t, j_\ell\rangle$, where j_ℓ is the spin associated with the link ℓ, the index i_s labels an orthonormal basis of the intertwiner space $\mathcal{K}^{(s)}_{j_1 j_2 j_3 j_4}$ associated with the node s and similarly for the target node t. In the holonomy representation, a spin-network state corresponds to:

$$\langle h_\ell | i_s, i_t, j_\ell \rangle = \sum_{m_\ell, n_\ell} \prod_\ell \left[D^{j_\ell}(h_\ell)\right]^{m_\ell}{}_{n_\ell} [i_s]^{n_1 n_2 n_3 n_4} [i_t]_{m_1 m_2 m_3 m_4} \,, \tag{3.62}$$

where spinor indices of intertwiners are lowered using the isomorphism $\epsilon_j : \mathcal{H}_j \to \mathcal{H}_j^*$ defined by $v_m = (-1)^{j-m} v^{-m}$. In the bosonic representation of $\mathcal{H}_{\Gamma_2}$ [97, 100], each link is associated with four harmonic oscillators. We denote the Hilbert space of states of this collection of sixteen oscillators by $\mathcal{H}^{16}_{bos}$ and label each link endpoint by an index i. The space of states of the quantum dipole graph is embedded unitarily in the oscillator model under the map:

$$\sqrt{2j_\ell + 1}\left[D^{j_\ell}(h_\ell)\right]^{m_\ell}{}_{n_\ell} \mapsto (-1)^{j_\ell - n_\ell} |j_\ell, m_\ell\rangle_{t(\ell)} |j_\ell, -n_\ell\rangle_{s(\ell)} \,, \tag{3.63}$$

where

$$|j, m\rangle_i = \frac{\left(a_i^{0\dagger}\right)^{j+m} \left(a_i^{1\dagger}\right)^{j-m}}{\sqrt{(j+m)!(j-m)!}} |0\rangle_i \,, \tag{3.64}$$

and $|0\rangle_i$ is the local vacuum state annihilated by the operators a_i^A. The states $|jm\rangle$ at each link endpoint can be seen as spin states with spin j and magnetic number m, so that (3.64) is the usual Schwinger oscillator model of angular momentum. Note that the map (3.63) is not surjective: the space of states of loop quantum gravity is a proper subspace $\mathcal{H}_{\Gamma_2} \subset \mathcal{H}^{16}_{bos}$ of the bosonic representation selected by

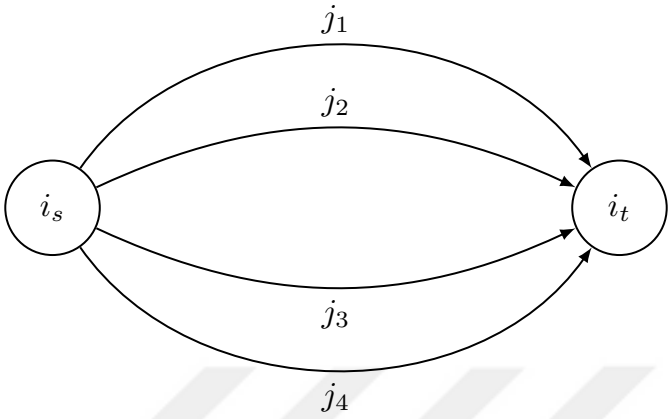

Figure 3.5. Dipole graph Γ_2. The source (s) and target (t) nodes are connected by four links $\ell = 1, \dots, 4$. The graph is dual to the triangulation of the 3-sphere formed by two tetrahedra glued along their boundaries. A spin-network state is labelled by spins j_ℓ and intertwiners i_s, i_t.

the area-matching and Gauss constraints (see [100]). The area-matching constraint is the requirement that only products of source and target local states $|j_\ell, m_\ell\rangle_t$ and $|j'_\ell, n_\ell\rangle_s$ with the same spins are allowed, $j_\ell = j'_\ell$, as required by the map (3.63). The Gauss constraint imposes gauge-invariance at each node n. We denote the projection to the space of area-matched, gauge-invariant states by $P_{\Gamma_2} : \mathcal{H}^{16}_{bos} \to \mathcal{H}_{\Gamma_2}$.

3.4.4.1 Bell states on Γ_2

Consider the Bell state $|\mathrm{B}_\gamma\rangle \in \mathcal{H}^{16}_{bos}$ obtained by squeezing the vacuum state with the matrix $\lambda_\ell \epsilon_{AB}$ at each link (Eq. (3.36)):

$$|\mathrm{B}_\gamma\rangle = \sum_{j_\ell} \bigotimes_\ell \lambda_\ell^{2j_\ell} \sum_{m_\ell=-j_\ell}^{j_\ell} (-1)^{j_\ell - m_\ell} |j_\ell, m_\ell\rangle_{t(\ell)} |j_\ell, -m_\ell\rangle_{s(\ell)} \,, \tag{3.65}$$

where we omit the normalization factor $\det\big(\mathbb{1} - \gamma\gamma^\dagger\big)^{1/4}$ since it will be changed by the projection P_{Γ_2}. This state is area-matched but not gauge invariant. In order to obtain the projection to $\mathcal{H}_{\Gamma_2}$, it is sufficient to act on $|\mathrm{B}_\gamma\rangle$ with the projection P_n to the space of gauge-invariant states at each node n of the graph. For each spin configuration j_ℓ, we expand the projection P_s at the source node with respect to a

basis of intertwiners $|i_k\rangle \in \mathcal{K}_{j_1 j_2 j_3 j_4}$ as

$$P_s = \sum_k |i_k\rangle\langle i_k| \,, \tag{3.66}$$

where $k = 1, \ldots, \dim \mathcal{K}_{j_1 j_2 j_3 j_4}$. We obtain after the projection:

$$|\Gamma_2, \mathrm{B}_\gamma\rangle = P_{\Gamma_2}|\mathrm{B}_\gamma\rangle = \sum_{j_\ell} \left(\prod_\ell \lambda^{2j_\ell} \right) \sum_k |i_k\rangle_t |\tilde{i}_k\rangle_s \,, \tag{3.67}$$

where the intertwiner $\tilde{i}_k$ is obtained from $|i_k\rangle$ by acting on all intertwiner indices with the antilinear map $\zeta : \mathcal{H}_j \to \mathcal{H}_j$ defined by

$$\tilde{v}^m = (\zeta v)^m = (v^{-m})^* (-1)^{j-m} \,. \tag{3.68}$$

The normalized projection of $P_{\Gamma_2}|\mathrm{B}_\gamma\rangle$ to the space of states with fixed spins j_ℓ is simply:

$$|\Gamma_2, \mathrm{B}_\gamma, j_\ell\rangle = \frac{1}{\sqrt{\dim \mathcal{K}_{j_1 j_2 j_3 j_4}}} \sum_k |i_k\rangle_t |\tilde{i}_k\rangle_s \,. \tag{3.69}$$

The map (3.68) corresponds to the operation of time-reversal for spin states in $\mathcal{H}_j$. Hence, if the states $|i_k\rangle$ form an orthonormal set of eigenstates of an observable $\hat{O}$, then the states $|\tilde{i}_k\rangle$ form an orthonormal basis of eigenstates of the time-reversed operator $\zeta \hat{O} \zeta^{-1}$. Now, the action of time-reversal on area operators $\mathbf{E}_a$ only amounts to a change of sign, $\zeta \mathbf{E}_a \zeta^{-1} = -\mathbf{E}_a$, and as a result the Penrose metric operator $\hat{g}_{ab}$ is not affected by this operation. Since any observable $\hat{O}$ of the intrinsic geometry can be written in terms of components of the Penrose metric, it follows that the intertwiners $|i_k\rangle$ and $|\tilde{i}_k\rangle$ describe the same local intrinsic geometry. This leads to a simple geometric interpretation of the projected state $|\Gamma_2, \mathrm{B}_\gamma, j_\ell\rangle$: it consists of a perfectly correlated state such that if the measurement of an observable O of the spatial metric at the tetrahedron s has a result O_k, then the observation of the same quantity at the tetrahedron t gives the same result. This property can be concisely represented as:

$$\mathrm{Measure}[\hat{O}_{s(\ell)}] = \mathrm{Measure}[\hat{O}_{t(\ell)}] \,. \tag{3.70}$$

Note that this property is valid for any observable $\hat{O}$, since any basis of orthonormal

intertwiners can be used in Eq. (3.66). Such a behavior mirrors that of Bell states for a pair of spin 1/2 systems, where observations of the individual spins $\sigma \cdot \mathbf{n}$ are perfectly correlated for measurements performed in arbitrary directions $\mathbf{n}$. In the present case, instead of spins, each subsystem is a quantum tetrahedron, and observations of individual metric properties are perfectly correlated.

Let us check that the pairwise mutual information I is maximized by the Bell state $|\Gamma_2, \mathrm{B}_\gamma, j_\ell\rangle$, for any spin configuration. Since the quantum dipole graph is formed by only two tetrahedra, we have $S_{st} = 0$, and the mutual information between source and target nodes reduces to:

$$I_{st} = S_s + S_t \,. \tag{3.71}$$

Tracing out the degrees of freedom of the target node, we find that the local state of the geometry at the source node is described by the density matrix:

$$\rho_s = \frac{1}{\dim \mathcal{K}_{j_1 j_2 j_3 j_4}} \sum_k |i_k\rangle_s \langle i_k|_s = \frac{\mathbb{1}_s}{\mathrm{Tr}_\mathrm{s}\, \mathbb{1}_s} \,. \tag{3.72}$$

The same result is obtained for ρ_t. It follows that the entanglement entropy of each subsystem is $S_s = S_t = \log \dim \mathcal{K}_{j_1 j_2 j_3 j_4}$, which is the maximal entropy at this dimensionality. The configuration of the local quantum geometry described by ρ_s is such that all states compatible with the prescribed spins j_ℓ are equally probable, and in this sense ρ_s is a microcanonical ensemble that maximizes the entropy in the space of quantum states of the tetrahedron compatible with a set of prescribed total areas for the faces at its boundary. We conclude that

$$I_{st} = 2 \log \dim \mathcal{K}_{j_1 j_2 j_3 j_4} \tag{3.73}$$

is the maximal pairwise mutual information, and $|\Gamma_2, \gamma, j_\ell\rangle$ satisfies all quantum shape-matching conditions introduced in Section 3.4.3, for any spin configuration.

Now let O_ℓ be an observable for a generic property of the shape of a face in Γ_2, and denote the operators associated with this quantity for the source and target tetrahedra by $\hat{O}_s$ and $\hat{O}_t$, respectively. We can choose the intertwiners states $|i_k\rangle_t$ in Eq. (3.66) to be the normalized eigenstates of $\hat{O}_t$. From the previous discussion, the intertwiners $|\tilde{i}_k\rangle$ are then eigenstates of $\hat{O}_s$ with the same eigenvalue. It follows

that, for any spin configuration:

$$\mathcal{C}_{SM}|\Gamma_2, \mathrm{B}_\gamma, j_\ell\rangle = (\hat{O}_s - \hat{O}_t)|\Gamma_2, \mathrm{B}_\gamma, j_\ell\rangle = 0\,. \tag{3.74}$$

Hence, the Bell state $|\Gamma_2, \mathrm{B}_\gamma, j_\ell\rangle$ also satisfies a stronger condition of shape-matching where $\mathcal{C}_{SM}$ is imposed as a constraint. This implies in particular that $\langle \mathcal{C}_{SM}\rangle = 0$, showing that average values for the geometry satisfy the classical shape-matching conditions. In addition, we also have $\langle \mathcal{C}^n_{SM}\rangle = 0$, $n \in \mathbb{N}$, consistent with a perfect correlation for measurements of arbitrary metric observables.

3.4.4.2 Bell states at fixed spins j_ℓ on Γ_2

Let us now focus on the study of the geometry described by the maximally entangled Bell states $|\Gamma_2, \mathrm{B}_\gamma, j_\ell\rangle$ for fixed spins j_ℓ. In particular, we wish to determine the average values, correlation functions and dispersions of the angle operators:

$$\widehat{\cos\theta_{ab}} = \frac{\mathbf{J}_a \cdot \mathbf{J}_b}{\sqrt{j_a(j_a+1)j_b(j_b+1)}}\,. \tag{3.75}$$

In order to compute the average value of an angle operator $\widehat{\cos\theta_{ab}}$, it is convenient to choose the interwiners $|i_k\rangle$ employed in the represention (3.69) to be normalized eigenstates of $(\mathbf{J}_a + \mathbf{J}_b)^2$:

$$(\mathbf{J}_a + \mathbf{J}_b)^2|i_k\rangle = k(k+1)|i_k\rangle\,, \qquad k \in \mathcal{I}_{ab} \cap \mathcal{I}_{cd}\,, \tag{3.76}$$

where we have introduced the interval $\mathcal{I}_{ab} = \{|j_a - j_b|, |j_a - j_b| + 1, \ldots, j_a + j_b - 1, j_a + j_b\}$ (similarly for $\mathcal{I}_{cd}$), and j_c, j_d are the spins at links opposite to j_a, j_b. Let χ_{cd} be the characteristic function associated with the interval $\mathcal{I}_{cd}$. The average value of an angle operator is then given by the explicit formula:

$$\langle \Gamma_2, \mathrm{B}_\gamma, j_\ell|\widehat{\cos\theta_{ab}}|\Gamma_2, \mathrm{B}_\gamma, j_\ell\rangle = \frac{1}{\dim \mathcal{K}_{j_1 j_2 j_3 j_4}} \sum_{k=|j_a - j_b|}^{j_a+j_b} \frac{k(k+1) - j_a(j_a+1) - j_b(j_b+1)}{2\sqrt{j_a(j_a+1)j_b(j_b+1)}}\chi_{cd}\,. \tag{3.77}$$

Similar expressions can be obtained for the Penrose metric g_{ab} and for polynomial functions of it.

Let us explore some special symmetric spin configurations. We start with the

case where all spins are equal, $j_\ell = j$:

$$|\Gamma_2, \mathrm{B}_\gamma, j_\ell = j\rangle = \frac{1}{\sqrt{2j+1}} \sum_k |i_k\rangle_t |\tilde{i}_k\rangle_s \,. \tag{3.78}$$

It is then straightforward to obtain:

$$\left\langle \widehat{\cos\theta_{ab}} \right\rangle = \frac{1}{j(j+1)(2j+1)} \left(\sum_{k=0}^{2j} \frac{1}{2} \big(k(k+1) - 2j(j+1) \big) \right) = -\frac{1}{3} \,, \tag{3.79}$$

for any pair a, b. We find that the average geometry describes a regular tetrahedron[3]. The maximization of the entanglement entropy for the individual nodes, which implies that the observation of any intertwiner state consistent with $j_\ell = j$ is equally probable and characterizes a microcanonical ensemble for the geometry, enforces a regular average geometry for the tetrahedron.

Next we compute the correlation function for operators $\mathbf{J}^s_a \cdot \mathbf{J}^s_b$ and $\mathbf{J}^t_a \cdot \mathbf{J}^t_b$ describing observations of the same angle in the two tetrahedra:

$$\mathcal{C}(j) = \frac{\big\langle \big(\mathbf{J}^s_a \cdot \mathbf{J}^s_b\big)\big(\mathbf{J}^t_a \cdot \mathbf{J}^t_b\big)\big\rangle - \big\langle \big(\mathbf{J}^s_a \cdot \mathbf{J}^s_b\big)\big\rangle \big\langle \big(\mathbf{J}^t_a \cdot \mathbf{J}^t_b\big)\big\rangle}{\big\langle \big(\mathbf{J}^s_a \cdot \mathbf{J}^s_a\big)\big\rangle \big\langle \big(\mathbf{J}^t_a \cdot \mathbf{J}^t_b\big)\big\rangle} \tag{3.80}$$

$$= \frac{16}{45} \left(\frac{j(j+1) + 3/16}{j(j+1)} \right) \xrightarrow{j\to\infty} \frac{16}{45} \,. \tag{3.81}$$

The correlation function $\mathcal{C}(j)$ remains finite in the large spin limit $j \to \infty$, showing that the fluctuations of the geometry remain correlated in the classical limit. The amplitude of the fluctuations is described by the dispersion $\Delta(\hat{g}_{ab}) = \sqrt{\langle \hat{g}^2_{ab} \rangle - \langle \hat{g}_{ab} \rangle^2}$ of the metric operator:

$$\frac{\Delta(\hat{g}_{ab})}{||\mathbf{E}_a||||\mathbf{E}_b||} = \frac{1}{3\sqrt{5}} \left(\sqrt{16 + \frac{3}{j} - \frac{3}{j+1}} \right) \xrightarrow{j\to\infty} \frac{4}{3\sqrt{5}} \,, \tag{3.82}$$

which shows that the states are not sharply peaked for large spins $j \to \infty$. The quantum state of the geometry is thus diffuse, describing on the average a pair of regular tetrahedra, with perfectly correlated fluctuations of the geometry of the two tetrahedra.

Consider now the more general case of two pairs of equal spins, $j_1 = j_2$ and

[3]Note that the angle θ_{ab} between the normals of two faces is the supplement of the corresponding dihedral angle. We still call θ_{ab} a dihedral angle for compactness of notation.

$j_3 = j_4$. The average values of the angle operators $\widehat{\cos\theta_{ab}}$ can be computed as before, leading to:

$$\left\langle \widehat{\cos\theta_{12}} \right\rangle = -\frac{1}{3}\,, \tag{3.83}$$

$$\left\langle \widehat{\cos\theta_{34}} \right\rangle = -1 + \frac{2}{3}\frac{j_1(j_1+1)}{j_3(j_3+1)}\,, \tag{3.84}$$

$$\left\langle \widehat{\cos\theta_{13}} \right\rangle = -\frac{1}{3}\sqrt{\frac{j_1(j_1+1)}{j_3(j_3+1)}}\,. \tag{3.85}$$

Owing to the asymmetry in the spin configurations, we have three distinct average values for dihedral angles. In the limit where all spins are the same, $j_1 \to j_3$, all averages reduce to $-1/3$, and we recover the previous result. For more general spin configurations j_ℓ, the general formula (3.77) is still valid, but a simple closed formula is not available.

3.4.5 Bell states on the pentagram

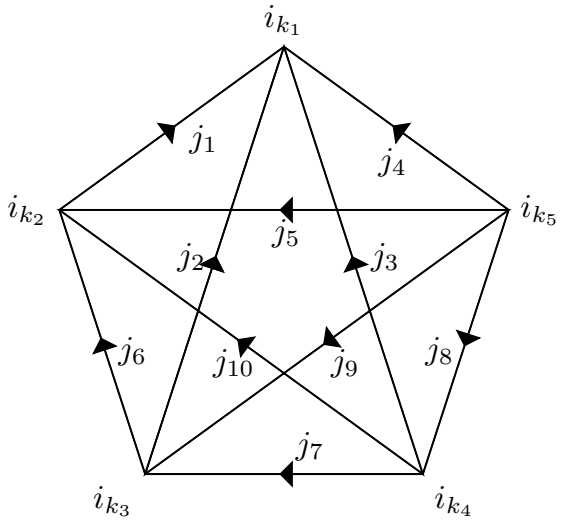

Figure 3.6. Pentagram graph Γ_5. The graph is dual to a triangulation of the three-sphere with five tetrahedra. A spin-network state on Γ_5 is labeled by five intertwiners i_{k_n} and ten spins j_ℓ attached to the nodes and links of the graph, respectively. The links are oriented according to $t(\ell) < s(\ell)$.

The pentagram graph Γ_5 is formed by five nodes connected by ten links as

shown in Fig. 3.6, and is dual to a triangulation Γ_5^* with five tetrahedra, ten faces and ten links. We label the nodes by an index $a = 1, \ldots, 5$. An oriented link corresponds to an ordered pair $\ell = (a, b)$, where a and b are the source and target nodes, respectively. Spin network states on Γ_5 are represented as $|\Gamma_5, j_{ab}, i_a\rangle$, where $j_{ab} (= j_{ba})$ is the spin at the link (a, b) and i_a is the intertwiner at the node a. At each node, an orthonormal basis of intertwiners can be labeled by a virtual spin i_a for some decomposition of the four-valent node as a gluing of two three-valent nodes. A spin network state on Γ_5 is then characterized by a set of 15 spins j_{ab}, i_a. The space of states of loop quantum gravity on Γ_5 is the Hilbert space $\mathcal{H}_{\Gamma_5} = L^2[SU(2)^{10}/SU(2)^5]$. The bosonic representation has now 40 oscillators, $\mathcal{H}_{\Gamma_5} \subset \mathcal{H}^{40}_{bos}$. Projecting the maximally entangled state $|\Gamma_5, \gamma\rangle \in \mathcal{H}^{40}_{bos}$ defined for general graphs in Eq. (3.36) to the space of gauge-invariant states with fixed spins j_ℓ, we obtain the Bell state (explicitly derived in Appendix D):

$$|\Gamma_5, \mathrm{B}_\gamma, j_{ab}\rangle = P_{\Gamma_5}|\mathrm{B}_\gamma, j_{ab}\rangle = \sum_{i_a} \overline{15j(j_{ab}, i_a)} \left(\bigotimes_{k=1}^{5} |i_k\rangle \right) , \tag{3.86}$$

where the $15j$-symbol is the contraction of the intertwiners i_a along the graph Γ_5, which can be seen as the $SU(2)$ vertex amplitude of the 4-simplex.

An alternative strategy for implementing the projection into the space of gauge-invariant states, which will lead us to a coherent state representation for the Bell state, consists in first writing the node projectors as

$$P_{\Gamma_5} = \bigotimes_a P_a \,, \qquad P_a = \sum_{i_a} |i_a\rangle\langle i_a| \equiv \int_{SU(2)} dX_a X_a \,, \tag{3.87}$$

where X_a acts unitarily on $\bigotimes_{b:a\neq b} V_{j_{ab}}$. Then we obtain from (3.36) that at fixed spins j_{ab}:

$$|\Gamma_5, \mathrm{B}_\gamma, j_{ab}\rangle = \int_{SU(2)^5} \left[\prod_{c=1}^{5} dX_c \right] \bigotimes_{a<b} \sum_{m_{ab}} (-1)^{j_{ab}-m_{ab}} X_a |j_{ab}, m_{ab}\rangle \otimes X_b |j_{ba}, -m_{ab}\rangle \,. \tag{3.88}$$

A resolution of the identity in terms of LS (Livine-Speziale) intertwiners $|\psi_a(j_{ab}, \mathbf{n}_{ab})\rangle$

[105] in the gauge-invariant space at the node a is given by [106]:

$$\mathbb{1}_\psi = \prod_{a\neq b} \mathrm{d}_{j_{ab}} \int_{P_j^{(0)}} d\mu_\psi(\mathbf{n}_{ab})\, |\psi_a(j_{ab},\mathbf{n}_{ab})\rangle\langle\psi_a(j_{ab},\mathbf{n}_{ab})|\,, \tag{3.89}$$

where the measure $d\mu_\psi(\mathbf{n}_{ab})$ is defined as

$$d\mu_\psi(\mathbf{n_{ab}}) = d\mu^{(0)}(\mathbf{n_{ab}})\,\rho_{j_{ab}}(\mathbf{n}_{ab})\,, \quad d\mu^{(0)}(\mathbf{n_{ab}}) \equiv \prod_{a\neq b} d^2\mathbf{n}_{ab}\ \delta^{(3)}\left(\sum_{a\neq b} j_{ab}\,\mathbf{n}_{ab}\right) \tag{3.90}$$

with an $SU(2)$ invariant measure $d\mu^{(0)}(\mathbf{n_{ab}})$ on the reduced phase space $P_j^{(0)}$ of solutions of the closure constraint $\sum_{a\neq b} j_{ab}\mathbf{n}_{ab} = 0.$, i.e., the integration in (3.89) is performed over the space of classical tetrahedra. The positive $SU(2)$ invariant function $\rho_{j_{ab}}(\mathbf{n}_{ab})$ is determined explicitly in [106]. Inserting the resolution of the identity (3.89) at each endpoint of the graph, and omitting irrelevant overall factors, we can write the Bell states $|\Gamma_5, \mathrm{B}_\gamma, j_{ab}\rangle$ in the form:

$$|\Gamma_5, \mathrm{B}_\gamma, j_{ab}\rangle = \int_{P_j^{(0)}} d\mu_\psi(\mathbf{n}_{ab})\, \overline{15j(j_{ab},\mathbf{n}_{ab})}\, |\psi(j_{ab},\mathbf{n}_{ab})\rangle\,, \tag{3.91}$$

where the boundary state

$$|\psi(\mathbf{n}_{ab}, j_{ab})\rangle = \bigotimes_a \int_{X_a\in SU(2)} dX_a \bigotimes_{b\neq a} X_a\, |\mathbf{n}_{ab}\rangle^{2j_{ab}} \tag{3.92}$$

is defined up to a phase (due to phase ambiguities in the definition of the $SU(2)$ coherent states $|\mathbf{n}_{ab}\rangle$), and the $SU(2)$ 15-j symbol is written in the coherent state basis as

$$15j(j_{ab},\mathbf{n}_{ab}) = \int_{SU(2)^5} \left[\prod_{c=1}^{5} dX_c\right] \prod_{a<b} \langle\zeta\mathbf{n}_{ab}|X_a^\dagger X_b|\mathbf{n}_{ba}\rangle^{2j_{ab}}\,. \tag{3.93}$$

By construction, the Bell states $|\Gamma_5, \mathrm{B}_\gamma, j_{ab}\rangle$ are quantum vector geometries, i.e., the average geometry and its fluctuations satisfy normal-matching conditions. In order to probe the geometric properties of these states in more detail, we wish now to check whether they also satisfy shape-matching conditions. We will focus on the weaker conditions (3.57) that characterize states peaked on Regge geometries in the mesoscopic limit of triangulations formed by large tetrahedra. Such an

analysis requires a careful description of the large spin behaviour of the $15j$-symbols appearing in the integral representation (3.91). The asymptotic behavior of the $15j$-symbols was studied in [83], and our calculations will rely heavily on the asymptotic formulas derived in that work. In what follows, we collect the relevant results for our purposes, and refer to [83, 84] for details.

The integral expression (3.93) can be analysed with stationary phase methods by rescaling all the spins simultaneously, $j_{ab} \to \lambda j_{ab}$, and letting $\lambda \to \infty$. Conditions for the critical points of the action, Eqs. (D.5) and (D.6), and formulas for the Hessian, Eqs. (D.8) and (D.9), are explicitly computed in Appendix D. Evaluating the Hessian of the action at critical points $v^i_{ab} = -n'^i_{ab}$, we find for off-diagonal elements:

$$H^{ij}_{cd}(\tilde{X}(\mathbf{n})) = -\frac{1}{2} j_{cd} \Big(-\delta_{ij} + i\epsilon_{ijk} n'^k_{cd} + n'^i_{cd} n'^j_{cd} \Big) \,, \tag{3.94}$$

and for diagonal elements:

$$H^{ij}_{cc}(\tilde{X}(\mathbf{n})) = -\tfrac{1}{2} \sum_{b \neq c} j_{bc} \Big(\delta_{ij} - i\epsilon_{ijk} n'^k_{cb} - n'^i_{cb} n'^j_{cb} \Big) = \sum_{b \neq c} -\tfrac{1}{2} j_{bc} \Big(\delta_{ij} - n'^i_{cb} n'^j_{cb} \Big) \tag{3.95}$$

The existence and classification of solutions to the critical equations depend on the boundary data $\{j_{ab}, \mathbf{n}_{ab}\}$. A configuration is said to be non-degenerate if, for each tetrahedron a, the four vectors $\mathbf{n}_{ab}$ with $b \neq a$ span a three-dimensional space. It is shown in [83] that if $\{j_{ab}, \mathbf{n}_{ab}\}$ is non-degenerate boundary data satisfying the closure equations

$$\sum_{b \neq a} j_{ab}\, \mathbf{n}_{ab} = 0 \,, \tag{3.96}$$

and $X_a \in SU(2)$ are a set of five group elements solving the critical equations

$$X_a\, \mathbf{n}_{ab} = -X_b\, \mathbf{n}_{ba} \,, \tag{3.97}$$

then there are at most two distinct sets of X_a. So we have three possibilities:

- There are no solutions for the set of fixed boundary data so that the tetrahedra do not glue at all.
- There is only one solution $\sim \{\tilde{X}\}$, up to equivalence.

- There are two distinct solutions $\sim \{\tilde{X}', \tilde{X}''\}$ which are not related by a symmetry.

If the four vectors $\mathbf{n}_{ab}$ satisfy the closure condition then they define a tetrahedron in $\mathbb{R}^3$ with outward face normals $\mathbf{n}_{ab}$ and areas j_{ab}. Each tetrahedron inherits a metric and an orientation from the ambient space but the metrics and orientations of different tetrahedra do not necessarily match. For a non-degenerate configuration, if the induced metrics on triangles agree for the two tetrahedra sharing the triangle and the induced orientations are opposite, the configuration is shape-matched. In this case the glued tetrahedra form a Regge geometry. In general, solutions of the critical conditions are vector geometries, normal-matched configurations up to gauge transformations.

For shape-matched boundary data, there exists a unique set of ten $SU(2)$ elements $g_{ab} = g_{ba}^{-1}$ which glue together the five tetrahedra and map the outward normal to one tetrahedron to the inward normal to the other,

$$g_{ba}\mathbf{n}_{ab} = -\mathbf{n}_{ba}\,. \tag{3.98}$$

The gluing maps g_{ba} parallel transport vectors in the tangent space T_a of the tetrahedron a to the tangent space T_b of the tetrahedron b, and can be used to fix a canonical choice of phase for the boundary state ψ through

$$|\mathbf{n}_{ba}\rangle = g_{ba}J|\mathbf{n}_{ab}\rangle\,, \tag{3.99}$$

defining a so-called Regge state. Interpreting the polyhedron obtained after gluing the five tetrahedra as the boundary of a 4-simplex, we can obtain three kinds of shape-matched configurations: the metric of the resulting 4-simplex can be $4d$ Lorentzian (with space-like tetrahedra), 4d Euclidean or 3d Euclidean geometry, with signatures $-+++, ++++$ or $0+++$, respectively. The signature of the 4d metric is determined by the number of inequivalent solutions to the critical point conditions for the given boundary data [84]: If the boundary data satisfies shape-matching conditions, then the critical point equations have two equivalence classes of solutions in the case of $4d$ Euclidean boundary data, one equivalence class in the case of $3d$ Euclidean boundary data, and none in the case of $4d$ Lorentzian boundary data. Moreover, in the $3d$ Euclidean one can always choose a gauge such

that the g_{ab} satisfies

$$g_{ab}^2 = \pm \mathbb{1}\,, \tag{3.100}$$

for each $a \neq b$. This means that the gluing map is either $g_{ab} = \mathbb{1}$ or $g_{ab} = R_\pi(\mathbf{n}_{ab})$, a rotation by π about the axis $\mathbf{n}_{ab}$.

In general, if the critical conditions have two inequivalent solutions, then the boundary data is necessarily shape-matched and $4d$ Euclidean (SM-2). When there is only one set of solutions to the critical equations up to equivalence, the boundary data can be shape-matched (SM-1) or normal-matched (NM-1). For a fixed non-degenerate but non shape-matching data, we can choose an arbitrary phase of the coherent states as there is at most one solution to the critical point equation such that the action at the critical points can be set to zero. Using this phase choice, the asymptotic behavior of the $15j$-symbol evaluated at the critical points is

$$15j(\lambda j, \mathbf{n})|_{\mathrm{NM}-1} \simeq \left(\frac{2\pi}{\lambda}\right)^6 \frac{2^4}{(4\pi)^8} \frac{1}{\sqrt{\det H}}\,. \tag{3.101}$$

For the case (SM-2), the action can be evaluated at the two distinct solutions:

$$S_{j,\mathbf{n}}|_\pm = \pm i \sum_{a<b} j_{ab}\theta_{ab} = \pm i S_R\,, \tag{3.102}$$

where S_R is the Regge action and θ_{ab} is the dihedral angle of the triangle shared by tetrahedra a and b. The full asymptotic behavior of the $15j$-symbol is then

$$15j(\lambda j, \mathbf{n})|_{\mathrm{SM}-2} \simeq \left(\frac{2\pi}{\lambda}\right)^6 \frac{2^4}{(4\pi)^8} \left(\frac{e^{i\lambda S_R}}{\sqrt{\det H_+}} + \frac{e^{-i\lambda S_R}}{\sqrt{\det H_-}} \right). \tag{3.103}$$

In the case (SM-1), we have the asymptotic behavior:

$$15j(\lambda j, \mathbf{n})|_{\mathrm{SM}-1} \simeq \pm \left(\frac{2\pi}{\lambda}\right)^6 \frac{2^4}{(4\pi)^8} \frac{1}{\sqrt{\det H}}\,. \tag{3.104}$$

Since these three possibilities exhaust the relevant contributions to the integral (3.91) in the asymptotic limit, our Bell state can be then expressed, for large spins, as a superposition of shape-matched and normal-matched configurations

$(|SM-2\rangle, |SM-1\rangle, |NM-1\rangle)$ as:

$$\lim_{\lambda\to\infty} |\Gamma_5, \mathrm{B}_\gamma, \lambda j_{ab}\rangle \simeq |SM-2\rangle + |SM-1\rangle + |NM-1\rangle\,. \tag{3.105}$$

In order to check whether the Bell state satisfies shape-matching conditions for large spins, we need to quantify the relative contributions of shape-matched (Regge) and normal-matched (vector geometry) configurations to the $15j$-symbol in the asymptotic limit. We will now explicitly verify that the normal-matched contribution $|NM-1\rangle$ is indeed subdominant for a family of spin configurations that admits shape-matched configurations.

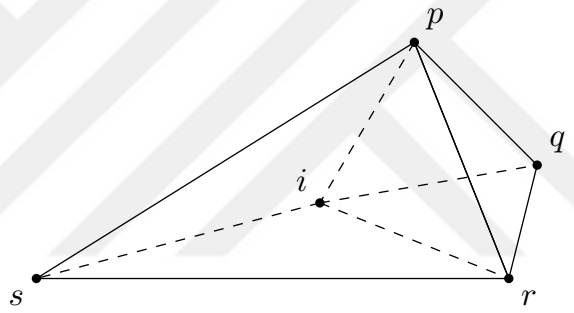

Figure 3.7. Pachner move 1-4. A single tetrahedron is divided into a gluing of four tetrahedra by the introduction of a new vertex i in its interior.

Let us start the analysis by describing the geometries we are interested in. First note that by choosing an arbitrary node a of the pentagram, the triangulation associated to Γ_5 can be seen as the gluing of two pieces related by a Pachner move 1-4: a single tetrahedron a and the polyhedron with four tetrahedra obtained from it by the inclusion of an internal point (see Fig. 3.7). Now, if the boundary data $\{j_{ab}, \mathbf{n}_{ab}\}$ is that of a shape-matched $3d$ Euclidean geometry, then these two pieces can be isometrically embedded in $\mathbb{R}^3$. Reversing the procedure, we obtain a method for constructing shape-matched configurations: we apply a Pachner move to a tetrahedron embedded in $\mathbb{R}^3$, and then just read off the boundary data from the explicit embedding in order to build an Euclidean $3d$ geometry for the boundary of the 4-simplex. This allows us, in particular, to determine the coordinates of the shape-matched configurations for a given parametrization of t solutions of the critical conditions, which is our main interest in the technique. The whole procedure can equally well be based on the Pachner move 2-3. In Appendix E,

we construct explicit shape-matched configurations (SM-1) for 1-4 and 2-3 vector geometries (Fig. 3.8) and compute the amplitude of the corresponding 15j-symbols by computing $|\det H|^{1/2}$.

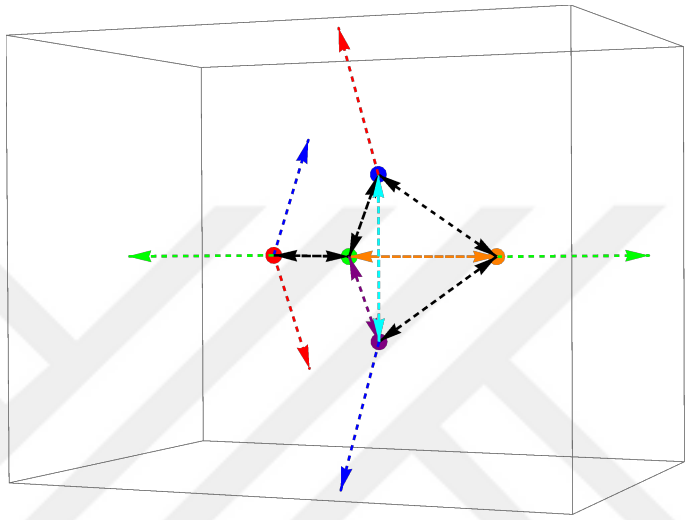

Figure 3.8. Graphical representation of a 1-4 vector geometry in a 3d box generated by using maximal tree method. Each colored point labels different node of the pentagram. The set of normals at each node satisfy the closure condition (3.96). Dashed black arrows stand for the anti-aligned normals which connect neighbor nodes: $\mathbf{n}_{a(a+1)} = -\mathbf{n}_{(a+1)a}$, $a = 1, \cdots, 4$. Dashed colored arrows stand for the remaining normals such that $\mathbf{n}_{ab} = -\mathbf{n}_{ba}$ with $\{(a,b) = 1, \cdots, 5 \mid a < b \wedge a \neq b-1\}$.

In [85], it is shown that algebraically vector geometries with fixed spins can be parametrized in terms of five independent variables ϕ. The five tetrahedra are represented in the Kapovich-Millson space as 4-sided polygons in $\mathbb{R}^3$ with edge vectors $j_{ab}\,\mathbf{m}_{ab}$, and the geometry is completely determined for a given set of spins if the face normals $\mathbf{m}_{ab}$ are written in terms of the five independent shape variables ϕ. Four of these shape variables are gauge-invariant $3d$ dihedral angles computed from the squared length of diagonals of the polygons:

$$(\mathbf{m}_{ca} + \mathbf{m}_{cd})(\mathbf{m}_{ca} + \mathbf{m}_{cd}) = 2\,(1 + \cos\phi_{ca,cd}) \tag{3.106}$$

$$(-\mathbf{m}_{ab} + \mathbf{m}_{ca})(-\mathbf{m}_{ab} + \mathbf{m}_{ca}) = 2\,(1 + \cos\phi_{ab,ca}) \tag{3.107}$$

$$(-\mathbf{m}_{db} + \mathbf{m}_{cd})(-\mathbf{m}_{db} + \mathbf{m}_{cd}) = 2\,(1 + \cos\phi_{db,cd}) \tag{3.108}$$

$$(\mathbf{m}_{ab} + \mathbf{m}_{db})(\mathbf{m}_{ab} + \mathbf{m}_{db}) = 2\,(1 + \cos\phi_{ab,db})\,, \tag{3.109}$$

and the remaining variable is a gauge-dependent quantity, an angle between faces at distinct tetrahedra,

$$(\mathbf{m}_{ab} + \mathbf{m}_{cd})\,(\mathbf{m}_{ab} + \mathbf{m}_{cd}) = 2\,(1 + \cos\phi_{cd,ab})\,, \tag{3.110}$$

computed from the squared length of the diagonal of the parallelogram $(\mathbf{m}_{cd}, \mathbf{m}_{dc}, \mathbf{m}_{ab}, \mathbf{m}_{ba})$.

We are interested in the 1-4 geometry obtained by the application of the Pachner move 1-4 to a regular tetrahedron. Accordingly, the exterior normals $(\mathbf{m}_{af}, \mathbf{m}_{bf}, \mathbf{m}_{cf}, \mathbf{m}_{df})$ are fixed to match the normals $(\mathbf{n}_{af}, \mathbf{n}_{bf}, \mathbf{n}_{cf}, \mathbf{n}_{df})$ of an explicit embedding of the regular tetrahedron in $\mathbb{R}^3$ (as described in Appendix E). In addition, the spin j_{in} of the interior faces is related to the spin j_{out} of the exterior faces by $j_{\rm in} = j_{\rm out}/\sqrt{6}$. This identity cannot hold for semi-integer spins, but can be arbitrarily well-approximated for large spins, which is the regime we are interested in. The two independent closure conditions for the interior tetrahedra read:

$$\mathbf{m}_{cb} = -\tfrac{1}{j_{\rm in}}(j_{\rm out}\,\mathbf{n}_{fb} + j_{\rm in}\,\mathbf{m}_{db} + j_{\rm in}\,\mathbf{m}_{ab})\,, \tag{3.111}$$

$$\mathbf{m}_{ad} = -\tfrac{1}{j_{\rm in}}(j_{\rm out}\,\mathbf{n}_{fd} + j_{\rm in}\,\mathbf{m}_{bd} + j_{\rm in}\,\mathbf{m}_{cd})\,. \tag{3.112}$$

Overall we obtained a 1-4 vector geometry with fixed spins from five shape variables where the non-gauge invariant quantity $\phi_{cd,ab}$ is the angle between normals of different tetrahedra and the other four variables are the dihedral angles $\phi_{ca,cd}, \phi_{ab,ca}, \phi_{db,ab}, \phi_{ab,db}$.[4]

We now proceed to compare the contributions of shape-matched and normal-matched configurations to the $15j$-symbols for the chosen spin configuration. The shape-matched configuration is $3d$ Euclidean, by construction, so it is enough to consider SM-1 and NM-1 contributions. In the limit of large spins, the $15j$-symbols have the asymptotic form given in Eqs. (3.101) and (3.104). Therefore, in the

[4]The 2-3 vector geometries are too constrained for our purposes. We could start with two regular tetrahedra glued back to back and let the interior geometry of the piece formed by three tetrahedra free. A simple counting argument shows, however, that this interior geometry is rigidly fixed. In general, a vector geometry is described by 40 parameters in 20 normalized vectors. We have 10 equations from the solutions to the critical equations. Two tetrahedra are constructed to be regular such that 7 normals are fixed in the vectorial geometry. There are also 3 closure conditions for the three free tetrahedra. The total number of constraints is $10 \times 2 + 7 \times 2 + 3 \times 2 = 40$ which is exactly the total number of parameters in a vector geometry. Therefore, the vectorial equations are too constrained to allow for configurations other than the shape-matched one.

asymptotic limit the ratio between the $15j$-symbols for normal-matched and shape-matched configurations is given by $\sqrt{|\det H_0|/|\det H|}$, where H_0 is the Hessian of the shape-matched configuration (whose coordinates are derived in Appendix E).

Using the parametrization introduced above, we first sample points of a subset of 1-4 vector geometries including the shape-matched solution. For this purpose, we first express $(\mathbf{m}_{cd}, \mathbf{m}_{ab})$ in terms of four parameters as

$$\mathbf{m}_{cd}^T = (\sin\theta_{cd}\cos\phi_{cd}, \sin\theta_{cd}\sin\phi_{cd}, \cos\theta_{cd})\,, \tag{3.113}$$

$$\mathbf{m}_{ab}^T = (\sin\theta_{ab}\cos\phi_{ab}, \sin\theta_{ab}\sin\phi_{ab}, \cos\theta_{ab})\,. \tag{3.114}$$

The other two interior normals in (3.106) are fixed to the shape-matched solutions $\mathbf{m}_{ca} = \mathbf{n}_{ca}$, $\mathbf{m}_{ca} = \mathbf{n}_{db}$, and $\mathbf{m}_{cb}, \mathbf{m}_{ad}$ are determined by the following closure conditions:

$$\mathbf{m}_{cb} = -\tfrac{1}{j_{\rm in}}(j_{\rm out}\mathbf{n}_{fb} + j_{\rm in}\mathbf{n}_{db} + j_{\rm in}\mathbf{m}_{ab})\,, \tag{3.115}$$

$$\mathbf{m}_{ad} = -\tfrac{1}{j_{\rm in}}(j_{\rm out}\mathbf{n}_{fd} + j_{\rm in}\mathbf{n}_{bd} + j_{\rm in}\mathbf{m}_{cd})\,. \tag{3.116}$$

Then we look for solutions within the interval $[0, 2\pi]$ of $\theta \equiv \theta_{cd} = \theta_{ab}$. This choice of parametrization leads to equalities among the gauge-invariant quantities:

$$\cos\phi_{ab,ca} - \cos\phi_{ab,db} = \cos\phi_{ca,cd} - \cos\phi_{db,cd} = \sqrt{2}\cos\theta\,, \tag{3.117}$$

where all these gauge-invariant quantities are exactly equal to $1/2$ at the shape-matched configuration. The corresponding solutions[5] for ϕ_{ab}, ϕ_{cd} are obtained by the normalization conditions on $\mathbf{m}_{cb}, \mathbf{m}_{ad}$.

Now we can plot the relative magnitude of $|\det H|^{-1/2}$ with respect to the shape-matched configuration for a sample of exact vector geometries. The results are displayed in Fig. 3.9.

We find that the typical scales for the contributions to $|\det H|^{-1/2}$ from normal-matched configurations are suppressed compared to the shape-matched configura-

[5]For each possible solution in this setting the degenerate outcomes for each tetrahedra should be eliminated from the total set of solutions which do not satisfy the folllowing:

$$\det G_a \neq 0\,, \qquad G_a = \sum_{b\neq a} \mathbf{b}_{ab}\,\mathbf{b}_{ab}^T\,. \tag{3.118}$$

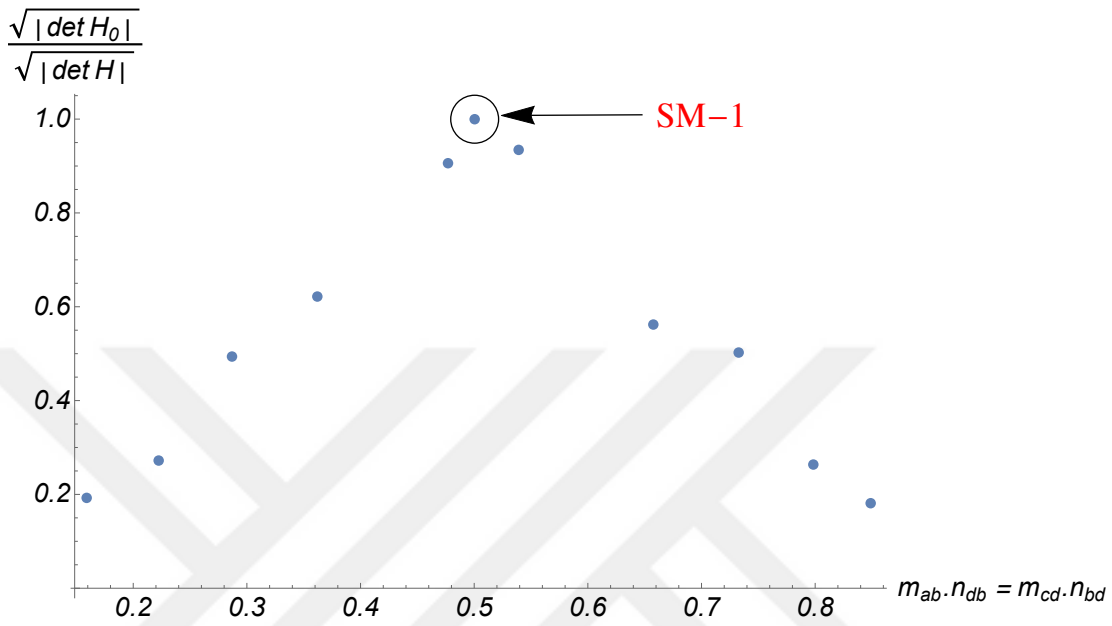

Figure 3.9. Sampling of exact relative magnitudes $(|\det H_0|^{1/2}_{1-4})/(|\det H|^{1/2}_{1-4})$ in terms of the cosine of the gauge-invariant 3d dihedral angles $\phi_{ab,db}$ and$\phi_{cd,bd}$. The relative magnitude reaches its maximum at the shape-matched configuration (SM-1) with $\mathbf{n}_{ab} \cdot \mathbf{n}_{db} = \mathbf{n}_{cd} \cdot \mathbf{n}_{bd} = 1/2$.

tion, showing that the $15j$-symbol is peaked at the shape-matched configuration. For the maximally suppressed configuration, the ratio is approximately 0.2, and the typical ratio is of the order of tenths. We show in Fig. 3.9 the suppression due to variations in a single shape variable. Since the geometry is parametrized by five shape variables, the suppression factor for the different variables will combine, and we can estimate a typical suppression of around two orders of magnitude, and a maximal suppression of about four orders of magnitude in the five-dimensional space of vector geometries.

The results of our analysis show that, in the coherent state representation, the Bell state $|\Gamma_5, \mathrm{B}_\gamma, j_{ab}\rangle$ on the pentagram is well-peaked on the shape-matched configuration in the asymptotic limit of large spins for the 1-4 geometry. The state is then well approximated in the regime of large spins by a wavefunction

concentrated at the shape-matched configuration:

$$\lim_{\lambda\to\infty} |\Gamma_5, \mathrm{B}_\gamma, \lambda j_{ab}\rangle \sim \left(\frac{2\pi}{\lambda}\right)^6 \frac{2^4}{(4\pi)^8} \int_{P_j^{(0)}} d\mu_\psi(\mathbf{n}_{ab}) \sum_{\sigma=-1,0,1} \frac{e^{i\sigma S_R}}{\sqrt{\det \mathrm{H}_\sigma}}\, \delta(\mathcal{C}_{\mathrm{SM}})\, |\psi(j_{ab}, \mathbf{n}_{ab})\rangle\,.$$

For the considered geometries, the shape-matched configuration lies within the family SM-1, and we can write accordingly $\lim_{\lambda\to\infty} |\Gamma_5, \mathrm{B}_\gamma, \lambda j_{ab}\rangle \simeq |SM-1\rangle$. In geometries with multiple shape-matched configurations, we expect the wavefunction of the Bell state to display peaks at each of the shape-matched configurations, leading to a zeroth-order approximation of the form:

$$\lim_{\lambda\to\infty} |\Gamma_5, \mathrm{B}_\gamma, \lambda j_{ab}\rangle \simeq |SM-2\rangle + |SM-1\rangle\,, \tag{3.119}$$

i.e., the state approaches a superposition of coherent states peaked at the shape-matched configurations compatible with the given choice of spins. In this sense, the Bell state corresponds to a wavefunction over the space of Regge geometries at fixed spins. In general, there are two distinct kinds of matched configurations [83, 84]: the term $|SM-2\rangle$ includes boundary data defining a $4d$ Euclidean metric in the associated 4-simplex, and $|SM-1\rangle$ includes the $3d$ Euclidean configurations with signature $0++$. Since the contribution of $15j$-symbols associated with normal-matched boundary data is suppressed in comparison to the shape-matched configurations, average values in the limit of large spins can be computed under the approximation (3.119), and we find that the weaker version of quantum shape-matching conditions for average values (3.57) discussed in Section 3.4.3 is satisfied:

$$\lim_{j_{ab}\to\infty} \frac{\langle \Gamma_5, \mathrm{B}_\gamma, j_{ab}|\mathcal{C}_{SM}(O_{ab})|\Gamma_5, \mathrm{B}_\gamma, j_{ab}\rangle}{\langle \psi, j_{ab}|\hat{O}_{s(ab)}|\Gamma_5, \mathrm{B}_\gamma, j_{ab}\rangle} \approx 0\,. \tag{3.120}$$

Chapter 4
Minisuperspace models of quantum spin systems

We introduced basic preliminaries 2.4 for a possible analysis of correlated complex quantum spin systems. Specifically, complexity can be understood for instance as introducing spin chains in higher dimensional cells, having a spin system consisting of at least three valent-node at each site or multiple types of spin operators at each site. This list can be well-extended to increase the complexity of the quantum spin systems.

In this chapter, we will analyze special classes of quantum spin chain models where in particular the dynamical evolution of spin correlations in the revelant system are computed using the canonical effective methods. In general, effective formalisms of fundamental theories are playing the role of understanding (or transmitting) intermediate steps to connect the extractable predictions from the fundamental theories such as canonical theory of quantum gravity to the phenomenological data from various experiments especially at high energy scales or observations from distant pasts of the universe such as cosmic microwave background. In particle physics approach (applied mostly in standard quantum field theory), a rigorous definition of an effective description of a more fundamental theory is that the effective action is obtained after some "heavy" degrees of freedom are integrated out above some specific energy scale of the relevant theory. Unlike in field theories on a Minkowski or fixed background, there are technical subtleties to define a well-defined representations of the Hilbert space for a quantum theory of general relativity where there is no fixed background geometry. For instance, one cannot no longer define a unique Fock vacuum state. In what follows we will

use an effective formalism, which can be also applied to background-independent theories, for a semi-classical analysis of a (minisuperspace) quantum spin system without explicitly referring a well-defined states and Hilbert space.

4.1 Introduction

Minisuperspace models of quantum-field theories, in particular quantum gravity, are usually constructed by quantizing a set of configurations obtained from the full classical theory by imposing spatial homogeneity. While homogeneous configurations are exact (though special) solutions of the classical theory, for various reasons they are not expected to be exact solutions of the full quantum-field theory. For instance, uncertainty relations would prevent both the amplitude and momentum of an inhomogeneous mode from having zero quantum fluctuations. In an interacting theory, fluctuations couple to expectation values, and non-zero fluctuations usually imply that the mode expectation values cannot remain zero in time. An exactly homogeneous (non-vacuum) solution therefore cannot be realized in a quantum-field theory. The question of what kind of an approximation to the full quantum theory a minisuperspace model may provide has remained open, but recently canonical effective methods have shed some light on this question for scalar quantum-field theories on a flat background space-time [107].

The main application of minisuperspace models is in the context of quantum gravity, where space-time is no longer a background but quantized as well. Several approaches to quantum gravity suggest that space or space-time may no longer be continuous in this setting. (See for instance [108, 109].) Discrete space may present a further obstacle to finding exact or approximate homogeneous solutions of the theory: even if we disregard quantum fluctuations or their back-reaction on expectation values, local moves in a discrete structure do not respect homogeneity. At most, a coarse-grained model which collects the accumulated action of many local moves in a single evolution step could lead to approximate homogeneous solutions. However, coarse-graining remains incompletely understood in discrete approaches to background-independent gravity. (See for instance [110, 111] for recent realizations.)

In order to probe these questions, we introduce here a discrete quantum system which exhibits several interesting aspects regarding minisuperspace models. Starting

from the discrete quantum theory rather than a classical continuum theory allows us to analyze how different features of the interacting dynamics can be captured in simpler systems. As is well known, a discrete theory can give rise to different continuum limits. Each of them would then lead to a different minisuperspace model. The same result can be seen directly by minisuperspace constructions performed for the discrete quantum theory.

We will also analyze the discrete quantum theory in qualitative terms. In particular, we are interested in the question of how long-range correlations can build up in a fundamental theory and under which conditions they are stable. If such correlations can be achieved, it is at least possible that nearly homogeneous configurations can be the result of evolution in the theory, rather than just of specific initial choices as implicitly made in minisuperspace constructions. Of course, homogeneous configurations require long-range correlations of a very specific kind which is more difficult to analyze for a generic interacting theory. But the building-up of some kind of long-range correlations is a pre-requisite for near homogeneity, and it can be studied in our model in qualitative terms. The stability question will lead us back to the ground-state configurations discussed for the various minisuperspace models introduced here. An interesting interplay between the full discrete theory and the models is important for the physical interpretation of minisuperspace results.

4.2 Canonical effective methods

Canonical effective methods [112–114] are primarily based on the functionals at expectation value level without knowing the wave function of the related quantum system. Instead of having a state space, we have expectation values of fundamental variables and their moments on an infinite-dimensional space. For a configuration of space consisting of N canonical degrees of freedom, a point in this infinite-dimensional space is completely determined by $(\langle\hat{q}_i\rangle, \langle\hat{p}_i\rangle)$ for $i = 1, \cdots, N$ and the moments

$$\Delta(q_i^a p_j^b) := \langle(\hat{q}_i - \langle\hat{q}_i\rangle)^a(\hat{p}_j - \langle\hat{p}_j\rangle)^b\rangle_{\rm symm}\,, \tag{4.1}$$

where all products in the expectation value are totally symmetric. In this chapter we prefer the hat notation $\hat{q}$ for quantum operators in order to distinguish from the

classical variables $q \equiv \langle \hat{q} \rangle$. The space of the classical variables and the moments is equipped with a Poisson structure defined by the commutator of the operator algebra:

$$\{\langle \hat{A} \rangle, \langle \hat{B} \rangle\} := \frac{1}{i\hbar} \langle [\hat{A}, \hat{B}] \rangle \,, \tag{4.2}$$

In particular, this relation satisfies the identical features realized for a commutator (linearity, anti-symmetricity and Jacobi identity). In fact, one can obtain a well-defined Poisson bracket on the space of all expectation values of fundamental operators and moments by extending (4.2) to the products of expectation values (Leibniz rule). The moments provide infinitely many quantum variables independent of expectation values but their values are limited by the Heisenberg uncertainty principle (2.12). For the case of $a + b = 2$ and a single degree of freedom (q, p), moments should satisfy the conventional uncertainty relation:

$$\Delta(q^2)\Delta(p^2) - \Delta(qp)^2 \geq \frac{\hbar^2}{4} \,. \tag{4.3}$$

Uncertainty relations for higher-order moments appear more complicated but all of them are derived from the Schwarz inequality (2.4). The correspondence between the points in the moments space and the rays in the state space can only occur if all the uncertainty relations of the moments at all orders are obeyed. In particular the moments, that correspond to the space of semiclassical states, obey the following hierarchy: order of $\Delta(q_i^a p_j^b) \sim \mathcal{O}(\hbar^{(a+b)/2})$ so that moments of a given order provide quantum corrections of that order in $\hbar$. This hierarchy relation enables then to truncate the infinite-dimensional space of moments and expectation values to finite-dimensional one. In this respect quantum corrections are then included in the quantum back-reaction of fluctuations and higher order correlations of a state on the evolution of expectation values. Therefore, we need to establish a definition for a time evolution of the effective system.

The dynamics for an effective description of a quantum system can be defined by introducing a quantum (effective) Hamiltonian from the Hamiltonian operator on the space of states:

$$H_Q\big(q_i, p_j, \Delta(q_i^a p_j^b)\big) := \langle \hat{H} \rangle \,. \tag{4.4}$$

The equations of motion are then generated by this quantum Hamiltonian referring

to Heisenberg equations of motion (2.34):

$$\frac{d}{dt}\langle\hat{A}\rangle := \{\langle\hat{A}\rangle, H_Q\} = \frac{1}{i\hbar}\langle[\hat{A},\hat{H}]\rangle\,. \tag{4.5}$$

For an explicit computation of the quantum Hamiltonian we will consider a system with a single degree of freedom. The quantum Hamiltonian can be expressed as $\langle H(\hat{q},\hat{p})\rangle = \langle H\big(q+(\hat{q}-q), p+(\hat{p}-p)\big)$ and this can formally Taylor expanded around the $\hat{q}-q$ and $\hat{p}-p$:

$$H_Q = \langle H(\hat{q},\hat{p})\rangle = \sum_{b=0}^{\infty}\sum_{a=0}^{\infty}\frac{1}{(a+b)!}\binom{a+b}{a}\frac{\partial^{a+b}H(q,p)}{\partial q^a\partial p^b}\Delta(q^a p^b)\,. \tag{4.6}$$

Specifically, a quantum Hamiltonian, that corresponds to a Hamiltonian operator with a canonical kinetic term $H(\hat{q},\hat{p}) = \frac{1}{2}\hat{p}^2 + V(\hat{q})$, is then

$$H_Q = \frac{1}{2}\big(p^2+\Delta(p^2)\big) + V(q) + \sum_{n=2}^{\infty}\frac{1}{n!}V^{(n)}(q)\Delta(q^n)\,. \tag{4.7}$$

For a first order correction in $\hbar$ to the effective potential, the Taylor expansion can be up to the second-order moments.

An overall report of using canonical effective methods is that firstly computing the moments, which are n-point correlation functions at the same time, can be performed on more general space of states. Secondly, this whole analysis does not fix the background geometry of the theory so that the canonical approach can be applied to the background-independent theories of quantum gravity. Therefore, we can use the canonical effective methods especially in cosmological settings of the primordial universe on a FLRW background. In what follows we will apply this effective framework for particular model of various discrete quantum spin systems.

4.3 The quantum spin chain model

In the absence of a consistent canonical quantum theory of gravity, it is not clear what Hamiltonian one should use to model its discrete dynamics. (See for instance [115–119] for some issues involved in such a construction.) In an attempt to construct tractable models, we focus here on some of the ingredients that

seem to be rather general. We do not intend to capture the precise dynamics of quantum gravity but rather plan to explore some properties of possible candidates for fundamental degrees of freedom.

Several proposals of quantum gravity, going back to [120], are based on mathematical versions of angular momentum or spin as a fundamental degrees of freedom. Not only spin eigenvalues but also their proposed arrangement on a graph in space, or a spin network, are discrete. Certain invariant combinations of spin quantum numbers can then be defined as discrete analogs of the common continuum expressions of geometrical measures. Moreover, spin-spin interactions can be used to introduce possible Hamiltonians.

Handling the arrangement of spins on an arbitrary graph in three spatial dimensions can be a difficult combinatorial problem. The first simplification we will use is a dimensional reduction: We will consider only one spatial dimension, which could be thought of as the radial direction measuring the distance from a non-rotating and spherical star or black hole, or more generally a so-called midisuperspace model of general relativity. Aligned in this direction are then several different types of spins, which roughly correspond to independent components of the spatial metric. We arrive at a 1-dimensional graph model as illustrated in Fig. 4.1. Here, spins on links in the horizontal direction, called "horizontal spins" in what follows, would then have a geometrical interpretation distinct from that of "vertical spins" on upward and open-ended links. However, such a geometrical interpretation will not be relevant for our analysis of the interacting dynamics.

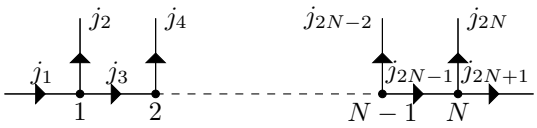

Figure 4.1. The inhomogeneous one-dimensional graph Γ with N nodes and $2N+1$ links. The Hamiltonian (4.8) is invariant under a mapping of spins that corresponds to a reflection of the graph in a horizontal direction. If the orientation of a link, indicated by an arrow, changes under this reflection, the corresponding mapped spin has a negative sign.

Specific versions of such quantum midisuperspace models with explicit Hamiltonians have been constructed for spherically symmetric models [121, 122] and certain types of gravitational waves [123, 124]. In tractable versions, one makes

use of a further reduction of the group SU(2) to the Abelian U(1). In order to have interesting spin-spin interactions, we will not make use of this reduction here. However, we will simplify the combinatorics by working with a single spin on each link, instead of distinguishing between left- and right-invariant vector fields on SU(2) as would be done in a full spin network.

The dynamics on a spin system, such as the one illustrated in Fig. 4.1, is in general spin-changing as well as graph-changing if it comes from a generic proposal of canonical quantum gravity. That is, the Hamiltonian can contain terms that change the irreducible representation of SU(2) on each link of the graph, as well as terms that can create new nodes and corresponding links of the graph. Such a dynamics is hard to control, and therefore we assume a simplified version in which no spin-changing or graph-changing terms occur. Therefore, for given irreducible representations and a fixed graph, only spin-spin interactions are present in the Hamiltonian. We consider only local (next-neighbor) pairwise interactions and require a certain reflection symmetry as indicated in Fig. 4.1 and spelled out in the explicit construction that follows.

As the discrete theory, we introduce a spin system which for a given integer N has $2N+1$ interacting spins J_i, $i = 1, \ldots, 2N+1$. We define the dynamics in canonical form, generated by the Hamiltonian

$$\hat{\mathrm{H}}_\Gamma = \alpha \sum_{i=1}^{N} \big(- \hat{\mathbf{J}}_{2i-1} \cdot \hat{\mathbf{J}}_{2i} + \hat{\mathbf{J}}_{2i-1} \cdot \hat{\mathbf{J}}_{2i+1} + \hat{\mathbf{J}}_{2i} \cdot \hat{\mathbf{J}}_{2i+1} \big) \tag{4.8}$$

with a coupling constant α. This operator is invariant under global rotations of the spins: the sum of all horizontal spins,

$$\mathbf{G} := \sum_{i=1}^{N+1} \hat{\mathbf{J}}_{2i-1} \,, \tag{4.9}$$

commutes with the Hamiltonian. This conserved quantity can be used in some cases to simplify equations of motion, as in Sec. 4.6.2. We have chosen the signs of individual coefficients of the spin products so as to make the Hamiltonian reflection symmetric under the operation $\hat{\mathbf{J}}_{2i-1} \mapsto -\hat{\mathbf{J}}_{2N-2i+3}$ while $\hat{\mathbf{J}}_{2i} \mapsto \hat{\mathbf{J}}_{2N-2i+2}$ (or $i \mapsto N-i+1$). These properties can be illustrated by the graph model presented in Fig. 4.1. The arrows indicate the sign in the reflection symmetry.

In 1-dimensional models of gravity, it is often convenient to impose polarization conditions which eliminate one of the metric components as an independent field. In our discrete model, such a condition would then relate the different types of spins (horizontal and vertical) to each other. Our polarization condition used here is a constraint that corresponds to the classical conditions

$$\mathbf{C}_i = -\mathbf{J}_{2i-1} + \mathbf{J}_{2i} + \mathbf{J}_{2i+1} = 0 \quad , \quad i = 1, \ldots, N \,. \tag{4.10}$$

They can be used to eliminate the vertical spins. Also this system of constraints has coefficients chosen so as to make it reflection symmetric: $\mathbf{C}_i \mapsto \mathbf{C}_{N-i+1}$.

We have a system of constraints in a non-symplectic Poisson manifold with coordinates given by spin components J_i^a, such that standard classifications of first or second class constraints are not available [125]. It is, however, straightforward to see that the constraints do not all (Poisson) commute with one another, nor with the Hamiltonian. The non-zero Poisson brackets are $\{C_i^a, C_i^b\} = \epsilon^{abc}(J_{2i-1}^c + J_{2i}^c + J_{2i+1}^c) \approx 2\epsilon^{abc} J_{2i-1}^c$ (the weak equality $\approx$ indicating that the constraints have been used) and $\{C_i^a, C_{i+1}^b\} = -\epsilon^{abc} J_{2i+1}^c$ for $a \neq b$, while all other components of the constraints commute. We are only interested in imposing the constraints as a reduction of vertical degrees of freedom. The constraint surface remains well-defined if the reduction constraints are imposed strongly. In particular, we can solve the constraints so as to eliminate all vertical spins $\mathbf{J}_{2i}$ (or $\hat{\mathbf{J}}_{2i}$), and use standard Poisson brackets (or commutators) for the remaining $\mathbf{J}_{2i-1}$ (or $\hat{\mathbf{J}}_{2i-1}$). All our derivations exclusively use Poisson brackets or commutators, and therefore the model is sufficient as a non-symplectic Poisson system.

We use the system of partially non-commuting constraints as an example of reduction, better known from the context of symmetry reduction. In fact, if we combine the constraints $\mathbf{C}_i$ with additional constraints that set all the vertical spins equal to zero, the reduction imposes homogeneity: it requires that the remaining, horizontal spins are all equal, $\mathbf{J}_{2i-1} = \mathbf{J}_{2i+1}$ for all $i = 1, \ldots, N$. If we impose only $\mathbf{C}_i = 0$ without restricting vertical spins, we can solve for the vertical spins and obtain a single 1-dimensional spin chain closely related to the next-neighbor Heisenberg spin chain. The fact that the quantized constraints do not commute with $\hat{H}$ allows us to probe for potential effects of local discrete moves not respecting reduction constraints.

An important question in classical symmetry reduction is whether variation commutes with reduction. It is not always guaranteed that equations of motion of the reduced system (extrema of the reduced action) agree with the field equations of the full theory restricted to fields that obey the reduction condition. Certain general conditions are known that guarantee this commutation property (symmetric criticality), formulated mainly as conditions on properties of the corresponding symmetry group [126,127]. In our case, we have a reduction constraint which shares with minisuperspace reductions the feature that it is (partially) non-commuting, but it does not directly correspond to a symmetry group. Moreover, we are working exclusively with Hamiltonians rather than action principles, and we do not have a symplectic phase space.

However, instead of using general conditions on symmetry groups, it is not difficult to test the commutation property directly. We have the reduced Hamiltonian

$$\hat{\mathrm{H}}_{\mathrm{red}} = \alpha \sum_{i=1}^{N} \left(-\hat{J}^2_{2i-1} + 3\,\hat{\mathbf{J}}_{2i-1}\cdot\hat{\mathbf{J}}_{2i+1} - \hat{J}^2_{2i+1}\right) \tag{4.11}$$

$$= \alpha \left(-\hat{J}^2_1 - 2\sum_{i=2}^{N} \hat{J}^2_{2i-1} - \hat{J}^2_{2N+1} + 3\sum_{i=1}^{N} \hat{\mathbf{J}}_{2i-1}\cdot\hat{\mathbf{J}}_{2i+1}\right) , \tag{4.12}$$

which generates Heisenberg equations of motion

$$\frac{\mathrm{d}\hat{J}^a_{2i+1}}{\mathrm{d}t} = 3\,\alpha\,\epsilon^{abc}\left(\hat{J}^b_{2i-1}\hat{J}^c_{2i+1} + \hat{J}^c_{2i+1}\hat{J}^b_{2i+3}\right) . \tag{4.13}$$

The full equations for horizontal spins are

$$\frac{\mathrm{d}\hat{J}^a_{2i+1}}{\mathrm{d}t} = \alpha\,\epsilon^{abc}\left(-\hat{J}^c_{2i+1}\hat{J}^b_{2i+2} + \hat{J}^b_{2i-1}\hat{J}^c_{2i+1} + \hat{J}^c_{2i+1}\hat{J}^b_{2i+3} + \hat{J}^b_{2i}\hat{J}^c_{2i+1}\right) , \tag{4.14}$$

coupled to vertical spins $\hat{\mathbf{J}}_{2i}$. If we use the constraint in order to eliminate the vertical spins in the equation of motion, we obtain

$$\frac{\mathrm{d}\hat{J}^a_{2i+1}}{\mathrm{d}t} = 2\,\alpha\,\epsilon^{abc}\left(\hat{J}^b_{2i-1}\hat{J}^c_{2i+1} + \hat{J}^c_{2i+1}\hat{J}^b_{2i+3}\right) \tag{4.15}$$

which are not identical with the equations generated by the reduced Hamiltonian. However, the difference is merely a constant numerical factor of the time derivatives.

We have interpreted the constraint imposed here as a polarization condition. The preceding calculations have shown that there is a small difference between imposing the polarization condition before or after deriving equations of motion. The coupling of modes is therefore slightly different if it is described by a reduced Hamiltonian, compared with the full Hamiltonian on whose equations of motion the same condition would be imposed. One can account for the difference by a simple rescaling (or a classical renormalization) of the coupling constant, using $\frac{2}{3}\alpha$ instead of α in the reduced Hamiltonian.

In what follows, we will, for simplicity, work mainly with reduced Hamiltonians. (The conserved quantity (4.9) now commutes strongly with the Hamiltonian.) We will compare different versions of homogeneous minisuperspace models and effective continuum theories.

4.4 Minisuperspace models

All spins in the model are coupled. It might therefore be possible that long-distance correlations build up over time, which could be of classical or quantum nature. A minisuperspace configuration would be one example of a classically correlated system. There is a difference between such a minisuperspace configuration and a homogeneous configuration as it might be realized as a ground state of the unreduced system because all spins would have to be identical as degrees of freedom, not just equal as values assigned to different links of the graph. In this subsection, we explore several questions related to this conceptual difference. We will also see that there is some freedom in defining different minisuperspace models, and that selecting a model that gives predictions close to the discrete theory requires knowledge of solutions of the discrete theory.

4.4.1 A minimal minisuperspace model

The smallest number of minisuperspace degrees of freedom can be realized by identifying all horizontal spins on the links. Setting $\hat{\mathbf{J}}_{2i-1} = \hat{\mathbf{J}}_{2i+1} =: \hat{\mathbf{J}}$ in the reduced Hamiltonian (4.11) gives us the minisuperspace Hamiltonian

$$\hat{H}^{(1)}_{\text{mini}} = \alpha N \hat{J}^2 \,. \tag{4.16}$$

We obtain the same result if we start with the unreduced Hamiltonian and set vertical spins equal to zero. Clearly, this Hamiltonian commutes with all minisuperspace degrees of freedom, given by the three components of a single $\hat{\mathbf{J}}$. The resulting trivial dynamics is very different from the coupled equations of the inhomogeneous theory.

4.4.2 A condensate model

Alternatively, homogeneity can be imposed at the level of states by working with condensate states of the full theory, given by

$$\Psi = \bigotimes_{i=1}^{N+1} \chi \tag{4.17}$$

where χ is a state in the Hilbert space of a single horizontal spin. The same individual state is therefore assumed for all links, but unlike in the minisuperspace model, the spins remain as independent degrees of freedom. This procedure is well known from the description of Bose–Einstein condensates, where it results in the non-linear Gross-Pitaevsky equation for the analog of χ. In quantum gravity, the procedure has been used in particular in the context of group-field theory [128–135], and it can also be seen in certain approximations that go beyond minisuperspace models by including perturbative inhomogeneity at an effective quantum level [136].

A non-linear equation for the single-spin wave function χ can be derived by first computing an effective Hamiltonian $\langle\Psi|\hat{H}|\Psi\rangle$ for (4.12) in a state of the form (4.17):

$$\langle\Psi|\hat{H}|\Psi\rangle = -2\alpha N\langle\chi|\hat{J}^2|\chi\rangle + 3\alpha N\langle\chi|\hat{\mathbf{J}}|\chi\rangle^2 \tag{4.18}$$

where we have identified $\langle\chi|\hat{\mathbf{J}}_i|\chi\rangle = \langle\chi|\hat{\mathbf{J}}_j|\chi\rangle$ for $i \neq j$. Effective equations of motion or variational ground states can be related to those of a state-dependent single-spin Hamiltonian

$$\hat{H}_{\text{condensate}} = -2\alpha N\hat{J}^2 + 3\alpha N\langle\hat{\mathbf{J}}\rangle\cdot\hat{\mathbf{J}}\,. \tag{4.19}$$

It generates the non-linear equation

$$i\hbar\frac{\mathrm{d}\chi}{\mathrm{d}t} = \hat{H}\chi = -2\alpha N\hat{J}^2\chi + 3\alpha N\langle\chi|\hat{\mathbf{J}}|\chi\rangle\cdot\hat{\mathbf{J}}\chi\,. \tag{4.20}$$

Unlike in the minimal minisuperspace model, the condensate dynamics is non-trivial.

4.4.3 Two interacting minisuperspace models

The inhomogeneous dynamics can be probed more faithfully by using more than one triple of degrees of freedom, but still of small number for a minisuperspace model. Starting with the unreduced Hamiltonian, we split the spins into different subsets by introducing the following notation:

$$\hat{\mathbf{J}}_{\mathrm{h1},j} := \hat{\mathbf{J}}_{4j-3} \tag{4.21}$$

$$\hat{\mathbf{J}}_{\mathrm{v1},j} := \hat{\mathbf{J}}_{4j-2} \tag{4.22}$$

$$\hat{\mathbf{J}}_{\mathrm{h2},j} := \hat{\mathbf{J}}_{4j-1} \tag{4.23}$$

$$\hat{\mathbf{J}}_{\mathrm{v2},j} := \hat{\mathbf{J}}_{4j} \,. \tag{4.24}$$

No analogous version of such a reduction has been used in quantum cosmology yet, but we will see that, in the present model, it can improve the simpler reduction given by $\hat{H}^{(1)}_{\mathrm{mini}}$.

Assuming even N, we can pair up neighboring nodes ($i = 2j-1$ and $i = 2j$ in (4.8)), and obtain the Hamiltonian

$$\hat{H} = \alpha \sum_{j=1}^{N/2} \Big(-\hat{\mathbf{J}}_{4j-3} \cdot \hat{\mathbf{J}}_{4j-2} + \hat{\mathbf{J}}_{4j-3} \cdot \hat{\mathbf{J}}_{4j-1} + \hat{\mathbf{J}}_{4j-2} \cdot \hat{\mathbf{J}}_{4j-1} \tag{4.25}$$

$$- \hat{\mathbf{J}}_{4j-1} \cdot \hat{\mathbf{J}}_{4j} + \hat{\mathbf{J}}_{4j-1} \cdot \hat{\mathbf{J}}_{4j+1} + \hat{\mathbf{J}}_{4j} \cdot \hat{\mathbf{J}}_{4j+1} \Big) \tag{4.26}$$

$$= \alpha \sum_{j=1}^{N/2} \Big(-\hat{\mathbf{J}}_{\mathrm{h1},j} \cdot \hat{\mathbf{J}}_{\mathrm{v1},j} + \hat{\mathbf{J}}_{\mathrm{h1},j} \cdot \hat{\mathbf{J}}_{\mathrm{h2},j} + \hat{\mathbf{J}}_{\mathrm{v1},j} \cdot \hat{\mathbf{J}}_{\mathrm{h2},j} \tag{4.27}$$

$$- \hat{\mathbf{J}}_{\mathrm{h2},j} \cdot \hat{\mathbf{J}}_{\mathrm{v2},j} + \hat{\mathbf{J}}_{\mathrm{h2},j} \cdot \hat{\mathbf{J}}_{\mathrm{h1},j+1} + \hat{\mathbf{J}}_{\mathrm{v2},j} \cdot \hat{\mathbf{J}}_{\mathrm{h1},j+1} \Big) \,. \tag{4.28}$$

(We refer to $\hat{\mathbf{J}}_{2N+1}$ as a single spin $\hat{\mathbf{J}}_{\mathrm{h1},N/2+1}$ without vertical or a second horizontal spins for $j = N/2+1$.) The new configurations and their interactions can be illustrated as in Fig. 4.2.

We have two constraints for each value of j:

$$\hat{C}_{1,j} = -\hat{\mathbf{J}}_{4j-3} + \hat{\mathbf{J}}_{4j-2} + \hat{\mathbf{J}}_{4j-1} = -\hat{\mathbf{J}}_{\mathrm{h1},j} + \hat{\mathbf{J}}_{\mathrm{v1},j} + \hat{\mathbf{J}}_{\mathrm{h2},j} \tag{4.29}$$

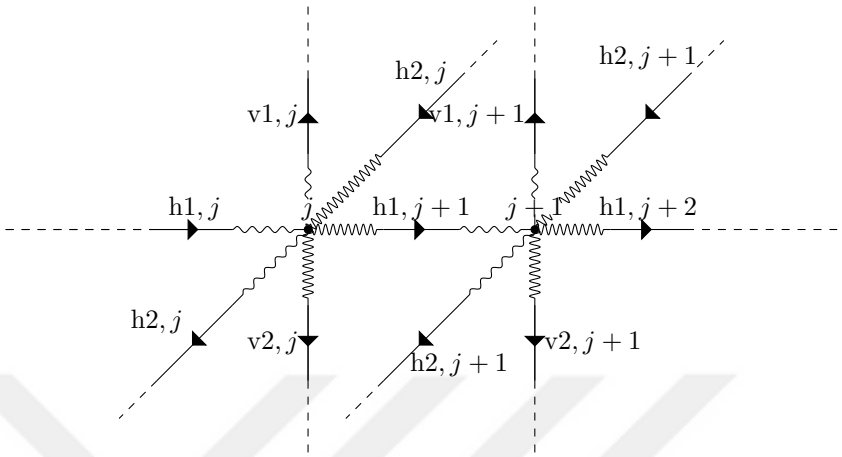

Figure 4.2. A re-arranged representation of the discrete spin model. As before, lines with a given orientation stand for the spin operators. There are now five different spins meeting at a given node j, among which only the two triplets $(\hat{\mathbf{J}}_{\mathrm{h1},j}, \hat{\mathbf{J}}_{\mathrm{v1},j}, \hat{\mathbf{J}}_{\mathrm{h2},j})$ and $(\hat{\mathbf{J}}_{\mathrm{h2},j}, \hat{\mathbf{J}}_{\mathrm{v2},j}, \hat{\mathbf{J}}_{\mathrm{h1},j+1})$ are interacting as indicated by wavy lines with different wave lengths. The spin $\hat{\mathbf{J}}_{\mathrm{h2},j}$ appears in both triplets, and is therefore doubled in the diagrammatic visualization. Also the constraints relate only the spins that occur together in a triplet.

$$\hat{C}_{2,j} \;=\; -\hat{\mathbf{J}}_{4j-1} + \hat{\mathbf{J}}_{4j} + \hat{\mathbf{J}}_{4j+1} = -\hat{\mathbf{J}}_{\mathrm{h2},j} + \hat{\mathbf{J}}_{\mathrm{v2},j} + \hat{\mathbf{J}}_{\mathrm{h1},j+1}\,. \tag{4.30}$$

The reduced Hamiltonian is

$$\hat{H}_{\mathrm{red}} = \alpha \sum_{j=1}^{N/2} \left(-\hat{J}^2_{\mathrm{h1},j} - 2\hat{J}^2_{\mathrm{h2},j} - \hat{J}^2_{\mathrm{h1},j+1} + 3\,\hat{\mathbf{J}}_{\mathrm{h1},j} \cdot \hat{\mathbf{J}}_{\mathrm{h2},j} + 3\,\hat{\mathbf{J}}_{\mathrm{h2},j} \cdot \hat{\mathbf{J}}_{\mathrm{h1},j+1} \right). \tag{4.31}$$

Setting $\hat{\mathbf{J}}_{\mathrm{h1},j} = \hat{\mathbf{J}}_{\mathrm{h1}}$ and $\hat{\mathbf{J}}_{\mathrm{h2},j} = \hat{\mathbf{J}}_{\mathrm{h2}}$ for all j (but $\hat{\mathbf{J}}_{\mathrm{h1}} \neq \hat{\mathbf{J}}_{\mathrm{h2}}$), we obtain a new minisuperspace Hamiltonian

$$\hat{H}^{(2)}_{\mathrm{mini}} = \alpha N(-\hat{J}^2_{\mathrm{h1}} - \hat{J}^2_{\mathrm{h2}} + 3\,\hat{\mathbf{J}}_{\mathrm{h1}} \cdot \hat{\mathbf{J}}_{\mathrm{h2}}) \tag{4.32}$$

with non-trivial dynamics. We note that this minisuperspace model is closely related to the mean-field model introduced for finite Heisenberg spin chains in [137]. The main difference is that our minisuperspace treatment identifies spin degrees of freedom on alternating links, while the mean-field treatment couples these spins. This relation, which we do not pursue further in this work (except for one conclusion drawn in Sec. 4.7), could be useful in an extension of discrete minisuperspace models

to controlled mean-field theories.

Alternatively, we can split up the range of N nodes into two disjoint averaging regions. Unlike $\hat{H}^{(2)}_{\rm mini}$, such a reduction can be interpreted as an analog of reductions proposed in quantum cosmology. In an attempt to include degrees of freedom relevant for the evolution of inhomogeneous perturbations on an isotropic background cosmology, [138] proposed that independent spatial regions can be pasted together to allow for more general degrees of freedom. (Our model here has only two such regions, but we will comment on effects of subdivisions in our discussion of stability in Sections 4.6.2 and 4.7.) Such a quantum cosmology is a version of the classical separate-universe approximation of [139–141].

In the reduced theory, we now assume N odd, such that we have an even number $N+1$ of horizontal spins. We can group them in two sets, one for the spins around nodes $i=1$ to $i=(N-1)/2$ and one for nodes from $i=(N+3)/2$ to $i=N$. (The central node $i_{\rm c}=(N+1)/2$ is not included in this counting. The spin $\hat{\mathbf{J}}_{2i_{\rm c}-1}=\hat{\mathbf{J}}_N$ to its left is contained in the first set, while $\hat{\mathbf{J}}_{2i_{\rm c}+1}=\hat{\mathbf{J}}_{N+2}$ to its right is contained in the second set.) Calling the first $(N+1)/2$ horizontal spins $\hat{\mathbf{J}}_{\rm h1}:=\hat{\mathbf{J}}_1=\hat{\mathbf{J}}_3\cdots=\hat{\mathbf{J}}_N$ and the last $(N+1)/2$ spins $\hat{\mathbf{J}}_{\rm h2}:=\hat{\mathbf{J}}_{N+2}=\hat{\mathbf{J}}_{N+4}=\cdots=\hat{\mathbf{J}}_{2N+1}$, we obtain, starting from the reduced Hamiltonian, the minisuperspace Hamiltonian

$$\hat{H}^{(3)}_{\rm mini}=\alpha\frac{N-3}{2}(\hat{J}^2_{\rm h1}+\hat{J}^2_{\rm h2})+3\alpha\hat{\mathbf{J}}_{\rm h1}\cdot\hat{\mathbf{J}}_{\rm h2}\,. \tag{4.33}$$

(There are $(N-1)/2$ non-interacting contributions of $\hat{J}^2_{\rm h1}$ and $\hat{J}^2_{\rm h2}$ from spins in the interior of the two averaging regions, as well as one contribution of $-\hat{J}^2_{\rm h1}+3\hat{\mathbf{J}}_{\rm h1}\cdot\hat{\mathbf{J}}_{\rm h2}-\hat{J}^2_{\rm h2}$ with interactions at the border between the regions, located at the central node $i_{\rm c}=(N+1)/2$.)

The two Hamiltonians are rather different from each other. They are both of the form

$$\hat{H}_{\beta\gamma}:=\beta(\hat{J}^2_{\rm h1}+\hat{J}^2_{\rm h2})+\gamma\hat{\mathbf{J}}_{\rm h1}\cdot\hat{\mathbf{J}}_{\rm h2}\,, \tag{4.34}$$

but while ${\rm sgn}\gamma={\rm sgn}\alpha$ in both cases, we have ${\rm sgn}\beta=-{\rm sgn}\alpha$ for $\hat{H}^{(2)}$ and ${\rm sgn}\beta={\rm sgn}\alpha$ for $\hat{H}^{(3)}$ (with $N>3$). We should therefore expect different ground states or effective potentials in the two cases. In particular, if $\langle\hat{J}^2_{\rm h1/2}\rangle$ is considered a free variable, we can minimize the energy of $\langle\hat{H}^{(3)}\rangle$ by zero spins, while the energy range of $\langle\hat{H}^{(2)}\rangle$ is unbounded from below. If $\langle\hat{J}^2_{\rm h1/2}\rangle$ is fixed, however, only the interaction term matters for ground states or effective potentials, for which the

two models provide the same sign. The ground-state properties are then similar to those of the Heisenberg spin chain related to the reduced Hamiltonian (4.11): parallel alignment of next-neighbor spins (ferromagnetic) if $\gamma < 0$ and antiparallel alignment (antiferromagnetic) if $\gamma > 0$.

We assume that the individual spin states have the same eigenvalue of $\hat{J}^2_{\mathrm{h1}}$ and $\hat{J}^2_{\mathrm{h2}}$, given by $s(s+1)\hbar^2$ with some half-integer s. We have two cases according to sgnγ: For $\gamma > 0$, the interaction term is minimized by antiparallel spins $\hat{\mathbf{J}}_{\mathrm{h1/2}}$. The two spins then form a combined spin eigenstate $|0,0\rangle$ of the total spin $\hat{\mathbf{J}} := \hat{\mathbf{J}}_{\mathrm{h1}} + \hat{\mathbf{J}}_{\mathrm{h2}}$ in which

$$\langle \hat{\mathbf{J}}_{\mathrm{h1}} \cdot \hat{\mathbf{J}}_{\mathrm{h2}} \rangle = \frac{1}{2} \langle \hat{J}^2 - \hat{J}^2_{\mathrm{h1}} - \hat{J}^2_{\mathrm{h2}} \rangle = -s(s+1)\hbar^2 \,, \tag{4.35}$$

and the energy eigenvalue is given by

$$E_{\gamma>0} = (2\beta - \gamma)s(s+1)\hbar^2 \,. \tag{4.36}$$

For $\gamma < 0$, the parallel configuration minimizes the interaction term, for which we have a whole multiplet of different sates with total spin $2s$. In any such state, $\langle \hat{\mathbf{J}}_{\mathrm{h1}} \cdot \hat{\mathbf{J}}_{\mathrm{h2}} \rangle = s^2\hbar^2$, and the energy eigenvalue is

$$E_{\gamma<0} = (2\beta s(s+1) + \gamma s^2)\hbar^2 \,. \tag{4.37}$$

The two different types of ground states, with antiparallel spins for $\gamma > 0$ and parallel spins for $\gamma < 0$, have interesting implications for the reliability of the two different interacting minisuperspace models. If $\gamma < 0$, the two models predict the same ground-state configuration with all fundamental spins aligned. There is only a quantitative difference between the models in the predicted ground-state energy. For $\gamma > 0$, however, the antiparallel alignment of $\hat{\mathbf{J}}_{\mathrm{h1}}$ and $\hat{\mathbf{J}}_{\mathrm{h2}}$ corresponds to very different fundamental configurations. With $\hat{H}^{(2)}_{\mathrm{mini}}$, the two antiparallel spins are alternating along the full spin chain, which agrees with the ground state of the discrete theory. With $\hat{H}^{(3)}_{\mathrm{mini}}$, however, we have two averaging regions with equal spins in each region, but antiparallel alignment between the two regions. Knowing the fundamental configuration, we can tell that an energy preference of antiparallel alignment at the border between the two regions means that the configuration should be unstable under splitting it up further into smaller and smaller averaging regions with antiparallel alignment at all borders. With complete splitting, each

link being an averaging region of its own, a configuration as with $\hat{H}^{(2)}_{\rm mini}$ or in the fundamental theory is obtained, but one would have left the minisuperspace stage. The second minisuperspace model with Hamiltonian $\hat{H}^{(2)}_{\rm mini}$, on the other hand, realizes the correct ground state within a minisuperspace model, and without the need for further refinement. (There is, however, a difference between the ground state of $\hat{H}^{(2)}_{\rm mini}$ and the corresponding discrete theory. The former has an even number of spins, but it is derived from a spin chain with an odd number of spins. These two cases are known to have different behaviors [142–144].)

We conclude that the way degrees of freedom are included in a minisuperspace model can have significant implications for how well fundamental properties are modelled, which however can be evaluated only if one knows a great deal about the fundamental theory. Transferring this lesson to quantum gravity suggests that caution toward minisuperspace results would be advisable. However, there is a difference between stability as discussed so far, where it is implicitly assumed that the spin chain can exchange energy with an environment and settle down to its ground state, and quantum-cosmology models, where there is no environment outside of the system. We will return to this question in Secs. 4.6 and 4.7.

4.4.4 Effective equations and potentials

We continue to analyze the dynamics by means of effective equations in canonical form. We assign infinitely many numbers to a set of quantum spin degrees of freedom with operator $\hat{\mathbf{J}}_i$. In a given state, these numbers correspond to the expectation values $\langle \hat{J}^a_i \rangle$ of spin components and the moments

$$\Delta(J^{a_1}_{i_1} \cdots J^{a_n}_{i_n}) := \langle (\hat{J}^{a_1}_{i_1} - \langle \hat{J}^{a_1}_{i_1} \rangle) \cdots (\hat{J}^{a_n}_{i_n} - \langle \hat{J}^{a_n}_{i_n} \rangle) \rangle_{\rm symm} \tag{4.38}$$

in totally symmetric ordering. (For uniform notation of all moments, we write fluctuations as $\Delta(J^a J^a) = (\Delta J^a)^2$.) In a semiclassical expansion, which we will perform in most of our derivations, it is sufficient to include only moments up to second order, $n = 2$. We then have a finite-dimensional system. For a semiclassical state, defined as a state with moments of the order $\Delta(J^{a_1}_{i_1} \cdots J^{a_n}_{i_n}) = \mathcal{O}(\hbar^{(a_1+\cdots+a_n)/2})$, terms of order $\hbar$ are included in a truncation up to second order in moments.

The quantum degrees of freedom form a phase space with Poisson bracket given

in (4.2). For instance,

$$\begin{aligned}
\{\langle\hat{J}_i^a\rangle, \langle\hat{J}_j^b\rangle\} &= \epsilon^{abc}\langle\hat{J}_i^c\rangle\delta_{ij} \\
\{\Delta(J_i^a J_j^b), \langle\hat{J}_k^c\rangle\} &= \delta_{ik}\epsilon^{acd}\Delta(J_i^d J_j^b) + \delta_{jk}\epsilon^{bcd}\Delta(J_i^a J_j^d) \\
\{\Delta(J_i^a J_j^b), \Delta(J_k^c J_l^d)\} &= \delta_{ik}\epsilon^{ace}\langle\hat{J}_i^e\rangle\Delta(J_j^b J_l^d) + \delta_{il}\epsilon^{ade}\langle\hat{J}_i^e\rangle\Delta(J_j^b J_k^c) + \delta_{jk}\epsilon^{bce}\langle\hat{J}_j^e\rangle\Delta(J_i^a J_l^d) \\
&+ \delta_{jl}\epsilon^{bde}\langle\hat{J}_j^e\rangle\Delta(J_i^a J_k^c) + \mathcal{O}(\Delta^3)\,.
\end{aligned} \tag{4.39}$$

The first two lines are exact, while the third line is valid to second order in moments.

In the minimal minisuperspace model we have the effective Hamiltonian

$$H_{\text{eff}}^{(1)} = \alpha N\left(\langle\hat{J}^x\rangle^2 + \langle\hat{J}^y\rangle^2 + \langle\hat{J}^z\rangle^2 + \Delta(J^x J^x) + \Delta(J^y J^y) + \Delta(J^z J^z)\right)\,. \tag{4.40}$$

All expectation values and moments then have zero time derivatives

$$\frac{\mathrm{d}O}{\mathrm{d}t} = \{O, H_{\text{eff}}^{(1)}\}\,, \tag{4.41}$$

as is to be expected from the non-interacting nature of the system.

4.4.4.1 Minimal minisuperspace model

The moments in (4.40) provide a quantum correction to the classical Hamiltonian. For the ground state, we can derive their minimal values by saturating uncertainty relations

$$\Delta(J^x J^x)\Delta(J^y J^y) \geq \frac{\hbar^2}{4}|\langle\hat{J}^z\rangle|^2 \tag{4.42}$$

and cyclic permutations. In order to evaluate these equations, we may assume that the expectation value $\langle\hat{\mathbf{J}}\rangle$ points in the z-direction. Therefore, only $\langle\hat{J}^z\rangle$ is non-zero among the spin components. The saturated uncertainty relations then require that $\Delta(J^z J^z) = 0$ while

$$\Delta(J^x J^x)\Delta(J^y J^y) = \frac{1}{4}\hbar^2|\langle\hat{J}^z\rangle|^2\,. \tag{4.43}$$

By symmetry, $\Delta(J^x J^x) = \Delta(J^y J^y)$. The quantum correction to the classical Hamiltonian, or the effective potential, is then

$$V_{\text{eff}}^{(1)} = \alpha N(\Delta(J^x J^x) + \Delta(J^y J^y) + \Delta(J^z J^z)) = \alpha N\hbar|\langle\hat{J}^z\rangle| = \alpha N\hbar\sqrt{\delta_{ab}\langle\hat{J}^a\rangle\langle\hat{J}^b\rangle}\,. \tag{4.44}$$

Although the effective potential is non-zero, it does not imply interactions but rather provides a zero-point energy because it only depends on a constant of motion. The effective Hamiltonian is given by

$$H_{\rm eff}^{(1)} = \alpha N \langle \hat{J}^z \rangle^2 + V_{\rm eff}^{(1)} = \alpha N \left(\langle \hat{J}^z \rangle^2 + \hbar |\langle \hat{J}^z \rangle| \right) = \alpha N s(s+1)\hbar^2 \tag{4.45}$$

if $\langle \hat{J}^z \rangle = \pm s\hbar$ for a spin pointing in the z-direction according to our assumptions. This value of the effective Hamiltonian is in agreement with the operator result, where the well-known eigenvalues of $\hat{J}^2$ are $s(s+1)\hbar^2$.

The same effective potential can be obtained from a canonical version of the spin system. Again assuming that the spin vector points in the z-direction, we introduce canonical coordinates

$$\begin{aligned} q &:= \frac{\delta\langle \hat{J}^x \rangle}{\sqrt{\langle \hat{J}^z \rangle}} = \frac{\delta\langle \hat{J}^x \rangle}{\sqrt[4]{\delta_{ab}\langle \hat{J}^a \rangle \langle \hat{J}^b \rangle - (\delta\langle \hat{J}^x \rangle)^2 - (\delta\langle \hat{J}^y \rangle)^2}} \\ p &:= \frac{\delta\langle \hat{J}^y \rangle}{\sqrt{\langle \hat{J}^z \rangle}} = \frac{\delta\langle \hat{J}^y \rangle}{\sqrt[4]{\delta_{ab}\langle \hat{J}^a \rangle \langle \hat{J}^b \rangle - (\delta\langle \hat{J}^x \rangle)^2 - (\delta\langle \hat{J}^y \rangle)^2}} \end{aligned} \tag{4.46}$$

for small values $\delta\langle \hat{J}^x \rangle$ and $\delta\langle \hat{J}^y \rangle$ much less than $\langle \hat{J}^z \rangle$: We have

$$\begin{aligned} \{q,p\} &= \frac{\{\delta\langle \hat{J}^x \rangle, \delta\langle \hat{J}^y \rangle\}}{\langle \hat{J}^z \rangle} + \frac{\delta\langle \hat{J}^x \rangle \{\delta\langle \hat{J}^y \rangle, \langle \hat{J}^z \rangle\} - \delta\langle \hat{J}^y \rangle \{\delta\langle \hat{J}^x \rangle, \langle \hat{J}^z \rangle\}}{2\langle \hat{J}^z \rangle^2} \\ &= 1 + \mathcal{O}((\delta\langle \hat{J}^{x/y} \rangle / \langle \hat{J}^z \rangle)^2)\,. \end{aligned} \tag{4.47}$$

These relations imply the quadratic equation

$$\left((\delta\langle \hat{J}^x \rangle)^2 + (\delta\langle \hat{J}^y \rangle)^2 \right)^2 + (q^2+p^2)^2 \left((\delta\langle \hat{J}^x \rangle)^2 + (\delta\langle \hat{J}^y \rangle)^2 \right) - (q^2+p^2)^2 \delta_{ab}\langle \hat{J}^a \rangle \langle \hat{J}^b \rangle = 0\,. \tag{4.48}$$

For $\delta_{ab}\langle \hat{J}^a \rangle \langle \hat{J}^b \rangle$ much greater than $(\delta\langle \hat{J}^x \rangle)^2 + (\delta\langle \hat{J}^y \rangle)^2$, we can solve (4.48) for $(\delta\langle \hat{J}^x \rangle)^2 + (\delta\langle \hat{J}^y \rangle)^2$ by

$$\begin{aligned} (\delta\langle \hat{J}^x \rangle)^2 + (\delta\langle \hat{J}^y \rangle)^2 &= -\frac{1}{2}(q^2+p^2)^2 \pm \sqrt{\delta_{ab}\langle \hat{J}^a \rangle \langle \hat{J}^b \rangle}(q^2+p^2)\sqrt{1 + \frac{(q^2+p^2)^2}{4\delta_{ab}\langle \hat{J}^a \rangle \langle \hat{J}^b \rangle}} \\ &\approx \sqrt{\delta_{ab}\langle \hat{J}^a \rangle \langle \hat{J}^b \rangle}(q^2+p^2) - \frac{1}{2}(q^2+p^2)^2 + \cdots\,. \end{aligned} \tag{4.49}$$

(Only the plus sign gives a positive solution.) The first term is a harmonic-oscillator Hamiltonian with $m^{-1} = 2\sqrt{\delta_{ab}\langle\hat{J}^a\rangle\langle\hat{J}^b\rangle} = \omega$, which has zero-point energy $\frac{1}{2}\hbar\omega = \hbar\sqrt{\delta_{ab}\langle\hat{J}^a\rangle\langle\hat{J}^b\rangle}$ in agreement with the effective potential (4.44).

4.4.4.2 Interacting minisuperspace models

For the two interacting models, we need the covariances $\Delta(J^a_{\rm h1}J^a_{\rm h2})$ for $a = x, y, z$ (no sum over a). In addition to the fluctuations as in the minimal minisuperspace model with a Hamiltonian of the type (4.34), we then have the term

$$\Delta V_{\rm interaction} = \gamma(\Delta(J^x_{\rm h1}J^x_{\rm h2}) + \Delta(J^y_{\rm h1}J^y_{\rm h2}) + \Delta(J^z_{\rm h1}J^z_{\rm h2})) \tag{4.50}$$

in the effective potential.

Covariances can often be ignored in the context of uncertainty relations, but they do contribute in the complete form

$$\Delta(A^2)\Delta(B^2) - \Delta(AB)^2 \geq \frac{1}{4}|\langle[\hat{A},\hat{B}]\rangle|^2\,. \tag{4.51}$$

Unlike fluctuations, which obtain a lower bound for non-commuting operators, covariances are subject to an upper bound depending on the fluctuations. For two commuting spin components as in (4.50), the uncertainty relation is

$$\Delta(J^x_{\rm h1}J^x_{\rm h1})\Delta(J^x_{\rm h2}J^x_{\rm h2}) \geq \Delta(J^x_{\rm h1}J^x_{\rm h2})^2\,. \tag{4.52}$$

If $\gamma > 0$ in (4.50), we can minimize the effective interaction potential by choosing the value

$$\Delta(J^x_{\rm h1}J^x_{\rm h2}) = -\sqrt{\Delta(J^x_{\rm h1}J^x_{\rm h1})\Delta(J^x_{\rm h2}J^x_{\rm h2})} = -\frac{1}{2}\hbar|\langle\hat{J}^z\rangle|\,. \tag{4.53}$$

The last equality holds if we also minimize the uncertainty relations for the two individual spins and use the antiparallel alignment for spin expectation values, without loss of generality assumed to point in the z-direction. The same value is obtained for $\Delta(J^y_{\rm h1}J^y_{\rm h2})$, while $\Delta(J^z_{\rm h1}J^z_{\rm h2}) = 0$ because the z-components have zero fluctuations with our choice of directions. Combining all terms in the effective Hamiltonian (4.34) then yields

$$H_{{\rm eff},\gamma>0} = 2\beta s(s+1)\hbar^2 - \gamma(s^2\hbar^2 + s\hbar^2) = s(s+1)(2\beta-\gamma)\hbar^2\,. \tag{4.54}$$

The first term is twice the non-interacting contribution from a single spin with the same form as in (4.45), the second term, $-\gamma s^2\hbar^2$, is $\gamma\langle\hat{J}^z_{\rm h1}\rangle\langle\hat{J}^z_{\rm h2}\rangle$ for antiparallel alignment in the z-direction, and the last term, $-\gamma s\hbar^2$, adds up the two non-zero covariances in (4.50). This result agrees with the ground-state energy (4.36). For $\gamma < 0$, one can see in the same way that the operator result (4.37) is reproduced if the covariances vanish and parallel alignment is used in $\gamma\langle\hat{J}^z_{\rm h1}\rangle\langle\hat{J}^z_{\rm h2}\rangle = \gamma s^2\hbar^2$.

4.4.4.3 Condensate model

The condensate model has provided non-trivial dynamics for a single spin. However, some of the equations for expectation values and moments are trivial. We can derive effective equations from the state-dependent Hamiltonian (4.19) if we assign to it the effective Hamiltonian

$$H_{\rm eff,\,cond} = -2\alpha N\delta_{ab}\left(\langle\hat{J}^a\rangle\langle\hat{J}^b\rangle + \Delta(J^aJ^b)\right) + 3\alpha N\delta_{ab}j^a\langle\hat{J}^b\rangle \tag{4.55}$$

where the vector j^a is treated in the following way: It is a constant for purposes of computing Poisson brackets, for instance in equations of motion. After the Poisson brackets have been derived, one sets $j^a = \langle\hat{J}^a\rangle$. In this way, the correct equations follow for expectation values taken in a state that evolves according to the non-linear equation (4.20).

Following this procedure, we obtain the equation

$$\frac{{\rm d}\langle\hat{J}^c\rangle}{{\rm d}t} = 3\alpha N\epsilon^{abc}\langle\hat{J}^a\rangle\langle\hat{J}^b\rangle = 0\,. \tag{4.56}$$

For second-order moments, we have the contribution

$$\frac{{\rm d}\langle\hat{J}^c\hat{J}^d\rangle}{{\rm d}t} = 3\alpha N\langle\hat{J}^a\rangle\left\langle\epsilon^{abc}\hat{J}^b\hat{J}^d + \epsilon^{abd}\hat{J}^c\hat{J}^b\right\rangle\,. \tag{4.57}$$

Since covariances couple to expectation values and fluctuations, non-zero correlations can build up during evolution even if they vanish in an initial state.

4.5 Continuum theories

One question about minisuperspace models derived from classical continuum theories, addressed in [107], is about the coordinate volume V_0 that characterizes the size of an averaging region. (See [145] for a review of minisuperspace models and quantum cosmology.) For the simplest minisuperspace models of general relativity, space is flat and infinite, and the canonical form $\int \mathrm{d}^3x\dot{\phi}p_\phi$ of any local degree of freedom $\phi(x)$ with momentum $p_\phi(x)$ is infinite for homogeneous configurations. In order to obtain a well-defined canonical structure, one can choose a finite region $\mathcal{V}$ of coordinate size $V_0 = \int_{\mathcal{V}} \mathrm{d}^3x$ and restrict integrations of the canonical form and the Lagrangian to this region.

If only homogeneous configurations are considered, the size and position of this region should not matter. The restricted canonical form is

$$\int_{\mathcal{V}} \mathrm{d}^3x\dot{\phi}(x)p_\phi(x) = V_0\dot{\bar{\phi}}\bar{p}_\phi \tag{4.58}$$

for homogeneous configurations $\phi(x) = \bar{\phi}$ and $p_\phi(x) = \bar{p}_\phi$. The momentum of $\bar{\phi}$ is therefore not equal to $\bar{p}_\phi$, but to $\bar{p} = V_0\bar{p}_\phi$. The standard Hamiltonian of a scalar field, just like other Hamiltonians for instance of gravitational degrees of freedom, then depends on V_0 when it is restricted to canonically conjugate minisuperspace configurations. For a scalar field, we have

$$\int_{\mathcal{V}} \mathrm{d}^3x \left(\frac{1}{2}\dot{\bar{\phi}}^2 + W(\bar{\phi})\right) = \frac{V_0}{2}\bar{p}_\phi^2 + V_0W(\bar{\phi}) = \frac{1}{2}\frac{\bar{p}^2}{V_0} + V_0W(\bar{\phi}) \tag{4.59}$$

and the dependence on V_0 is not just by a multiplicative factor. While the classical theory does not depend on the choice of V_0, the quantum theory does, for instance via V_0-dependent effective potentials.

In [107], it was shown that the V_0-dependent semiclassical corrections in minisuperspace effective potentials of a scalar-field theory are related to infrared contributions to field-theory effective potentials. The choice of V_0 then has physical relevance in the number of infrared modes included in the minisuperspace model, but it is a property of the minisuperspace truncation rather than of physical interactions. It is therefore difficult to justify interpretations of minisuperspace effects in quantitative terms.

In order to test this question in our spin system, we now derive a continuum theory from which our minimal minisuperspace model can be obtained by using homogeneous configurations. Generalizations corresponding to the interacting minisuperspace models will also be considered. As we will see, for this kind of spin systems the nature of averaging regions is less problematic than for canonical field theories. There may therefore be an advantage in deriving minisuperspace models directly from discrete quantum theories.

4.5.1 Continuum models

Starting with the unreduced theory, we introduce two continuum fields $\hat{\mathbf{J}}_{\rm h}(x)$ and $\hat{\mathbf{J}}_{\rm v}(x)$ where x runs through the entire length of our graph. In terms of the measure provided by the choice of x, we introduce the coordinate distance between two nodes i at $x = x_i$ and $i+1$ at $x = x_{i+1}$ by $\delta = \int_{x_i}^{x_{i+1}} {\rm d}x$, assumed to be independent of i. The total length of the graph is $L_0 = \int_{x_1}^{x_{N+1}} {\rm d}x = N\delta$. For integer values of $x = x_i$, we identify $\hat{\mathbf{J}}_{\rm v}(x_i) = \hat{\mathbf{J}}_{{\rm v},i} = \hat{\mathbf{J}}_{2i}$, $\hat{\mathbf{J}}_{{\rm h}1,i} = \hat{\mathbf{J}}_{2i-1}$ and $\hat{\mathbf{J}}_{{\rm h}2,i} = \hat{\mathbf{J}}_{2i+1}$.

4.5.1.1 Minimal model

For the minimal model, we do not treat $\hat{\mathbf{J}}_{{\rm h}1,i}$ and $\hat{\mathbf{J}}_{{\rm h}2,i}$ as independent fields but rather view them as one horizontal field evaluated at different positions $x_i \pm \delta/2$: We set $\hat{\mathbf{J}}_{\rm h}(x_i - \delta/2) = \hat{\mathbf{J}}_{{\rm h}1,i}$ and $\hat{\mathbf{J}}_{\rm h}(x_i + \delta/2) = \hat{\mathbf{J}}_{{\rm h}2,i}$. The leading terms in a continuum limit of the Hamiltonian and the constraint can then be obtained by an expansion in δ up to second order. Derivatives by x appear in the process, and will be denoted by a prime.

The constraints are

$$\begin{aligned} \hat{C}^a(x_i) &= -\hat{J}^a_{\rm h}(x_i - \delta/2) + \hat{J}^a_{\rm v}(x_i) + \hat{J}^a_{\rm h}(x_i + \delta/2) && (4.60)\\ &= \hat{J}^a_{\rm v}(x_i) + \delta \hat{J}^a_{\rm h}(x_i)' \,. && (4.61) \end{aligned}$$

The Hamiltonian is

$$\hat{H} = \alpha\delta_{ab} \sum_{i=1}^{N} \Big(-\hat{J}^a_{\rm h}(x_i - \delta/2)\hat{J}^b_{\rm v}(x_i) + \hat{J}^a_{\rm h}(x_i - \delta/2)\hat{J}^b_{\rm h}(x_i + \delta/2) + \hat{J}^a_{\rm v}(x_i)\hat{J}^b_{\rm h}(x_i + \delta/2) \Big)$$

$$= \alpha \sum_{i=1}^{N} \left(\hat{J}_{\rm h}(x_i)^2 + \delta \hat{\mathbf{J}}_{\rm v}(x_i) \cdot \hat{\mathbf{J}}_{\rm h}(x_i)' + \frac{1}{4}\delta^2 (\hat{\mathbf{J}}_{\rm h}(x_i) \cdot \hat{\mathbf{J}}_{\rm h}(x_i)'' - (\hat{J}_{\rm h}(x_i)')^2) \right) . \quad (4.62)$$

Solving the constraint, the Hamiltonian becomes

$$\hat{H} = \alpha \sum_{i=1}^{N} \left(\hat{J}_{\rm h}(x_i)^2 + \frac{1}{4}\delta^2 (\hat{\mathbf{J}}_{\rm h}(x_i) \cdot \hat{\mathbf{J}}_{\rm h}(x_i)'' - 5(\hat{J}_{\rm h}(x_i)')^2) \right) \quad (4.63)$$

and gives rise to the continuum limit

$$\hat{H}^{(1)}_{\rm cont} = \frac{\alpha}{\delta} \int {\rm d}x \left(\hat{J}^2_{\rm h} + \frac{1}{4}\delta^2 (\hat{\mathbf{J}}_{\rm h} \cdot \hat{\mathbf{J}}''_{\rm h} - 5(\hat{J}'_{\rm h})^2) \right) \quad (4.64)$$

$$= \frac{\alpha}{\delta} \int {\rm d}x \left(\hat{J}^2_{\rm h} - \frac{3}{2}\delta^2 (\hat{J}'_{\rm h})^2 \right) + \frac{1}{4}\alpha\delta \hat{\mathbf{J}}_{\rm h} \cdot \hat{\mathbf{J}}'_{\rm h}|_{\partial} \quad (4.65)$$

with a boundary term denoted by a subscript ∂. The continuum limit for the reduced Hamiltonian (4.11) is the same as (4.65).

The minisuperspace model obtained from this continuum Hamiltonian is

$$H^{(1)}_{\rm mini} = \frac{\alpha}{\delta} L_0 \hat{J}^2_{\rm h} = \alpha N \hat{J}^2_{\rm h} . \quad (4.66)$$

It is identical with the Hamiltonian in our minimal minisuperspace model. Any reference to the averaging length L_0 can be expressed in terms of the number N of nodes of the fundamental discrete theory, which has physical meaning free of truncation choices. Therefore, there are no such problems as may be related to the appearance of V_0 in minisuperspace models derived from classical continuum theories.

4.5.1.2 Interacting minisuperspace models

If we do distinguish between $\hat{\mathbf{J}}_{\rm h1}(x_i)$ and $\hat{\mathbf{J}}_{\rm h2}(x_i)$, we obtain the continuum Hamiltonian

$$\hat{H}^{(2)}_{\rm cont} = \frac{\alpha}{\delta} \int {\rm d}x \left(-\hat{\mathbf{J}}_{\rm h1} \cdot \hat{\mathbf{J}}_{\rm v} + \hat{\mathbf{J}}_{\rm h1} \cdot \hat{\mathbf{J}}_{\rm h2} + \hat{\mathbf{J}}_{\rm v} \cdot \hat{\mathbf{J}}_{\rm h2} \right) \quad (4.67)$$

with constraint

$$\hat{C} = -\hat{\mathbf{J}}_{\rm h1} + \hat{\mathbf{J}}_{\rm v} + \hat{\mathbf{J}}_{\rm h2} = 0 . \quad (4.68)$$

Solving the constraint gives the Hamiltonian

$$\hat{H}^{(2)}_{\rm cont} = \frac{\alpha}{\delta}\int \mathrm{d}x \left(-\hat{J}^2_{\rm h1} + 3\hat{\mathbf{J}}_{\rm h1}\cdot\hat{\mathbf{J}}_{\rm h2} - \hat{J}^2_{\rm h2}\right) , \tag{4.69}$$

from which we obtain the interacting minisuperspace Hamiltonian $\hat{H}^{(2)}_{\rm mini}$.

For the second interacting model, we do not distinguish between $\hat{\mathbf{J}}_{\rm h1}(x_i)$ and $\hat{\mathbf{J}}_{\rm h2}(x_i)$, but introduce two averaging regions of length $L_0/2$ each in which we have the constant fields $\hat{\mathbf{J}}_1$ and $\hat{\mathbf{J}}_2$, respectively. Starting with the first continuum theory with Hamiltonian (4.65), we obtain

$$\hat{H}^{(3)}_{\rm hom} = \frac{\alpha}{\delta}\frac{L_0}{2}\left(\hat{J}^2_1 + \hat{J}^2_2\right) + \frac{1}{4}\alpha\delta\left(\hat{\mathbf{J}}_1 - \hat{\mathbf{J}}_2\right)\cdot\hat{\mathbf{J}}' . \tag{4.70}$$

The last term, originating from the boundary term, needs further discussion. We have left a $\hat{\mathbf{J}}'$ in the equation, still referring to an inhomogeneous continuum field. It gives us the difference between the two averaged fields $\hat{\mathbf{J}}_1$ and $\hat{\mathbf{J}}_2$. It is infinite if we have two constant fields taking different values in the two regions, but it is multiplied with the spacing δ which goes to zero in the continuum limit. We can regularize this product to a finite number by defining it as

$$\lim_{\delta\to 0}(\delta\hat{\mathbf{J}}') = \lim_{\delta\to 0}\left(\delta\frac{\hat{\mathbf{J}}_2 - \hat{\mathbf{J}}_1}{\delta}\right) = \hat{\mathbf{J}}_2 - \hat{\mathbf{J}}_1 . \tag{4.71}$$

The minisuperspace Hamiltonian is then equal to

$$\begin{aligned}\hat{H}^{(3)}_{\rm mini} &= \frac{\alpha}{\delta}\frac{L_0}{2}\left(\hat{J}^2_1 + \hat{J}^2_2\right) - \frac{1}{4}\alpha\left(\hat{\mathbf{J}}_1 - \hat{\mathbf{J}}_2\right)^2 &(4.72)\\ &= \alpha(N/2 - 1/4)\left(\hat{J}^2_1 + \hat{J}^2_2\right) + \frac{1}{2}\alpha\hat{\mathbf{J}}_1\cdot\hat{\mathbf{J}}_2 . &(4.73)\end{aligned}$$

Unlike what we saw for $\hat{H}^{(2)}_{\rm mini}$, this result is not identical with the previous derivation (4.33) from the discrete theory. However, if we slightly modify our boundary regularization by introducing an additional factor of six in the definition (4.71), the minisuperspace Hamiltonians are the same. The initial disagreement is a result only of the fact that the boundary regularization is ambiguous, which is necessary for $\hat{H}^{(3)}_{\rm mini}$ derived from the continuum theory, but not for $\hat{H}^{(2)}_{\rm mini}$. Notice that the final agreement is non-trivial, because changing the factor in (4.71) modifies the

interacting as well as non-interacting terms in the resulting $\hat{H}^{(3)}_{\rm mini}$, which then both agree with (4.33).

4.6 Effective analysis of the discrete theory

So far, we have analyzed different minisuperspace models, their ground states and effective potentials, as well as relations with continuum theories. Minisuperspace models of quantum gravity are used to analyze homogeneous solutions, which necessarily have long-range correlations as seen from the fundamental theory because distant degrees of freedom are identified. Non-zero fluctuations of a single minisuperspace variable are therefore the same as long-range correlations in the fundamental theory.

Homogeneity and long-range correlations can easily be achieved in the ground state of the fundamental theory. However, discrete ground states are not suitable as nearly classical geometries of a discrete model of quantum gravity, in which degrees of freedom must be excited in order to have non-degenerate geometries. We therefore need excited states with approximate homogeneity and long-range correlations, which poses a question very different from just finding ground states. Long-range correlations related to homogeneity easily build up us a system settles down to its ground state, but it is not guaranteed that this can happen also in an excited state of an isolated system (such as the whole universe) which does not have a drain for surplus energy. In our discrete model, the evolution of long-range correlations can be studied in qualitative terms.

4.6.1 Effective dynamics

For the full or reduced discrete theories, we have large systems of coupled equations generated by the effective Hamiltonians

$$\begin{aligned} H_{\rm eff} &= \alpha\delta_{ab}\sum_{i=1}^{N}\big(-\langle\hat{J}^a_{2i-1}\rangle\langle\hat{J}^b_{2i}\rangle+\langle\hat{J}^a_{2i-1}\rangle\langle\hat{J}^b_{2i+1}\rangle+\langle\hat{J}^a_{2i}\rangle\langle\hat{J}^b_{2i+1}\rangle-\Delta(J^a_{2i-1}J^b_{2i}) \\ &+ \Delta(J^a_{2i-1}J^b_{2i+1})+\Delta(J^a_{2i}J^b_{2i+1})\big) \end{aligned} \tag{4.74}$$

and

$$H_{\rm eff,red} = \alpha\delta_{ab}\sum_{i=1}^{N}\big(-\langle\hat{J}^a_{2i-1}\rangle\langle\hat{J}^b_{2i-1}\rangle + 3\langle\hat{J}^a_{2i-1}\rangle\langle\hat{J}^b_{2i+1}\rangle - \langle\hat{J}^a_{2i+1}\rangle\langle\hat{J}^b_{2i+1}\rangle - \Delta(J^a_{2i-1}J^b_{2i-1}) + 3\Delta(J^a_{2i-1}J^b_{2i+1}) - \Delta(J^a_{2i+1}J^b_{2i+1})\big)\,, \tag{4.75}$$

respectively. The Poisson brackets between expectation values and moments are as in (4.39), except that the subscript takes values in a larger set.

For the unreduced system, we have effective constraints in addition to the effective Hamiltonian. A single constraint operator generates infinitely many effective constraints because it restricts not only expectation values but also the associated moments [146, 147]. In states annihilated by the constraint, we have

$$C^a_i := \langle\hat{C}^a_i\rangle = -\langle\hat{J}^a_{2i-1}\rangle + \langle\hat{J}^a_{2i}\rangle + \langle\hat{J}^a_{2i+1}\rangle = 0 \tag{4.76}$$

as well as

$$C^a_{i,J^b_j} := \langle(\hat{J}^b_j - \langle\hat{J}^b_j\rangle)\hat{C}^a_i\rangle = -\Delta(J^b_jJ^a_{2i-1}) + \Delta(J^b_jJ^a_{2i}) + \Delta(J^b_jJ^a_{2i+1}) = 0 \tag{4.77}$$

and higher-order constraints.

For the boundary expectation values, the equations of motion are

$$\frac{{\rm d}\langle\hat{J}^a_1\rangle}{{\rm d}t} = \alpha\,\epsilon^{abc}\left(\langle\hat{J}^b_3\rangle\langle\hat{J}^c_1\rangle + \Delta(J^b_3J^c_1) - \langle\hat{J}^b_2\rangle\langle\hat{J}^c_1\rangle - \Delta(J^b_2J^c_1)\right) \tag{4.78}$$

and

$$\frac{{\rm d}\langle\hat{J}^a_{2N+1}\rangle}{{\rm d}t} = \alpha\,\epsilon^{abc}\left(\langle\hat{J}^b_{2N}\rangle\langle\hat{J}^c_{2N+1}\rangle + \Delta(J^b_{2N}J^c_{2N+1}) - \langle\hat{J}^b_{2N-1}\rangle\langle\hat{J}^c_{2N+1}\rangle - \Delta(J^b_{2N-1}J^c_{2N+1})\right). \tag{4.79}$$

Implementing the constraint, we obtain

$$\frac{{\rm d}\langle\hat{J}^a_1\rangle}{{\rm d}t} = 2\,\alpha\,\epsilon^{abc}\left(\langle\hat{J}^b_3\rangle\langle\hat{J}^c_1\rangle + \Delta(J^b_3J^c_1)\right) \tag{4.80}$$

and

$$\frac{{\rm d}\langle\hat{J}^a_{2N+1}\rangle}{{\rm d}t} = 2\,\alpha\,\epsilon^{abc}\left(\langle\hat{J}^b_{2N-1}\rangle\langle\hat{J}^c_{2N+1}\rangle + \Delta(J^b_{2N-1}J^c_{2N+1})\right). \tag{4.81}$$

The reduced equations for internal spins are

$$\frac{\mathrm{d}\langle \hat{J}^a_{2i+1}\rangle}{\mathrm{d}t} = 2\,\alpha\,\epsilon^{abc}\left(\langle \hat{J}^b_{2i-1}\rangle\langle \hat{J}^c_{2i+1}\rangle + \Delta(J^b_{2i-1}J^c_{2i+1}) + \langle \hat{J}^b_{2i+3}\rangle\langle \hat{J}^c_{2i+1}\rangle + \Delta(J^b_{2i+3}J^c_{2i+1})\right) \tag{4.82}$$

where $i = \{2, \cdots, N-1\}$. The equation of motion generated by the effective version of the reduced quantum Hamiltonian (4.75) are

$$\frac{\mathrm{d}\langle \hat{J}^{\mathrm{red},a}_{2i+1}\rangle}{\mathrm{d}t} = 3\,\alpha\,\epsilon^{abc}\left(\langle \hat{J}^b_{2i-1}\rangle\langle \hat{J}^c_{2i+1}\rangle + \Delta(J^b_{2i-1}J^c_{2i+1}) + \langle \hat{J}^b_{2i+3}\rangle\langle \hat{J}^c_{2i+1}\rangle + \Delta(J^b_{2i+3}J^c_{2i+1})\right). \tag{4.83}$$

As in the case of operator equations, the equations can be mapped into each other by a constant rescaling of the time coordinate. We note that these equations are exact as no truncation by moments has been necessary. However, equations of motion for second-order moments depend on third-order moments and have to be truncated for a self-contained semiclassical approximation to first order in $\hbar$.

Analytical solutions of these non-linear equations for large N are difficult to find. However, it is possible to analyze some general properties of interest in the context of long-range correlations. In particular, we are interested in correlations between spins at the two boundaries of the graph, which are certainly long-range for large N. We will assume that initially there are no correlations between different spins, but they will build up over time as the system evolves.

The reduced equation of motion for the correlation $\Delta(J^a_1 J^b_{2i+1})$ is

$$\begin{aligned}\frac{\mathrm{d}\Delta(J^a_1 J^b_{2i+1})}{\mathrm{d}t} &= 2\,\alpha\left\{\epsilon^{acd}\left(\langle \hat{J}^d_1\rangle\Delta(J^c_3 J^b_{2i+1}) + \langle \hat{J}^c_3\rangle\Delta(J^d_1 J^b_{2i+1}\right)\right. \\ &\quad \left. + \epsilon^{bef}\left(\langle \hat{J}^e_{2i-1}\rangle\Delta(J^a_1 J^f_{2i+1}) + \langle \hat{J}^f_{2i+1}\rangle\Delta(J^a_1 J^e_{2i-1})\right)\right\}. \end{aligned} \tag{4.84}$$

If we start with an uncorrelated state, the initial conditions are such that the only non-zero initial values are the expectation value of $\hat{J}_1$ and $\hat{J}_{2N+1}$ and their variances chosen such that uncertainty relations are respected. For interior spins, only the fluctuations are assumed non-zero (although they would be allowed to be zero for a general spin system).

The expectation values and second-order moments of the state for all spins are coupled to one another through the evolution equations. One may solve them perturbatively by orders of α. To zeroth order, all expectation values and moments

are constant and no correlations build up. To first order, using (4.84), $\mathrm{d}\Delta(J_1J_3)/\mathrm{d}t$ has a non-zero contribution of the form $\alpha\langle\hat{J}_1\rangle\Delta(J_3J_3)$ and after some time $\Delta(J_1J_3)$ is non-zero to first order in α. The expectation value $\langle\hat{J}_3\rangle$ has a time derivative of the form (4.82) or (4.83) with one non-zero term of the form $\alpha\Delta(J_1J_3)$ and after some time is non-zero to second order in α. We can iterate this procedure and generate non-zero expectation values on all links, as well as non-zero correlations between the links. The first step has generated a covariance $\Delta(J_1J_3) = \mathcal{O}(\alpha\hbar)$ because we used one solution perturbative in α and one fluctuation. For the next step, moving up to $\Delta(J_1J_5)$, we first need to generate a non-zero $\langle\hat{J}_3\rangle$ and $\Delta(J_3J_5)$, using one additional fluctuation and repeated perturbative solutions. We therefore obtain a non-zero $\Delta(J_1J_5) = \mathcal{O}(\alpha^4\hbar^2)$. By iteration, we obtain a non-zero $\Delta(J_1J_{2i+1}) = \mathcal{O}(\alpha^{3i-2}\hbar^i)$. For long-range correlations between the boundary spins, we need to apply the procedure up to $i = N/2$, after which all spins are correlated from non-zero seed expectation values on both boundaries; see Figs. 4.3 and 4.4. A small number of iterations, $M \ll N$, does not lead to strong long-range correlations. The building-up of long-range correlations from local dynamics can therefore be seen only to high perturbative orders, or non-perturbatively, and it requires high orders in an $\hbar$-expansion.

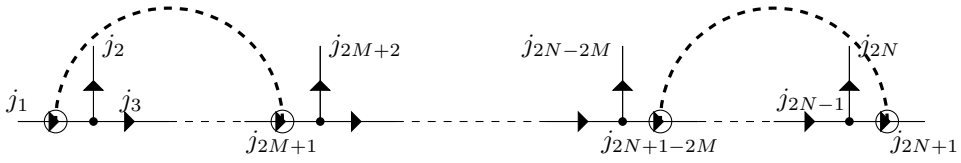

Figure 4.3. Correlations between the farthest spin sets for $\hat{\mathbf{J}}_1$ and $\hat{\mathbf{J}}_{2N+1}$ after solving the equations M times iteratively for a graph with N nodes for $2M \leq N+1$. The semi-circles represent non-zero covariances $\Delta(J^a_1 J^b_{2M+1})$ and $\Delta(J^a_{2N+1}J^b_{2N+1-2M})$.

4.6.2 Dynamical stability for small number of nodes

We now return to the question of dynamical stability of states of the spin chain as an isolated system. We will consider discrete theories with small number of nodes and choose initial values corresponding to the different ground states found in our minisuperspace models. The effective evolution equations can be solved perturbatively and indicate dynamical stability in some cases. (We will not analyze

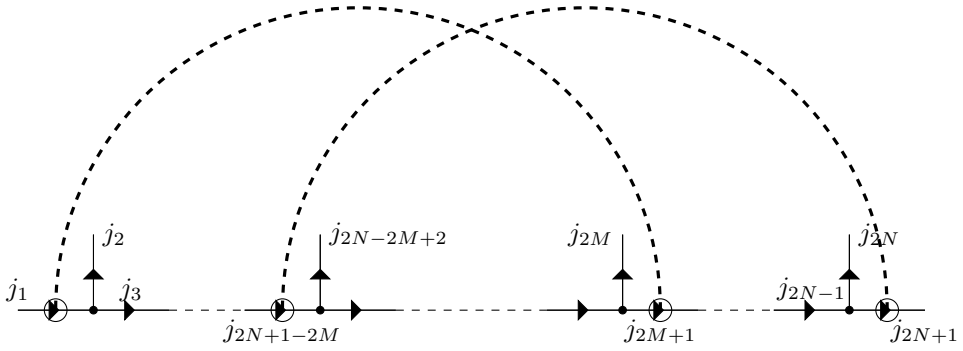

Figure 4.4. Correlations between the farthest spin sets for $\hat{\mathbf{J}}_1$ and $\hat{\mathbf{J}}_{2N+1}$ after solving the equations M times iteratively for a graph with N nodes for $N < 2M$. The semi-circles represent non-zero covariances $\Delta(J^a_1 J^b_{2M+1})$ and $\Delta(J^a_{2N+1} J^b_{2N+1-2M})$.

stability under perturbations of initial configurations.) Although we present explicit solutions only for small numbers of nodes, the relevant features are generic and can be seen also for large numbers of nodes, but it is more cumbersome to produce explicit expressions.

4.6.2.1 Single-node graph

For $N = 1$, we have two horizontal spins which we can identify with the spins in our two interacting minisuperspace models, or view as a theory beyond the minimal minisuperspace model. In this case, correlations between the boundary spins are next-neighbour correlations. The reduced equations of motion are

$$\frac{\mathrm{d}\langle \hat{J}^x_1\rangle}{\mathrm{d}t} = 2\,\alpha\left(\langle \hat{J}^z_1\rangle\langle \hat{J}^y_3\rangle - \langle \hat{J}^y_1\rangle\langle \hat{J}^z_3\rangle + \Delta(J^z_1 J^y_3) - \Delta(J^y_1 J^z_3)\right) \tag{4.85}$$

and cyclic for the y and z components. For the second horizontal spin, $\mathbf{J}_3$, we have

$$\frac{\mathrm{d}\langle \hat{J}^x_3\rangle}{\mathrm{d}t} = 2\,\alpha\left(\langle \hat{J}^y_1\rangle\langle \hat{J}^z_3\rangle - \langle \hat{J}^z_1\rangle\langle \hat{J}^y_3\rangle + \Delta(J^y_1 J^z_3) - \Delta(J^z_1 J^y_3)\right) = -\frac{\mathrm{d}\langle \hat{J}^x_1\rangle}{\mathrm{d}t} \tag{4.86}$$

and again cyclic for the y and z components. The equality $\mathrm{d}\langle\hat{\mathbf{J}}_1\rangle/\mathrm{d}t = -\mathrm{d}\langle\hat{\mathbf{J}}_3\rangle/\mathrm{d}t$ can be read off from the equations of motion, but it also follows directly from the conservation of (4.9). The vertical spin can be obtained from the horizontal ones by the simple constraint $\langle\hat{\mathbf{J}}_2\rangle = \langle\hat{\mathbf{J}}_1\rangle - \langle\hat{\mathbf{J}}_3\rangle$.

We will first solve the corresponding classical equations, which are as above but

with zero covariances. We proceed by perturbation theory with respect to α, so that we have constant spins to zeroth order. Upon repeatedly inserting lower-order solutions in the equations of motion, we proceed up to second order and obtain

$$\mathbf{J}_1^{(2)}(t) = \mathbf{A}_1 + 2\,\alpha\,\mathbf{B}_1\,t + 4\,\alpha^2\,\mathbf{C}_1 t^2 + \cdots \tag{4.87}$$

$$\mathbf{J}_3^{(2)}(t) = \mathbf{A}_3 + 2\,\alpha\,\mathbf{B}_3\,t + 4\,\alpha^2\,\mathbf{C}_3 t^2 + \cdots\,, \tag{4.88}$$

where $\mathbf{A}_i$ are free constant vectors. These approximate solutions are valid up to $t \sim 1/\alpha$, respecting the perturbative regime.

The remaining coefficients

$$B_1^x = A_1^z A_3^y - A_1^y A_3^z \tag{4.89}$$

and

$$C_1^x = -A_1^y B_3^z - B_1^y A_3^z + A_1^z B_3^y + B_1^z A_3^y\,, \tag{4.90}$$

and cyclic for the y and z components, are also constant but strictly related to $\mathbf{A}_i$. From (4.86), we have that $\mathbf{B}_1 = -\mathbf{B}_3$ and $\mathbf{C}_1 = -\mathbf{C}_3$. Therefore,

$$\begin{aligned} C_1^x &= (A_1^z A_3^x - A_1^x A_3^z)A_3^z - A_1^y(A_1^x A_3^y - A_1^y A_3^x) - (A_1^x A_3^y - A_1^y A_3^x)A_3^y + A_1^z(A_1^z A_3^x - A_1^x A_3^z) \\ &= -A_1^x\left((A_3^y)^2 + (A_3^z)^2\right) + A_3^x\left((A_1^y)^2 + (A_1^z)^2\right) + A_1^z A_3^z\,(A_3^x - A_1^x) + A_1^y A_3^y\,(A_3^x - A_1^x) \\ &= A_3^x\,|\mathbf{A}_1|^2 - A_1^x\,|\mathbf{A}_3|^2 + (\mathbf{A}_1\cdot\mathbf{A}_3)\,(A_3^x - A_1^x)\,, \end{aligned} \tag{4.91}$$

which enables the vector coefficient $\mathbf{C}_3$ expressing purely in terms of constant vectors $\mathbf{A}_i = A_i\hat{A}_i$:

$$\begin{aligned} \mathbf{C}_3 = -\mathbf{C}_1 &= A_3^2\mathbf{A}_1 - A_1^2\mathbf{A}_3 + (\mathbf{A}_1\cdot\mathbf{A}_3)\,(\mathbf{A}_1 - \mathbf{A}_3) \\ &= A_1 A_3\big[(A_3 + (\hat{A}_1\cdot\hat{A}_3)A_1)\hat{A}_1 - (A_1 + (\hat{A}_1\cdot\hat{A}_3)A_3)\hat{A}_3\big]\,. \end{aligned} \tag{4.92}$$

As one possible choice of initial conditions, we could impose that all spins other than the boundary ones (that is, only the vertical spin in the present model) are zero. Therefore, for a single node, $\mathbf{J}_2(0) = 0$ and $\mathbf{A}_1 = \mathbf{A}_3$. Equations (4.89) and (4.90) then imply that $\mathbf{B}_i = 0 = \mathbf{C}_i$, and all spins remain constant in time. This result, although it is classical, agrees with the trivial dynamics in our minimal minisuperspace model.

We now include moment terms and find solutions of the quantum theory, again perturbative in α. In order to obtain information about the boundary correlations, we should compute quantities such as $\Delta(J_1^x J_3^y)$ from

$$\frac{\mathrm{d}\Delta(J_1^x J_3^y)}{\mathrm{d}t} = 2\,\alpha\,\big(- \langle \hat{J}_1^y\rangle \Delta(J_3^y J_3^z) + \langle \hat{J}_3^y\rangle \Delta(J_1^z J_3^y) + \langle \hat{J}_1^z\rangle \Delta((J_3^y)^2) - \langle \hat{J}_3^z\rangle \Delta(J_1^y J_3^y) + \langle \hat{J}_1^z\rangle \Delta(J_1^x J_3^x) - \langle \hat{J}_1^x\rangle \Delta(J_1^x J_3^z) - \langle \hat{J}_3^z\rangle \Delta((J_1^x)^2) + \langle \hat{J}_3^x\rangle \Delta(J_1^x J_1^z)\big) \tag{4.93}$$

We will also need to consider

$$\frac{\mathrm{d}\Delta(J_1^y J_3^z)}{\mathrm{d}t} = 2\,\alpha\,\big(- \langle \hat{J}_1^z\rangle \Delta(J_3^z J_3^x) + \langle \hat{J}_3^z\rangle \Delta(J_1^x J_3^z) + \langle \hat{J}_1^x\rangle \Delta((J_3^z)^2) - \langle \hat{J}_3^x\rangle \Delta(J_1^z J_3^z) + \langle \hat{J}_1^x\rangle \Delta(J_1^y J_3^y) - \langle \hat{J}_1^y\rangle \Delta(J_1^y J_3^x) - \langle \hat{J}_3^x\rangle \Delta((J_1^y)^2) + \langle \hat{J}_3^y\rangle \Delta(J_1^y J_1^x)\big) \tag{4.94}$$

and

$$\frac{\mathrm{d}\Delta(J_1^x J_3^z)}{\mathrm{d}t} = 2\,\alpha\,\big(- \langle \hat{J}_1^y\rangle \Delta((J_3^z)^2) + \langle \hat{J}_3^y\rangle \Delta(J_1^z J_3^z) + \langle \hat{J}_1^z\rangle \Delta(J_3^y J_3^z) - \langle \hat{J}_3^z\rangle \Delta(J_1^y J_3^z) + \langle \hat{J}_1^x\rangle \Delta(J_1^x J_3^y) - \langle \hat{J}_1^y\rangle \Delta(J_1^x J_3^x) - \langle \hat{J}_3^x\rangle \Delta(J_1^x J_1^y) + \langle \hat{J}_3^y\rangle \Delta((J_1^x)^2)\big) \tag{4.95}$$

For generic initial conditions, these covariances will have the same quadratic form to second order in α, using non-zero initial fluctuations. However, in some specific cases the covariances remain constant, corresponding to stable initial configurations. In particular, we are interested in whether our classical solutions (4.87) are perturbatively stable within a semiclassical treatment of the quantum dynamics. We must then test whether the covariance terms in (4.85) change the behavior.

As before, we first assume that the initial expectation values are such that $\mathbf{J}_2(0) = 0$, or $\mathbf{A}_1 = \mathbf{A}_3$. Moreover, we assume fluctuations and covariances as we found them for the corresponding ground state in the minimal minisuperspace model, given by (4.43): $\Delta((J^x)^2) = \Delta((J^y)^2) = \frac{1}{2}\hbar|\langle \hat{J}^z\rangle|$, now for both horizontal spins in the single-node model. This result had been derived by assuming the spin expectation values to point in the z-direction, which we will also do now. Moreover, we have initially zero covariances between components of the two spins.

Assuming the spin expectation values to point in the z-direction leaves only three non-zero terms in (4.93), two of which vanish for zero initial covariances. We are left with $\langle \hat{J}_1^z\rangle \Delta((J_3^y)^2) - \langle \hat{J}_3^z\rangle \Delta((J_1^y)^2)$. This difference is zero initially

because the fluctuations and expectation values on the two horizontal links are the same. Therefore, $\mathrm{d}\Delta(J_1^x J_3^y)/\mathrm{d}t = 0$ and this covariance remains zero to the orders considered here. Similarly, (4.94) and (4.95) remain zero, and the covariance terms in (4.85) do not contribute for this choice of initial values. The configuration corresponding to the minimal minisuperspace model is therefore dynamically stable within the single-node model.

For the ground-state configurations of the interacting minisuperspace models we also obtain perturbative stability, but the arguments are slightly different in the case of antiparallel alignment. In (4.93), the fluctuation terms no longer cancel out because $\langle \hat{J}_3^z \rangle = -\langle \hat{J}_1^z \rangle$. However, there are now two non-zero covariance terms in (4.93) because $\Delta(J_1^x J_3^x) = \Delta(J_1^y J_3^y) = -\frac{1}{2}\hbar|\langle \hat{J}^z \rangle|$ from (4.53), where $\langle \hat{J}^z \rangle$ on the right could now refer to either $\hat{J}_1^z$ or $\hat{J}_3^z$ because their absolute values are equal. We now have four non-zero individual terms in (4.93), but they all cancel out for the given initial values. Again, we have dynamical stability of the ground state.

Before we move on to two nodes, we confirm the ground-state covariances for a spin-1/2 system. For $\gamma < 0$ and spins pointing in the z-direction, the ground state $|J_1^z, J_3^z\rangle = |1/2, 1/2\rangle$ is uncorrelated and has zero spin-spin covariance $\Delta(J_1^x J_3^x)$ as used. For $\gamma < 0$, the ground state is the singlet $2^{-1/2}(|1/2, -1/2\rangle - |-1/2, 1/2\rangle$, which is correlated and leads to $\langle \hat{J}_1^x \hat{J}_3^x \rangle = -\frac{1}{4}\hbar^2$ by standard calculations. Since $\langle \hat{J}_1^x \rangle = 0 = \langle \hat{J}_3^x \rangle$ in this state, we have $\Delta(J_1^x J_3^x) = -\frac{1}{4}\hbar^2 = -\frac{1}{2}\hbar|\langle \hat{J}_3^z \rangle|$ as derived in (4.53).

4.6.2.2 Two-node graph and beyond

For the two-node graph, the evolution equations of the boundary spins at the edges are of a similar form as in the case of a single-node graph:

$$\frac{\mathrm{d}\langle \hat{J}_1^x \rangle}{\mathrm{d}t} = 2\,\alpha \left(\langle \hat{J}_1^z \rangle \langle \hat{J}_3^y \rangle - \langle \hat{J}_1^y \rangle \langle \hat{J}_3^z \rangle + \Delta(J_1^z J_3^y) - \Delta(J_1^y J_3^z) \right) \tag{4.96}$$

$$\frac{\mathrm{d}\langle \hat{J}_5^x \rangle}{\mathrm{d}t} = 2\,\alpha \left(\langle \hat{J}_3^y \rangle \langle \hat{J}_5^z \rangle - \langle \hat{J}_3^z \rangle \langle \hat{J}_5^y \rangle + \Delta(J_3^y J_5^z) - \Delta(J_3^z J_5^y) \right) \tag{4.97}$$

but now they couple to internal spins. For the internal horizontal spin, $\hat{\mathbf{J}}_3$, we have

$$\frac{\mathrm{d}\langle \hat{J}_3^x\rangle}{\mathrm{d}t} = 2\,\alpha\,\big((\langle \hat{J}_1^y\rangle + \langle \hat{J}_5^y\rangle)\langle \hat{J}_3^z\rangle - (\langle \hat{J}_1^z\rangle + \langle \hat{J}_5^z\rangle)\langle \hat{J}_3^y\rangle + \Delta(J_1^y J_3^z) - \Delta(J_1^z J_3^y) + \Delta(J_3^z J_5^y) - \Delta(J_3^y J_5^z)\big) = -\tfrac{\mathrm{d}\langle \hat{J}_1^x\rangle}{\mathrm{d}t} - \tfrac{\mathrm{d}\langle \hat{J}_5^x\rangle}{\mathrm{d}t}\,. \tag{4.98}$$

Classical solutions up to second order in α are

$$\mathbf{J}_1^{(2)}(t) = \mathbf{A}_1 + 2\,\alpha\,\mathbf{B}_1\,t + 4\,\alpha^2\,\mathbf{C}_1 t^2 + \cdots \tag{4.99}$$

$$\mathbf{J}_5^{(2)}(t) = \mathbf{A}_5 + 2\,\alpha\,\mathbf{B}_5\,t + 4\,\alpha^2\,\mathbf{C}_5 t^2 + \cdots\,. \tag{4.100}$$

With (4.98), the solution for the internal spin is

$$\mathbf{J}_3^{(2)}(t) = \mathbf{A}_3 + 2\,\alpha\,\mathbf{B}_3\,t + 4\,\alpha^2\,\mathbf{C}_3 t^2 + \cdots\,, \tag{4.101}$$

where $\mathbf{B}_3 = -(\mathbf{B}_1 + \mathbf{B}_5)$ and $\mathbf{C}_3 = -(\mathbf{C}_1 + \mathbf{C}_5)$ follow from the conversation of the total spin. The coefficients $\mathbf{C}_3$ can be obtained by replacing $\mathbf{A}_1 \to \mathbf{A}_1 + \mathbf{A}_5$ in (4.92):

$$\mathbf{C}_3 = A_3^2\,(\mathbf{A}_1 + \mathbf{A}_5) - |\mathbf{A}_1 + \mathbf{A}_5|^2\mathbf{A}_3 + \big[(\mathbf{A}_1 + \mathbf{A}_5)\cdot\mathbf{A}_3\big]\,(\mathbf{A}_1 + \mathbf{A}_5 - \mathbf{A}_3)\,. \tag{4.102}$$

For the vertical spins $\mathbf{J}_2$ and $\mathbf{J}_4$ we then have

$$\mathbf{J}_2^{(2)}(t) = \mathbf{J}_1^{(2)}(t) - \mathbf{J}_3^{(2)}(t) = \mathbf{A}_1 - \mathbf{A}_3 + 2\,\alpha\,(2\mathbf{B}_1 + \mathbf{B}_5)\,t + 4\,\alpha^2\,(2\mathbf{C}_1 + \mathbf{C}_5)t^2 + \cdots$$
$$\mathbf{J}_4^{(2)}(t) = \mathbf{J}_3^{(2)}(t) - \mathbf{J}_5^{(2)}(t) = \mathbf{A}_3 - \mathbf{A}_5 - 2\,\alpha\,(\mathbf{B}_1 + 2\,\mathbf{B}_5)\,t - 4\,\alpha^2\,(\mathbf{C}_1 + 2\mathbf{C}_5)t^2 + \cdots$$

We need equations of motion for covariances in order to extend the classical solutions to the semiclassical regime. These equations for correlations of neighboring spins are very similar to the equations of the single-node case, but we can now also have changing values of more distant spins, such as

$$\frac{\mathrm{d}\Delta(J_1^x J_5^y)}{\mathrm{d}t} = 2\,\alpha\,\big(-\langle \hat{J}_1^y\rangle\Delta(J_3^z J_5^y) + \langle \hat{J}_3^y\rangle\Delta(J_1^z J_5^y) + \langle \hat{J}_1^z\rangle\Delta(J_3^y J_5^y) - \langle \hat{J}_3^z\rangle\Delta(J_1^y J_5^y) - \langle \hat{J}_3^x\rangle\Delta(J_1^x J_5^z) - \langle \hat{J}_5^z\rangle\Delta(J_1^x J_3^x) + \langle \hat{J}_3^z\rangle\Delta(J_1^x J_5^x) + \langle \hat{J}_5^x\rangle\Delta(J_1^x J_3^z)\big) \tag{4.103}$$

for the boundary spins of the two-node graph. For spin expectation values pointing in the z-direction, there are four potentially non-zero terms, $\langle \hat{J}_1^z\rangle\Delta(J_3^y J_5^y) -$

$\langle\hat{J}_5^z\rangle\Delta(J_1^xJ_3^x)+\langle\hat{J}_3^z\rangle(\Delta(J_1^xJ_5^x)-\Delta(J_1^yJ_5^y))$. The covariances are zero unless we have a state with antiparallel orientation of neighboring spins. The four remaining terms then cancel out because $\langle\hat{J}_1^z\rangle=-\langle\hat{J}_3^z\rangle=\langle\hat{J}_5^z\rangle$ and $\Delta(J_1^xJ_5^x)=\Delta(J_1^yJ_5^y)$.

At this point we have to be careful when we compare minisuperspace configurations with the exact ground state(s) of the two-node model, which is an odd-number spin chain and has strong finite-size effects. Diagonalizing the Hamiltonian $\alpha(\hat{\mathbf{J}}_1\cdot\hat{\mathbf{J}}_3+\hat{\mathbf{J}}_3\cdot\hat{\mathbf{J}}_5)$ in the spin-1/2 case leads to the degenerate ground states $\psi_1=6^{-1/2}(|-1/2,1/2,1/2\rangle-2|1/2,-1/2,1/2\rangle+|1/2,1/2,-1/2\rangle)$ and $\psi_2=6^{-1/2}(|-1/2,-1/2,1/2\rangle-2|-1/2,1/2,-1/2\rangle+|1/2,-1/2,-1/2\rangle)$. Choosing the first state to be specific, one can then compute the expectation values $\langle\hat{J}_1^z\rangle=\frac{1}{3}\hbar=\langle\hat{J}_5^z\rangle$ and $\langle\hat{J}_3^z\rangle=-\frac{1}{6}\hbar$. These values are next-neighbor antiparallel, but do not obey $\langle\hat{J}_1^z\rangle=-\langle\hat{J}_3^z\rangle=\langle\hat{J}_5^z\rangle$. Moreover, we have the covariances $\Delta(J_1^xJ_3^x)=-\frac{1}{6}\hbar^2=\Delta(J_1^yJ_3^y)$ which do not obey (4.53), and we have $\Delta(J_1^zJ_3^z)=-\frac{1}{9}\hbar^2$. There are also distant covariances such as $\Delta(J_1^xJ_5^x)=\frac{1}{12}\hbar^2=\Delta(J_1^yJ_5^y)$ and $\Delta(J_1^zJ_5^z)=-\frac{1}{36}\hbar^2$. Although these values do not show the generic antiparallel behavior, one can still see that all terms in (4.103) cancel out.

The expressions for $\mathbf{B}_i$ and $\mathbf{C}_i$ in terms of $\mathbf{A}_i$ are very similar to those in (4.89) and (4.90), just with different labels. (The relation (4.91) for $\mathbf{C}_i$ in terms of $\mathbf{A}_i$, however, has a different form for multiple nodes because it has been derived for the single-node graph using $\mathbf{B}_3=-\mathbf{B}_1$.) For ground-state configurations of minisuperspace models we therefore obtain the same cancelations as in the single-node model because these considerations depend only on the expectation values and moments of horizontal spins on neighboring links. In the two-node model, one can choose initial conditions such that all vertical spins have zero expectation values and covariances with any other spins. Therefore, $\mathbf{J}_4^{(2)}(0)=\mathbf{J}_2^{(2)}(0)=0$ and $\mathbf{A}_1^{(0)}=\mathbf{A}_3^{(0)}=\mathbf{A}_5^{(0)}$. This implies that $\mathbf{B}_i=0=\mathbf{C}_i$, and all spins remain constant in time as in the single-node.

The same pattern is then realized also for more nodes, and we conclude that the various ground states are dynamically stable. The minisuperspace models with Hamiltonians $\hat{H}^{(1)}_{\text{mini}}$ and $\hat{H}^{(2)}_{\text{mini}}$ predict the same ground-state configurations as the discrete theory, and these minisuperspace states are therefore stable within the discrete model. The minisuperspace model with Hamiltonian $\hat{H}^{(3)}_{\text{mini}}$, however, is unstable. It not only predicts a ground-state configuration that does not agree with any fundamental ground state, it also has unstable dynamics when its ground-state

configuration is embedded in a fundamental spin chain. Unlike in the other two models, there are then three neighboring spins $\mathbf{J}_{2i_c-3}$, $\mathbf{J}_{2i_c-1}$ and $\mathbf{J}_{2i_c+1}$ around the central node at $i_c = (N+1)/2$, such that $\langle\hat{\mathbf{J}}_{2i_c-3}\rangle = \langle\hat{\mathbf{J}}_{2i_c-1}\rangle = -\langle\hat{\mathbf{J}}_{2i_c+1}\rangle$, and no cancellations happen in (4.103).

4.7 Possible implications for quantum cosmology

We have analyzed four different minisuperspace models of a spin system related to the Heisenberg spin chain. The first model resembles the traditional construction of quantum-cosmology models in which only homogeneous degrees od freedom without spatial variation are considered. In the present context, such a model does not capture the dynamical nature of coupled spins. The second model is a more recent proposal to apply mathematical constructions of condensate states to quantum cosmology. The dynamics is then quite different from a traditional minisuperspace model. In particular, a non-trivial dynamics is now realized even though the degrees of freedom included in the model are the same. The remaining models incorporate additional degrees of freedom in two different ways. They both lead to non-trivial dynamics and in this sense improve the reduction. However, details of ground states and stability are very different in the two models, indicating that good knowledge of the fundamental dynamics is important for a successful construction of minisuperspace models. This conclusion is our first result in an application to quantum cosmology: Traditional minisuperspace models start with a reduction of the classical theory, and then quantize by using some ideas related to candidates for full quantum gravity. But if they do not directly address the full dynamics, they may be in danger of missing crucial information, just as our model Hamiltonian $\hat{H}^{(4)}_{\rm mini}$ does compared with $\hat{H}^{(3)}_{\rm mini}$.

Our successful Hamiltonian $\hat{H}^{(3)}_{\rm mini}$ is similar to the sublattice Hamiltonians introduced in [137] for Heisenberg spin chains. The detailed analysis of this work showed that such an approximation, for given chain length N, is better for larger spin lengths s on the chain. If a similar statement is true for the dynamics of quantum cosmology, it would indicate that a coarse-graining procedure applied before symmetry reduction could improve models of quantum cosmology, for such a procedure would combine the small fundamental spins of $s = 1/2$ to systems of larger spin lengths. Coarse graining in gravitational, and in particular background-

independent theories, is not well-understood, but proposals have been made for instance in [110, 111]. It is also encouraging that sublattice structures can be found in spin systems with more than one dimensions [148, 149].

Our minisuperspace Hamiltonian $\hat{H}^{(4)}_{\rm mini}$ is based on a construction similar to the separate-universe approximation of classical cosmology. Its failure to model properties of ground states and stability indicates that it is not a good quantum approximation for all kinds of fundamental dynamics. Its lack of stability is of particular concern, resulting from the fact that in this model the minisuperspace ground state does not correspond to the ground state of the discrete theory. We therefore have provided an explicit example of important fundamental properties not captured by a minisuperspace model. Such models are unstable if energy can be exchanged with an environment, and one might conclude that they are unreliable.

However, not just ground states but also excited states may be stable in an isolated system if no energy can be exchanged with an environment. This is the situation usually realized in models of quantum cosmology, where the state represents the whole universe with nothing outside. The stability of excited states then results in a large variety of candidates for homogeneous configurations. Nevertheless, some caution toward such minisuperspace states used in quantum cosmology is still required: Our spin system can be taken as a model for quantum space, in which near homogeneity should be possible and stable under evolution. However, there should also be matter, with additional degrees of freedom that could be placed on the same graph used for our spin chain but representing a different system of degrees of freedom. There could then be energy exchange between the spin system analyzed here and the new matter system. We would be back at the question whether a homogeneous spin configuration, representing quantum space, can be stable within the coupled system if it does not capture the correct ground state. The question of how matter is coupled to quantum space therefore seems important in the context of the emergence and stability of correlated quantum-cosmology states.

Chapter 5
Super cosmic variance from non-Gaussian statistics

In section 2.6 we simply compute two-point correlation function of a free quantum field on a Minkowski spacetime which served as a toy model in order to perform more sophisticated and realistic (connectable to observations) calculations about correlation functions of quantum fields on curved spacetimes. In this chapter our primary focus will be the statistical properties (correlation functions) primordial perturbations fields which originated from the quantum fluctuations during inflationary era that is assumed in the very early universe.

5.1 Introduction

On larger scales of space, the energy-mass contents of the observable universe can be approximated by a homogeneous and isotropic distribution. One of the clearest picture of this type of distributions is the *Cosmic Microwave Background* (CMB) where the thermal fluctuations are only up to one part in 10^5. This particular type of possible anisotropy reveals a picture of the early universe due to the fact that the CMB photons decoupled from matter contents when the interaction rate of the photons with baryons becomes close to the expansion rate of the universe. The significance of these CMB anisotropies along the history of cosmological physics is that the tiny observed anisotropies are not causally connected at the very early moments of the observable universe according to standard hot "Big Bang" approach.

The prominent candidate of resolving the origin of the CMB anisotropies (or so called "homogeneity problem") is known as *inflationary* mechanism [150–153]. This

mechanism describes a period of exponentially accelerated expansion at a typical energy scale around four orders of magnitude less than the Planck energy 10^{19} GeV at the very early moment of the universe. The remarkable consequence of the presence of inflation is that all the perturbations, which are responsible for CMB or Large Scale Structure, are originated from primordial quantum fluctuations [153–155]. The equation of state for a standard inflationary mechanism is established by taking $p \approx -\rho$ for pressure p and energy density ρ and on equal footing the energy density should stay constant during the accelerated expansion so that the inflationary era can sustain sufficiently to resolve the largest modes in CMB. An exact exponentially expanding spaces are characterized by spatial foliations of de Sitter spacetimes which is one of classes of maximally symmetric spacetimes as in Minkowski spacetimes but with a positive cosmological constant [59, 156]. However, the inflationary era must be finite for the observable universe so that the breaking of the time translation symmetry for a de Sitter spacetime is quantified by a parameter knowns as *slow-roll* parameter ϵ.

Possible inhomogeneities that are observed today are related to the primordial perturbations in spacetime metric or the energy density of possible matter contents at the very early moment of the universe. In particular, we will be mainly interested in the scalar perturbations Φ part of the spatial metric with a specific gauge: $a(t)^2\big[\delta_{ij}(1+2\Phi(\mathbf{x}))\big]dx^i dx^j$ right after the inflation where $a(t)$ is the scale factor. According to general relativity [157], the spacetime metric is an dynamical entity and coupled to the matter content, which simply implies that any variations in the energy density of matter and radiation are directly related to the perturbations in the metric. Specifically, if a single degree of freedom is responsible both for inflationary mechanism and seeds the inhomogeneities then we call the perturbations of different quantities as *adiabatic* (the different contributions have the same relative amplitude during the inflation).

The gauge-invariant primordial curvature perturbations $\zeta \equiv \Phi - (\dot{a}\delta\rho)/(a\dot{\rho})$ [158, 159] are our primary source of information about the inflationary era of the universe. Ideally, we can extract an understanding of the underlying physics responsible for inflation from the details of the correlations observed in the Cosmic Microwave Background (CMB) inhomogeneities and the large scale structure. The adiabatic curvature perturbations serve as determining the evolution of cosmological perturbations so that focusing on the statistics of the curvature perturbations enable

to extract the statistical features of the relevant cosmological structures.

The primordial curvature perturbations, as initial conditions for the history of universe, are generated from the quantum fluctuations during inflation in the ground state such that each Fourier mode as in (2.64) can be built out of a quantum harmonic oscillator with a finite dispersion around the mean of the mode. More importantly, due to the exponential expansion the uncertainties intrinsic to the quantum field during inflation stretched to the cosmological scales. Therefore, there is direct way of conditioning the probability distributions for the observable quantities in the sky by the probability distributions for the primordial perturbations. Complete derivations and explanations of the gauge-invariant curvature perturbations can be found in these prominent review lectures and books [160–162].

5.2 Super cosmic variance

We have a natural limitation called as *cosmic variance* of obtaining the probability distributions for cosmological quantities since we only have one realization of these perturbations unlike the experiments in particle physics. Sampling a probability distribution for a quantity around a global ensemble distribution leads to a sample variance which is inversely proportional to the number possible samples for that quantity. For the primordial perturbations $\zeta(\mathbf{x})$ there are very small number of modes are accessible on large scales such that there is one only realization that causes larger cosmic variance for the global ensemble distribution of $\zeta(\mathbf{x})$.

Another actual limitation for extracting distributions for perturbations is that we can only access to a finitely sized universe. In particular a long duration of inflation leads to a large post-inflationary volume. The length of inflation is quantified by so called number of *e-folds*, $dN \equiv d\log a$. For resolving the homogeneity problem such that in order to have the largest modes in CMB, the minimum e-folds needs to be ~ 60. Therefore, the possibility that inflation lasts longer than this threshold number of e-folds, corresponds to a post-inflationary volume which is larger than the observable universe. This fact, observing only a finite volume universe, limits us to access perturbations on larger scales.

These limitations naturally lead to investigate whether the probability distributions of the perturbations in our observed volume correspond to a representative of the global distribution or not. Otherwise, they may be biased due to our particular

sampling. Assuming that the post-inflationary volume is larger than the observed volume, then if the long modes (scales larger than typical Hubble scale H_0^{-1}) of curvature perturbations correlated with short modes of curvature perturbations so that the different Fourier modes $\mathbf{k}$ are correlated in the probability distribution of ζ, then the small scales perturbations are affected by the long scales ones and the considered sample in the observed volume is systematically biased. This phenomena is called as *super cosmic variance* (SCV). In particular this type of *mode coupling* of different scales can emerge for a non-Gaussian probability distribution.

We observe only a finite volume of the universe and have no reason to expect that the current size of that volume is anything special: there are likely to be at least some *super horizon* modes with more or less the same properties as those that have already re-entered the horizon. That supposition is critically important in comparing statistical observations to theory. In the case of exactly Gaussian fluctuations the finite size of our Hubble volume is the origin of the familiar cosmic variance uncertainties in the power spectrum fit.

5.3 Primordial non-Gaussianity

The origin of the primordial non-Gaussianity for a given simple inflationary model can be seen by studying higher order perturbations in the action of a scalar field minimally coupled to gravity (with unit Planck mass $M_P = 1$):

$$S = \int d^4x\sqrt{g}\left[\frac{R}{2} - \frac{1}{2}(\nabla\phi)^2 - V(\phi)\right], \tag{5.1}$$

For the perturbations, we only restrict to the scalar perturbations with a specific gauge $\delta\phi$ such that all the scalar perturbations degrees of freedom are derived from metric perturbations. The metric is expanded in terms of the curvature perturbations ζ on uniform density hypersurfaces. At linear order of canonical perturbation theory the two point function at equal time in the Fourier space at the end of inflation is

$$\langle\zeta(\mathbf{k}_1)\zeta(\mathbf{k}_2)\rangle = (2\pi)^3 P_\zeta \delta^3(\mathbf{k}_1 + \mathbf{k}_2), \quad P_\zeta = \frac{\dot{a}^2}{8\pi a^2 \epsilon} \tag{5.2}$$

where $\epsilon := 1 - \ddot{a}a/\dot{a}^2$ is the first order slow roll parameter. This expectation value is the ensemble average of realization in statistics but in this case there is only one realization such that the ensemble is at the same time averaging over space or all possible Fourier modes (Ergodic theorem) [163]. Naturally, the inflationary initial conditions can be taken as Gaussian random which means for a single mode there are infinitely many realizations by infinite number of directions drawn from a Gaussian distribution. But these initial conditions are actually quantum fluctuations of the scalar field in its ground state. Now we can calculate two-point function of the canonically quantized scalar field $\hat{\phi}$ in its vacuum state on a curved background geometry, FRLW [164]:

$$\langle 0|\hat{\phi}(\mathbf{k}_1)\hat{\phi}(\mathbf{k}_2)|0\rangle = |u_k|^2\delta^3(\mathbf{k}_1 + \mathbf{k}_2)\,, \tag{5.3}$$

where u_k is the mode function of the operator field $\hat{\phi}$ similar to the case in Minkowski spacetimes (2.64)

$$\hat{\phi}(\mathbf{x}, t) = \int \frac{d^3k}{(2\pi)^3}\left[a(\mathbf{k})u_k(t)e^{i\mathbf{k}\cdot\mathbf{x}} + a^\dagger(\mathbf{k})u_k^*(t)e^{-i\mathbf{k}\cdot\mathbf{x}}\right]. \tag{5.4}$$

The mode function $|u_k|^2 \Longleftrightarrow P(k)$ can be in fact identified to the variance of some Gaussian distribution for a field $\phi(\mathbf{k})$. Although current constraints show no sign of primordial non-Gaussianities, it is natural to expect deviations from Gaussian distributions since we know that the expansion and acceleration are driven by gravity which is highly non-linear. Therefore, it is promising to concentrate on the higher-order correlations by going beyond linear perturbation theory where the leading correction to the two-point function is three-point function of correlated three modes.

In general, the non-Gaussian probability distribution of the curvature perturbation ζ can be completely determined by all the set of connected N-point correlation functions[1], for instance in Fourier space:

$$\langle\zeta(\mathbf{k}_1)\zeta(\mathbf{k}_2)\cdots\zeta(\mathbf{k}_N)\rangle_c := (2\pi)^3\delta^3\Big(\sum \mathbf{k}_i\Big)P_\zeta^{(N)}(\mathbf{k}_1, \mathbf{k}_2, \cdots, \mathbf{k}_N)\,, \tag{5.5}$$

where *polyspectra* $P_\zeta^{(N)}$ is so called *polyspectra* which characterize the momentum

[1]The connected part of the N-point function (non-Gaussian) part is not captured by applying Wick?s theorem to express Gaussian part as a product of two-point functions.

dependence of the correlation functions. They are directly related to the size and shape of the momentum-space polygons formed by the N momenta (see Fig.5.1) by assuming statistical isotropy and to the "momentum conservation" in the delta function expression in (5.5) by assuming translation invariance. The leading-order non-Gaussian statistics is called the *bispectrum*: $B_\zeta \equiv P_\zeta^{(3)}$.

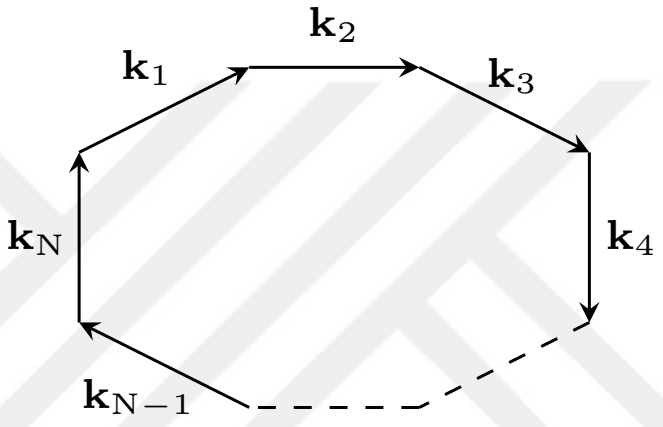

Figure 5.1. Momentum-space polygons formed by the N momenta $\mathbf{k}_i$ such that $\sum_{i=1}^{N} \mathbf{k}_i = 0$.

5.4 Super cosmic variance from general type non-Gaussian fields

A particular part of the non-Gaussian space, the coupling between long and short wavelength fluctuations, is of interest from both of these viewpoints. The bias from super horizon modes is completely unmeasurable, but the qualitative conclusions we draw about the origin of fluctuations can change when we allow for it [165–175]. The *Planck* satellite bounds demonstrate that the fluctuations are very close to Gaussian [176], but the constraints have not crossed the theoretically interesting threshold to rule out entire classes of physics beyond single field slow-roll [177]. Fortunately, no such mode coupling has been detected within our universe yet, but current observational limits (e.g., from the Planck satellite results [176] and the most recent constraints from quasars [178]) do not rule out this possibility.

The expectation for interesting threshold levels of non-Gaussianity comes from

our current understanding of the space of likely models for inflation and the primordial fluctuations. Indeed, many inflation scenarios predict some degree of non-Gaussianity and the details of the correlations would ideally provide a means to distinguish qualitatively different primordial physics. In weighing observational evidence for or against any inflation model that couples modes of different wavelengths we must include these SCV uncertainties. In addition, if *any* non-Gaussianity is detected, we must be sure we understand how to draw robust conclusions about the set of primordial universe models consistent with those measurements. This is a non-trivial task because it is not clear if there are types of non-Gaussianity inflation *cannot* generate and because it is far from obvious how the statistics in biased sub-volumes are related to those of parent distributions with arbitrary non-Gaussian fluctuations. Future constraints on non-Gaussianity will continue to test various inflation scenarios but can also have implications for our understanding of the universe that are independent of the origin of the fluctuations.

Here we consider several scenarios motivated by predictions from currently studied inflation models and demonstrate how the presence of correlations beyond the bispectrum can alter the shape of lower order correlation functions in biased sub-volumes. We will demonstrate that although observations could prove that the source of the primordial fluctuations was not single-clock inflation, constraints on or detections of the shape of the bispectrum can be consistent with single-clock predictions even when super cosmic variance is at work.

5.4.1 The model

An attractive discriminating feature of inflation scenarios is the behavior of the squeezed limit of the primordial bispectrum: that is, how significantly it couples two short wavelength modes to one long wavelength mode (represented by a squeezed triangle in momentum space, with side lengths $k_1 \equiv k_l \ll k_2 \approx k_3 \equiv k_s$) [179]. This limit also indicates how significantly the bispectrum can cause the power spectrum in biased sub-volumes to differ from the global power spectrum (for a concrete example entirely within our universe, see the discussion of non-Gaussian halo bias [180, 181]). A bispectrum of the type generated by single clock inflation, which primarily couples modes of the same wavelength, will give a negligible shift to the power spectrum regardless of the realization of the long wavelength modes. A local

type coupling, on the other hand, can give an interesting amplitude shift [166, 168].

Beyond the bispectrum, all higher order correlation functions can contribute to the biasing of lower order statistics when some modes have longer wavelengths than the size of the spatial region of interest. Scenarios where the non-Gaussian field is any local but non-linear function of a Gaussian field have the nice property that the bispectrum is of the standard local type (up to at most logarithmic corrections) even in biased sub-volumes. And, in sufficiently biased sub-volumes the observed statistics of *any* local, non-linear function (polynomial and without derivatives) of a Gaussian field will be those of a field with the local ansatz [166].

Here, we explore the question of biased statistics for scenarios with non-local bispectra. Our goal is to understand how observations of a necessarily limited set of correlation functions can constrain the space of models of the primordial universe. In particular, the single-clock inflation consistency relations [179, 182–189] indicate how one could rule out single clock inflation, but would a detection of $f_{\rm NL}^{\rm local} = 0$ and $f_{\rm NL}^{\rm equil} \neq 0$ confirm single clock inflation? To address this question we consider bispectral shapes characterized by their degree of divergence with the long wavelength mode, k_l, in the squeezed limit, including k_l^{-1} (equilateral type), k_l^{-2} (sometimes called 'orthogonal' type[2]), and k_l^{-3} (local type).

To consider non-Gaussian scenarios with the desired n-point correlations, we build the field Φ from a series of nonlocal functionals of a Gaussian random field $\phi(x)$,

$$\Phi[\phi(\mathbf{x})] = \phi(\mathbf{x}) + f_{\rm NL}\Phi_2[\phi(\mathbf{x})] + g_{\rm NL}\Phi_3[\phi(\mathbf{x})] + \cdots \,, \tag{5.6}$$

where the subscript on Φ_n indicates how many copies of the Gaussian field appear in the term. The Φ_n will generate the connected parts of the tree-level correlations at order $n+1$ and higher, and we require $\langle \Phi_n \rangle = 0$. We assume the Gaussian field is homogeneous and isotropic. Its statistics are completely determined by the power spectrum, which we take to be scale-invariant for simplicity:

$$\langle \phi(\mathbf{k}_1)\phi(\mathbf{k}_2)\rangle = (2\pi)^3\delta^3(\mathbf{k}_1+\mathbf{k}_2)P_\phi(k_1) \tag{5.7}$$

$$P_\phi(k) = 2\pi^2\frac{\Delta_\phi^2}{k^3} \,. \tag{5.8}$$

[2] A different, also very useful definition of 'orthogonal' comes from looking at possible scale-invariant shapes produced by single clock inflation [190]. With that definition, the orthogonal template diverges as k_l^{-1}.

We will primarily work with the Fourier transform of Φ:

$$\begin{aligned}
\Phi(\mathbf{k}) &= \phi(\mathbf{k}) + f_{\rm NL}\Phi_2(\mathbf{k}) + g_{\rm NL}\Phi_3(\mathbf{k}) + \dots \\
&= \phi(\mathbf{k}) + \frac{f_{\rm NL}}{2!}\int \frac{d^3p_1}{(2\pi)^3}\int d^3p_2\,[\phi(\mathbf{p}_1)\phi(\mathbf{p}_2) - \langle\phi(\mathbf{p}_1)\phi(\mathbf{p}_2)\rangle] \\
&\quad \times N_2(\mathbf{p}_1,\mathbf{p}_2,\mathbf{k})\delta^3(\mathbf{k}-\mathbf{p}_1-\mathbf{p}_2) \\
&\quad + \frac{g_{\rm NL}}{3!(2\pi)^6}\prod_{\ell=1}^{3}\int d^3p_\ell \left[\phi(\mathbf{p}_1)\phi(\mathbf{p}_2)\phi(\mathbf{p}_3) - \sum_{\substack{i=1\\k\neq j\neq i}}^{3}\phi(\mathbf{p}_i)\langle\phi(\mathbf{p}_j)\phi(\mathbf{p}_k)\rangle\right] \\
&\quad \times N_3(\mathbf{p}_1,\mathbf{p}_2,\mathbf{p}_3,\mathbf{k})\delta^3(\mathbf{k}-\sum_{\ell=1}^{3}\mathbf{p}_\ell) + \cdots\,, \qquad (5.9)
\end{aligned}$$

The kernels $N_n(\mathbf{p}_1,\mathbf{p}_2,\dots,\mathbf{p}_n,\mathbf{k})$ are symmetric in the first n entries. The subtracted terms inside the square brackets maintain $\langle\Phi_n\rangle = 0$ and ensure that only connected parts of the n-point functions are generated by each term. Loop corrections to the power spectrum from the non-Gaussian terms go like $(f_{\rm NL}\Delta_\phi)^2$ and $(g_{\rm NL}\Delta_\phi^2)^2$ and the one-loop correction to the bispectrum goes like $g_{\rm NL}\Delta_\phi^2$ (relative to the $\mathcal{O}(f_{\rm NL})$ tree-level bispectrum). Weak non-Gaussianity is defined by requiring those quantities to be $\ll 1$, and if $g_{\rm NL} \lesssim \mathcal{O}(f_{\rm NL}^2)$ the loop correction to the power spectrum from the three point function is parametrically larger than that from the four-point.

To generate our full set of desired correlations, the Φ_n must be non-local. It is notationally easier to first generate the appropriate set of terms in real space, so we consider Φ_n of the form

$$\Phi_n = \partial^{\beta_{2n-1}}(\partial^{\beta_{2n-2}}\phi(\dots(\partial^{\beta_2}\phi\partial^{\beta_1}\phi)))(\mathbf{x})\,, \qquad (5.10)$$

where the β_i can be negative. To generate the corresponding Fourier transformed terms, we define derivative operators acting on $\phi(\mathbf{x})$ based on the corresponding

momentum space behavior,[3]

$$\partial^n \phi(\mathbf{x}) \equiv \int \frac{d^3k}{(2\pi)^3} k^n \phi(\mathbf{k}) e^{i\mathbf{k}\cdot\mathbf{x}} \,. \tag{5.12}$$

A Φ_2 that can generate the equilateral, orthogonal or local bispectral templates was derived by Scoccimarro et al in [191]. In the next section we review the choice of quadratic terms, taking a slightly different perspective but arriving at the same Φ_2 as [191]. In Section 5.4.3 we generalize the procedure for generating the quadratic terms and consider a Φ_3 designed to induce only the terms in Φ_2 in biased sub-volumes. In Section 5.4.3.4 we examine subsets of the cubic terms that restrict the bispectra induced in biased sub-volumes to local, equilateral, or orthogonal type and consider the implications for theory and observations. In Section 6 we conclude and comment on how our analysis might be further developed.

5.4.2 Quadratic Terms

In this section we derive an expression for Φ_2 using a procedure that can be easily generalized to the cubic term, Φ_3, and beyond. Although our motivation and procedure are slightly different, the result reproduces the expressions derived by Scoccimarro et al [191].

We limit our considerations to bispectra that diverge in the squeezed limit as one, two, or three inverse powers of the long wavelength momentum. Since a local quadratic function, $\phi^2(x)$, yields the most divergent bispectrum, we need to include inverse derivative operators in order to reduce the divergence. We therefore start with the following family of terms quadratic in the Gaussian field

$$\partial^{\alpha_3}(\partial^{\alpha_2}\phi\partial^{\alpha_1}\phi), \tag{5.13}$$

[3]Note that ∂^n is not in general a genuine derivative operator because it does not obey the Leibniz rule,

$$\begin{aligned}
[\partial^n(\phi_1\phi_2)](\mathbf{k}) &= k^n \int \frac{d^3p}{(2\pi)^3} \phi_1(\mathbf{p})\phi_2(\mathbf{k}-\mathbf{p}) \\
\left[\phi_1\partial^n\phi_2 + \phi_2\partial^n\phi_1\right](\mathbf{k}) &= \int \frac{d^3p}{(2\pi)^3} \phi_1(\mathbf{p})\phi_2(\mathbf{k}-\mathbf{p})(p^n + |\mathbf{k}-\mathbf{p}|^n) \\
\rightarrow \partial^n(\phi_1\phi_2) &\neq \phi_1\partial^n\phi_2 + \phi_2\partial^n\phi_1.
\end{aligned} \tag{5.11}$$

Our notation is related to the one used in Scoccimarro et al [191] by: $(\partial^2)_{\text{here}} = (-\nabla^2)_{\text{there}}$.

with restrictions on the α_i:

- $\sum \alpha_i = 0$. This condition maintains scale-invariance.
- $\alpha_{1,2} \geq 0$. Together with the previous condition, this automatically sets $\alpha_3 \leq 0$. This condition ensures that the infrared (IR) sensitivity to ϕ_l is no stronger than that of local non-Gaussianity. In other words, this rule ensures that the squeezed limit of the bispectrum does not grow like k_l^{-4} or more for small k_l.
- $|\alpha_i| \leq 2$. This restriction generates the *minimal* set of terms required to produce equilateral (k_l^{-1}), orthogonal (k_l^{-2}) or local (k_l^{-3}) type behavior (and corresponds to to setting $u = s = 0$ in [191]). However, there are certainly additional terms with $|\alpha_i| > 2$ that will also generate bispectra with the same squeezed limit behavior. We comment on relaxing this condition in Section 6.

The generic quadratic functional with terms obeying these constraints is

$$\Phi_2[\phi(x)] = [a_1\phi^2 + a_2\partial^{-1}(\phi\partial\phi) + a_3\partial^{-2}(\phi\partial^2\phi) + a_4\partial^{-2}(\partial\phi)^2] - [\text{E.V.}] \ . \quad (5.14)$$

where $-[\text{E.V.}]$ indicates that the expectation values of the terms should be subtracted. The corresponding N_2 kernel (which in this case depends only on the magnitudes of the momenta) is

$$N_2(p_1, p_2, k) = 2a_1 + a_2\frac{p_1 + p_2}{k} + a_3\frac{p_1^2 + p_2^2}{k^2} + 2a_4\frac{p_1 p_2}{k^2} \ . \quad (5.15)$$

A generic homogeneous and isotropic bispectrum for the potential Φ can be written as

$$\langle\Phi(\mathbf{k}_1)\Phi(\mathbf{k}_2)\Phi(\mathbf{k}_3)\rangle = (2\pi)^3\delta^3(\mathbf{k}_1 + \mathbf{k}_2 + \mathbf{k}_3)\ B(k_1, k_2, k_3) \ . \quad (5.16)$$

Our ansatz gives a bispectrum

$$B_\Phi(k_1, k_2, k_3) = f_{\rm NL}P_\phi(k_1)P_\phi(k_2)N_2(k_1, k_2, k_3) + \text{cyc.} \quad (5.17)$$

where there are 2 additional cyclic permutations. Notice that both the a_2 and a_3 terms in Eq.(5.67) generate terms of the type $P(k_1)^{1/3}P(k_2)^{2/3}P(k_3)$ in the bispectrum.

We have already factored out an overall amplitude, $f_{\rm NL}$, from Φ_2. With the usual convention $f_{\rm NL} \equiv 6B_\Phi(k, k, k)/P_\Phi^2(k)$, this leaves a normalization condition

for the coefficients of the individual quadratic terms:

$$a_1 + a_2 + a_3 + a_4 = 1 \ . \tag{5.18}$$

The constraints on the α_i so far allow us to restrict consideration to a subset of possible non-Gaussian fields based on the behavior of the bispectrum. However, any quadratic term will also contribute to the power spectrum of the full, non-Gaussian field

$$\langle \Phi(\mathbf{k}_1)\Phi(\mathbf{k}_2)\rangle = \langle \phi(\mathbf{k}_1)\phi(\mathbf{k}_2)\rangle + f_{\rm NL}^2 \langle \Phi_2(\mathbf{k}_1)\Phi_2(\mathbf{k}_2)\rangle + \dots \tag{5.19}$$

where the dots contain contributions from Φ_3 and higher. The contributions to $P_\Phi(k)$ from the terms in Φ_2 contain an extra integral over momenta p and go like $[N_2(p, |\mathbf{k}-\mathbf{p}|, k)]^2$. The contributions from the a_3 and a_4 terms go like $1/k^4$ times a divergent integral over momenta p (this is easiest to see by considering $k \ll p$). We can force this badly behaved contribution to the loop to vanish by setting

$$a_4 = -a_3 \ . \tag{5.20}$$

We will impose this condition from now on to remove a_4 from all expressions. Insisting on Eq.(5.20) is equivalent to the choice of the coefficient t for the equilateral and orthogonal cases in [191].

5.4.2.1 Recovering the standard bispectral templates

Frequently used bispectral templates with fixed degree of divergence with the long wavelength mode are

$$\begin{aligned}
B_{\rm local} &= 2f_{\rm NL}^{\rm local}(P_\phi(k_1)P_\phi(k_2) + P_\phi(k_1)P_\phi(k_3) + P_\phi(k_2)P_\phi(k_3)) \qquad (5.21)\\
B_{\rm equil} &= 6f_{\rm NL}^{\rm equil}[-P_\phi(k_1)P_\phi(k_2) + 2 \text{ perm.} - 2(P_\phi(k_1)P_\phi(k_2)P_\phi(k_3))^{2/3}\\
&\quad + P_\phi(k_1)^{1/3}P_\phi(k_2)^{2/3}P_\phi(k_3) + 5 \text{ perm.}]\\
B_{\rm orth} &= 6f_{\rm NL}^{\rm orth}[-3P_\phi(k_1)P_\phi(k_2) + 2 \text{ perm.} - 8(P_\phi(k_1)P_\phi(k_2)P_\phi(k_3))^{2/3}\\
&\quad + 3P_\phi(k_1)^{1/3}P_\phi(k_2)^{2/3}P_\phi(k_3) + 5 \text{ perm.}]
\end{aligned}$$

The best constraints on the amplitudes $f_{\rm NL}$ of these templates come from the *Planck* satellite: [192], which limit $f_{\rm NL}^{\rm local} = 2.7 \pm 5.8$, $f_{\rm NL}^{\rm equil} = -42 \pm 75$, and $f_{\rm NL}^{\rm orth} = -25 \pm 39$ at the 68.3% confidence level.

The ansatz in Eq.(5.14) clearly contains the local ansatz

$$\text{Local Bispectrum}: \qquad a_2 = a_3 = a_4 = 0\ . \tag{5.22}$$

To see the conditions that recover the orthogonal and equilateral templates, insert the N_2 kernel from Eq. (5.67) into the general expression for the bispectrum, Eq. (5.66), and take the squeezed limit $k_1 \equiv k_l \ll k_2, k_3 \equiv k_s$:

$$\lim_{k_l \ll k_s} B(k_s, k_s, k_l) = f_{NL} P_\phi(k_l) P_\phi(k_s) \Bigg[(4a_1 + 2a_2 + 2a_3) + (2a_2 - 4a_3)\Big(\frac{k_l}{k_s}\Big) + (2a_2 + 2a_3)\Big(\frac{k_l}{k_s}\Big)^2 + 2a_1\Big(\frac{k_l}{k_s}\Big)^3 \Bigg]. \tag{5.23}$$

where we have already used $a_4 = -a_3$. The equilateral bispectrum scaling k_l^{-1} requires that the coefficients of both the k_l^{-3} and the k_l^{-2} contributions vanish. Since $P(k_l) \propto k_l^{-3}$, these conditions are, respectively

$$4a_1 + 2a_2 + 2a_3 = 0 \qquad \text{and} \qquad 2a_2 - 4a_3 = 0\ . \tag{5.24}$$

Including the normalization condition (5.18), these are sufficient equations to uniquely fix the a_i. The result exactly recovers the equilateral template:

$$\text{Equilateral Bispectrum}: \qquad a_1 = -3,\ a_2 = 4,\ a_3 = 2, a_4 = -2\ . \tag{5.25}$$

The orthogonal bispectrum scaling k_l^{-2} requires only the coefficient of k_l^{-3} to vanish, which is not sufficient information to completely fix all the a_i. That is reasonable since the orthogonal shape was originally defined not by its squeezed limit but by minimizing its overlap with the other templates over a range of momentum configurations. To generate the standard orthogonal template we can add an additional condition, comparable to the orthogonality condition required by [190],

$$a_1^{\text{orth}} = 3\ a_1^{\text{equil}} \tag{5.26}$$

so that all the a_i are fixed:

$$\text{Orthogonal Bispectrum}: \qquad a_1 = -9,\ a_2 = 10,\ a_3 = 8, a_4 = -8\ . \tag{5.27}$$

In the next section we will introduce the long-short wavelength split and see how the conditions in Eq.(5.24) that fix the squeezed limit behavior of the bispectrum can also be directly read off of the real-space expression in Eq.(5.14).

5.4.2.2 The long-short wavelength split

We are interested in the effect of long wavelength background modes on the statistics measured in spatial sub-volumes. To that end, we split the field Φ in Fourier space at a scale k_*,

$$\begin{aligned}\Phi_s(\mathbf{k}) &= \Phi(\mathbf{k})\Theta(k-k_*)\\ \Phi_l(\mathbf{k}) &= \Phi(\mathbf{k})\Theta(k_*-k)\ ,\end{aligned} \tag{5.28}$$

where Θ is the step function. This is only an approximation to splitting the field with a top hat in real space, but our results will not depend on this distinction. Also, in what follows, we will mainly consider momenta far away from the scale k_*, and ignore complications arising from those close to k_*. Applying the Θ-function on the right hand side of $\Phi(\mathbf{k})$, defined in Eq.(5.65), gives

$$\Phi_s(\mathbf{k}) = \phi_s(\mathbf{k}) + f_{\rm NL}\Phi_2^{(s)}(\mathbf{k}) + \dots \tag{5.29}$$

$$\Phi_l(\mathbf{k}) = \phi_l(\mathbf{k}) + f_{\rm NL}\Phi_2^{(l)}(\mathbf{k}) + \dots \tag{5.30}$$

where $\phi_s(\mathbf{k})$ and $\phi_l(\mathbf{k})$ are defined analogously to Eq.(5.28). Writing out the effect of the Θ-function on the quadratic term gives, for the short wavelength quadratic piece,

$$\begin{aligned}\Phi_2^{(s)}(\mathbf{k}) &= \frac{1}{2!(2\pi)^3}\int d^3p_1\, d^3p_2\, N_2(\mathbf{p}_1,\mathbf{p}_2,\mathbf{k})[\phi(\mathbf{p}_1)\phi(\mathbf{p}_2) - [\text{E.V.}]]\,\delta^3(\mathbf{k}-\mathbf{p}_1-\mathbf{p}_2)\\ &\Theta(|\mathbf{p}_1+\mathbf{p}_2|-k_*) = \frac{1}{2!(2\pi)^3}\int_{|\mathbf{p}_1+\mathbf{p}_2|>\mathbf{k}_*} d^3p_1 d^3p_2\, N_2(\mathbf{p}_1,\mathbf{p}_2,\mathbf{k})[\phi_s(\mathbf{p}_1)\phi_s(\mathbf{p}_2)\\ &+2\phi_s(\mathbf{p}_1)\phi_l(\mathbf{p}_2) - [\text{E.V.}]]\,\delta^3(\mathbf{k}-\mathbf{p}_1-\mathbf{p}_2)\end{aligned} \tag{5.31}$$

Here, the second line is obtained from by considering the separate momentum regimes for p_1 and p_2 that satisfy the step function: $\Theta(|\mathbf{p}_1+\mathbf{p}_2|-k_*) = [\Theta(p_1-k_*)\Theta(p_2-k_*)+\Theta(p_1-k_*)\Theta(k_*-p_2)+\Theta(k_*-p_1)\Theta(p_2-k_*)]\Theta(|\mathbf{p}_1+\mathbf{p}_2|-k_*)$. In

the same manner we can write $\Phi_2^{(l)}$ (with some redundancy) as

$$\Phi_2^{(l)}(\mathbf{k}) = \frac{1}{2!(2\pi)^3} \int_{|\mathbf{p}_1+\mathbf{p}_2|<\mathbf{k}_*} d^3p_1\, d^3p_2\, N_2(\mathbf{p}_1,\mathbf{p}_2,\mathbf{k})[\phi_s(\mathbf{p}_1)\phi_s(\mathbf{p}_2)+\phi_l(\mathbf{p}_1)\phi_l(\mathbf{p}_2) - [\text{E.V.}]] \times\delta^3(\mathbf{k}-\mathbf{p}_1-\mathbf{p}_2) \tag{5.32}$$

Notice that in the first term of Eq.(5.32), the angle between short scale modes $\mathbf{p}_1$ and $\mathbf{p}_2$ must be nearly π so they sum to a long mode with magnitude k below the splitting scale.

5.4.2.3 The field observed in biased sub-volumes

We now examine the difference in the global and local statistics of the power spectrum when the quadratic terms above are included. Very generally, the observed field, restricted to points $\mathbf{x}$ within a sub-volume V_S, will take the form

$$\Phi^{\rm obs}(\mathbf{x})|_{x\in V_S} = (\phi+\Phi_1^{\rm SCV}) + f_{\rm NL}(\Phi_2+\Phi_2^{\rm SCV}) + g_{\rm NL}(\Phi_3+\Phi_3^{\rm SCV})\dots\,, \tag{5.33}$$

where the contributions from the Super Cosmic Variance (SCV) terms, $\Phi_n^{\rm SCV}$, vanish in sub-volumes where all long wavelength modes take their mean value (0). Since an observer with access to only a single sub-volume cannot separate the mean contributions from the SCV contributions it is more natural to write the right hand side of the equation above in terms of the observer's linear field, $\chi(\mathbf{x})$, and kernels, and amplitudes:

$$\Phi^{\rm obs}[\chi(\mathbf{x})]|_{x\in V_S} = \chi(\mathbf{x}) + \tilde{f}_{\rm NL}\tilde{\Phi}_2[\chi(\mathbf{x})] + \tilde{g}_{\rm NL}\tilde{\Phi}_3[\chi(\mathbf{x})]\dots\,, \tag{5.34}$$

Note that the standard way of defining the normalizations $\tilde{f}_{\rm NL}$ and $\tilde{g}_{\rm NL}$ only works for scale-invariant contributions from the SCV terms.

For the set of quadratic terms we are considering here, using the kernel N_2 from Eq.(5.67) in the expression for the short wavelength field, Eq.(5.31) gives

$$\Phi_s(\mathbf{k}) \approx \phi_s(\mathbf{k})\left\{1+f_{\rm NL}\left[(2a_1+a_2+a_3)\phi_l + (a_2-2a_3)\partial\phi_l\frac{1}{k} + a_3\partial^2\phi_l\frac{1}{k^2}\right]\right\}$$

$$+\frac{f_{\rm NL}}{2!(2\pi)^3}\int\limits_{p_1,p_2>k_*} d^3p_1 d^3p_2 N_2(p_1,p_2,k)\Big[\phi_s(\mathbf{p}_1)\phi_s(\mathbf{p}_2)-[\text{E.V.}]\Big]\delta^3(\mathbf{k}-\mathbf{p}_1-\mathbf{p}_2) \tag{5.35}$$

where the approximation comes because we have taken $\mathbf{k}-\mathbf{p}_2 \simeq \mathbf{k}$ in the $\phi_s(\mathbf{p}_1)\phi_l(\mathbf{p}_2)$ term in Eq.(5.31). The functions of the long wavelength modes are

$$\phi_l \equiv \int_\Lambda^{k_*} \frac{d^3p}{(2\pi)^3}\,\phi(\mathbf{p}), \quad \partial\phi_l \equiv \int_\Lambda^{k_*} \frac{d^3p}{(2\pi)^3}\,p\phi(\mathbf{p}), \quad \partial^2\phi_l \equiv \int_\Lambda^{k_*} \frac{d^3p}{(2\pi)^3}\,p^2\phi(\mathbf{p}) \tag{5.36}$$

where Λ is an infrared scale corresponding to the longest wave mode that exited the horizon during inflation. We will treat the quantities in Eq.(5.36) as constants in any particular sub-volume. While this is not exactly true, since a nonzero gradient $\partial\phi_l$ implies non-constant $\phi_l(\mathbf{x})$, we show below that this difference is small compared to the effect of the average value of ϕ_l.

The observed linear term in a biased sub-volume is shifted from the original $\phi(k)$ by a term whose amplitude and scale-dependence depends on the bispectrum and the bias:

$$\begin{aligned}\chi_G(\mathbf{k}) \;\equiv\; & \phi_s(\mathbf{k})[1+f_{\rm NL}\Phi_1^{\rm SCV}(k)] = \phi_s(\mathbf{k})\bigg(1+f_{\rm NL}\Big[(2a_1+a_2+a_3)\phi_l \\ & +(a_2-2a_3)\partial\phi_l\frac{1}{k}+a_3\partial^2\phi_l\frac{1}{k^2}\Big]\bigg)\end{aligned} \tag{5.37}$$

Then, using the observed linear field everywhere, the observed non-Gaussian field is

$$\begin{aligned}\Phi^{\rm obs}(k) \;=\; & \chi_G(\mathbf{k}) \\ & +\frac{f_{\rm NL}}{2!(2\pi)^3}\int d^3p_1\,d^3p_2\,\frac{N_2(\mathbf{p}_1,\mathbf{p}_2,\mathbf{k})}{[1+f_{\rm NL}\Phi_1^{\rm SCV}(p_1)][1+f_{\rm NL}\Phi_1^{\rm SCV}(p_2)]} \\ & \times[\chi_G(\mathbf{p}_1)\chi_G(\mathbf{p}_2)-[\text{E.V.}]]\delta^3(\mathbf{k}-\mathbf{p}_1-\mathbf{p}_2)\;.\end{aligned} \tag{5.38}$$

The power spectrum and bispectrum observed in sub-volumes can be computed as usual from this expression, and will differ in amplitude and scale-dependence (shape) from the corresponding quantities in unbiased sub-volumes.

The observed power spectrum is shifted from the input power spectrum by

(assuming weak non-Gaussianity)

$$P_\Phi^{\rm obs} \approx P_\chi^{\rm obs}(k) = P_\phi(k)\left\{1 + f_{\rm NL}\left[(2a_1+a_2+a_3)\phi_l + (a_2-2a_3)\partial\phi_l\frac{1}{k} + a_3\partial^2\phi_l\frac{1}{k^2}\right]\right\}^2 \quad (5.39)$$

This effect was discussed and quantified in detail for the case of local non-Gaussianity in [168]. There it was shown that the correction proportional to ϕ_l can be large and interesting. The other terms here, proportional to $\partial\phi_l$ and $\partial^2\phi_l$ are sensitive to only a very small range of modes beyond the horizon. If the universe was inflating for N_e e-folds before the mode of scale k_* exited the horizon, the super cosmic variance contributions from non-local bispectra are of order

$$\begin{aligned}\frac{\langle(\partial\phi_l)^2\rangle}{k_*^2} &= \frac{1}{k_*^2}\int_\Lambda^{k_*} dk\, k\, \Delta_\phi^2(k) = \frac{\Delta_\phi^2(k_*)}{(n_s+1)}\left(1-e^{-(n_s+1)N_e}\right), \\ \frac{\langle(\partial^2\phi_l)^2\rangle}{k_*^4} &= \frac{1}{k_*^4}\int_\Lambda^{k_*} dk\, k^3\, \Delta_\phi^2(k) = \frac{\Delta_\phi^2(k_*)}{(n_s+3)}\left(1-e^{-(n_s+3)N_e}\right) \end{aligned} \quad (5.40)$$

Here we have assumed for simplicity that the super horizon power spectrum is $\Delta_\phi^2 = A_0(k/k_*)^{n_s-1}$ with constant spectral index n_s and used $N_e = ln(k_*/\Lambda)$. Notice that with $k_* = H_0$ the second quantity in Eq.(5.40) is of the order of the contribution of fluctuations to the spatial curvature, $\langle\Omega_k^2\rangle$.

Figure 5.2 shows that the quantities in Eq.(5.40) are very small, of order 10^{-5}. As expected, there is no appreciable cosmic variance shift to the power spectrum, Eq.(5.39), from non-local bispectra. Figure 5.2 assumes that the power spectrum is consistent with the current best fit from the Planck satellite (Planck+WP) [2] ($\Delta_\Phi^2(k) = 3.98772\times10^{-9}(k/k_*)^{n_s-1}$, $n_s = 0.9619$) and uses $k_* = 0.05\,{\rm Mpc}^{-1}$ as the reference infrared scale. (H_0 is the appropriate scale for considering our current universe.) The strong suppression with extra powers of k in the integrands makes these quantities insensitive to small variations in the spectral index. Specifically, there is no considerable difference between flat spectral index ($n_s = 1$) and $n_s = 0.9619$ (in contrast to the significant enhancement $\langle\phi_l^2\rangle^{1/2}$ receives from a red tilt over sufficiently many super horizon e-folds).

Although these terms have a substantial scale-dependence, the maximum shift to the spectral index at the CMB pivot point is of order 10^{-4}, which is within the current 68% confidence interval from measurements by the *Planck* satellite. (Notice that allowing mild scale-dependence in a_1, a_2 or a_3 *would* generate interesting shifts

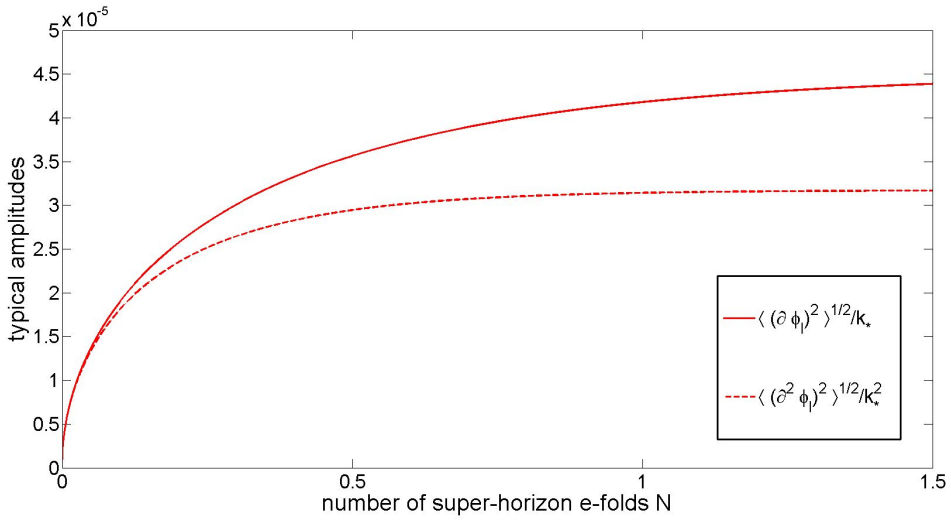

Figure 5.2. Graph of the RMS amplitude of long-wavelength super cosmic variance terms from non-local bispectra, $\frac{1}{k_*}\langle(\partial\phi_l)^2\rangle^{1/2}$ and $\frac{1}{k_*^2}\langle(\partial^2\phi_l)^2\rangle^{1/2}$. This plot assumes that the power spectrum on scales larger than $k_* = 0.05\,\mathrm{Mpc}^{-1}$ remains consistent with *Planck* satellite observations: $\Delta^2_\Phi(k) = 3.98772\times10^{-9}(k/k_*)^{n_s-1}$ with $n_s = 0.9619$ [2]. Notice that the plotted quantities are not sensitive to more than about an e-fold of inflation and remain $\mathcal{O}(10^{-5})$ so, as expected, only the local bispectrum can generate a significant super cosmic variance contribution to the power spectrum.

to the spectral index. The example of scale-dependent a_1 was discussed in [173].)

The bispectrum observed in biased sub-volumes is also shifted. For the exact local ansatz, the change in the observed level of non-Gaussianity was discussed in [166, 168]. When the super cosmic variance shifts to the power spectrum are scale-dependent, the shape of the observed bispectrum changes:

$$B^{\rm obs}(k_1,k_2,k_3) = P_\chi(k_1)P_\chi(k_2)\frac{f_{\rm NL}N_2(k_1,k_2,k_3)}{[1+f_{\rm NL}\Phi_1^{\rm SCV}(k_1)][1+f_{\rm NL}\Phi_1^{\rm SCV}(k_2)]} + \text{cyc.} \quad (5.41)$$

However, as with the scale-dependent corrections to the power spectrum, the changes in shape are too small to be observationally relevant. We will find much

more interesting effects from the inclusion of cubic terms in the ansatz for the non-Gaussian field, which we turn to next.

5.4.3 Cubic Terms

In this section we establish a method to generate cubic terms that induce the four quadratic terms of Eq.(5.14) in biased sub-volumes.

5.4.3.1 Generation of cubic terms

In general, we consider cubic terms that take the form

$$\partial^{\beta_5}(\partial^{\beta_4}\phi\partial^{\beta_3}(\partial^{\beta_2}\phi\partial^{\beta_1}\phi)) \ . \tag{5.42}$$

Similarly to the rules we used to limit the quadratic terms, we consider only cubic terms that satisfy the following restrictions:

1. $\sum \beta_i = 0$ to maintain scale-invariance,
2. $\beta_{1,2,4} \geq 0$ to ensure that the induced quadratic terms do not depend on $\partial^{-1}\phi_l$ or higher inverse derivatives, controlling sensitivity to the infrared (IR) scale.
3. $|\beta_i| \leq 2$ restricts to a minimal set of terms to consider. Note that conditions 1-3 imply $\beta_5 \leq 0$.
4. $\beta_1 + \beta_2 + \beta_3 \geq 0$ to ensure that the induced linear terms are no more sensitive to the IR scale than in local non-Gaussianity (logarithmic sensitivity).
5. At least one of β_1, β_2, or β_4 must be zero and the $\{\beta_1, \beta_2\}$ pairs should be drawn from the same set of values as the $\{\alpha_1, \alpha_2\}$ pairs in Eq.(5.14). This ensures that all the leading order quadratic terms induced in biased sub-volumes are one of those in Eq.(5.14).

As a guide to understanding the origin of these restrictions, an example of the quadratic terms induced in biased sub-volumes by a cubic term is given in Appendix F.1. There are 18 cubic terms, listed in Appendix F, which satisfy these five rules. As with the quadratic terms, it is certainly possible to consider a larger set of terms that have interesting behavior in biased sub-volumes. In Section 5.4.3.4 we discuss

the consequences of the minimal set of terms and also comment on the role of some terms we have discarded. Appendix F also gives the cubic kernel, $N_3(\mathbf{p}_1, \mathbf{p}_2, \mathbf{p}_3, \mathbf{k})$, from these 18 terms.

The addition of this cubic functional adds a leading order trispectrum to the model:

$$\begin{aligned}\langle\Phi(\mathbf{k}_1)\Phi(\mathbf{k}_2)\Phi(\mathbf{k}_3)\Phi(\mathbf{k}_4)\rangle &= (2\pi)^3\delta_D^3(\mathbf{k}_1+\mathbf{k}_2+\mathbf{k}_3+\mathbf{k}_4)\; T_\Phi(\mathbf{k}_1,\mathbf{k}_2,\mathbf{k}_3,\mathbf{k}_4)\\ T_\Phi(\mathbf{k}_1,\mathbf{k}_2,\mathbf{k}_3,\mathbf{k}_4) &= g_{\rm NL}P_\phi(k_1)P_\phi(k_2)P_\phi(k_3)N_3(\mathbf{k}_1,\mathbf{k}_2,\mathbf{k}_3,\mathbf{k}_4) + \text{cyc.}\end{aligned} \tag{5.43}$$

where there are three additional terms in the +cyc. Notice that our definition of $g_{\rm NL}$ as the amplitude of the trispectrum goes beyond the usual definition. The typical conventions for defining the amplitudes of trispectra in various momentum configurations are [193, 194]:

$$\begin{aligned} gnl^{\rm standard} &\equiv \frac{1}{6}\lim_{k_1\to 0}\frac{T_\Phi(\mathbf{k}_1,\mathbf{k}_2,\mathbf{k}_3,\mathbf{k}_4)}{P_\Phi(k_1)P_\Phi(k_2)P_\Phi(k_3)}\\ \tau_{\rm NL} &\equiv \frac{1}{4}\frac{9}{25}\lim_{|\mathbf{k}_1+\mathbf{k}_2|\to 0}\frac{T_\Phi(\mathbf{k}_1,\mathbf{k}_2,\mathbf{k}_3,\mathbf{k}_4)}{P_\Phi(|\mathbf{k}_1+\mathbf{k}_2|)P_\Phi(k_1)P_\Phi(k_3)}\end{aligned} \tag{5.44}$$

Because we have imposed $|\beta_i| \leq 2$ (and specifically $\beta_3 \geq -2$), all of our trispectra have $\tau_{\rm NL} = 0$. Current constraints on the trispectrum from *Planck* satellite data are (allowing both standard shapes to be non-zero) $\tau_{\rm NL} = 0.3 \pm 0.9 \times 10^4$, $g_{\rm NL}^{\rm standard} = -1.2 \pm 2.8 \times 10^5$ [195] at 68% CL, or assuming only one non-zero template at a time $\tau_{\rm NL} < 2800$ at 95% CL [192], $g_{\rm NL}^{\rm standard} = -1.3 \pm 1.8 \times 10^5$ at 68% CL [195].

5.4.3.2 Constraints on cubic terms from their contributions to the power spectrum

As with the quadratic terms, we impose additional restrictions based on the behavior of (classical) loop corrections from the cubic terms, requiring that UV divergences are not stronger than the log divergence of the tree-level case.

The cubic field Φ_3 contributes to the power spectrum at order $g_{\rm NL}^2$ (from $\langle\Phi_3(\mathbf{k}_1)\Phi_3(\mathbf{k}_2)\rangle$):

$$\begin{aligned}\delta P_{\Phi_3}(k) &= g_{\rm NL}^2\int\frac{d^3p_1}{(2\pi)^3}\frac{d^3p_2}{(2\pi)^3}\,d^3p_3\,N_3^2(\mathbf{p}_1,\mathbf{p}_2,\mathbf{p}_3,\mathbf{k})P(p_1)P(p_2)P(p_3)\\ &\quad\times\delta^3(\mathbf{k}-\mathbf{p}_1-\mathbf{p}_2-\mathbf{p}_3)\,.\end{aligned} \tag{5.45}$$

Since this contribution has two momentum integrals (two classical loops), there are several different momentum configurations to consider. The resulting constraints (details appear in Appendix F.2) are

$$\begin{aligned} b_{10} = b_{14} = b_{16} = b_{18} &= 0 \\ b_3 + b_4 &= 0 \\ b_6 + b_7 &= 0 \\ b_{12} + b_{13} &= 0 \\ b_{11} + b_{15} + b_{17} &= 0 \\ 2(b_5 + b_8) + b_6 + b_9 + b_{12} &= 0 \end{aligned} \tag{5.46}$$

After imposing these restrictions, we are left with a 9 parameter set of cubic terms to explore. Corrections to the bispectrum from the cubic term (proportional to $f_{\rm NL}g_{\rm NL}$ at lowest order) do not give any additional constraints that are not covered by conditions imposed on the quadratic term.

5.4.3.3 The field observed in biased sub-volumes

To work out the statistics observed in biased sub-volumes of a field described by Eq.(5.61) and the cubic functional from the previous section, we again split $\Phi(\mathbf{k})$ into long and short wavelength components:

$$\Phi_s(\mathbf{k}) = \phi_s(\mathbf{k}) + \mathrm{f_{NL}}\Phi_2^{(\mathrm{s})}(\mathbf{k}) + \mathrm{g_{NL}}\Phi_3^{(\mathrm{s})}(\mathbf{k}) \tag{5.47}$$

$$\Phi_l(\mathbf{k}) = \phi_l(\mathbf{k}) + \mathrm{f_{NL}}\Phi_2^{(\mathrm{l})}(\mathbf{k}) + \mathrm{g_{NL}}\Phi_3^{(\mathrm{l})}(\mathbf{k}) \tag{5.48}$$

where

$$\begin{aligned} \Phi_3^{(s)}(\mathbf{k}) = \frac{1}{3!}\iiint \frac{d^3p_1}{(2\pi)^3}\frac{d^3p_2}{(2\pi)^3}d^3p_3\, N_3(\mathbf{p}_1,\mathbf{p}_2,\mathbf{p}_3,\mathbf{k})\,\delta^3(\mathbf{k}-\mathbf{p}_1-\mathbf{p}_2-\mathbf{p}_3) \\ \times\,\Theta(|\mathbf{p}_1+\mathbf{p}_2+\mathbf{p}_3|-k_*)\left[\phi(\mathbf{p}_1)\phi(\mathbf{p}_2)\phi(\mathbf{p}_3) - \sum_{\substack{i=1\\k\neq j\neq i}}^{3}\phi(\mathbf{p}_i)\langle\phi(\mathbf{p}_j)\phi(\mathbf{p}_k)\rangle\right] + \text{cyc} \end{aligned} \tag{5.49}$$

$$\Phi_3^{(l)}(\mathbf{k}) = \frac{1}{3!}\iiint \frac{d^3p_1}{(2\pi)^3}\frac{d^3p_2}{(2\pi)^3} d^3p_3\, N_3(\mathbf{p}_1,\mathbf{p}_2,\mathbf{p}_3,\mathbf{k})\,\delta^3(\mathbf{k}-\mathbf{p}_1-\mathbf{p}_2-\mathbf{p}_3)$$
$$\times\,\Theta(k_* - |\mathbf{p}_1+\mathbf{p}_2+\mathbf{p}_3|)\Big[\phi(\mathbf{p}_1)\phi(\mathbf{p}_2)\phi(\mathbf{p}_3) - \sum_{\substack{i=1\\k\neq j\neq i}}^{3}\phi(\mathbf{p}_i)\langle\phi(\mathbf{p}_j)\phi(\mathbf{p}_k)\rangle\Big] + \text{cyc} \tag{5.50}$$

The step function in Eq.(5.49) allows several different types of terms (analogous to the two terms in Eq.(5.31)). In particular, there is a term with all three fields ϕ_s which ensures that all sub-volumes have the same cubic term as the parent volume. There is also a term with a single ϕ_l that contributes to the quadratic term in biased sub-volumes. In other words, the quadratic term that describes the non-Gaussian field in the sub-volume (see Eq.(5.33)) is

$$(f_{\rm NL}\Phi_2)^{\rm obs} = f_{\rm NL}(\Phi_2 + \Phi_2^{SCV}) \tag{5.51}$$

where

$$\begin{aligned} f_{\rm NL}\Phi_2^{SCV} = g_{\rm NL}\Big[\phi_l\Big\{&(3b_1+b_2+b_3+b_8+b_{17})\phi_s^2 + (b_2+b_{13})\partial^{-1}(\phi_s\partial\phi_s)\\ &+(b_3+b_6+2b_{11}+b_{13}+2b_{17})\partial^{-2}(\phi_s\partial^2\phi_s) + (b_4+b_7+b_{12}+2b_{15})\\ &\partial^{-2}(\partial\phi_s)^2\Big\} + \partial\phi_l\Big\{(b_2+2b_4)\phi_s\partial^{-1}\phi_s + (b_5+2b_7+b_{15})\partial^{-1}(\phi_s^2)\\ &+b_9\partial^{-1}\partial\phi_s\partial^{-1}\phi_s + (b_9+2b_{12})\partial^{-2}(\phi_s\partial\phi_s) + b_{13}\partial^{-2}(\partial^2\phi_s\partial^{-1}\phi_s)\Big\}\\ &+\partial^2\phi_l\Big\{b_3\phi_s\partial^{-2}\phi_s + b_6\partial^{-1}(\phi_s\partial^{-1}\phi_s) + b_{11}\partial^{-2}(\phi_s^2)\\ &+b_{13}\partial^{-3}(\phi_s\partial\phi_s)\Big\}\Big] - [\text{E.V.}]. \end{aligned} \tag{5.52}$$

Here the subscript 'SCV' indicates that this is a super cosmic variance contribution to the quadratic term and we have used the conditions from Eq.(5.46) to remove some of the original 18 b_i. By design, the largest cosmic variance terms (those terms proportional ϕ_l) regenerate the four quadratic terms which span the local, equilateral, and orthogonal bispectra types. The contributions proportional to $\partial\phi_l$ or $\partial^2\phi_l$ are subleading, and likely to be unobservably small (although we will comment further on those terms in the next section). Focussing on the leading

contributions, we can more clearly make contact with our discussion of bispectral shapes (Eq.(5.14)) by writing

$$\Phi_2^{SCV} = \frac{g_{\rm NL}\phi_l}{f_{\rm NL}}\Big\{[A_1\phi_s^2 + A_2\partial^{-1}(\phi_s\partial\phi_s) + A_3\partial^{-2}(\phi_s\partial^2\phi_s) + A_4\partial^{-2}(\partial\phi_s)^2] + \cdots - [\text{E.V.}]\Big\} \tag{5.53}$$

There is also a term in Eq.(5.49), $\Phi_3^{(s)}$, with a single ϕ_s: the cubic terms also contribute to the linear term in biased sub-volumes. Including the shift to the linear term from Φ_2 (see Eq.(5.37)), the induced linear term is

$$\begin{aligned}
\Phi_1^{\rm SCV} \;=\;& f_{\rm NL}\left[\phi_s\Big\{(2a_1+a_2+a_3)\phi_l + (a_2-2a_3)\partial\phi_l\frac{1}{k} + a_3\partial^2\phi_l\frac{1}{k^2}\Big\}\right] \\
&+ g_{\rm NL}\left[\phi_s\Big\{[3b_1+b_2+b_3+b_5+b_6+2b_8+b_{11}+2b_{17}]\phi_l^2\right. \\
&\qquad \left.[b_2+b_9+b_{13}]\partial^{-1}(\phi_l\partial\phi_l) + b_3\partial^{-2}(\phi_l\partial^2\phi_l) + b_4\partial^{-2}(\partial\phi_l)^2\Big\}\right. \\
&+\partial^{-1}\phi_s\Big\{[b_2+2b_4+2b_5+2b_7+b_9+2b_{12}+2b_{15}](\phi_l\partial\phi_l) \\
&+b_6\partial^{-1}(\phi_l\partial^2\phi_l) + b_7\partial^{-1}(\partial\phi_l)^2 + [b_8+b_{15}]\partial(\phi_l^2)\Big\} \\
&+\partial^{-2}\phi_s\Big\{[b_3+b_6+2b_{11}+b_{13}](\phi_l\partial^2\phi_l) + [b_9+b_{12}](\partial\phi_l)^2 \\
&\left.+b_{17}\partial^2(\phi_l)^2\Big\} + \partial^{-3}\phi_s\Big\{b_{13}(\partial^2\phi_l\partial\phi_l)\Big\}\right] - [\text{E.V.}]
\end{aligned} \tag{5.54}$$

All the terms inside the first set of curly brackets in the $g_{\rm NL}$ term generate SCV of the same order (that is, $\langle(\phi_l^2)^2\rangle \sim \langle(\partial^{-1}(\phi_l\partial\phi_l))^2\rangle$, etc), while the terms on the fourth line and below give contributions that are significantly smaller. Furthermore, since the individual terms inside each set of $g_{\rm NL}$ curly brackets have the same dimension, there is no way to distinguish them. The only relevant feature is the degree of scale-dependence of the prefactor.

Finally, notice that the short-wavelength field contains terms where, for example, p_1, p_2, $p_3 > k_*$ but $|\mathbf{p}_1+\mathbf{p}_2| < k_*$. This momentum range allows us to consider the limit of correlation functions where momentum modes accessible in a sub-volume sum up to a long wavelength mode. The information in that limit is about the variation of lower order correlations over spatial distances the size of the long wavelength mode [184, 194].

5.4.3.4 Families of cubic terms from the super cosmic variance point of view

In this section, we point out various interesting special cases of the general formulae from the previous section. In each of the subsections below we impose additional constraints (beyond the loop correction considerations) that restrict the super cosmic variance contributions to the bispectrum and power spectrum. That is, we impose constraints on the various combinations of the b_i parameters in Equations (5.52) and (5.54).

Before considering the results of the previous section organized by the squeezed limit behavior of the bispectrum, we first note some general features of the possible super cosmic variance consequences from our cubic terms.

- We find cubic terms that shift the bispectrum at order ϕ_ℓ but that give no shift to the power spectrum at order ϕ_s (the terms in Eq.(5.54) proportional to ϕ_l^2, $\partial^{-1}(\phi_l\partial\phi_l)$, $\partial^{-2}(\phi_l\partial^2\phi_l)$ and $\partial^{-2}(\partial\phi_l)^2$ individually vanish). This set of cubic terms only generates $\Phi_2^{\rm SCV}$ where the $\{A_i\}$ are linear combinations of $\{1,0,-2,2\}$ and $\{1,-2,0,0\}$.

- We find cubic terms that shift the power spectrum at order ϕ_s but that generate no significant shift to the bispectrum (all terms proportional to ϕ_ℓ in the induced quadratic term individually vanish). The $\Phi_1^{\rm SCV}$ generated by any terms in this set are indistinguishable at order ϕ_s. Some can, in principle, be distinguished by the relative amplitude of the sub-leading terms (proportional to $\partial^{-1}\phi_s$ and $\partial^{-2}\phi_s$).

- We find cubic terms that generate neither a shift proportional to ϕ_ℓ in the induced quadratic term, Eq.(5.52), nor a shift proportional to ϕ_s in the induced linear term, Eq.(5.54). From an observational point of view, these cubic terms generate no super cosmic variance of an interesting size. One of these induces no sub-leading shift to the power spectrum and at most a $\partial^2\phi_l$ shift to the bispectrum and so is a candidate for a trispectrum template consistent with single clock inflation. The kernel and trispectra for this case can be found in Appendix F.3.

To summarize, our set of cubic terms demonstrates that it is possible to find examples with significant cosmic variance in the bispectrum but not the power

spectrum, in the power spectrum but not the bispectrum. As may be expected, our set also contains terms that generate no interesting cosmic variance. Furthermore, there is, in general, a degeneracy in the induced lower order terms: Multiple cubic terms (eg, terms that give different trispectra) can generate indistinguishable $\Phi_1^{\rm SCV}$, $\Phi_2^{\rm SCV}$.

If we impose the conditions $4A_1 + 2A_2 + 2A_3 = 0$, and $2A_2 - 4A_3 = 0$, the SCV induced quadratic term will generate a bispectrum of the equilateral shape (the condition $A_3 + A_4 = 0$ is already enforced by the loop constraints on Φ_3). Most cubic terms satisfying those constraints shift the power spectrum at leading order. However, there are cases that generate an equilateral bispectrum but no leading order shift to the power spectrum (no term proportional to ϕ_s in Eq.(5.54)). This case may, in principle, be distinguished from a purely equilateral bispectrum by a sub-leading term (proportional to $\partial\phi_l$), although in practice that contribution is quite small. There is also a cubic term whose SCV contribution gives an equilateral bispectrum at leading order and no contributions to the bispectrum of size $\partial\phi_l$ (although this solution does affect the power spectrum at order ϕ_s).

We can define an equilateral family of statistics by those Φ_n whose SCV contributions induce only an equilateral shape bispectrum at leading order and shift the power spectrum by at most terms proportional to $\partial^{-2}\phi_s$ (the same effect that an equilateral bispectrum gives). Note that although this family is distinct from the set of correlations with no SCV at all, it is not observationally distinct if only the power spectrum and the shape of the bispectrum have been measured. A set of non-zero $\{b_i\}$ for the cubic term that induces the equilateral bispectrum but no significant shift to the power spectrum is

$$b_1 = -5/3\ , \quad b_2 = 2\ , \quad b_5 = 3\ , \quad b_9 = -4\ , \quad b_{12} = -2\ , \quad b_{13} = 2. \tag{5.55}$$

The field observed in biased sub-volumes in this scenario (assuming only an equilateral bispectrum in the mean statistics) takes the form

$$\begin{aligned}\Phi^{\rm obs}(\mathbf{k}) &= \phi(\mathbf{k}) \\ &\quad + \frac{(f_{\rm NL}^{\rm equil} + g_{\rm NL}^{\rm equil}\phi_l)}{2!(2\pi)^3}\int d^3p_1 d^3p_2\,[\phi(\mathbf{p}_1)\phi(\mathbf{p}_2) - \langle\phi(\mathbf{p}_1)\phi(\mathbf{p}_2)\rangle] \\ &\quad \times N_2^{\rm equil}(\mathbf{p}_1, \mathbf{p}_2, \mathbf{k})\delta^3(\mathbf{k} - \mathbf{p}_1 - \mathbf{p}_2)\end{aligned} \tag{5.56}$$

$$+\frac{g_{\rm NL}^{\rm equil}}{3!(2\pi)^6}\prod_{\ell=1}^{3}\int d^3p_\ell\left[\phi(\mathbf{p}_1)\phi(\mathbf{p}_2)\phi(\mathbf{p}_3)-\sum_{\substack{i=1\\k\neq j\neq i}}^{3}\phi(\mathbf{p}_i)\langle\phi(\mathbf{p}_j)\phi(\mathbf{p}_k)\rangle\right]$$
$$\times N_3^{\rm equil}(\mathbf{p}_1,\mathbf{p}_2,\mathbf{p}_3,\mathbf{k})\delta^3(\mathbf{k}-\sum_{\ell=1}^{3}\mathbf{p}_\ell) \tag{5.57}$$

where $N_2^{\rm equil}$ is Eq.(5.67) with $\{a_i\}=\{-3,4,2,-2\}$ (see Eq.(5.69)) and $N_3^{\rm equil}$ with the set of $\{b_i\}$ from Eq.(5.55). Figure 5.3 shows an example quantification of the qualitatively important result for this scenario: there is a range of values of $f_{\rm NL}^{\rm equil}$ in the mean or parent statistics that are consistent with a particular value of $f_{\rm NL}^{\rm equil,obs}$ in sub-volumes. Note that the parent volume can have an input $f_{\rm NL}^{\rm equil}$ of either sign. Appendix F.3 contains more details of some of the interesting cubic terms that induce an equilateral bispectrum in biased sub-volumes.

If we impose the conditions $A_2=A_3=A_4=0$, the SCV induced quadratic term will generate a local shape bispectrum. All such cubic terms also shift the power spectrum at order ϕ_s and most also give sub-leading shifts. If we define the local family as the set Φ_n whose SCV contributions induce only a local bispectrum and only shift the power spectrum as ϕ_s (no sub-leading terms, to match the behavior of the local bispectrum), our ansatz contains several cubic terms in the family. If we are more restrictive and insist that the induced bispectrum has no piece proportional to either $\partial\phi_l$ or $\partial^2\phi_l$ in the bispectrum, the only solution is $b_i=0$ except for $i=1$ (the local $g_{\rm NL}$ term). Super cosmic variance from a local cubic term and beyond was previously considered in [166, 193].

If we impose the conditions $2A_1+A_2+A_3=0$, the SCV induced quadratic term will generate a bispectrum with a squeezed limit that diverges as $1/k_l^2$ (the condition $A_3+A_4=0$ is already enforced by the loop constraints on Φ_3). All such cubic terms in our set generate no shift to the power spectrum at leading order. Notice that this does not insist on the orthogonal template, only the squeezed limit behavior. However, it is possible to have the exact orthogonal template bispectrum induced with or without also inducing a shift to the power spectrum. As in the local and equilateral case, we can define the orthogonal family as the set of terms in $\Phi[\phi(\mathbf{x})]=\phi(\mathbf{x})+f_{\rm NL}\Phi_2[\phi(\mathbf{x})]+g_{\rm NL}\Phi_3[\phi(\mathbf{x})]+\cdots$ that has no stronger than ϕ_s/k SCV in the power spectrum and maintains a bispectrum with only $1/k_l^2$ divergence.

In the following section we will demonstrate a particular way to generate

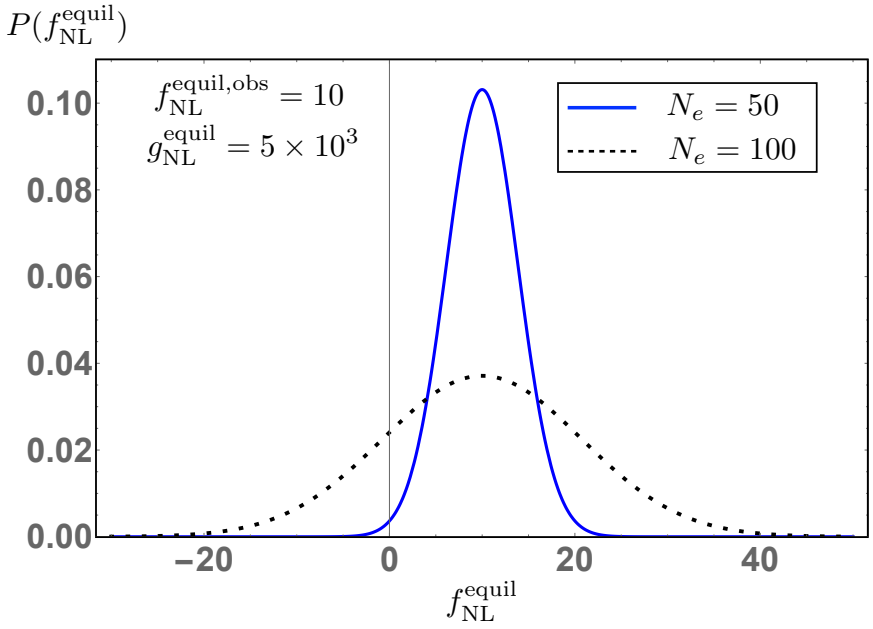

Figure 5.3. Assuming that a single sub-volume measurement of $f_{\rm NL}^{\rm equil} = 10$, this plot shows the probability distribution for the value of $f_{\rm NL}^{\rm equil}$ that could be present in the (mean statistics of the) parent volume. Both curves assume the parent volume has a power spectrum consistent with *Planck* satellite observations and $g_{\rm NL}^{\rm equil} = 5 \times 10^3$ (where $g_{\rm NL}^{\rm equil}$ is defined as the amplitude of the non-local cubic term specified in Eq.(5.55)). If there are no further SCV effects from higher order terms, any sub-volume will have the same power spectrum and $g_{\rm NL}^{\rm equil}$ as the parent volume. The solid (blue) curve considers a parent volume larger than the sub-volume by a factor of 50 extra e-folds. The dotted (black) curve show a parent volume larger by a factor of 100 extra e-folds. For the best fit *Planck* power spectrum and $N_e = 50$, 100, the RMS variance of the long wavelength modes is $\sqrt{\langle \phi_l^2 \rangle} \approx 0.0008$ and 0.0022 respectively.

bispectra which lead to no dominant super cosmic variance uncertainties. The space of generated bispectra will also provide to compare them with the space of shapes that are predicted by the single-clock inflationary models. This is relevant since single-clock inflation expects no mode coupling from bispectra induced in the power spectrum uncertainties of the curvature perturbations. We will try to cover all the possible set of shapes that reveals no SCV.

5.5 Space of non-Gaussian fields with single-clock bispectra

5.5.1 Introduction

From the inflationary theory perspective, the presence or absence of the mode coupling is a tool to qualitatively distinguish the number of degrees of freedom relevant for generating the inflationary background and fluctuations: In so-called 'single-clock' models, short and long wavelengths are decoupled, so that fluctuations in any post-inflationary patch have intrinsic correlation functions[4] entirely determined by the background at the moment the fluctuations exited the horizon [179, 183–186, 188, 189, 198]. The amplitude of long wavelength fluctuations is irrelevant. But, if fluctuations of a light degree of freedom other than the 'clock' field contribute to the observed curvature perturbations, long-short mode coupling generically occurs [3, 170, 175, 199–205]. Interesting coupling between long and short wavelength modes can occur at any order in correlation functions, beginning with the bispectrum (Fourier space 3pt function). The consistency relations for single clock inflation require, among other things, that the bispectrum in the squeezed limit ($k_l \equiv k_1 \ll k_2 \approx k_3$) depend no more strongly on the long wavelength mode than $1/k_l$. Requiring such a scaling in the "initial conditions" for the hot big bang universe (even without a dynamical model for generating it) ensures that these bispectra lead to no additional cosmic variance uncertainties in the power spectrum of the perturbations.

The importance of long-short mode coupling, both as a discriminator of inflationary scenarios and as a source of cosmic variance relating observations to theory, suggests that it be used to organize model-independent tests of non-Gaussianity. Such an approach was developed for the bispectrum in [206], who demonstrated that such a basis efficiently covers a wide range of inflationary models in the literature. (There are other basis proposals, either overlapping or complementary to this one, and organized by other considerations [207–209]). They also found a basis template with the single-clock degree of long-short mode coupling but that was not well covered by the two standard single-clock templates. Since that

[4] The intrinsic correlations may be different from correlations an observer at a particular point sees, due to projection effects [196, 197].

work, the space of templates from single-clock inflationary Lagrangians has continued to grow, eg [210], and the implications of cosmic variance consequences of mode-coupling have been developed [169–175]. In addition, the *Planck* satellite's tightest constraints on non-Gaussianity were published [176], and the focus for the next generation of constraints on single-clock scenarios has turned to Large Scale Structure surveys [211, 212].

Looking toward the future of non-Gaussianity constraints, in this work we revisit the relationship between elements in a mathematical basis for non-Gaussian fields and the set produced by inflation. We are particularly motivated by asking whether or not a detection of a shape satisfying the single-clock consistency relation rules out multi-source scenarios. At one level, certainly not: knowing the form of one correlation function in a non-Gaussian field implies nothing about the shapes of the other correlation functions. In particular, there exist trispectra that generate equilateral shape bispectra in biased sub-volumes through long-short mode-coupling [3]. These cannot be single-clock models, but they would be entirely consistent with the detection of an equilateral bispectrum[5]. However, even without cosmic variance from higher order correlations, we can ask whether every bispectrum that has the single-clock scaling in the squeezed limit can be generated (naturally or not) by single-clock inflation. The templates for single-clock inflation contain additional signatures of inflationary physics in momentum configurations away from the squeezed limit, so by constructing a basis and focusing on templates so far not in the literature we might hope to either "reverse engineer" interesting single-clock inflation scenarios or find some additional physical limits on what they can produce.

To address the relationship between the space of bispectra with no super cosmic variance and single-clock inflation models, we begin in the next section by generating non-Gaussian fields as non-linear, non-local functionals of a Gaussian field. The field will be fully specified (so all correlation functions can be computed and the field can be numerically generated), and one can add new terms order by order to control the details of higher order correlations. We focus on the first non-linear term, which is quadratic in the Gaussian field and so gives a tree-level bispectrum. We generate the space of fields by characterizing the quadratic term according to the number of inverse derivatives allowed per field, and then restrict the set

[5]Such an effect may be detectable through constraints on higher order correlations, but requires sufficiently precise constraints of more general correlations, which will be challenging.

by requiring the squeezed limit of the bispectrum diverge no more strongly than $1/k_l$. We call this set the super cosmic variance free set since there is no significant long-short mode coupling. At the same order that this procedure recovers the two simplest single clock templates, we also find a third, orthogonal bispectrum that peaks in folded configurations and has very small coupling in the equilateral limit. We conclude in chapter 6 with some discussion of the implications of these results and how they can be extended.

5.5.2 Generating super cosmic variance free models

In this section, we first review a procedure to generate an expression for a non-Gaussian field with a bispectrum that matches the equilateral template. Then we show how the procedure may be generalized to non-Gaussian fields with the other standard ("orthogonal") template proposed for single-clock inflation. In the process we will uncover an additional bispectral template that also has the single-clock squeezed limit.

5.5.3 Constructing a non-Gaussian field with an equilateral bispectrum

The lowest order statistic that is zero for a Gaussian field but non-zero more generally is the three-point function. Assuming the non-Gaussian field Φ is homogeneous, the bispectrum $B(\mathbf{k}_1, \mathbf{k}_2, \mathbf{k}_3)$ is defined by

$$\langle \Phi(\mathbf{k}_1)\Phi(\mathbf{k}_2)\Phi(\mathbf{k}_3)\rangle = (2\pi)^3\delta^3(\mathbf{k}_1+\mathbf{k}_2+\mathbf{k}_3)\; B(\mathbf{k}_1,\mathbf{k}_2,\mathbf{k}_3)\;. \tag{5.58}$$

We also restrict to isotropic bispectra. In a generic single-clock inflation model, the form of the bispectrum need not be particularly simple. However, the bispectra of many models can be well approximated by "templates" built from a sum of terms that are each simple products of the three momenta [190, 206, 207]. For example, the equilateral template is:

$$\begin{aligned} B_{\rm equil}(k_1,k_2,k_3) = 6 f_{\rm NL}^{equil} A_\Phi^2 \Bigg[&-\left(\frac{1}{k_1^3 k_2^3} + 2 \text{ perm.}\right) \\ &-\frac{2}{(k_1k_2k_3)^2} + \left(\frac{1}{k_1 k_2^2 k_3^3} + 5 \text{ perm.}\right)\Bigg]\,. \end{aligned} \tag{5.59}$$

We have assumed a scale-invariant power spectrum for simplicity, with amplitude $A_\Phi^2 = k^3 P_\Phi(k)$, and f_{NL}^{equil} is the amplitude parameter of the bispectrum, defined at the equilateral point in momentum space ($k_1 = k_2 = k_3$). Notice that even though the individual terms in the template have as many as 3 powers of a particular momentum in the denominator, in the squeezed limit (e.g., $k_1 \equiv k_l \ll k_2 \approx k_3 \equiv k_s$) the entire template scales like:

$$\lim_{k_l \ll k_s} B_{\rm equil} \propto \frac{1}{k_l k_s^5} + \dots \tag{5.60}$$

To write an expression for a non-Gaussian field Φ (the Bardeen potential after reheating) with a bispectrum that matches the equilateral template we use a series of nonlocal functionals of a Gaussian random field $\phi(x)$ [3, 191]:

$$\Phi[\phi(\mathbf{x})] = \phi(\mathbf{x}) + f_{\rm NL}\Phi_2[\phi(\mathbf{x})] + \dots \tag{5.61}$$

where the subscript on Φ_2 indicates the term is quadratic in the Gaussian field. Including higher order terms Φ_n would add tree-level $(n+1)$ point functions to the model. Since a quadratic term that is local in the Gaussian field, $\Phi_2(x) = [\phi(x)]^2$, gives a bispectrum that diverges as $1/k_l^3$ in the squeezed limit, we must allow $\Phi_2(x)$ to be non-local in order to reduce the degree of divergence. So, we consider

$$\Phi_2(x) = \partial^{\alpha_3}(\partial^{\alpha_2}\phi\partial^{\alpha_1}\phi)(\mathbf{x}) \ , \tag{5.62}$$

where the α_i can be negative and the derivative is defined by

$$\partial^n\phi(x) \equiv \int \frac{d^3k}{(2\pi)^3} k^n \phi(\mathbf{k}) e^{i\mathbf{k}\cdot\mathbf{x}} \ . \tag{5.63}$$

We will restrict consideration to scale-invariant bispectra, which imposes the requirement $\alpha_1 + \alpha_2 + \alpha_3 = 0$.

To find the form of Φ_2 that generates a bispectrum for Φ matching the equilateral template in Eq.(5.59), notice that there are individual terms in the template that diverge as $1/k_l^3$, $1/k_l^2$, and $1/k_l$. Each of these terms can be recovered from the ansatz Eq.(5.62) by considering $|\alpha_i| \leq 2$. In addition, individual terms that diverge more strongly than $1/k_l^3$ can be avoided by requiring $\alpha_1, \alpha_2 > 0$. The quadratic

term that satisfies those restrictions is [3, 191]

$$\Phi_2[\phi(x)] = [a_1\phi^2 + a_2\partial^{-1}(\phi\partial\phi) + a_3\partial^{-2}(\phi\partial^2\phi) + a_4\partial^{-2}(\partial\phi)^2] - [\text{E.V.}] \ . \tag{5.64}$$

where $-$[E.V.] indicates that the expectation values of the terms should be subtracted.

To see the bispectrum generated by this quadratic term, it is easiest to first write the general non-Gaussian field in Fourier space (Fourier transform of Eq.(5.61)):

$$\Phi(\mathbf{k}) = \phi(\mathbf{k}) + \frac{f_{\rm NL}}{2!}\int\frac{d^3p_1}{(2\pi)^3}\int d^3p_2\,[\phi(\mathbf{p}_1)\phi(\mathbf{p}_2) - \langle\phi(\mathbf{p}_1)\phi(\mathbf{p}_2)\rangle]\,N_2(\mathbf{p}_1,\mathbf{p}_2,\mathbf{k})\delta^3(\mathbf{k}-\mathbf{p}_1-\mathbf{p}_2) \tag{5.65}$$

where the kernel N_2 is symmetric in the first two entries. Then the bispectrum is easily computed:

$$B(k_1,k_2,k_3) = f_{\rm NL}P_\phi(k_1)P_\phi(k_2)N_2(k_1,k_2,k_3) + \text{perm.} \tag{5.66}$$

where $P_\phi(k)$ is the power in the Gaussian field. For the quadratic term in Eq.(5.64), the kernel is

$$N_2(p_1,p_2,k) = 2a_1 + a_2\frac{p_1+p_2}{k} + a_3\frac{p_1^2+p_2^2}{k^2} + 2a_4\frac{p_1p_2}{k^2} \ . \tag{5.67}$$

Not every part of the parameter space covered by the four-parameter kernel N_2 in Eq.(5.67) above is well behaved. In particular, consider the power spectrum including the (1-loop) non-Gaussian contribution:

$$\langle\Phi(k)\Phi(k')\rangle = (2\pi)^3\delta(\mathbf{k}+\mathbf{k}')\Big[P_\phi(k) + 2f_{\rm NL}^2 \times\int d^3p\,P_\phi(p)\,P_\phi(|\mathbf{k}-\mathbf{p}|)\,N_2^2(p,|\mathbf{k}-\mathbf{p}|,k)\Big] \tag{5.68}$$

The last two terms in the kernel, Eq.(5.67), scale like $(p/k)^2$ in the limit $p \gg k$ and so give loop contributions that diverge in the UV. This divergence can be removed by requiring $a_3 + a_4 = 0$. After insisting on good behavior of the loop term (logarithmic divergences only), bispectra from the kernel N_2 can still have squeezed

limits that diverge like k_l^{-3}, k_l^{-2}, or k_l^{-1}. Restricting to bispectra that are consistent with the single-clock degree of divergence requires that the coefficients of both the k_l^{-3} and the k_l^{-2} contributions vanish. These conditions lead a unique solution, which (with a choice of normalization) corresponds to the equilateral template

$$\text{Equilateral Bispectrum :}$$
$$a_1 = -3,\ a_2 = 4,\ a_3 = 2, a_4 = -2\ . \tag{5.69}$$

Notice that terms a_2 and a_3 give identical contributions to the shape of the bispectrum. However, they differ in their contributions to the 1-loop power spectrum and so both terms are required to both recover the equilateral template and keep the power spectrum well-behaved.

5.5.4 Obtaining the single-clock orthogonal template

The equilateral template is not sufficient to cover the space of single-clock inflation models that are equally natural within even the simplest effective field theory of single-clock fluctuations [213]. A second template with squeezed limit proportional to $1/k_l$ but distinct from the equilateral template in other momentum configurations was proposed in [190]. (See also the proposal in [214].) We will show the orthogonal template in Eq.(5.75) below, but the most important point for our purposes in this section is that the orthogonal bispectrum contains terms with up to four powers of any single momentum in the denominator, i.e., $k_1/k_2^3k_3^4$. This suggests that quadratic terms in the field expansion with a less restrictive set of α_i may generate bispectra with the single-clock squeezed limit but otherwise very little overlap with the equilateral template. Allowing $|\alpha_3| \leq 3$ does not generate any new solutions, but $|\alpha_3| \leq 4$ will be sufficient.

To derive additional factorizable bispectra with the single-clock squeezed limit, we add the following quadratic terms to those in Eq.(5.64):

$$\begin{aligned} &a_5\partial^{-3}(\phi\partial^3\phi),\ a_6\partial^{-3}(\partial\phi\partial^2\phi) \\ &a_7\partial^{-4}(\phi\partial^4\phi),\ a_8\partial^{-4}(\partial^2\phi\partial^2\phi),\ a_9\partial^{-4}(\partial\phi\partial^3\phi) \\ &a_{10}\partial^2(\partial^{-1}\phi)^2,\ a_{11}\partial^{-4}(\partial^{-1}\phi\partial^5\phi) \end{aligned} \tag{5.70}$$

The terms in the last line come from allowing $\alpha_1, \alpha_2 \geq -1$. When we restricted

to $|\alpha_3| \leq 2$, allowing $\alpha_1, \alpha_2 < 0$ only generated terms in the bispectrum that were the same as those generated by the four terms in Eq.(5.64) (or that were more divergent than $1/k^3$). And, since negative values of α_1, α_2 lead to terms with 1-loop contributions to the power spectrum that diverge in the infra-red rather than the UV those terms also would not change the loop constraints. So, including them would have been redundant. However, because the power spectrum goes like $1/k^3$, when we are interested in terms in the bispectra that go as four or more powers of a single momenta the $\alpha_1, \alpha_2 < 0$ terms do give new functions of momenta at this order. (Table (G.1) in the Appendix shows a complete list of quadratic terms, including $\alpha_1, \alpha_2 < 0$ organized by the bispectra they generate to illustrate these redundancies.)

Now, in this new set we need to introduce new constraints which avoid the divergences in the one-loop correction to the power spectrum

$$\begin{aligned} a_5 + a_6 &= 0, \\ a_7 + a_8 + a_9 + a_{11} &= 0 \\ 2a_{10} + a_{11} &= 0 \, . \end{aligned} \tag{5.71}$$

where the first two conditions ensure the UV divergence in the loop integral is no more than logarithmic and the last condition does the same for the IR divergence. Finally, after again imposing that in the squeezed limit the bispectrum diverges no more strongly than $1/k_l$, there are four linearly independent (and non-trivial) solutions for the $\{a_i\}$

$$\begin{aligned} \{a_i\} = \{&\{-3, 4, 2, -2, 0, 0, 0, 0, 0, 0, 0\}, \\ &\{1, 0, 0, 0, 0, 0, -2, 2, 0, 0, 0\}, \\ &\{1, -1, 0, 0, 0, 0, -1, 0, 1, 0, 0\}, \\ &\{1, 0, 0, 0, 0, 0, -2, 0, 0, -1, 2\}\} \end{aligned} \tag{5.72}$$

The kernels $N_2^{(i)}$, each corresponding to the i^{th} solution from the list above, are

$$\begin{aligned}
N_2^{(1)}(k_1,k_2,k_3) &= -6 + 4\frac{k_1+k_2}{k_3} + 2\frac{k_1^2+k_2^2}{k_3^2} - 4\frac{k_1k_2}{k_3^2} \\
N_2^{(2)}(k_1,k_2,k_3) &= 2 - 2\frac{k_1^4+k_2^4}{k_3^4} + 4\frac{k_1^2k_2^2}{k_3^4} \\
N_2^{(3)}(k_1,k_2,k_3) &= 2 - \frac{k_1+k_2}{k_3} - \frac{k_1^4+k_2^4}{k_3^4} + \frac{k_1k_2^3+k_2k_1^3}{k_3^4} \\
N_2^{(4)}(k_1,k_2,k_3) &= 2 - 2\frac{k_1^4+k_2^4}{k_3^4} - 2\frac{k_3^2}{k_1k_2} + \frac{2}{k_3^4}\left(\frac{k_2^5}{k_1}+\frac{k_1^5}{k_2}\right)
\end{aligned} \tag{5.73}$$

where the first line ($N_2^{(1)}$) is again the kernel for the equilateral template. Notice that the fourth kernel is actually less divergent than the equilateral template and is just proportional to $1/k_s^6$ in the squeezed limit. We label the bispectra generated by each of these kernels as

$$B_i(k_1,k_2,k_3) \propto P_\phi(k_1)P_\phi(k_2)N_2^{(i)}(k_1,k_2,k_3) + \text{perm.} \tag{5.74}$$

Now we can show that this space of solutions is sufficient to cover the standard orthogonal template [190]:

$$\begin{aligned}
\frac{B_{ortho}(k_1,k_2,k_3)}{f_{\rm NL}^{orth}A_\Phi^2(k)} = (1+p)\Bigg[6\left(\frac{1}{k_1k_2^2k_3^3}+5\,\text{perm.}\right) - 6\left(\frac{1}{k_1^3k_2^3}+2\,\text{perm.}\right) - \frac{12}{k_1^2k_2^2k_3^2}\Bigg] \\
-\frac{6\,p}{27}\Bigg[-\left(\frac{k_1^2}{k_2^4k_3^4}+2\,\text{perm.}\right) + 6\left(\frac{k_1}{k_2^3k_3^4}+5\,\text{perm.}\right) - 15\left(\frac{1}{k_1^2k_2^4}+5\,\text{perm.}\right) \\
-18\left(\frac{1}{k_1^3k_2^3}+2\,\text{perm.}\right) + 20\left(\frac{1}{k_1k_2k_3^4}+2\,\text{perm.}\right) + 12\left(\frac{1}{k_1k_2^2k_3^3}+5\,\text{perms.}\right) + \frac{6}{k_1^2k_2^2k_3^2}\Bigg]
\end{aligned} \tag{5.75}$$

where $p \simeq 8.52$. The first term in square brackets (multiplied by the factor $(1+p)$), is just the usual equilateral template and the second term with a factor of p itself has the correct single-clock behavior in the squeezed limit. This template can be expressed in terms of the bispectra generated by the kernels we found above:

$$B_{ortho} = \left(\frac{10p}{9}+1\right)B_1 - \left(\frac{10p}{9}\right)B_2$$

$$+\left(\frac{10p}{3}\right)B_3+\left(\frac{p}{9}\right)B_4 \tag{5.76}$$

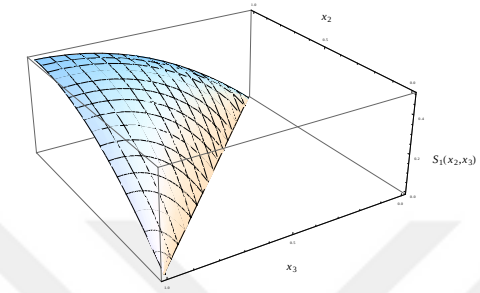

$S_1(x_2, x_3) \propto (k_1k_2k_3)^2 B_1(k_1, k_2, k_3)$

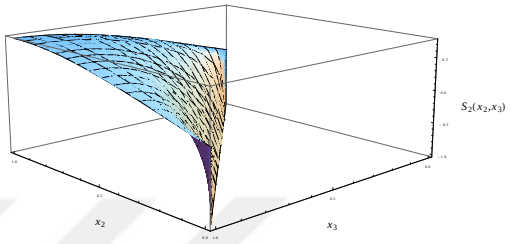

$S_2(x_2, x_3) \propto (k_1k_2k_3)^2 B_2(k_1, k_2, k_3)$

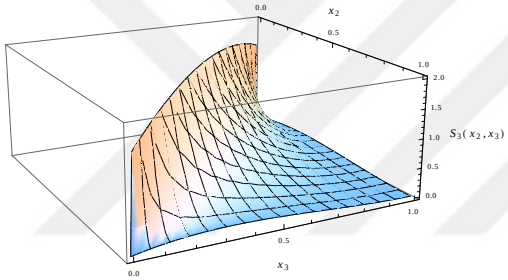

$S_3(x_2, x_3) \propto (k_1k_2k_3)^2 B_3(k_1, k_2, k_3)$

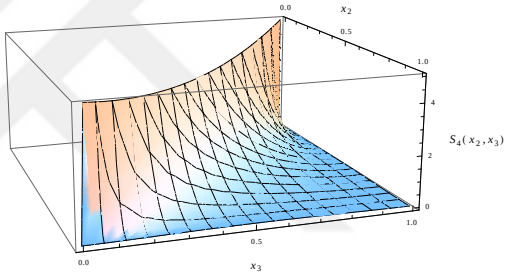

$S_4(x_2, x_3) \propto (k_1k_2k_3)^2 B_4(k_1, k_2, k_3)$

At this point, we have sufficient terms to recover the two standard templates, but do we have anything new? To answer this question we need to define the overlap between two bispectra. This depends on the similarity between the dimensionless "shapes", $S(k_1, k_2, k_3)$, defined by

$$S_i(k_1, k_2, k_3) = (k_1k_2k_3)^2 \frac{B_i(k_1, k_2, k_3)}{N f_{\rm NL} A_\phi^2}, \tag{5.77}$$

where N is a normalization factor. Although it is standard in the literature to define N in the equilateral limit, here we are insisting only on a non-vanishing *squeezed* limit, and in fact two of our kernels as defined above vanish in the equilateral limit. So, we instead normalize in the squeezed limit. The choice of normalization is, however, irrelevant for comparing any two terms and is irrelevant for expressions involving only the bispectrum. The exact expression for each shape is given in the Appendix, Eq.(G.7), and they are plotted in Figures 1-4.

We can now compare two shapes using the cosine introduced by [215]:

$$\cos\theta = \frac{S_1 \cdot S_2}{(S_1 \cdot S_1)^{1/2}(S_2 \cdot S_2)^{1/2}}, \tag{5.78}$$

where the dot product can be simplified to a two dimensional integral (from three) since the shape is symmetric in the momenta. Defining $k_2/k_1 = x_2$ and $k_3/k_1 = x_3$ gives

$$S_1 \cdot S_2 = \int_{\texttt{triangle}} dx_2 dx_3 \; S_1(x_2, x_3)\, S_2(x_2, x_3)\; . \tag{5.79}$$

The domain of integration can be restricted using rotational invariance and the triangle inequality. Since divergences occur in some shapes at the boundary of the parameter space (when $x_2 = 0$ or 1) we consider a slightly restricted domain, $(0.01 \leq x_2 \leq 0.99,\; 1 - x_2 \leq x_3 \leq 1)$. Table 5.1 shows the correlation coefficients between our four shapes. (Note that if one is interested in a more specific question like the degree to which the bispectrum measured from the cosmic microwave background can distinguish shapes, the definition of the scalar product should be modified with an appropriate weighting function in the integral [207].)

	S_1	S_2	S_3	S_4
S_1	1	0.74	0.38	0.30
S_2		1	-0.33	-0.41
S_3			1	0.99
S_4				1

Table 5.1. The overlap between the shapes associated with the four linearly independent kernels with the single-clock squeezed limit.

The table shows significant overlap between S_3 and S_4, so we expect that our basis includes just one additional shape with very little overlap with the standard equilateral and orthogonal templates. We express this new shape by searching for a linear combination of the shapes associated to B_1, B_2, and B_3 with minimal cosine with both the equilateral and orthogonal templates. This procedure gives $\cos(B_{new}, B_{ortho})$, $\cos(B_{new}, B_{equil})\} \lesssim \mathcal{O}(10^{-2})$ for

$$B_{flat-only} = 0.486\, B_1 - 0.484\, B_2 + 0.998\, B_3 \tag{5.80}$$

(We have written this in terms of the bispectrum rather than the shape functions,

so it is independent of normalization convention for the individual shapes associated with the B_i. To understand the shape above qualitatively, we plot it in both 3D (Figure 5.4) and as a contour plot (Figure 5.5).

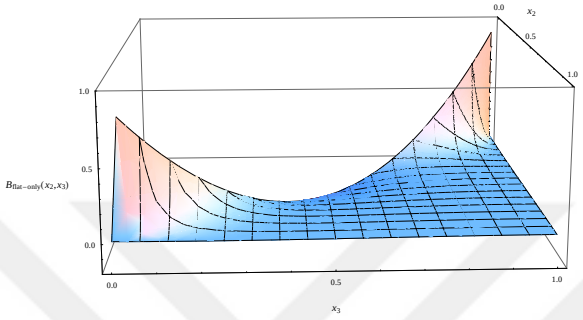

Figure 5.4. This is the 3D plot of the flat-only shape $S_{flat-only}(x_2, x_3)$ proportional to $(k_1k_2k_3)^2 B_{flat-only}(k_1, k_2, k_3)$

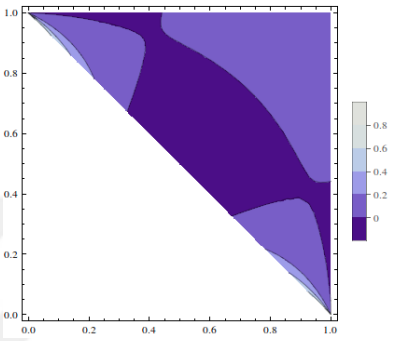

Figure 5.5. Contour plot of the flat-only shape.

The graph peaks along flattened configurations $x_2 + x_3 = 1$ and has essentially very small amplitude away from that line, including at the equilateral point. We label it “flat-only" to emphasize both where it peaks and the small equilateral amplitude. Below, we will compare this shape in detail with a variety of single-clock models, but the fact we will find low overlap is perhaps already not surprising: because the shape is nearly zero away from the flat limit, its cosine with other shapes is predominantly a function of the behavior only along the flat limit. For reference in the next section, note that the oscillation along the line $x_2 + x_3 = 1$ can be well approximated by

$$S_{\text{flat-only}}(1, x_2, x_3 = 1 - x_2) \approx 0.86 \\ -\text{Sin}\left[(1 + x_2 - x_3)\left(\frac{\pi}{2}\right)\right] . \tag{5.81}$$

This simple oscillatory behavior turns out not to be an easy feature to find. For reference, the cosine of the flat-only shape with the local shape is about 0.5.

5.5.5 Comparison with previous work

Although our approach and motivation were rather different, it is interesting to note that our results can be mapped to terms in the basis constructed in [206]. We have constructed a non-Gaussian field while they focused on a basis for bispectra. The

system of constraints we are solving is different since we have several field terms that produce the same polynomials in the bispectrum, and additional constraints on the behavior of UV loops. In both their basis and ours, one has to choose some order to truncate the list of terms considered, and truncating at the appropriate order to recover the single-clock orthogonal template turns out to give a set of four linearly independent solutions in either case. Appendix G shows in detail the relationship between these approaches and the results. In [206] they similarly computed cosines and identified the existence of a shape ($S_4^{\rm BB}$ in Appendix G) that had cosines of 0.07 and 0.8 with the equilateral and orthogonal templates, respectively. So, this shape is not well covered by the two standard templates. Although $S_4^{\rm BB}$ itself only has cosine of about 0.1 with the flat-only shape, it is an essential ingredient in the linear combination of the basis in [206]that is equivalent to the flat-only shape.

In the next section, we examine in detail the relationship of this flat-only shape to the shapes that can be produced by single-clock Lagrangians, including some natural shapes proposed after [206] appeared.

Chapter 6
Summary and Outlook

In this chapter we will consider the implications of the preceding chapters for further understanding the significance of analyzing all possible features of the correlations between physical observables in a given system or modeling. In the first place we will summarize briefly the results presented in the preceding chapters and then we will discuss the outlooks of these works in this thesis.

6.1 Entanglement and quantum spacetimes

In chapter 3 we demonstrated how a particular set of highly entangled states in loop quantum gravity can be associated to geometrical structures at quantum level and approximate discrete geometries in three dimensional space. States of the geometry in the classical phase space of loop quantum gravity on a graph Γ describe twisted geometries [75–77], polyhedral spaces that in general display metric discontinuities on two-dimensional faces. Regge geometries corrrespond to the continuous geometries in the space of twisted geometries, and are selected by shape-matching conditions discussed in [80, 86]. An intermediate class of states is given by vector geometries, for which identified faces of neighboring tetrahedra are always parallel, allowing them to be glued together, but may have different shapes. Vector geometries are described by a set of normal-matching conditions [83–85]. In this work, we introduced a class of entangled states in the Hilbert space $\mathcal{H}_\Gamma$ of loop quantum gravity that can be assigned to vector geometries. Such quantum vector geometries are defined as solutions to gluing conditions that ensure both mean values and fluctuations of the geometry to be compatible with classical vector geometries. They are distinct from coherent states peaked on a vector geometry in that for

coherent states only the mean geometry satisfies normal-matching conditions, and correspond not to isolated vector geometries, but to special surfaces in the space of classical vector geometries. In order to check whether a given state approximates a Regge geometry, we also introduced a set of quantum shape-matching conditions designed as tests of the continuity of the geometry. We were able to identify states in the space of quantum vector geometries that are well-peaked on Regge geometries and showed that they satisfy the proposed shape-matching conditions. Such states provide explicit examples of how continuous geometries can be constructed on Γ for the generally discontinuous quantum geometry of loop quantum gravity in $\mathcal{H}_\Gamma$.

The definition of quantum vector geometries was guided by a prescription discussed in Section 3.2 for the construction of general classical vector geometries. The classical phase space of gauge-invariant twisted geometries on Γ is the symplectic reduction $\mathcal{P}_\Gamma//\mathcal{C}$, where $\mathcal{P}_\Gamma$ is the space of twisted geometries and $\mathcal{C}$ is the closure constraint that implements gauge invariance. Vector geometries are defined in $\mathcal{P}_\Gamma$ as states that, in addition to $\mathcal{C}$, also satisfy normal-matching constraints $\mathbf{T}_\ell$ (Eq. (3.9)) that ensure normals of glued faces to be antialigned at each link ℓ. A gauge-invariant vector geometry is then a gauge orbit that intersects some normal-matched geometry. Accordingly, we defined a quantum vector geometry as the projection to the space of gauge-invariant states $\mathcal{H}_\Gamma$ of a state $|\psi\rangle$ satisfying the normal-matching conditions $\langle\psi|\mathbf{T}_\ell \cdot \mathbf{T}_\ell|\psi\rangle = 0$ in the space of gauge-dependent states. The space of solutions to these conditions was fully determined in the bosonic representation of LQG, in which states of the theory are mapped into states of a set of harmonic oscillators satisfying constraints that implement gauge invariance and area matching [97–100]. The simplest class of solutions is given by a family $|\Gamma, \mathrm{B}_\gamma\rangle$ (Eqs. (3.53)–(3.55)) of squeezed vacua in the oscillator model [65, 100]. We called these solutions Bell states, since they are built out of perfectly correlated spin states at each link. In order to explore the properties of quantum vector geometries, we performed a careful analysis of Bell states on the dipole and pentagram graphs, and presented analytical and numerical results for their mean geometry and correlation functions.

We found that the Bell state $|\Gamma_2, \mathrm{B}_\gamma, j_\ell\rangle$ on the dipole graph Γ_2 at fixed spins is the direct analogue in LQG of the well-known Bell states for spin 1/2 systems [216]. The fluctuations of the quantum geometry are perfectly correlated: if an observable O of the local geometry is measured in both tetrahedra, the outcomes are always the same. In particular, measurements of edge lengths give the same result regardless

of where they were performed. This implies that the Bell states satisfy the shape-matching conditions proposed in Section 3.4.3. Moreover, if the degrees of freedom of one tetrahedron t are traced out, then the density matrix ρ_s of the remaining tetrahedron describes a microcanonical ensemble: all configurations compatible with the chosen spins are equally probable. Interestingly, if all spins are chosen to be the same, $j_\ell = j$, this is sufficient to enforce the mean geometry to be that of a regular tetrahedron. At fixed spins, the quantum mutual information between the two tetrahedra is maximized.

On the pentagram Γ_5, amplitudes of Bell states $|\Gamma_5, \mathrm{B}_\gamma, j_\ell\rangle$ are simply given by $SU(2)$ $15j$-symbols (Eq. (3.86)). This allowed us to apply the asymptotic analysis of the $15j$-symbols presented in [83,84] to study their geometry for large spins. This limit is conveniently analyzed in the coherent state representation, where states of the geometry are represented as superpositions of coherent states $|\psi(j_{ab}, \mathbf{n}_{ab})\rangle$ associated with classical geometries on Γ_5 specified by boundary data $\{j_{ab}, \mathbf{n}_{ab}\}$ describing areas and normals of $2d$ faces. For the Bell state $|\Gamma_5, \mathrm{B}_\gamma, j_\ell\rangle$, only the subspace of vector geometries is relevant in the asymptotic regime, including both shape-matched (Regge) and general normal-matched (vector) geometries [83,84]. We addressed the key question of the relative importance of shape-matched and normal-matched configurations in the mesoscopic limit. When the former dominate, the state is peaked on a Regge geometry. The amplitudes of vector geometries are determined by the Hessian of the action in the integral representation (3.93) of the $15j$-symbols. We computed numerically these amplitudes for special spin configurations and found that the mesoscopic limit is indeed dominated by shape-matched configurations. We proceeded in three steps. We first selected spins j_ℓ for which a shape-matched configuration exists. For that purpose, we considered geometries describing boundaries of 4-simplices with a $3d$ Euclidean metric (signature $0+++$) [83,84], which can be conveniently represented as the gluing of 5 tetrahedra divided in two subsystems related by 1-4 or 2-3 Pachner moves in $\mathbb{R}^3$. Next, we determined the full space of vector geometries including normal-matched configurations for such spins. Finally, we computed the Hessian for these vector geometries. We found that contributions to the $15j$-symbol from normal-matched configurations are suppressed compared to the shape-matched configurations. The wavefunction of $|\Gamma_5, \mathrm{B}_\gamma, j_\ell\rangle$ in the coherent state representation is peaked on an orbit of normal-matched geometries, where the mean geometry is a

Regge geometry in the limit of large spins. Moreover, in the case of a $4d$ Euclidean metric (signature $++++$), the $15j$-symbol is known to be peaked on a matched geometry, and the same result follows.

For general graphs Γ, the amplitudes of Bell states in the spin network basis are given by the spin network evaluation $A_\Gamma(j_{ab}, i_a)$ of the graph (Eq. (3.55)). The asymptotic analysis of the 15-j symbols associated with the pentagram Γ_5 was recently extended to the case of amplitudes A_Γ on arbitrary graphs in [85], and could be applied to a similar analysis of the mesoscopic limit of Bell states on general graphs. This requires a clear geometric interpretation of the boundary data that determines the amplitude A_Γ. The asymptotics of A_Γ have a similar structure as that of the $15j$-symbol in terms of the saddle point approximation: general vector geometries are those with at least one saddle point, while the existence of two saddle points characterizes a special subset including boundaries of flat $4d$ polytopes. Unlike the case of Γ_5, however, one cannot directly recognize the boundary of a flat $4d$ polytope from the existence of two saddle points. In fact, for general graphs this special subset spans more general geometries called angle-matched vector geometries, for which areas and internal angles of $2d$ faces are matched, but residual shape-matching conditions must be imposed to ensure that the diagonals of $2d$ faces also match. In addition, there are no $3d$ Regge geometries with a single saddle point. Accordingly, the identification of $3d$ continuous geometries must be modified, but one could in principle study the asymptotics of states $|\Gamma, \mathrm{B}_\gamma, j_\ell\rangle$ in arbitrary graphs in a similar way as done for the pentagram. In the limit of large spins, we expect that averaging contributions from vector geometries will lead again to $3d$ Regge geometries.

The normal-matching condition $\langle\psi|\mathbf{T}_\ell \cdot \mathbf{T}_\ell|\psi\rangle = 0$ imposed at each link (before the projection to the space of gauge-invariant states) can be rephrased in information theoretic language as the condition of maximization of the quantum mutual information for the subsystems at the two endpoints of the link, which describe the dual faces glued by the link. The projection to $\mathcal{H}_\Gamma$ considerably affects the state, but we still expect it to display strong correlations for the intrinsic geometry of nearest neighboors, as the projector acts locally at each node. This provides a simple picture for the mechanism responsible for the emergence of a continuous geometry in the limit of large spins for Bell states: the information describing the geometry of a boundary surface is shared between the regions of space connected by

the surface, so that discontinuities of the metric are suppressed. In a more general tone, we see that for normal-matched states on arbitrary graphs Γ the notion of adjacency of nodes in the spin network coincides with that of large entanglement. This property is clearly not valid in general, as one can easily conceive states where intertwiners in far away regions in the graph are perfectly correlated and the geometry of nearest neighbors fluctuate independently in intertwiner space. If this behavior occurred in the mesoscopic limit, the resulting geometry would not resemble a continuous classical geometry under the usual assumption that links in the graph describe relations of spatial adjacency for the quantum tetrahedra. The possibility that relations of adjacency (and, more generally, measurements of distance) could be derived directly from the network of correlations in a given state has been suggested in [217], and has also been recently discussed in [66,67] in connection with efforts to characterize the geometry of LQG states in terms of the entanglement among subsystems using information theoretic tools.

Another question that could be addressed in future works concerns the behavior of the entanglement entropy for collections of nodes in large graphs. Moreover, we considered a squeezing matrix which does not couple variables at distinct links for the construction of the Bell states, but one could also introduce additional long-range correlations for distant links as in [65], and it is not clear how spin correlations behave in the presence of short and long-ranged couplings and in what level quantum matching conditions are affected.

6.2 Discrete spin systems and canonical quantum gravity

In [5] we have analyzed a discrete spin model with different methods from canonical quantum gravity. Our aim is to test the latter, rather than revealing new properties of spin systems in general. We have found new results in three different classes: minisuperspace truncations, effective theories, and dynamical long-range correlations.

We have derived different minisuperspace models directly from the discrete theory, which is a new procedure compared with the usual construction of minisuperspace models by quantizing homogeneous configurations of a continuum

theory. Several novel features could be seen, for instance the existence of different minisuperspace models of the same discrete theory, paralleling the existence of different continuum limits of one discrete theory. In our specific constructions, starting with the discrete theory has the advantage that no problems related to infrared scales of traditional minisuperspace models occur. We have seen that it can be of advantage to keep more degrees of freedom in a minisuperspace model than simple homogeneous configurations would suggest, in particular when non-trivial dynamical properties should be obtained. Good knowledge of the fundamental theory is required in order to select a reliable minisuperspace model. Alternatively, non-trivial dynamics can be obtained by using condensate states, as employed also in cosmological models of group-field theories [128–135].

In several examples of our minisuperspace models, we have computed canonical effective potentials and equations and found good agreement with known ground-state energies and configurations. Our results provide further support for the canonical effective methods proposed for quantum gravity in [112, 113], with an extension to the computation of effective potentials in [218].

We have also analyzed the discrete spin system directly, with an emphasis on properties that should be important for the dynamical building-up of long-range correlations as they are likely to be relevant for the dynamical emergence of states as they may be described by minisuperspace models, a question related to the continuum limit of discrete quantum gravity. Our analysis, based on rather general properties of the underlying equations of motion, suggests that such features can only be seen in a full non-perturbative treatment of the dynamics.

Concerning stability, we have seen that not all minisuperspace ground states correspond to the ground state of the discrete theory. Some models are therefore unstable if energy can be exchanged with an environment, and one could conclude that such models are unreliable. This model is also dynamically unstable within second order perturbation theory if it is embedded in a spin chain.

Not just ground states but also excited states may be stable in an isolated system if no energy can be exchanged with an environment. This is the situation usually realized in models of quantum cosmology, where the state represents the whole universe with nothing outside it. There are then further candidates for homogeneous configurations. Nevertheless, some caution toward such minisuperspace models in quantum gravity is still required: Our spin system can be taken as a model for

quantum space, in which near homogeneity should be possible and stable under evolution. However, there should also be matter, with additional degrees of freedom that could be placed on the same graph used for our spin chain but representing a different system. There could then be energy exchange between our spin system and the new matter system, and we would be back to the question whether a homogeneous spin configuration, representing quantum space, can be stable within the coupled system. The question of how matter is coupled to quantum space therefore seems important in the context of the emergence and stability of correlated quantum-cosmology states.

6.3 Non-local bispectra from super cosmic variance

In [3] we have considered non-Gaussian fields built from non-local real space expressions with up to cubic dependence on a Gaussian field. This ansatz, Eq.(5.61), can generate a variety of tree-level bispectra and trispectra, including shapes consistent with either single-clock or multi-field inflationary models. By examining the ways in which statistics in spatial sub-volumes can differ from the mean statistics of the parent volume we draw the following important conclusions:

- Terms at order n in a non-local expression for a non-Gaussian field $\Phi(\mathbf{x})$ can generically shift the amplitudes and momentum dependence of the power spectrum and correlations up to order $\langle\Phi(k_1)...\Phi(k_n)\rangle$ in biased sub-volumes, but need not shift *all* of them.

- More specifically, super cosmic variance effects can induce bispectra in biased subvolumes to match any of the equilateral, orthogonal, or local templates. The amplitude and sign of the induced bispectrum depends in a degenerate way on the background over- or under-density of the sub-volume as well as the amplitude and sign of the mean trispectrum. Depending on the specific form of the trispectrum, the power spectrum may or may not display a dependence on background density within the sub-volume.

Mathematically, our results are very reasonable: non-Gaussian statistics at each order are independent, so of course measuring the 3-point function alone constrains neither the shape nor the amplitude of higher order correlations. Furthermore,

different n-point correlations can induce indistinguishable contributions to lower order correlations in biased sub-volumes. When neither the bias nor the higher order correlations can be measured, there is a large degeneracy of correlation functions (and so inflation models) that can be consistent with just a few measurements. Specifically, we have demonstrated that a limited set of measurements of the primordial density correlations (e.g., a detection of $f_{\rm NL}^{\rm local} = 0$ and $f_{\rm NL}^{\rm equil} \neq 0$) could be consistent with single-clock inflation *or* a multi-field scenario. Measurement of a purely equilateral bispectrum does not in and of itself imply that there can be no super cosmic variance at work. To rule out super cosmic variance (at least, to rule it out of observational relevance) we must also constrain any correlation between statistics measured within smaller regions of our own Hubble volume and the background density of those regions.

We have hardly covered the space of non-Gaussian statistics: our set of examples was chosen to be a minimal set that allows us to explore the possible implications of cosmic variance from super horizon modes for non-local, scale-independent bispectra[1]. We see no obstruction to extending our results to find quartic terms in the non-local expansion that could bias, for example, the trispectrum but not the bispectrum. One might complain that super cosmic variance that evades detection in the simplest measurements (e.g., in the power spectrum) but biases higher order terms (e.g., the trispectrum) would require too much of a conspiracy to be realistic. Addressing this discomfort systematically requires a measure on the space of super cosmic variance effects from multi-field inflation models. It would be interesting to find an inflation model that contains trispectra of the sort we have found or to prove that no model can generate them, nor their higher order generalizations.

[1]There are many other terms one might wish to include to study further aspects of this problem. At the level of the quadratic terms, for example, we have not been sufficiently general to cover the other standard template for single-clock inflation (the 'orthogonal' template in the appendix of reference [190]). To expand the model to include this template would require allowing $\alpha_i < -2$. At cubic order, we eliminated some terms since they did not induce one of our desired quadratic terms at leading order. Keeping those terms would add more parameters that would relax some of the restrictions on the b_i from removing sub-leading terms (and badly behaved loop contributions).

6.4 Shapes for super cosmic variance free from non-Gaussianities

In [4] we have constructed a set of non-Gaussian fields built from non-local real space expressions up to second order in Gaussian field, and by expanding the second order term in the number of inverse derivatives. We restricted to fields with tree-level bispectra that couple short and long wavelength modes no more strongly than single-clock inflation does. Long wavelength background modes from these bispectra just act like curvature and so the coupling introduces no additional cosmic variance in the locally observed power spectrum. At the same order that we recover the familiar equilateral and orthogonal templates, we also find we can construct a third 'flat-only' shape with negligible overlap with those two. The shape is characterized by primarily coupling modes in flattened triangle configurations (and very little in the equilateral limit). In addition, it has a simple oscillation along the flat line.

We systematically investigated physics that can enhance terms beyond the minimal, lowest order shapes in the effective field theory of single-clock fluctuations including multiple ways to enhance terms with more derivatives and terms where one π carries no derivatives. We also computed cosines between the flat-only shape and typical suppressed terms with more or fewer derivatives. Finally, we looked at some shapes produced by non-trivial modifications of the background dynamics (dissipation). We found that none of these cases had the structure to naturally provide the oscillation along the flat-only limit that the template has. This all suggests that the flat-only shape may not describe any 'natural' single-clock model so far in the literature. We have checked a subset of linear combinations of single-clock shapes, but we have not been exhaustive. The shape could potentially be constructed from a fine-tuned combination of these standard effects, in which case it is not clear whether behavior along the flat limit indicative of any particular physics. It is also possible that the flat-only shape occurs naturally in a model that is not single-clock, but whose bispectrum accidentally realizes the symmetries associated with single-clock inflation. It would be interesting to try to reverse-engineer a model that generates this shape.

The broader context for this work is a better understanding of how best to frame

constraints from data on the space of possible non-Gaussian correlations. We have taken the point of view that the degree to which long modes are coupled to short modes is the most important qualitative feature and used that as an organizing principle. At any order, the space of fields whose bispectra have no appreciable cosmic variance from mode coupling must be greater than or equal to the space of shapes (natural or fine-tuned) from single-clock inflation. The details of the bispectrum away from the squeezed limit carry information about the physics of the model beyond its single-clock nature, and possibly even about whether the single-clock squeezed limit could be accidental.

Rather than finding a basis for the bispectrum, we have used a basis for the non-Gaussian field. This is useful because the field can be numerically realized. However, in the case where we expand only to the first non-Gaussian term and insist that it generates no cosmic variance in lower order correlation functions, correlations at different orders are only related via loop corrections. And, as we have shown by comparison with the earlier work in [206], there is sufficient degeneracy in going between the bispectrum shape and the field that loop corrections can always be satisfied. In other words, the correlation functions are pretty much decoupled and one may as well construct a basis for each order independently. But, when we expand the space of allowed correlations to include significant mode-coupling, the relationship between correlations at different orders is very informative (think, eg, of the non-Gaussian halo bias) and so constructing the field rather than the bispectrum alone is a better approach. As we showed in [3], mode coupling from higher order correlation functions can be entirely consistent with the presence of a bispectrum that has the single-clock (no cosmic variance) squeezed limit.

Finally, we note that the existing literature suggests that it would be worthwhile to continue this procedure of constructing the quadratic term to higher order in inverse derivatives. One can continue to compare to the construction in [206], and the natural single-clock bispectra proposed in [210] should be recovered. it would be interesting to compare the number total number of orthogonal, super cosmic variance free shapes constructed this way to the number so far discussed in the single-clock inflation literature.

Appendix A
Vector geometry for equal spins $j_{ab} = j$

Let us illustrate the structure of the space of vector geometries in the concrete case of equiareal tetrahedra. It is convenient to introduce the unit vectors $\mathbf{w}_{ab} := X_a \mathbf{n}_{ab}$. We will determine the dimensionality of the space of solutions to the critical point equations and discuss the relevant subspaces. From the condition $\mathbf{w}_{ab} = -\mathbf{w}_{ba}$, only ten of the twenty vectors $\mathbf{w}_{ab}$ can be independent—one per link. Consider the node 1. There are four vectors $\mathbf{w}_{1b}$ at the node. We can use the symmetry under global rotations to fix:

$$\mathbf{w}_{12} = \hat{\mathbf{z}}\,, \qquad \mathbf{w}_{13} = (\sin\theta, 0, \cos\theta)\,, \tag{A.1}$$

so that the two first vectors are described by a single parameter.

- For $\theta = 0$, we have $\mathbf{w}_{12} = \mathbf{w}_{13} = \hat{\mathbf{z}}$, and the closure relation gives $\mathbf{w}_{14} = \mathbf{w}_{15} = -\hat{\mathbf{z}}$. This is a degenerate case, where the normals form a linear object. This subspace contains a single solution.

- For $\theta = \pi$, $\mathbf{w}_{13} = -\mathbf{w}_{12} = -\hat{\mathbf{z}}$, and the closure relation gives $\mathbf{w}_{15} = -\mathbf{w}_{14}$, where $\mathbf{w}_{14}$ can be freely chosen. The symmetry under global rotations can be used to force one of the components of $\mathbf{w}_{14}$ to vanish, leaving one free parameter. Hence, this subspace is one-dimensional. If $\mathbf{w}_{14} = \pm\hat{\mathbf{z}}$, then the geometry is the same as for $\theta = 0$. The normals form a planar object, and we have again a degenerate geometry.

- Now take $\theta \neq 0, \pi$. From the closure relation $\sum_{b\neq 1} \mathbf{w}_{1b} = 0$, it follows that

the partial sum $\mathbf{w}_{12} + \mathbf{w}_{13} + \mathbf{w}_{14}$ must be a unit vector, equal to $-\mathbf{w}_{15}$. The possible choices of $\mathbf{w}_{14}$ form a unit sphere centered at $0 + \mathbf{w}_{12} + \mathbf{w}_{13}$, which intersects the unit sphere centered at the origin 0 at a one-dimensional loop. Therefore, we have one free parameter associated with $\mathbf{w}_{14}$, and the space of solutions to the closure relation, up to global rotations, is two-dimensional. If one takes $\mathbf{w}_{14} = -\mathbf{w}_{13}$ or $-\mathbf{w}_{12}$, then the normals form a parallelogram, and we have a degenerate geometry. For any other choice, the normals form a nondegenerate geometry of nonzero volume, describing a unique tetrahedron.

In short, the space of solutions of the closure relation at a node, up to rotations, is two-dimensional, and the subset of degenerate solutions forms a lower dimensional subspace.

Consider now the node 2. We have $\mathbf{w}_{21} = -\mathbf{w}_{12}$. The vector $\mathbf{w}_{23}$ is completely free, requiring two free parameters for its description. As before, we have a single extra parameter for the description of $\mathbf{w}_{24}$, in order for the closure relation to admit a solution. The last vector $\mathbf{w}_{25}$ is then fixed by the closure relation. We have three additional parameters associated with the second node.

For the node 3, the vectors $\mathbf{w}_{31}$ and $\mathbf{w}_{32}$ are fixed by the previous choices of normals for the nodes 1 and 2. We have again one free parameter for the possible choices of $\mathbf{w}_{34}$. However, the same is true for $\mathbf{w}_{43} = -\mathbf{w}_{34}$ at the node 4, and the intersection of two loops on the sphere is in general formed by isolated points, and we do not have a new degree of freedom associated with these nodes. All remaining vectors at the nodes 3 and 4 are then fixed by the closure relations. The closure relation at the node 5 imposes an additional condition, but this is automatically satisfied when the closure relations at the nodes 1 to 4 and the link conditions are satisfied.

We conclude that the space of solutions to the critical point conditions on the pentagram with all spins equal, $j_\ell = j$, is characterized by five parameters, and the subset of degenerate geometries forms a lower-dimensional subset at the boundary of the parameter space.

Appendix B
Entanglement entropy at fixed total area J

It is interesting to test whether the entanglement entropy of the Bell states $|\Gamma_2, \mathrm{B}_\gamma, j_\ell\rangle$ obeys an area-law in the limit of large spins characterizing the semi-classical regime for the geometry of the dipole graph. We start by expressing the projection of the squeezed vacua $|\Gamma_2, \mathrm{B}_\gamma\rangle$ to the subspace of states with total area $J = \sum_\ell j_\ell$ in the basis of Bell intertwiners:

$$|\Gamma_2, \mathrm{B}_\gamma, J\rangle = \frac{1}{\sqrt{N(J)}} \sum_{\substack{\sum_\ell j_\ell = J \\ \text{s.t. } \exists\, \mathrm{i_k}}} \sum_{k=0}^{\dim(\mathcal{K}_{j_1 \cdots j_L})-1} |i_k\rangle_t |\tilde{i}_k\rangle_s \,, \tag{B.1}$$

where the normalization constant is determined by the dimensionality of the intertwiner space with L links and for a fixed total area J, which is given by [219]:

$$N(J) = \frac{1}{(J+1)} \binom{J+L-1}{J} \binom{J+L-2}{J} . \tag{B.2}$$

The reduced density matrix $\rho_s(\lambda)$ at the source node is obtained by tracing out the degrees of freedom of the target node:

$$\rho_s = \frac{\mathbb{1}_s}{\mathrm{Tr_s}\, \mathbb{1}_s} . \tag{B.3}$$

This density matrix describes a uniform distribution of probabilities in the intertwiner space, corresponding to a microcanonical ensemble for the local geometry at the source node compatible with the condition that the total area is equal to J.

The entanglement entropy is given by:

$$S(J) = \log N(J)\,. \tag{B.4}$$

The asymptotics of the entropy $S(J)$ can be computed for large total area J using Stirling approximation for the factorials. At the leading order, the dimension of interwiner space $N(J)$ is:

$$N(J) \sim \frac{1}{2\pi J L^2}\left(1+\frac{L}{N}\right)^{2J}\left(1+\frac{J}{N}\right)^{2L-3}. \tag{B.5}$$

If the number of links L is fixed and the total area J is sent to infinity, then we obtain a logarithmic entropy [219]:

$$\lim_{J\to\infty} S(J) \sim (2L-4)\log J\,. \tag{B.6}$$

We can conclude that the Bell state $|\Gamma, \mathrm{B}_\gamma, J\rangle$ on a dipole graph with arbitrary number of links and at fixed total area does not obey an area-law for the entanglement (or black hole) entropy. Moreover, we can obtain an entanglement entropy linear in J with potentially logarithmic divergent factor by letting the number of links $N \gg 1$.

Appendix C
Derivation of the Bell states on a pentagram graph

The projection of $|\mathrm{B}_\gamma\rangle \in \mathcal{H}_{bos}$ to the space of spin network states $\mathcal{H}_{\Gamma_5} \subset \mathcal{H}_{bos}$ is

$$|\Gamma_5, \mathrm{B}_\gamma\rangle = P_{\Gamma_5}|\mathrm{B}_\gamma\rangle\,. \tag{C.1}$$

Fixing the spins, we obtain a Bell state with determined spins:

$$|\Gamma_5, \mathrm{B}_\gamma, j_{ab}\rangle = P_{\Gamma_5}|\mathrm{B}_\gamma, j_{ab}\rangle\,, \tag{C.2}$$

where

$$|\mathrm{B}_\gamma, j_{ab}\rangle = \bigotimes_{a<b}\sum_{m_{ab}}(-1)^{j_{ab}-m_{ab}}|j_{ab}, m_{ab}\rangle \otimes |j_{ba}, -m_{ab}\rangle\,. \tag{C.3}$$

We adopt the convention that a ket $|j_{ab}, m_{ab}\rangle$ with spin j_{ab} lives at the endpoint a of the link $\overline{ab}$. The state $|\mathrm{B}_\gamma, j_{ab}\rangle$ is by construction area-matched. The projection to the space of gauge-invariant states is easily constructed using the orthonormal intertwiner basis labeled by the virtual spins i_a:

$$P_{\Gamma_5} = \bigotimes_a P_a\,, \qquad P_a = \sum_{i_a}|i_a\rangle\langle i_a|\,, \tag{C.4}$$

where $|i_a\rangle \in \mathcal{H}_a = \mathrm{Inv}[\bigotimes_{b:a\neq b} V_{j_{ab}}]$.

We represent the orthonormal intertwiners in the magnetic basis as:

$$|i_1\rangle = \sum_m [i_1]^{m_{12}m_{13}m_{14}m_{15}}|j_{12}, m_{12}\rangle \otimes |j_{13}, m_{13}\rangle \otimes |j_{14}, m_{14}\rangle \otimes |j_{15}, m_{15}\rangle\,, \tag{C.5}$$

and similarly for the other values of a. The dual bases with respect to the standard Hilbert space inner product and to the ϵ bilinear form are:

$$\langle i_1| = \sum_m [\bar{i_1}]^{m_{12}m_{13}m_{14}m_{15}} \langle j_{12}, m_{12}| \otimes \langle j_{13}, m_{13}| \otimes \langle j_{14}, m_{14}| \otimes \langle j_{15}, m_{15}| \,,$$

$$[i_1| = \sum_m \left[\prod_b (-1)^{j_{1b}-m_{1b}}\right] [i_1]^{-m_{12},-m_{13},-m_{14},-m_{15}} \langle j_{12}, m_{12}| \otimes \langle j_{13}, m_{13}| \otimes \langle j_{14}, m_{14}| \otimes \langle j_{15}, m_{15}| \,.$$

The antilinear time-reversal operator is defined as $\zeta|i_1\rangle = |i_1]$, with

$$|i_1] = \sum_m \left[\prod_{b\neq 1} (-1)^{j_{1b}-m_{1b}}\right] [\bar{i_1}]^{-m_{12},-m_{13},-m_{14},-m_{15}} |j_{12}, m_{12}\rangle \otimes |j_{13}, m_{13}\rangle \otimes |j_{14}, m_{14}\rangle \otimes |j_{15}, m_{15}\rangle \,.$$

The projector P_{Γ_5} can be implemented node by node. We first represent the state $|\mathrm{B}_\gamma, j_{ab}\rangle$ (before the projection) as a superposition of tensor products of node states in the form:

$$|\mathrm{B}_\gamma, j_{ab}\rangle = \sum_{m_{ab}} \bigotimes_a |\mathrm{B}_{\gamma_a}(m_{ab})\rangle \,. \tag{C.6}$$

Then we project each of the components in the above expansion to the gauge-invariant subspace. The representation (C.6) is not unique, and we can choose, for instance:

$$\begin{aligned}
|\mathrm{B}_{\gamma_1}\rangle &= |j_{12}, m_{12}\rangle \otimes \cdots \otimes |j_{15}, m_{15}\rangle \,, \\
|\mathrm{B}_{\gamma_2}\rangle &= (-1)^{j_{12}-m_{12}} |j_{21}, -m_{12}\rangle \otimes |j_{23}, m_{23}\rangle \otimes |j_{14}, m_{14}\rangle \otimes |j_{15}, m_{15}\rangle \,, \\
|\mathrm{B}_{\gamma_3}\rangle &= \left[\prod_{b<3} (-1)^{j_{b3}-m_{b3}}\right] |j_{31}, -m_{13}\rangle \otimes |j_{32}, -m_{23}\rangle \otimes |j_{34}, m_{34}\rangle \otimes |j_{35}, m_{35}\rangle \,, \\
|\mathrm{B}_{\gamma_4}\rangle &= \left[\prod_{b<4} (-1)^{j_{b4}-m_{b4}}\right] |j_{41}, -m_{14}\rangle \otimes |j_{42}, -m_{24}\rangle \otimes |j_{43}, -m_{34}\rangle \otimes |j_{45}, m_{45}\rangle \,, \\
|\mathrm{B}_{\gamma_5}\rangle &= \left[\prod_{b<5} (-1)^{j_{b5}-m_{b5}}\right] |j_{51}, -m_{15}\rangle \otimes |j_{52}, -m_{25}\rangle \otimes |j_{53}, -m_{35}\rangle \otimes |j_{54}, -m_{45}\rangle \,,
\end{aligned}$$

by attaching the signs $(-1)^{j_{ab}-m_{ab}}$ in (C.3) always to the source node, at all links.

Then the projected node states are:

$$
\begin{aligned}
P_1|\mathrm{B}_{\gamma_1}(m_{ab})\rangle &= \sum_{i_1} [\bar{i_1}]^{m_{12},m_{13},m_{14},m_{15}}|i_1\rangle\,,\\
P_2|\mathrm{B}_{\gamma_2}(m_{ab})\rangle &= \sum_{i_2} (-1)^{j_{12}-m_{12}}[\bar{i_2}]^{-m_{12},m_{23},m_{24},m_{25}}|i_2\rangle\,,\\
P_3|\mathrm{B}_{\gamma_3}(m_{ab})\rangle &= \sum_{i_3} \left[\prod_{b<3}(-1)^{j_{b3}-m_{b3}}\right] [\bar{i_3}]^{-m_{13},-m_{23},m_{34},m_{35}}|i_3\rangle\,,\\
P_4|\mathrm{B}_{\gamma_4}(m_{ab})\rangle &= \sum_{i_4} \left[\prod_{b<4}(-1)^{j_{b4}-m_{b4}}\right] [\bar{i_4}]^{-m_{14},-m_{24},-m_{34},m_{45}}|i_4\rangle\,,\\
P_5|\mathrm{B}_{\gamma_5}(m_{ab})\rangle &= \sum_{i_5} \left[\prod_{b<5}(-1)^{j_{b5}-m_{b5}}\right] [\bar{i_5}]^{-m_{15},-m_{25},-m_{35},-m_{45}}|i_5\rangle\,.
\end{aligned}
$$

Taking their tensor product and summing over the indices m_{ab}, we obtain:

$$
\begin{aligned}
|\Gamma_5, \mathrm{B}_\gamma, j_{ab}\rangle =& \sum_{m_{ab}} \left[\prod_{c<d}(-1)^{j_{cd}-m_{cd}}\right] \sum_{i_a} \left(\bigotimes_{k=1}^{5}|i_k\rangle\right) [\bar{i_1}]^{m_{12},m_{13},m_{14},m_{15}}[\bar{i_2}]^{-m_{12},m_{23},m_{24},m_{25}}\\
&\times [\bar{i_3}]^{-m_{13},-m_{23},m_{34},m_{35}}[\bar{i_4}]^{-m_{14},-m_{24},-m_{34},m_{45}}[\bar{i_5}]^{-m_{15},-m_{25},-m_{35},-m_{45}}\\
=& \sum_{m_{ab}} \sum_{i_a} \left(\bigotimes_{k=1}^{5}|i_k\rangle\right) [\bar{i_1}]^{m_{12},m_{13},m_{14},m_{15}}[\bar{i_2}]_{m_{12}}{}^{m_{23},m_{24},m_{25}}\\
&\times [\bar{i_3}]_{m_{13},m_{23}}{}^{m_{34},m_{35}}[\bar{i_4}]_{m_{14},m_{24},m_{34}}{}^{m_{45}}[\bar{i_5}]_{m_{15},m_{25},m_{35},m_{45}}\\
=& \sum_{i_a} \left(\bigotimes_{k=1}^{5}|i_k\rangle\right) \overline{15j(j_{ab}, i_a)}\,,
\end{aligned}
\tag{C.7}
$$

where the $15j$ symbol is the contraction of the intertwiners determined by the graph Γ_5:

$$
15j = [i_1]^{m_{12}m_{13}m_{14}m_{15}}[i_2]_{m_{12}}{}^{m_{23}m_{24}m_{25}}[i_3]_{m_{13}m_{23}}{}^{m_{34}m_{35}}[i_4]_{m_{14}m_{24}m_{34}}{}^{m_{45}}[i_5]_{m_{15}m_{25}m_{35}m_{45}}\,,
\tag{C.8}
$$

with indices raised and lowered with the ϵ-isomorphism.

Appendix D
Hessian of the action for $15j$-symbol

Now we will derive explicitly the Hessian of the action for $15j$-symbol. The action for the asymptotic problem of the $15j(j_{ab}, \mathbf{n}_{ab})$ symbol is

$$S_{(j,\mathbf{n})}[X] = \sum_{b<a} 2j_{ab} \ln \langle \zeta \mathbf{n}_{ab} | X_a^{-1} X_b | \mathbf{n}_{ab} \rangle \,, \tag{D.1}$$

where it encodes a global $SU(2)$ continuous symmetry and a discrete $\pm$ symmetry at each vertex a, given by $X'_a = \epsilon_a Y X_a$ with $Y \in SU(2)$ and $\epsilon_a = \pm$. In order to find the critical points to the action, we need to compute the variation of the action with respect to the $SU(2)$ group elements X_a. The variation of the $SU(2)$ group element is simply $\delta X = \tau X$ with the variation of its inverse $\delta X^{-1} = -X^{-1}\tau$, where $\tau_i = \frac{1}{2} i \sigma_i$ is the $su(2)$ algebra element. Therefore, the partial derivative of the action with respect to a $SU(2)$ element X_d^j is

$$\begin{aligned}
\frac{\partial S_{(j,\mathbf{n})}[X]}{\partial X_d^j} &= \sum_{b<a} 2j_{ab} \left\{ \frac{\langle -\mathbf{n}_{db} | X_d^{-1}(-\tau_j)\delta_{ad} X_b | \mathbf{n}_{bd} \rangle}{\langle -\mathbf{n}_{db} | X_d^{-1} X_b | \mathbf{n}_{bd} \rangle} + \frac{\langle -\mathbf{n}_{ad} | X_a^{-1} \tau_j \delta_{bd} X_d | \mathbf{n}_{da} \rangle}{\langle -\mathbf{n}_{ad} | X_a^{-1} X_d | \mathbf{n}_{da} \rangle} \right\} \\
&= \sum_{b<d} 2j_{db} \frac{\langle -\mathbf{n}_{db} | X_d^{-1}(-\tau_j) X_b | \mathbf{n}_{bd} \rangle}{\langle -\mathbf{n}_{db} | X_d^{-1} X_b | \mathbf{n}_{bd} \rangle} + \sum_{a>d} 2j_{ad} \frac{\langle -\mathbf{n}_{ad} | X_a^{-1} \tau_j X_d | \mathbf{n}_{da} \rangle}{\langle -\mathbf{n}_{ad} | X_a^{-1} X_d | \mathbf{n}_{da} \rangle} \,,
\end{aligned}$$

where $|-\mathbf{n}_{ab}\rangle$ is obtained by the action of the antilinear map ζ on coherent states, which takes $\mathbf{n}$ to $-\mathbf{n}$. The stationarity of the action $\delta S_{(j,\mathbf{n})}[X] = 0$ leads to a set of

complex vector equations:

$$\sum_{b\neq a} j_{ab}\mathbf{v}_{ab} = 0, \;\; \mathbf{v}_{ab} = -\mathbf{v}_{ba}\,, \tag{D.2}$$

where the vector $\mathbf{v}_{ab}$ is defined as

$$\mathbf{v}_{ab} = \frac{\langle -\mathbf{n}_{ab}|X_a^{-1}\boldsymbol{\sigma}X_b|\mathbf{n}_{ba}\rangle}{\langle -\mathbf{n}_{ab}|X_a^{-1}X_b|\mathbf{n}_{ba}\rangle} \tag{D.3}$$

and the minus sign of the second term in the variation of the action can be taken in a single expression by knowing that the epsilon inner product $\epsilon(T\alpha,\beta) = -\epsilon(\alpha,T\beta)$ for algebra element T and $\epsilon(g\alpha,\beta) = \epsilon(\alpha,g^{-1}\beta)$ for group element g. As the action of the group element on coherent states $|\mathbf{n}_{ab}\rangle$ produces new set of coherent states $|\mathbf{n'}_{ab}\rangle$, $X_a|\mathbf{n}_{ab}\rangle = |\mathbf{n'}_{ab}\rangle$, we can simplify the vector $\mathbf{v}_{ab}$ expression:

$$\mathbf{v}_{ab} = \frac{\langle -\mathbf{n'}_{ab}|\boldsymbol{\sigma}|\mathbf{n'}_{ba}\rangle}{\langle -\mathbf{n'}_{ab}||\mathbf{n'}_{ba}\rangle} = \frac{(\mathbf{n'}_{ba}-\mathbf{n'}_{ab}) - i(-\mathbf{n'}_{ab}\times\mathbf{n'}_{ba})}{1-\mathbf{n'}_{ab}\mathbf{n'}_{ba}} = -\mathbf{n'}_{ab}\,, \tag{D.4}$$

where we used the scalar product of coherent states and the projector $P_n = |\mathbf{n}\rangle\langle\mathbf{n}| = \frac{1}{2}(\mathbb{I}+\boldsymbol{\sigma}\cdot\mathbf{n})$. It is clear that the stationary methods can be extended for real part of the function so that the real part of the action is maximized by setting the imaginary part to zero, $\mathbf{n'}_{ab}$ and $\mathbf{n'}_{ba}$ should be anti-parallel, $X_a\mathbf{n}_{ab} = -X_b\mathbf{n}_{ba}$. Therefore we have ten equations

$$X_a\mathbf{n}_{ab} = -X_b\mathbf{n}_{ba} \tag{D.5}$$

for maximizing the action and five equations for the stationarity of the action

$$\sum_{b\neq a} j_{ab}\mathbf{n}_{ab} = 0\,. \tag{D.6}$$

The solutions to the critical equations (D.5)-(D.6) contain an interpretation in terms of the BF theory. They can be considered as the solutions of a four-dimensional BF theory with group $SU(2)$ discretized on a 4-simplex. Therefore, the solutions can be parametrized by the X_a and $\mathbf{b}_{ab} = j_{ab}X_a\mathbf{n}_{ab}$. These are the discrete connection and B-field variables, respectively. The critical equations are now expressed in

terms of the $\mathbf{b}_{ab}$:

$$\sum_{b:b\neq a} \mathbf{b}_{ab} = 0, \quad \mathbf{b}_{ab} = -\mathbf{b}_{ba}\,, \tag{D.7}$$

which determines a vector geometry by twenty three-dimensional vectors $\mathbf{b}_{ab}$. The X_a variables are a discrete version of the connection on a BF theory. This is due to the gluing of two 4-simplexes followed by the identification of the $\mathbf{n}_{ab}$ variables on a common tetrahedron. In terms of the vector geometry ($\mathbf{b}_{ab}$ variables), this implies that the gluing takes place after the action of the corresponding X_a for the tetrahedron.

As we have the critical points to the action, we can evaluate the Hessian of the action. The Hessian is the second derivative of the action with respect to the group element:

$$\begin{aligned}
H^{ij}_{cd} \equiv \frac{\partial^2 S_{(j,\mathbf{n})}[X]}{\partial X^i_c \partial X^j_d} = \sum_{b<d} 2j_{db} \Bigg\{ & \frac{\langle -\mathbf{n}_{cb}|X_c^{-1}(\tau_i\tau_j)\delta_{cd}X_b|\mathbf{n}_{bc}\rangle}{\langle -\mathbf{n}_{cb}|X_c^{-1}X_b|\mathbf{n}_{bc}\rangle} + \frac{\langle -\mathbf{n}_{dc}|X_d^{-1}(-\tau_j\tau_i)\delta_{bc}X_c|\mathbf{n}_{cd}\rangle}{\langle -\mathbf{n}_{dc}|X_d^{-1}X_c|\mathbf{n}_{cd}\rangle} \\
& - \frac{\langle -\mathbf{n}_{db}|X_d^{-1}(-\tau_j)X_b|\mathbf{n}_{bd}\rangle}{\langle -\mathbf{n}_{db}|X_d^{-1}X_b|\mathbf{n}_{bd}\rangle^2}\Big(\langle -\mathbf{n}_{cb}|X_c^{-1}(-\tau_i)\delta_{cd}X_b|\mathbf{n}_{bc}\rangle + \langle -\mathbf{n}_{dc}|X_d^{-1}\tau_i\delta_{bc}X_c|\mathbf{n}_{cd}\rangle\Big) \Bigg\} \\
+ \sum_{a>d} 2j_{ad} \Bigg\{ & \frac{\langle -\mathbf{n}_{cd}|X_c^{-1}(-\tau_i\tau_j)\delta_{ca}X_d|\mathbf{n}_{dc}\rangle}{\langle -\mathbf{n}_{cd}|X_c^{-1}X_d|\mathbf{n}_{dc}\rangle} + \frac{\langle -\mathbf{n}_{ac}|X_a^{-1}(\tau_j\tau_i)\delta_{cd}X_c|\mathbf{n}_{ca}\rangle}{\langle -\mathbf{n}_{ac}|X_a^{-1}X_c|\mathbf{n}_{cd}\rangle} \\
& - \frac{\langle -\mathbf{n}_{ad}|X_a^{-1}(\tau_j)X_d|\mathbf{n}_{da}\rangle}{\langle -\mathbf{n}_{ad}|X_a^{-1}X_d|\mathbf{n}_{da}\rangle^2}\Big(\langle -\mathbf{n}_{cd}|X_c^{-1}(-\tau_i)\delta_{ac}X_d|\mathbf{n}_{dc}\rangle + \langle -\mathbf{n}_{ac}|X_a^{-1}\tau_i\delta_{cd}X_c|\mathbf{n}_{ca}\rangle\Big) \Bigg\}
\end{aligned}$$

for the case $c < d$ and $c > d$ with using the definition of $\mathbf{v}_{ab}$ we have:

$$\begin{aligned}
c<d : & -\frac{1}{2}j_{cd}\left[\frac{\langle -\mathbf{n}_{dc}|X_d^{-1}(-\delta_{ij}-i\epsilon_{ijk}\sigma_k)X_c|\mathbf{n}_{cd}\rangle}{\langle -\mathbf{n}_{dc}|X_d^{-1}X_c|\mathbf{n}_{cd}\rangle} + v^j_{dc}v^i_{dc}\right] \\
& = -\frac{1}{2}j_{cd}\big(-\delta_{ij} - i\epsilon_{ijk}v^k_{cd} + v^i_{cd}v^j_{cd}\big) \\
c>d : & -\frac{1}{2}j_{cd}\left[\frac{\langle -\mathbf{n}_{cd}|X_c^{-1}(-\delta_{ij}-i\epsilon_{ijk}\sigma_k)X_d|\mathbf{n}_{dc}\rangle}{\langle -\mathbf{n}_{cd}|X_c^{-1}X_d|\mathbf{n}_{dc}\rangle} + v^j_{cd}v^i_{cd}\right] \\
& = -\frac{1}{2}j_{cd}\big(-\delta_{ij} - i\epsilon_{ijk}v^k_{cd} + v^i_{cd}v^j_{cd}\big)\,,
\end{aligned} \tag{D.8}$$

and for $c = d$:

$$c = d : -\frac{1}{4}\Bigg\{ \sum_{b<c} 2j_{bc}\left(\frac{\langle -\mathbf{n}_{bc}|X_c^{-1}(\delta_{ij} + i\epsilon_{ijk}\sigma_k)X_b|\mathbf{n}_{bc}\rangle}{\langle -\mathbf{n}_{cb}X_c^{-1}X_b|\mathbf{n}_{bc}\rangle|} - v^j_{cb}v^i_{cb}\right) + \sum_{a>c} 2j_{ac}\left(\frac{\langle -\mathbf{n}_{ac}|X_a^{-1}(\delta_{ij} + i\epsilon_{ijk}\sigma_k)X_c|\mathbf{n}_{ca}\rangle}{\langle -\mathbf{n}_{ac}|X_a^{-1}X_c|\mathbf{n}_{ca}\rangle} - v^j_{ac}v^i_{ac}\right)\Bigg\} = -\frac{1}{4}\sum_{b\neq c} 2j_{bc}(\delta_{ij} + i\epsilon_{ijk}v^k_{cb} - v^i_{cb}v^j_{cb})\,, \tag{D.9}$$

where we have used the identity $\sigma_i\sigma_j = \delta_{ij} + i\epsilon_{ijk}\sigma_k$. The Hessian of the action, as a second derivative test of a function, can be used to express the asymptotic expansion of the integral over the group elements X, which corresponds to 15j-symbol proportional to $e^{\lambda S}$ given by the boundary data:

$$15j(\lambda j, n) \sim \left(\frac{2\pi}{\lambda}\right)^6 \frac{1}{\sqrt{\det H}}\, e^{\lambda S(X)}\,, \tag{D.10}$$

where the action S for the $15j$-symbol is evaluated at the critical points derived above. In order to apply the method of extended stationary phase we need to ensure that the stationary points are isolated. This is accomplished by fixing $SU(2)$ elements as: $X'_a = (X_5)^{-1}X_a$ for $a = \{1, \cdots, 4\}$. The "gauge fixed" integral formulas then have isolated critical points related only by the discrete symmetries and can now be evaluated using extended stationary phase. After gauge fixing and deriving the expression of the Hessian H^{ij}_{cd} for a given boundary data $\{j_{ab}, \mathbf{n}_{ab}\}$, we can perform the explicit calculation of the Hessian matrix H:

$$H = \begin{bmatrix} H_{11} & H_{12} & \dots & H_{14} \\ H_{21} & H_{22} & \dots & H_{24} \\ \vdots & \vdots & \vdots & \vdots \\ H_{41} & H_{42} & \dots & H_{44} \end{bmatrix}\,. \tag{D.11}$$

Appendix E
Shape-matched configurations for a 4-simplex in $\mathbb{R}^3$

The boundary data of a 4-simplex in $\mathbb{R}^3$ is equipped with a metric of signature $0++$ and has the same metric geometry as a linear immersion of the simplex into $\mathbb{R}^3$. For a single solution set X_a to the critical point equations, the gluing map g_{ab} can be either an identity or π rotation with which the boundary data coincides with the $3d$ Euclidean geometry. In other words, the shape-matched normals in $3d$ space should form the boundary of a 4-simplex via geometric way. It is obvious to start with gluing five copies of a tetrahedron in order to form a shape-matched configuration for the boundary of a 4-simplex but gluing five copies of a tetrahedron consistently requires boosts in $\mathbb{R}^4$ such that the induced metrics on the triangle agree for both of the tetrahedra sharing any given triangle, and the induced orientations are opposite. For this geometric set, we can have two inequivalent set of solutions $\{X_a, X'_a\}$ for shape-matching configurations. Let us construct a table of possible class of set of solutions (SM-2 and no solution $\times$) for gluing five copies of a tetrahedron for a 4-simplex with a particular spin choice:

Boundary data $(j, \mathbf{n})$	SM-2, $\times$
5 copies of an equiareal tetrahedron ($j_1 = j_2 = j_3 = j_4$)	SM-2
5 copies of a tetrahedron ($j_1 = j_2 \neq j_3 = j_4$ or perms.)	SM-2
5 copies of a tetrahedron ($j_1 \neq j_2 \neq j_3 = j_4$ or perms.)	$\times$
5 copies of a tetrahedron ($j_1 \neq j_2 \neq j_3 \neq j_4$)	$\times$

Table E.1. A table for solutions for gluing five copies of a tetrahedron for a 4-simplex with a fixed spin configuration

There are two types of boundary data which do not have any solutions due to the fact that they do not satisfy area matching constraints $j_{ab} = j_{ba}$, i.e. they do not glue at all.

E.1 Pachner move: 1-4

We will construct the boundary of a 4-simplex in $\mathbb{R}^3$ out of local modifications to a 3-manifold triangulation, where a collection of five tetrahedra whose twenty faces are glued together in ten pairs. There are four such modifications knowns as Pachner moves: **1-4** move is replacing a single tetrahedron with four distinct tetrahedra meeting at a common internal vertex. **2-3** move is taking two distinct tetrahedra joined along a common face with three distinct tetrahedra joined along a common edge. The remaining moves, 3-2 and 4-1 moves, are just inverse to the 2-3 and 1-4 moves. These moves do not change the topology of the triangulation at all. We will consider only 1-4 and 2-3 moves since their critical point equations or the orientation conditions for the relevant vector geometry are exactly the same as in 4-1 and 3-2, respectively.

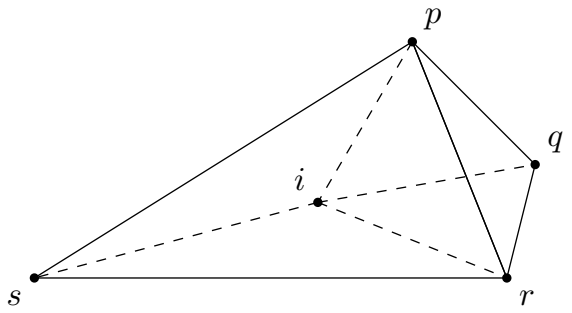

Figure E.1. This is a description of a 1-4 move to construct five glued tetrahedra by placing a fifth vertex i, origin of the coordinates, in the center point of the tetrahedra $pqrs$ labeled by τ_f.

Consider a regular tetrahedron τ_f with side length 2 by having four position vectors of four vertices where the regular tetrahedron is centered at the origin of the coordinates:

$$\mathbf{p}^T = (1, 0, -\frac{1}{\sqrt{2}}),\ \ \mathbf{q}^T = (-1, 0, -\frac{1}{\sqrt{2}}),\ \ \mathbf{r}^T = (0, 1, \frac{1}{\sqrt{2}}),\ \ \mathbf{s}^T = (0, -1, \frac{1}{\sqrt{2}}) \,. \quad \text{(E.1)}$$

We can construct the edge vectors $\mathbf{e}_k$ in order to fully determine the regular tetrahedron:

$$\mathbf{e}_1 = \mathbf{p} - \mathbf{s}, \;\; \mathbf{e}_2 = \mathbf{q} - \mathbf{s}, \;\; \mathbf{e}_3 = \mathbf{r} - \mathbf{s}\,. \tag{E.2}$$

One can obtain the outward normals of the regular tetrahedron ($\mathbf{E} = A_{\rm out}^{1-4}\,\mathbf{n}$, $A_{\rm out}^{1-4} = \sqrt{3}$) from the "electric field" on each face of the tetrahedron:

$$\mathbf{E}_1 = \frac{1}{2}(\mathbf{e}_2 \times \mathbf{e}_3), \;\; \mathbf{E}_2 = \frac{1}{2}(\mathbf{e}_3 \times \mathbf{e}_1), \;\; \mathbf{E}_3 = \frac{1}{2}(\mathbf{e}_1 \times \mathbf{e}_2) \tag{E.3}$$

with satisfying the closure condition on the regular tetrahedron $\mathbf{E}_4 = -(\mathbf{E}_1 + \mathbf{E}_2 + \mathbf{E}_3)$ and the normals related to the exterior faces of τ_f are then:

$$\mathbf{n}_{cf} = (1/A_{\rm out}^{1-4})\,\mathbf{E}_3, \;\; \mathbf{n}_{af} = (1/A_{\rm out}^{1-4})\,\mathbf{E}_1, \;\; \mathbf{n}_{bf} = (1/A_{\rm out}^{1-4})\,\mathbf{E}_2, \;\; \mathbf{n}_{df} = -(\mathbf{n}_{cf} + \mathbf{n}_{af} + \mathbf{n}_{bf})\,,$$

where the labelings a, b, c, d correspond to the four interior tetrahedra $\tau_a, \tau_b, \tau_c, \tau_d$, respectively. The normals of the interior faces with area $A_{\rm in}^{1-4} = 1/\sqrt{2}$ belonging to the four interior tetrahedra are:

$$\tau_b : \mathbf{n}_{cb} = \frac{1}{2A_{\rm in}^{1-4}}(\mathbf{d} - \mathbf{f}) \times (\mathbf{a} - \mathbf{f}), \;\; \mathbf{n}_{db} = \frac{1}{2A_{\rm in}^{1-4}}(\mathbf{a} - \mathbf{f}) \times (\mathbf{c} - \mathbf{f}),$$
$$\mathbf{n}_{ab} = \frac{1}{2A_{\rm in}^{1-4}}(\mathbf{c} - \mathbf{f}) \times (\mathbf{d} - \mathbf{f}), \;\; \mathbf{n}_{fb} = \mathbf{n}_{bf}$$

$$\tau_d : \mathbf{n}_{ad} = \frac{1}{2A_{\rm in}^{1-4}}(\mathbf{b} - \mathbf{f}) \times (\mathbf{c} - \mathbf{f}), \;\; \mathbf{n}_{cd} = \frac{1}{2A_{\rm in}^{1-4}}(\mathbf{a} - \mathbf{f}) \times (\mathbf{b} - \mathbf{f}),$$
$$\mathbf{n}_{bd} = -\mathbf{n}_{db}, \;\; \mathbf{n}_{fd} = \mathbf{n}_{df}$$

$$\tau_a : \mathbf{n}_{ca} = \frac{1}{2A_{\rm in}^{1-4}}(\mathbf{b} - \mathbf{f}) \times (\mathbf{d} - \mathbf{f}), \;\; \mathbf{n}_{fa} = \mathbf{n}_{af}, \;\; \mathbf{n}_{da} = -\mathbf{n}_{ad}, \;\; \mathbf{n}_{ba} = -\mathbf{n}_{ab}$$

$$\tau_c : \mathbf{n}_{fc} = \mathbf{n}_{cf}, \, \mathbf{n}_{ac} = -\mathbf{n}_{ca}, \;\; \mathbf{n}_{dc} = -\mathbf{n}_{cd}, \;\; \mathbf{n}_{bc} = -\mathbf{n}_{cb}\,, \tag{E.4}$$

where there are in total 4 aligned and 6 back to back conditions on the normals. These conditions can be applied to the configurations other than shape-matched

in the 1-4 vector geometry. As the normals are obtained on a shape-matched configuration for a 4-simplex, we can compute $|\det H|^{-1/2}$ for fixed spins $j_{\rm out} = 2, j_{\rm in} = 2/\sqrt{6}$, which is related to the ratio of the areas $(A_{\rm out}, A_{\rm in})$ of the exterior and interior faces, on this boundary data:

$$|\det H_0|^{1/2}_{1-4} = 0.204947\,. \tag{E.5}$$

E.2 Pachner move: 2-3

Now we can consider 2-3 move to construct a 4-simplex in $\mathbb{R}^3$ which shown in Fig. E.2.

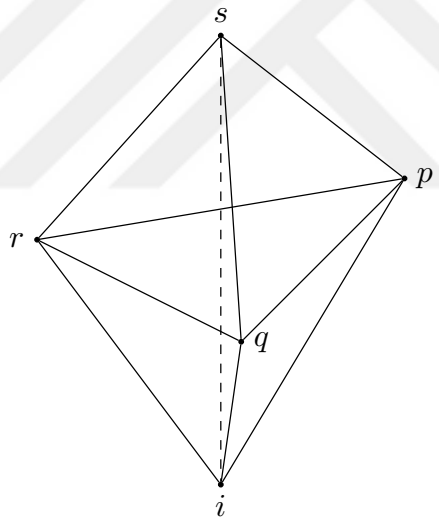

Figure E.2. Pachner move 2-3. Two tetrahedra glued back to back are transformed into three tetrahedra with the inclusion of a new edge from the vertex s to the vertex i.

Consider two regular tetrahedra glued back to back with side length of 2 by having five position vectors of five vertices where the regular tetrahedron at the top is centered at the origin of the coordinates:

$$\mathbf{p}^T = (1, 0, -\frac{1}{\sqrt{2}}),\ \mathbf{q}^T = (-1, 0, -\frac{1}{\sqrt{2}}),\ \mathbf{r}^T = (0, 1, \frac{1}{\sqrt{2}}),\ \mathbf{s}^T = (0, -1, \frac{1}{\sqrt{2}}),\ \mathbf{i}^T = (0, \frac{5}{3}, -\frac{5}{3\sqrt{2}})\,.$$

The normals of the two regular tetrahedra τ_f and τ_d with exterior and interior areas

$A^{2-3}_{\rm out}=\sqrt{3}, A^{2-3}_{\rm in}=(4/3)\sqrt{2}$ are then respectively as follows

$$\mathbf{n}_{cf}=(1/A^{2-3}_{\rm out})\,\mathbf{E}_3,\ \mathbf{n}_{af}=(1/A^{2-3}_{\rm out})\,\mathbf{E}_1,\ \mathbf{n}_{bf}=(1/A^{2-3}_{\rm out})\,\mathbf{E}_2,\ \mathbf{n}_{df}=-(\mathbf{n}_{cf}+\mathbf{n}_{af}+\mathbf{n}_{bf})$$

$$\mathbf{n}_{cd}=(1/A^{2-3}_{\rm out})\,\mathbf{F}_3,\ \mathbf{n}_{ad}=(1/A^{2-3}_{\rm out})\,\mathbf{F}_1,\ \mathbf{n}_{bd}=(1/A^{2-3}_{\rm out})\,\mathbf{F}_2,\ \mathbf{n}_{fd}=-\mathbf{n}_{df}\,, \quad \text{(E.6)}$$

where the vectors $\mathbf{E}_k$ are given in (E.3) and $\mathbf{F}_k$ have the same expression as in the $\mathbf{E}_k$ via replacing the vertex s by the vertex i. The sets of the normals belonging to three interior tetrahedra τ_c, τ_a and τ_b are as follows

$$\tau_c:\mathbf{n}_{bc}=\frac{1}{2A^{2-3}_{\rm in}}(\mathbf{a}-\mathbf{f})\times(\mathbf{d}-\mathbf{f}),\ \mathbf{n}_{ac}=\frac{1}{2A^{2-3}_{\rm in}}(\mathbf{d}-\mathbf{f})\times(\mathbf{b}-\mathbf{f}),\ \mathbf{n}_{fc}=\mathbf{n}_{cf},\ \mathbf{n}_{dc}=\mathbf{n}_{cd}$$

$$\tau_a:\mathbf{n}_{ba}=\frac{1}{2A^{2-3}_{\rm in}}(\mathbf{d}-\mathbf{f})\times(\mathbf{c}-\mathbf{f}),\ \mathbf{n}_{da}=\mathbf{n}_{ad},\ \mathbf{n}_{fa}=\mathbf{n}_{af},\ \mathbf{n}_{ca}=-\mathbf{n}_{ac}$$

$$\tau_b:\mathbf{n}_{fb}=\mathbf{n}_{bf},\ \mathbf{n}_{db}=\mathbf{n}_{bd},\ \mathbf{n}_{ab}=-\mathbf{n}_{ba},\ \mathbf{n}_{cb}=-\mathbf{n}_{bc}\,. \quad \text{(E.7)}$$

In the 2-3 vector geometry, there are in total 6 aligned and 4 back to back conditions on the normals and the $|\det H|^{-1/2}$ for fixed spins $j_{\rm out}=2, j_{\rm in}=j_{\rm out}\,(4/3)\sqrt{2/3}$ on this boundary data is

$$|\det H_0|^{1/2}_{2-3}=0.262621\,. \quad \text{(E.8)}$$

Appendix F
Cubic terms and the cubic kernel

The functional $\Phi_3[\phi(\mathbf{x})]$ built from the 18 terms derived in Section 5.4.3.1 is[1]

$$\begin{aligned}\Phi_3(\mathbf{x}) = {} & b_1\phi^3 + b_2\phi\partial^{-1}(\phi\partial\phi) + b_3\phi\partial^{-2}(\phi\partial^2\phi) + b_4\phi\partial^{-2}((\partial\phi)^2) + b_5\partial^{-1}(\phi^2\partial\phi) \\ & + b_6\partial^{-1}(\phi\partial^{-1}(\phi\partial^2\phi)) + b_7\partial^{-1}(\phi\partial^{-1}((\partial\phi)^2)) + b_8\partial^{-1}(\phi\partial(\phi^2)) + b_9\partial^{-1}(\partial\phi\partial^{-1}(\phi\partial\phi)) \\ & + b_{10}\partial^{-1}(\partial\phi\partial^{-2}(\phi\partial^2\phi)) + b_{11}\partial^{-2}(\phi^2\partial^2\phi) + b_{12}\partial^{-2}(\phi(\partial\phi)^2) + b_{13}\partial^{-2}(\partial^2\phi\partial^{-1}(\phi\partial\phi)) \\ & + b_{14}\partial^{-2}(\partial^2\phi\partial^{-2}(\phi\partial^2\phi)) + b_{15}\partial^{-2}(\partial\phi\partial(\phi^2)) + b_{16}\partial^{-2}(\phi\partial(\phi\partial\phi)) \\ & + b_{17}\partial^{-2}(\phi\partial^2(\phi^2)) + b_{18}\partial^{-2}(\partial\phi\partial^{-1}(\phi\partial^2\phi)) \,. \end{aligned} \tag{F.1}$$

To compute the kernel associated with $\Phi_3(\mathbf{x})$, we need to take the Fourier transform of each term. As an example, consider the Fourier transform of the 13th term:

$$\begin{aligned}&\partial^{-2}(\partial^2\phi\partial^{-1}(\phi\partial\phi))(\mathbf{k}) \\ &\quad = \int d^3x \frac{1}{k^2}\Bigg\{\int \frac{d^3p_1}{(2\pi)^3} p_1^2\phi(\mathbf{p}_1)e^{i\mathbf{p}_1\cdot\mathbf{x}} \int \frac{d^3q}{(2\pi)^3}\frac{1}{q}\Big[\int \frac{d^3p_2}{(2\pi)^3}\int d^3p_3 \\ &\quad \times\delta^3(\mathbf{q}-\mathbf{p}_2-\mathbf{p}_3)\phi(\mathbf{p}_2)p_3\phi(\mathbf{p}_3)\Big]e^{i\mathbf{q}\cdot\mathbf{x}}\Bigg\}e^{-i\mathbf{k}\cdot\mathbf{x}}\end{aligned}$$

[1] We note that three terms - $\partial^{-1}(\partial\phi\partial^{-2}(\partial\phi)^2)$, $\partial^{-2}(\partial^2\phi\partial^{-2}(\partial\phi)^2))$, $\partial^{-2}(\partial\phi\partial^{-1}(\partial\phi)^2)$ - have been neglected because they do not have nonzero β_1, β_2, or β_4 and thus do not regenerate the original four quadratic terms, but only terms suppressed by $\partial\phi_l$. Allowing these terms would introduce new parametric freedom among the 18 terms above, allowing some to be nonzero after the imposition of convergence on loop corrections.

$$= \int \frac{d^3p_1}{(2\pi)^3} \int \frac{d^3p_2}{(2\pi)^3} \int d^3p_3 \int d^3q \; \delta^3(\mathbf{k}-\mathbf{p}_1-\mathbf{q})$$
$$\times\delta^3(\mathbf{q}-\mathbf{p}_2-\mathbf{p}_3)\frac{p_1^2 p_3}{k^2 q}\phi(\mathbf{p}_1)\phi(\mathbf{p}_2)\phi(\mathbf{p}_3) \tag{F.2}$$

We can use a Dirac delta function to integrate over any of the four momenta ($\mathbf{p}_1, \mathbf{p}_2, \mathbf{p}_3$ or $\mathbf{q}$) but to make the calculations more transparent we will treat these possibilities symmetrically and write

$$\partial^{-2}(\partial^2\phi\partial^{-1}(\phi\partial\phi))(\mathbf{k}) = \frac{1}{3!}\int \frac{d^3p_1}{(2\pi)^3} \int \frac{d^3p_2}{(2\pi)^3} \int d^3p_3 \, \delta^3(\mathbf{k}-\mathbf{p}_1-\mathbf{p}_2-\mathbf{p}_3)$$
$$\times\phi(\mathbf{p}_1)\phi(\mathbf{p}_2)\phi(\mathbf{p}_3)\left[\frac{p_1 p_3^2}{k^2|\mathbf{p}_1+\mathbf{p}_2|} + \frac{p_2 p_3^2}{k^2|\mathbf{p}_1+\mathbf{p}_2|} + \frac{p_1 p_2^2}{k^2|\mathbf{p}_1+\mathbf{p}_3|}\right.$$
$$\left. + \frac{p_2^2 p_3}{k^2|\mathbf{p}_1+\mathbf{p}_3|} + \frac{p_1^2 p_2}{k^2|\mathbf{p}_2+\mathbf{p}_3|} + \frac{p_1^2 p_3}{k^2|\mathbf{p}_2+\mathbf{p}_3|}\right]. \tag{F.3}$$

Now we can read off the contribution to the cubic kernel from the 13th term:

$$N_3^{13\text{th}}(\mathbf{p}_1,\mathbf{p}_2,\mathbf{p}_3,k) \equiv \frac{p_1 p_3^2}{k^2|\mathbf{p}_1+\mathbf{p}_2|} + \frac{p_2 p_3^2}{k^2|\mathbf{p}_1+\mathbf{p}_2|} + \frac{p_1 p_2^2}{k^2|\mathbf{p}_1+\mathbf{p}_3|} + \frac{p_2^2 p_3}{k^2|\mathbf{p}_1+\mathbf{p}_3|}$$
$$+\frac{p_1^2 p_2}{k^2|\mathbf{p}_2+\mathbf{p}_3|} + \frac{p_1^2 p_3}{k^2|\mathbf{p}_2+\mathbf{p}_3|} \tag{F.4}$$

Applying this procedure to each term gives the full cubic kernel $N_3(\mathbf{p}_1,\mathbf{p}_2,\mathbf{p}_3,k)$:

$$\begin{aligned}
&N_3(\mathbf{p}_1,\mathbf{p}_2,\mathbf{p}_3,k)\\
&= 6b_1 + b_2\left[\frac{p_1+p_2}{|\mathbf{p}_1+\mathbf{p}_2|} + \frac{p_1+p_3}{|\mathbf{p}_1+\mathbf{p}_3|} + \frac{p_2+p_3}{|\mathbf{p}_2+\mathbf{p}_3|}\right]\\
&\quad + b_3\left[\frac{p_1^2+p_2^2}{|\mathbf{p}_1+\mathbf{p}_2|^2} + \frac{p_1^2+p_3^2}{|\mathbf{p}_1+\mathbf{p}_3|^2} + \frac{p_2^2+p_3^2}{|\mathbf{p}_2+\mathbf{p}_3|^2}\right]\\
&\quad + 2b_4\left[\frac{p_1 p_2}{|\mathbf{p}_1+\mathbf{p}_2|^2} + \frac{p_1 p_3}{|\mathbf{p}_1+\mathbf{p}_3|^2} + \frac{p_2 p_3}{|\mathbf{p}_2+\mathbf{p}_3|^2}\right] + 2b_5\left[\frac{p_1+p_2+p_3}{k}\right]\\
&\quad + b_6\left[\frac{p_1^2+p_2^2}{k|\mathbf{p}_1+\mathbf{p}_2|} + \frac{p_1^2+p_3^2}{k|\mathbf{p}_1+\mathbf{p}_3|} + \frac{p_2^2+p_3^2}{k|\mathbf{p}_2+\mathbf{p}_3|}\right]\\
&\quad + 2b_7\left[\frac{p_1 p_2}{k|\mathbf{p}_1+\mathbf{p}_2|} + \frac{p_1 p_3}{k|\mathbf{p}_1+\mathbf{p}_3|} + \frac{p_2 p_3}{k|\mathbf{p}_2+\mathbf{p}_3|}\right]\\
&\quad + 2b_8\left[\frac{|\mathbf{p}_1+\mathbf{p}_2|}{k} + \frac{|\mathbf{p}_1+\mathbf{p}_3|}{k} + \frac{|\mathbf{p}_2+\mathbf{p}_3|}{k}\right]
\end{aligned}$$

$$
\begin{aligned}
&+b_9\left[\frac{p_3(p_1+p_2)}{k|\mathbf{p}_1+\mathbf{p}_2|}+\frac{p_2(p_1+p_3)}{k|\mathbf{p}_1+\mathbf{p}_3|}+\frac{p_1(p_2+p_3)}{k|\mathbf{p}_2+\mathbf{p}_3|}\right]\\
&+b_{10}\left[\frac{p_3(p_1^2+p_2^2)}{k|\mathbf{p}_1+\mathbf{p}_2|^2}+\frac{p_2(p_1^2+p_3^2)}{k|\mathbf{p}_1+\mathbf{p}_3|^2}+\frac{p_1(p_2^2+p_3^2)}{k|\mathbf{p}_2+\mathbf{p}_3|^2}\right]+2b_{11}\left[\frac{p_1^2+p_2^2+p_3^2}{k^2}\right]\\
&+2b_{12}\left[\frac{p_1p_2}{k^2}+\frac{p_1p_3}{k^2}+\frac{p_2p_3}{k^2}\right]+b_{13}\left[\frac{p_3^2(p_1+p_2)}{k^2|\mathbf{p}_1+\mathbf{p}_2|}+\frac{p_2^2(p_1+p_3)}{k^2|\mathbf{p}_1+\mathbf{p}_3|}+\frac{p_1^2(p_2+p_3)}{k^2|\mathbf{p}_2+\mathbf{p}_3|}\right]\\
&+b_{14}\left[\frac{p_3^2(p_1^2+p_2^2)}{k^2|\mathbf{p}_1+\mathbf{p}_2|^2}+\frac{p_2^2(p_1^2+p_3^2)}{k^2|\mathbf{p}_1+\mathbf{p}_3|^2}+\frac{p_1^2(p_2^2+p_3^2)}{k^2|\mathbf{p}_2+\mathbf{p}_3|^2}\right]\\
&+2b_{15}\left[\frac{p_1|\mathbf{p}_2+\mathbf{p}_3|}{k^2}+\frac{p_2|\mathbf{p}_1+\mathbf{p}_3|}{k^2}+\frac{p_3|\mathbf{p}_1+\mathbf{p}_2|}{k^2}\right]\\
&+b_{16}\left[\frac{(p_1+p_2)|\mathbf{p}_1+\mathbf{p}_2|}{k^2}+\frac{(p_1+p_3)|\mathbf{p}_1+\mathbf{p}_3|}{k^2}+\frac{(p_2+p_3)|\mathbf{p}_2+\mathbf{p}_3|}{k^2}\right]\\
&+2b_{17}\left[\frac{|\mathbf{p}_1+\mathbf{p}_2|^2}{k^2}+\frac{|\mathbf{p}_1+\mathbf{p}_3|^2}{k^2}+\frac{|\mathbf{p}_2+\mathbf{p}_3|^2}{k^2}\right]\\
&+b_{18}\left[\frac{(p_1^2+p_2^2)p_3}{k^2|\mathbf{p}_1+\mathbf{p}_2|}+\frac{(p_1^2+p_3^2)p_2}{k^2|\mathbf{p}_1+\mathbf{p}_3|}+\frac{(p_2^2+p_3^2)p_1}{k^2|\mathbf{p}_2+\mathbf{p}_3|}\right]
\end{aligned}
\tag{F.5}
$$

F.1 Quadratic terms induced by a cubic term in biased sub-volumes

We again use the 13th term, $\partial^{-2}(\partial^2\phi\partial^{-1}(\phi\partial\phi))$, to illustrate how to read off the induced quadratic terms from the limit of a cubic term when one momentum is much smaller than the other two. Choosing any one of the three momenta (e.g., p_3) as the long wavelength mode k_l and the other two (p_1, p_2) as the short wavelength modes k_s, and using the fact that the kernel is symmetric in the p_i:

$$
\begin{aligned}
&\partial^{-2}(\partial^2\phi\partial^{-1}(\phi\partial\phi))(\mathbf{k})\\
&\quad\longrightarrow 3\times\frac{1}{3!}\int_\Lambda^{k_*}\frac{d^3p_3}{(2\pi)^3}\phi(\mathbf{p}_3)\int_{k_*}^{k_{\max}}\frac{d^3p_1}{(2\pi)^3}\int_{k_*}^{k_{\max}}d^3p_2\delta^3(\mathbf{k}-\mathbf{p}_1-\mathbf{p}_2)\phi(\mathbf{p}_1)\phi(\mathbf{p}_2)\\
&\qquad\times\left\{\frac{p_1^2}{k^2}+\frac{p_2^2}{k^2}+p_3\left[\frac{p_1^2}{k^2p_2}+\frac{p_2^2}{k^2p_1}\right]+p_3^2\left[\frac{p_1}{k^3}+\frac{p_2}{k^3}\right]\right\}\\
&\quad\equiv\left[\phi_l\partial^{-2}(\phi_s\partial^2\phi_s)+\partial\phi_l\partial^{-2}(\partial^2\phi_s\partial^{-1}\phi_s)+\partial^2\phi_l\partial^{-3}(\phi_s\partial\phi_s)\right]
\end{aligned}
\tag{F.6}
$$

where Λ is the largest scale in the problem (eg, corresponding to the mode that first exited during inflation) and k_* is the scale that defines the size of the sub-volume. The corresponding procedure in real space is

$$\begin{aligned}\partial^{-2}(\partial^2\phi\partial^{-1}(\phi\partial\phi)) \longrightarrow &\Big[\partial^{-2}(\partial^2\phi_l\partial^{-1}(\phi_s\partial\phi_s)) + \partial^{-2}(\partial^2\phi_s\partial^{-1}(\phi_l\partial\phi_s)) + \partial^{-2}(\partial^2\phi_s\partial^{-1}(\phi_s\partial\phi_l))\Big] \\ &= \Big[\partial^2\phi_l\partial^{-2}(\partial^{-1}(\phi_s\partial\phi_s)) + \phi_l\partial^{-2}(\partial^2\phi_s\partial^{-1}(\partial\phi_s)) + \partial\phi_l\partial^{-2}(\partial^2\phi_s\partial^{-1}(\phi_s))\Big] \\ &= \Big[\phi_l\partial^{-2}(\phi_s\partial^2\phi_s) + \partial\phi_l\partial^{-2}(\partial^2\phi_s\partial^{-1}\phi_s) + \partial^2\phi_l\partial^{-3}(\phi_s\partial\phi_s)\Big] \qquad \text{(F.7)}\end{aligned}$$

Note that to go from the first line to the second, all the long modes $\phi_l, \partial\phi_l$ and $\partial^2\phi_l$ are treated as constants.

F.2 Power spectrum from the cubic field Φ_3

In this Appendix we derive the constraints on the terms in Φ_3 from their contribution to the power spectrum:

$$\begin{aligned}&\Big\langle \Phi_3(\mathbf{k}')\Phi_3(\mathbf{k})\Big\rangle \equiv \delta P_{\Phi_3}(k)\,\delta^3(\mathbf{k}'+\mathbf{k}) \\ &\quad= \left(\frac{g_{\rm NL}}{3!}\right)^2 \prod_{\ell=1}^{3}\int \frac{d^3p_\ell}{(2\pi)^3}\prod_{m=1}^{3}\int\frac{d^3q_m}{(2\pi)^3} N_3(\mathbf{p}_1,\mathbf{p}_2,\mathbf{p}_3,\mathbf{k})N_3(\mathbf{q}_1,\mathbf{q}_2,\mathbf{q}_3,\mathbf{k}') \\ &\quad\times\delta^3(\mathbf{k}'-\sum_{m=1}^{3}\mathbf{q}_m)\delta^3(\mathbf{k}-\sum_{\ell=1}^{3}\mathbf{p}_\ell)\Big\langle\Big[\phi(\mathbf{p}_1)\phi(\mathbf{p}_2)\phi(\mathbf{p}_3) - \sum_{\substack{i=1\\k\neq j\neq i}}^{3}\phi(\mathbf{p}_i)\langle\phi(\mathbf{p}_j)\phi(\mathbf{p}_k)\rangle\Big] \\ &\quad\Big[\phi(\mathbf{q}_1)\phi(\mathbf{q}_2)\phi(\mathbf{q}_3) - \sum_{\substack{i'=1\\k'\neq j'\neq i}}^{3}\phi(\mathbf{q}'_i)\langle\phi(\mathbf{q}'_j)\phi(\mathbf{q}'_k)\rangle\Big]\Big\rangle = g_{\rm NL}^2\int\frac{d^3p_1}{(2\pi)^3}\frac{d^3p_2}{(2\pi)^3}\,d^3p_3 \\ &\quad N_3^2(\mathbf{p}_1,\mathbf{p}_2,\mathbf{p}_3,\mathbf{k})P(p_1)P(p_2)P(p_3)\,\delta^3(\mathbf{k}-\mathbf{p}_1-\mathbf{p}_2-\mathbf{p}_3)\,. \qquad \text{(F.8)}\end{aligned}$$

In order to obtain the constraints on the terms in N_3 we need to find those that give divergent integrals in the expression above. The divergences are in the UV, where some of the internal momenta are large, and there are several configurations to consider:

For $k \ll |\mathbf{p}_1+\mathbf{p}_2|, p_1; k \gg p_2$:

$$b_{14} = 0$$

$$
\begin{aligned}
b_{10} + b_{18} &= 0 \\
b_3 + b_4 + b_6 + b_7 + 2b_{11} + b_{12} + b_{13} + b_{14} + 2b_{15} + b_{16} + 2b_{17} + b_{18} &= 0
\end{aligned}
\tag{F.9}
$$

For $k \ll |\mathbf{p}_1 + \mathbf{p}_2|, p_1, p_2$:

$$
\begin{aligned}
b_{12} + b_{13} + b_{16} &= 0 \\
b_{11} + b_{14} + b_{15} + b_{17} + b_{18} &= 0
\end{aligned}
\tag{F.10}
$$

For $k \ll p_1, p_2; k \gg |\mathbf{p}_1 + \mathbf{p}_2|$:

$$
\begin{aligned}
b_{16} &= 0 \\
(b_{11} + b_{15} + b_{17}) + (b_{12} + b_{13} + b_{16}) + (b_{11} + b_{14} + b_{15} + b_{17} + b_{18}) &= 0 \\
b_6 + b_7 + b_{18} &= 0 \\
(2b_5 + b_6 + 2b_8 + b_9 + b_{10} + b_{12}) + (b_{12} + b_{13} + b_{16}) &= 0
\end{aligned}
\tag{F.11}
$$

We have verified that other loop corrections (e.g., to the bispectrum) do not give additional constraints.

F.3 Special cubic kernels and its corresponding trispectra

A cubic kernel that gives no cosmic variance contributions stronger than $\partial^2\phi_l$ to the power spectrum or bispectrum has $\{b_1 = 1, b_{11} = 3, b_{17} = -3\}$. This is a candidate for a single-clock inflation trispectrum:

$$
N_3(\mathbf{k}_1, \mathbf{k}_2, \mathbf{k}_3, \mathbf{k}_4) = 6\left[1 + \frac{k_1^2 + k_2^2 + k_3^2}{k_4^2} - \frac{|\mathbf{k}_1 + \mathbf{k}_2|^2 + |\mathbf{k}_1 + \mathbf{k}_3|^2 + |\mathbf{k}_2 + \mathbf{k}_3|^2}{k_4^2}\right]
$$

Recall that the trispectrum is related to the cubic kernel by

$$
T_\Phi(\mathbf{k}_1, \mathbf{k}_2, \mathbf{k}_3, \mathbf{k}_4) = g_{\rm NL} P_\phi(k_1) P_\phi(k_2) P_\phi(k_3) N_3(\mathbf{k}_1, \mathbf{k}_2, \mathbf{k}_3, \mathbf{k}_4) + \text{cyc.} \tag{F.12}
$$

For the kernel above, the trispectrum has no factors of $|\mathbf{k}_i + \mathbf{k}_j|$ in the denominator and $\lim_{k_i \to 0} T_\Phi = 0$.

A cubic kernel that induces an equilateral bispectrum and a leading order ($\propto \phi_s$) SCV shift to the power spectrum is $\{b_1 = -3, b_2 = 4, b_3 = 2, b_4 = -2\}$. We start writing the non-Gaussian field up to cubic order with implementing our parameter set for the cubic terms

Induce equilateral bispectrum and shift PS:

$$\begin{aligned} N_3(\mathbf{k}_1, \mathbf{k}_2, \mathbf{k}_3, \mathbf{k}_4) &= -18 + 4\left[\frac{k_1+k_2}{|\mathbf{k}_1+\mathbf{k}_2|} + \frac{k_1+k_3}{|\mathbf{k}_1+\mathbf{k}_3|} + \frac{k_2+k_3}{|\mathbf{k}_2+\mathbf{k}_3|}\right] \\ &\quad +2\left[\frac{k_1^2+k_2^2}{|\mathbf{k}_1+\mathbf{k}_2|^2} + \frac{k_1^2+k_3^2}{|\mathbf{k}_1+\mathbf{k}_3|^2} + \frac{k_2^2+k_3^2}{|\mathbf{k}_2+\mathbf{k}_3|^2}\right] \\ &\quad -4\left[\frac{k_1k_2}{|\mathbf{k}_1+\mathbf{k}_2|^2} + \frac{k_1k_3}{|\mathbf{k}_1+\mathbf{k}_3|^2} + \frac{k_2k_3}{|\mathbf{k}_2+\mathbf{k}_3|^2}\right] \end{aligned} \tag{F.13}$$

One can see directly from the trispectrum that this term induces the equilateral bispectrum:

$$\begin{aligned} k_4^3 \lim_{k_4\to 0} T_\Phi(\mathbf{k}_1, \mathbf{k}_2, \mathbf{k}_3, \mathbf{k}_4) &= P(k_1)P(k_2)\left[-6 + 4\frac{k_1+k_2}{k_3} + 2\frac{k_1^2+k_2^2}{k_3^2} - 4\frac{k_1k_2}{k_3^2}\right] \\ &\quad +\text{perm.} \end{aligned} \tag{F.14}$$

The cubic term with $\{b_1 = -5/3, b_2 = 2, b_5 = 3, b_9 = -4, b_{12} = -2, b_{13} = 2\}$ also induces the equilateral bispectrum but does not shift the power spectrum at leading order ($\propto \phi_s$). This kernel is

$$\begin{aligned} N_3(\mathbf{k}_1, \mathbf{k}_2, \mathbf{k}_3, \mathbf{k}_4) &= -10 + 2\left[\frac{k_1+k_2}{|\mathbf{k}_1+\mathbf{k}_2|} + \frac{k_1+k_3}{|\mathbf{k}_1+\mathbf{k}_3|} + \frac{k_2+k_3}{|\mathbf{k}_2+\mathbf{k}_3|}\right] + 6\left[\frac{k_1+k_2+k_3}{k_4}\right] \\ &\quad -4\left[\frac{k_3(k_1+k_2)}{k_4|\mathbf{k}_1+\mathbf{k}_2|} + \frac{k_2(k_1+k_3)}{k_4|\mathbf{k}_1+\mathbf{k}_3|} + \frac{k_1(k_2+k_3)}{k_4|\mathbf{k}_2+\mathbf{k}_3|}\right] \\ &\quad -4\left[\frac{k_1k_2+k_1k_3+k_2k_3}{k_4^2}\right] \\ &\quad +2\left[\frac{k_3^2(k_1+k_2)}{k_4^2|\mathbf{k}_1+\mathbf{k}_2|} + \frac{k_2^2(k_1+k_3)}{k_4^2|\mathbf{k}_1+\mathbf{k}_3|} + \frac{k_1^2(k_2+k_3)}{k_4^2|\mathbf{k}_2+\mathbf{k}_3|}\right] \end{aligned} \tag{F.15}$$

In this case the trispectrum again satisfies Eq.(F.14) but in addition

$$\text{No shift to power spectrum}: \; k_1^3k_2^3 \lim_{k_1,k_2\to 0} T_\Phi(\mathbf{k}_1, \mathbf{k}_2, \mathbf{k}_3, \mathbf{k}_4) = 0\,. \tag{F.16}$$

Appendix G
Basis functions for bispectra

In [206] there is a set of basis functions, $\{\mathcal{K}_n\}$, that describes nearly scale-invariant bispectral shapes (recall shape S is proportional to $(k_1k_2k_3)^2B(k_1,k_2,k_3)$) with various levels of divergence in the squeezed limit. The $\mathcal{K}_n$ are symmetrized, separable polynomials of momenta

$$\mathcal{K}_n(k_1,k_2,k_3) \equiv \frac{1}{N_n}\left(k_1^p k_2^r k_3^s + perms.\right), \tag{G.1}$$

where n labels the particular triple of (positive and negative) integers $\{p,r,s\}$ and N_n is the number of distinct permutations. We will restrict to exact scale-invariance of the power spectrum and bispectrum for simplicity, so $p+r+s=0$. The constant shape is labeled by $\mathcal{K}_0 = 1$. Then, sets of polynomials grouped according to the minimum power of momenta appearing, $R=-1,-2,-3$, etc. There are six additional terms up to $R=-2$ divergence:

$$\begin{aligned}
\mathcal{K}_1 &= \frac{1}{6}\left(\frac{k_3}{k_1} + 5\ perms\right),\ \mathcal{K}_2 = \frac{1}{3}\left(\frac{k_1^2}{k_3k_2} + 2perms\right)\\
\mathcal{K}_3 &= \frac{1}{3}\left(\frac{k_1k_2}{k_3^2} + 2\ perms\right),\ \mathcal{K}_4 = \frac{1}{6}\left(\frac{k_1^2}{k_3^2} + 5\ perms\right)\\
\mathcal{K}_5 &= \frac{1}{6}\left(\frac{k_1^3}{k_2k_3^2} + 5\ perms\right),\ \mathcal{K}_6 = \frac{1}{3}\left(\frac{k_1^4}{k_2^2k_3^2} + 2\ perms\right)
\end{aligned} \tag{G.2}$$

In [206] they find four linear combinations of these shapes that have the same squeezed limit as the equilateral template

$$S_1^{\rm BB} = -2\mathcal{K}_0 + 6\mathcal{K}_1 - 3\mathcal{K}_2 \tag{G.3}$$

$\mathcal{K}_n$	$\{p,r,s\}$	$\Phi_2(x)$			$\{a_i\}$
$\mathcal{K}_0$	$(0,0,0)$	$\partial^{-2}(\partial\phi)^2$	–	–	$\{a_4\}$
$\mathcal{K}_1$	$(-1,0,1)$	$\partial^{-1}(\phi\partial\phi)$	$\partial^{-2}(\phi\partial^2\phi)$	$\partial^{-3}(\partial\phi\partial^2\phi)$	$\{a_2,a_3,a_6\}$
$\mathcal{K}_2$	$(-1,-1,2)$	ϕ^2	$\partial^{-3}(\phi\partial^3\phi)$	–	$\{a_1,a_5\}$
$\mathcal{K}_3$	$(-2,1,1)$	$\partial^{-4}(\partial^2\phi)^2$	$\partial^{-1}(\partial^2\phi\partial^{-1}\phi)$	–	$\{a_8,\times\}$
$\mathcal{K}_4$	$(-2,0,2)$	$\partial^{-4}(\partial^3\phi\partial\phi)$	$\partial^{-2}(\partial^{-1}\phi\partial^3\phi)$	$\partial^{-1}\phi\partial\phi$	$\{a_9,\times,\times\}$
$\mathcal{K}_5$	$(-2,-1,3)$	$\partial^{-4}(\phi\partial^4\phi)$	$\partial^{-3}(\partial^{-1}\phi\partial^4\phi)$	$\partial(\phi\partial^{-1}\phi)$	$\{a_7,\times,\times\}$
$\mathcal{K}_6$	$(-2,-2,4)$	$\partial^2(\partial^{-1}\phi)^2$	$\partial^{-4}(\partial^{-1}\phi\partial^5\phi)$	–	$\{a_{10},a_{11}\}$

Table G.1. The set of terms in the real space field expansion, $\Phi_2(x)$ that correspond to each polynomial $\mathcal{K}_n$ (see Eq.(G.1)) appearing in the shape of the bispectrum. The different $\Phi_2(x)$ terms on a given horizontal line result in redundant terms in the shape of the bispectrum but contribute differently to the lowest order non-Gaussian (loop) contribution to the power spectrum. The conditions of a well-behaved loop correction in general introduce constraints among terms corresponding to different from $\mathcal{K}_n$. However, some $\Phi_2(x)$ terms are truly redundant even once loops are considered (eg, they come with unconstrained coefficients) and so are not needed. The last column lists the labels a_i we used in the main text, where $\times$ indicates the term was redundant for our purposes and so was not included.

$$S_2^{\rm BB} = \mathcal{K}_0 + 3\mathcal{K}_3 - 3\mathcal{K}_4 \tag{G.4}$$

$$S_3^{\rm BB} = \mathcal{K}_2 + 2\mathcal{K}_3 - 2\mathcal{K}_5 \tag{G.5}$$

$$S_4^{\rm BB} = 2\mathcal{K}_3 - \mathcal{K}_6, \tag{G.6}$$

where $S_1^{\rm BB}$ is the equilateral template.

In our expansion of the non-Gaussian field, the number of operators that can generate a term in the bispectrum associated with $\{\mathcal{K}_n\}$ [206] is equal to the number of distinct entries in $\{p,r,s\}$. This redundancy allows us to cancel loop divergences in the first non-Gaussian correction to the power spectrum. The relationship between $\{\mathcal{K}_n\}$, all possible terms in $\Phi_2(x)$ that can generate that shape in the bispectrum, and the coefficients $\{a_i\}$ of the set of terms used in the body of the thesis is shown in Table G.1. Some terms in $\Phi_2(x)$ are truly redundant for our purposes here, and so we did not include them (they are marked with an $\times$ in the last column of the table).

After imposing loop constraints, we imposed that the bispectrum is no more divergent than k_l^{-1} in the squeezed limit and found four linearly independent solutions (Eq.5.73) that generate shapes

$$S_1(k_1,k_2,k_3) = \frac{1}{2}\left(\frac{k_1}{k_2}+cyc\right) - \frac{1}{2}\left(\frac{k_1^2}{k_2k_3}+cyc\right) - 1 \tag{G.7}$$

$$S_2(k_1,k_2,k_3) = \frac{1}{4}\left(\frac{k_3^2}{k_1k_2}+cyc\right) - \frac{1}{4}\left(\frac{k_1^3}{k_3^2k_2}+cyc\right) + \frac{1}{2}\left(\frac{k_1k_2}{k_3^2}+cyc\right) \tag{G.8}$$

$$S_3(k_1,k_2,k_3) = -\left(\frac{k_1^2}{k_2k_3}+cyc\right) + \frac{1}{2}\left(\frac{k_1}{k_2}+cyc\right) + \frac{1}{2}\left(\frac{k_1^3}{k_3^2k_2}+cyc\right) - \frac{1}{2}\left(\frac{k_2^2}{k_3^2}+cyc\right) \tag{G.9}$$

$$S_4(k_1,k_2,k_3) = \left(\frac{k_1^2}{k_2k_3}+cyc\right) - \left(\frac{k_1^3}{k_3^2k_2}+cyc\right) + \left(\frac{k_1^4}{k_2^2k_3^2}+cyc\right). \tag{G.10}$$

A little bit of algebra shows that these shapes are related to those in [206] by

$$S_1^{\rm BB} = 2S_1, \tag{G.11}$$

$$S_2^{\rm BB} = -S_1 + S_3 + 2S_2 \tag{G.12}$$

$$S_3^{\rm BB} = \frac{4}{3}S_2, \tag{G.13}$$

$$S_4^{\rm BB} = \frac{4}{3}S_2 - \frac{1}{3}S_4\,. \tag{G.14}$$

Although it is maybe not immediately obvious that the procedure for constructing non-Gaussian fields $\Phi_{\rm NG}(x)$ with $1/k_l$ squeezed limit bispectra would lead to the same results as constructing bispectral shapes only, studying the structure of the loop constraints shows that the redundancy between $\mathcal{K}_n$ and $\Phi_2(x)$ is exactly enough to be sure the loop constraints are always satisfied. Notice that this is not the case for shapes that correspond to bispectra with $1/k_l^2$ divergence: $\mathcal{K}_0$ corresponds to only one field term, which does not have good loop behavior. So, although $\mathcal{K}_0$ appears to be a fine basis element at the level of bispectral shapes, we should not take $\partial^{-2}(\partial\phi)^2$ as a basis element of the quadratic term for a well-behaved non-Gaussian field.

Bibliography

[1] Sherman, G. (November 14, 1999) "The completely connected graph for 31 vertices," .
URL http://homepages.which.net/~gk.sherman/kbaaaa.htm

[2] Ade, P. A. R. and others (2014) "Planck 2013 results. XVI. Cosmological parameters," *Astron. Astrophys.*, **571**, p. A16.

[3] Baytaş, B., A. Kesavan, E. Nelson, S. Park, and S. Shandera (2015) "Nonlocal bispectra from super cosmic variance," *Phys. Rev.*, **D91**(8), p. 083518, 1502.01009.

[4] Baytaş, B. and S. Shandera (2016) "Space of non-Gaussian fields with single-clock bispectra," *Phys. Rev.*, **D94**(4), p. 043510, 1605.07206.

[5] Baytaş, B. and M. Bojowald (2017) "Minisuperspace models of discrete systems," *Phys. Rev.*, **D95**(8), p. 086007, 1611.06255.

[6] Baytaş, B., E. Bianchi, and N. Yokomizo (2018) "Gluing polyhedra with entanglement in loop quantum gravity," 1805.05856.

[7] Chandler, D. (1987) *Introduction to Modern Statistical Mechanics*, Oxford University Press.

[8] Fierz, M. (1939) "Ú́ber die relativistische Theorie kŕaftefreier Teilchen mit beliebigem Spin," *Helvetica Physica Acta*, **12**(1), pp. 3–37.

[9] Pauli, W. (1940) "The Connection Between Spin and Statistics," *Physical Review.*, **58**(8), pp. 716–722.

[10] Sethna, J. P. (2006) *Statistical Mechanics: Entropy, Order Parameters and Complexity*, Oxford University Press.

[11] Kardar, M. (2007) *Statistical Mechanics of Particles*, Cambridge University Press.

[12] Dirac, P. A. M. (1926) "On the Theory of Quantum Mechanics," *Proceedings of the Royal Society A.*, **112**(762), pp. 661–677.

[13] Hilbert, D. (1915-1927) *Lectures on Quantum Theory.*

[14] Neumann, J. V. (1955) *Mathematical Foundations of Quantum Mechanics*, Princeton University Press, Reprinted in paperback form.

[15] Schrodinger, E. (1926) "Quantisierung als Eigenwertproblem (Erste Mitteilung)," *Annalen der Physik*, **79**, pp. 361–376.

[16] Heisenberg, W. (1925) "Uber quantentheoretische Umdeutung kinematischer und mechanischer Beziehungen." *Zeitschrift fur Physik*, **33**(1), pp. 879–893.

[17] Born, M. and P. Jordan (1925) "Zur Quantenmechanik," *Zeitschrift fur Physik*, **34**, pp. 854–888.

[18] Born, J. P., M. and W. Heisenberg (1926) "Zur Quantenmechanik II," *Zeitschrift fur Physik*, **35**, pp. 557–615.

[19] Nielsen, M. A. and I. L. Chuang (2010) *Quantum computation and quantum information*, Cambridge University Press, Cambridge, New York: 10th anniversary ed.

[20] Schrodinger, E. (1926) "An Undulatory Theory of the Mechanics of Atoms and Molecules," *Physical Review.*, **28**, pp. 1049–1070.

[21] Heisenberg, W. (1927) "'Uber den anschaulichen Inhalt der quantentheoretischen Kinematik und Mechanik," *Zeitschrift f'ur Physik*, **43**, pp. 172–198.

[22] Einstein, A., B. Podolsky, and N. Rosen (1935) "Can Quantum-Mechanical Description of Physical Reality Be Considered Complete?" *Physical Review*, **47**, pp. 777–780.

[23] Bell, J. S. (1966) "On the problem of hidden variables in quantum mechanics," *Rev. Mod. Phys.*, **38**, pp. 447–452.

[24] Werner, R. F. (1989) "Quantum states with Einstein-Podolsky-Rosen correlations admitting a hidden-variable model," *Phys. Rev. A*, **40**, p. 4277.

[25] Bell, J. S. (1987) *Speakable and unspeakable in Quantum Mechanics*, Cambridge University Press, Cambridge.

[26] Peres, A. (1993) *Quantum Theory: Concepts and Methods*, Kluwer, Dordrecht.

[27] Ferraro, A., L. Aolita, D. Cavalcanti, F. M. Cucchietti, and A. Acín (2010) "Almost all quantum states have nonclassical correlations," *Phys. Rev. A*, **81**, p. 052318.

[28] Piani, M., P. Horodecki, and R. Horodecki (2008) "No-Local-Broadcasting Theorem for Multipartite Quantum Correlations," *Phys. Rev. Lett.*, **100**, p. 090502.

[29] Horodecki, R., P. Horodecki, M. Horodecki, and K. Horodecki (2009) "Quantum entanglement," *Rev. Mod. Phys.*, **81**, pp. 865–942.

[30] Shannon, C. and W. Weaver (1949) *The Mathematical Theory of Communication*, University of Illinois Press, Urbana.

[31] Girolami, D. (2013) *Quantum Correlations in Information Theory*, Ph.D. thesis, The University of Nottingham.

[32] Latorre, J. I. and A. Riera (2009) "A short review on entanglement in quantum spin systems," *Journal of Physics A: Mathematical and Theoretical*, **42**(50), p. 504002.

[33] Wolf, M. M., F. Verstraete, M. B. Hastings, and J. I. Cirac (2008) "Area Laws in Quantum Systems: Mutual Information and Correlations," *Phys. Rev. Lett.*, **100**, p. 070502.

[34] Hayden, S. D. L. P., P. and A. Winter (2004) "Randomizing quantum states: constructions and applications," *Comm. in Math. Phys.*, **250**(371).

[35] Joel, K., D. Kollmar, and L. F. Santos (2013) "An introduction to the spectrum, symmetries, and dynamics of spin-1/2 Heisenberg chains," *American Journal of Physics*, **81**, pp. 450–457, 1209.0115.

[36] Nepomechie, R. I. (1999) "A Spin chain primer," *Int. J. Mod. Phys.*, **B13**, pp. 2973–2986.

[37] Bethe, H. (1931) "On the theory of metal I. Eigenvalues and eigenfunctions of a linear chain of atoms," *Z. Phys.*, **71**(205-226).

[38] Sutherland, B. (2005) *Beautiful Models*, New Jersey: World Scientific.

[39] Mattis, D. C. (2006) *The Theory of Magnetism Made Simple: An Introduction to Physical Concepts and to Some Useful Mathematical Methods*, Singapore: World Scientific.

[40] Chen, W. L. G. J., S. and Y. Wang (2007) "Fidelity and quantum phase transition for the Heisenberg chain with next-nearest-neighbor interaction," *Phys. Rev. E*, **76**(061108).

[41] Santos, L. F. (2009) "Transport and control in one-dimensional systems," *J. Math. Phys.*, **50**(095211).

[42] Santos, B. F., L. F. and F. M. Izrailev (2012) "Chaos and statistical relaxation in quantum systems of interacting particles," *Phys. Rev. Lett.*, **108**(094102).

[43] Amico, L., R. Fazio, A. Osterloh, and V. Vedral (2008) "Entanglement in many-body systems," *Rev. Mod. Phys.*, **80**, pp. 517–576.

[44] Rovelli, C. (2011) "Zakopane lectures on loop gravity," *PoS*, **QGQGS2011**, p. 003.

[45] Perez, A. (2013) "The Spin Foam Approach to Quantum Gravity," *Living Rev. Rel.*, **16**, p. 3.

[46] Landau, L. E., L. (1958) *Quantum Mechanics Non-Relativistic Theory*, vol. 3, Pergamon, UK.

[47] Ponzano, R. T., G. (1968) *Semiclassical limit of Racah coefficients, in: Spectroscopic and Group Theoretical Methods in Physics*, ed. F. Block, North Holland, Amsterdam.

[48] Regge, T. (1961) "General relativity without coordinates," *Il Nuovo Cimento (1955-1965)*, **19**(3), pp. 558–571.

[49] Rovelli, C. (2004) *Quantum Gravity*, Cambridge: Cambridge University Press.

[50] Thiemann, T. (2007) *Modern Canonical Quantum General Relativity*, Cambridge: Cambridge University Press.

[51] Major, S. A. and S. M. D. (2002) "Modelling space with an atom of quantum geometry," *Class. Quantum Grav.*, **19**, p. 2211.

[52] Barbieri, A. (1998) "Quantum tetrahedra and simplicial spin networks," *Nucl. Phys. B*, **518**, p. 714.

[53] Baez, J. C. and J. W. Barrett (1999) "The quantum tetrahedron in 3 and 4 dimensions," *Adv. Theor. Math. Phys.*, **3**, p. 815.

[54] Bianchi, E. (2013), "QUANTUM GEOMETRY OF SPACE IN SPINFOAM GRAVITY," Lectures "Conformal Symmetry and Perspectives in Quantum and Mathematical Gravity", Zakopane, Poland.

[55] Terno, D. R. (2009) "Quantum tetrahedron and its classical limit," *Class. Quant. Grav.*, **26**, p. 035010.

[56] Rovelli, C. and S. Speziale (2006) "A Semiclassical tetrahedron," *Class. Quant. Grav.*, **23**, pp. 5861–5870.

[57] Peskin, S. D. V., M. E. (1995) *An Introduction To Quantum Field Theory*, Avalon Publishing.

[58] Brown, L. S. (1994) *Quantum Field Theory*, Cambridge University Press.

[59] Mukhanov, W. S., V. (2007) *Introduction to Quantum Effects in Gravity*, Butterworth-Heinemann.

[60] Van Raamsdonk, M. (2009) "Comments on quantum gravity and entanglement," 0907.2939.

[61] ——— (2010) "Building up spacetime with quantum entanglement," *Gen. Rel. Grav.*, **42**, pp. 2323–2329, [Int. J. Mod. Phys.D19,2429(2010)], 1005.3035.

[62] Bianchi, E. and R. C. Myers (2014) "On the Architecture of Spacetime Geometry," *Class. Quant. Grav.*, **31**, p. 214002, 1212.5183.

[63] Jacobson, T. (1995) "Thermodynamics of space-time: The Einstein equation of state," *Phys. Rev. Lett.*, **75**, pp. 1260–1263, gr-qc/9504004.

[64] ——— (2016) "Entanglement Equilibrium and the Einstein Equation," *Phys. Rev. Lett.*, **116**(20), p. 201101, 1505.04753.

[65] Bianchi, E., J. Guglielmon, L. Hackl, and N. Yokomizo (2016) "Squeezed vacua in loop quantum gravity," 1605.05356.

[66] Chirco, G., F. M. Mele, D. Oriti, and P. Vitale (2017) "Fisher Metric, Geometric Entanglement and Spin Networks," 1703.05231.

[67] Livine, E. R. (2017) "Intertwiner Entanglement on Spin Networks," 1709.08511.

[68] Saravani, M., S. Aslanbeigi, and A. Kempf (2016) "Spacetime Curvature in terms of Scalar Field Propagators," *Phys. Rev.*, **D93**(4), p. 045026, 1510.02725.

[69] Cao, C., S. M. Carroll, and S. Michalakis (2017) "Space from Hilbert Space: Recovering Geometry from Bulk Entanglement," *Phys. Rev.*, **D95**(2), p. 024031, 1606.08444.

[70] Rovelli, C. (2004) *Quantum Gravity*, Cambridge University Press, UK.

[71] Thiemann, T. (2007) *Modern canonical quantum general relativity*, Cambridge University Press, UK.

[72] Ashtekar, A. and J. Lewandowski (2004) "Background independent quantum gravity: A status report," *Class. Quant. Grav.*, **21**, p. R53, gr-qc/0404018.

[73] Rovelli, C. and L. Smolin (1995) "Spin networks and quantum gravity," *Phys. Rev.*, **D52**, pp. 5743–5759, gr-qc/9505006.

[74] Baez, J. C. (1996) "Spin network states in gauge theory," *Adv. Math.*, **117**, pp. 253–272, gr-qc/9411007.

[75] Freidel, L. and S. Speziale (2010) "Twisted geometries: A geometric parametrisation of SU(2) phase space," *Phys. Rev.*, **D82**, p. 084040, 1001.2748.

[76] ——— (2010) "From twistors to twisted geometries," *Phys. Rev.*, **D82**, p. 084041, 1006.0199.

[77] Rovelli, C. and S. Speziale (2010) "On the geometry of loop quantum gravity on a graph," 1005.2927.

[78] Regge, T. (1961) "General relativity without coordinates," *Il Nuovo Cimento (1955-1965)*, **19**(3), pp. 558–571.
URL http://dx.doi.org/10.1007/BF02733251

[79] Regge, T. and R. M. Williams (2000) "Discrete structures in gravity," *J. Math. Phys.*, **41**, pp. 3964–3984, gr-qc/0012035.

[80] Bianchi, E., P. Dona, and S. Speziale (2011) "Polyhedra in loop quantum gravity," *Phys. Rev.*, **D83**, p. 044035, 1009.3402.

[81] Barbieri, A. (1998) "Quantum tetrahedra and simplicial spin networks," *Nucl. Phys.*, **B518**, pp. 714–728, gr-qc/9707010.

[82] Baez, J. C. and J. W. Barrett (1999) "The Quantum tetrahedron in three-dimensions and four-dimensions," *Adv. Theor. Math. Phys.*, **3**, pp. 815–850, gr-qc/9903060.

[83] Barrett, J. W., W. J. Fairbairn, and F. Hellmann (2010) "Quantum gravity asymptotics from the SU(2) 15j symbol," *Int. J. Mod. Phys.*, **A25**, pp. 2897–2916, 0912.4907.

[84] Barrett, J. W., R. J. Dowdall, W. J. Fairbairn, H. Gomes, and F. Hellmann (2009) "Asymptotic analysis of the EPRL four-simplex amplitude," *J. Math. Phys.*, **50**, p. 112504, 0902.1170.

[85] Dona, P., M. Fanizza, G. Sarno, and S. Speziale (2017) "SU(2) graph invariants, Regge actions and polytopes," 1708.01727.

[86] Dittrich, B. and S. Speziale (2008) "Area-angle variables for general relativity," *New J. Phys.*, **10**, p. 083006, 0802.0864.

[87] Minkowski, H. (1897) "Allgemeine Lehrsʹatze ʹuber die Konvexe Polyeder," *Nachr. Ges. Wiss., Gottingen*, pp. 198–219.

[88] Kapovich, M. J., M. *J. Differential Geom.*, p. 479.

[89] Montvay, I. and G. Mʹunster (1997) *Quantum fields on a lattice*, Cambridge University Press, Cambridge.

[90] Aquilanti, V., H. M. Haggard, R. G. Littlejohn, and L. Yu (2007) "Semiclassical Analysis of Wigner 3j-symbol," *Journal of Physics A: Mathematical and Theoretical*, **40**, p. 5637.

[91] Aquilanti, V., H. M. Haggard, A. Hedeman, N. Jeevanjee, R. G. Littlejohn, and L. Yu (2012) "Semiclassical Mechanics of the Wigner 6j-symbol," *Journal of Physics A: Mathematical and Theoretical*, **45**, p. 065209.

[92] Haggard, H. M. and R. G. Littlejohn (2010) "Asymptotics of the Wigner 9j-symbol," *Classical and Quantum Gravity*, **27**, p. 35010.

[93] Roberts, J. (1999) "Classical 6j-symbols and the tetrahedron," *Geom. Topol.*, **3**, pp. 21–66, math-ph/9812013.

[94] Major, S. A. (1999) "Operators for quantized directions," *Class. Quant. Grav.*, **16**, pp. 3859–3877, gr-qc/9905019.

[95] Penrose, R. (1971) *Angular momentum: An approach to combinatorial space-time in Quantum Theory and Beyond, edited by T. Bastin (Cambridge University Press,Cambridge).*

[96] ——— (1973) *On the Nature of Quantum Geometry, in: Magic Without Magic: J.A. Wheeler Festschrift, ed. J.R. Klauder, W.H.Freeman and Co Ltd.*

[97] Girelli, F. and E. R. Livine (2005) "Reconstructing quantum geometry from quantum information: Spin networks as harmonic oscillators," *Class. Quant. Grav.*, **22**, pp. 3295–3314, gr-qc/0501075.

[98] Borja, E. F., L. Freidel, I. Garay, and E. R. Livine (2011) "U(N) tools for Loop Quantum Gravity: The Return of the Spinor," *Class. Quant. Grav.*, **28**, p. 055005, 1010.5451.

[99] Livine, E. R. and J. Tambornino (2012) "Spinor Representation for Loop Quantum Gravity," *J. Math. Phys.*, **53**, p. 012503, 1105.3385.

[100] Bianchi, E., J. Guglielmon, L. Hackl, and N. Yokomizo (2016) "Loop expansion and the bosonic representation of loop quantum gravity," *Phys. Rev.*, **D94**(8), p. 086009, 1609.02219.

[101] Bianchi, E., E. Magliaro, and C. Perini (2010) "Coherent spin-networks," *Phys. Rev.*, **D82**, p. 024012, 0912.4054.

[102] Thiemann, T. (2001) "Gauge field theory coherent states (GCS): 1. General properties," *Class. Quant. Grav.*, **18**, pp. 2025–2064, hep-th/0005233.

[103] Freidel, L. and J. Hnybida (2013) "On the exact evaluation of spin networks," *J. Math. Phys.*, **54**, p. 112301, 1201.3613.

[104] Bauer, B. and C. Nayak (2013) "Area laws in a many-body localized state and its implications for topological order," *Journal of Statistical Mechanics: Theory and Experiment*, **2013**(09), p. P09005.

[105] Livine, E. R. and S. Speziale (2007) "A New spinfoam vertex for quantum gravity," *Phys. Rev.*, **D76**, p. 084028, 0705.0674.

[106] Conrady, F. and L. Freidel (2009) "Quantum geometry from phase space reduction," *J. Math. Phys.*, **50**, p. 123510, 0902.0351.

[107] Bojowald, M. and S. Brahma (2016) "Minisuperspace models as infrared contributions," *Phys. Rev.*, **D93**(12), p. 125001.

[108] Kiefer, C. (2012) *Quantum Gravity*, Oxford University Press, Oxford.

[109] Oriti, D. (2009) *Approaches to Quantum Gravity: Toward a New Understanding of Space, Time and Matter*, Cambridge University Press, Cambridge.

[110] Dittrich, B. and W. Kaminski (2013) "Topological lattice field theories from intertwiner dynamics," 1311.1798.

[111] Dittrich, B., E. Schnetter, C. J. Seth, and S. Steinhaus (2016) "Coarse graining flow of spin foam intertwiners," *Phys. Rev.*, **D94**(12), p. 124050.

[112] Bojowald, M. and A. Skirzewski (2006) "Effective equations of motion for quantum systems," *Rev. Math. Phys.*, **18**, pp. 713–746.

[113] Bojowald, Martin and Skirzewski, Aureliano (2006) "Quantum gravity and higher curvature actions," *eConf*, **C0602061**, p. 03, [Int. J. Geom. Meth. Mod. Phys.4,25(2007)].

[114] Tsobanjan, A. (2015) "Semiclassical States on Lie Algebras," *J. Math. Phys.*, **56**(3), p. 033501.

[115] Thiemann, T. (1998) "Quantum spin dynamics (QSD)," *Class. Quant. Grav.*, **15**, pp. 839–873.

[116] Giesel, K. and T. Thiemann (2007) "Algebraic Quantum Gravity (AQG). I. Conceptual Setup," *Class. Quant. Grav.*, **24**, pp. 2465–2498.

[117] Henderson, A., A. Laddha, and C. Tomlin (2013) "Constraint algebra in loop quantum gravity reloaded. I. Toy model of a $U(1)^3$ gauge theory," *Phys. Rev.*, **D88**(4), p. 044028.

[118] Tomlin, C. and M. Varadarajan (2013) "Towards an Anomaly-Free Quantum Dynamics for a Weak Coupling Limit of Euclidean Gravity," *Phys. Rev.*, **D87**(4), p. 044039.

[119] Laddha, A. (2014) "Hamiltonian constraint in Euclidean LQG revisited: First hints of off-shell Closure," 1401.0931.

[120] Oriti, D. (1971) *Quantum Theory and Beyond*, Cambridge University Press, Cambridge, UK.

[121] Bojowald, M. (2004) "Spherically symmetric quantum geometry: States and basic operators," *Class. Quant. Grav.*, **21**, pp. 3733–3753.

[122] Bojowald, M. and R. Swiderski (2006) "Spherically symmetric quantum geometry: Hamiltonian constraint," *Class. Quant. Grav.*, **23**, pp. 2129–2154.

[123] Neville, D. E. (1999) "Long range correlations in quantum gravity," *Phys. Rev.*, **D59**, p. 044032.

[124] Banerjee, K. and G. Date (2008) "Loop Quantization of Polarized Gowdy Model on T**3: Kinematical States and Constraint Operators," *Class. Quant. Grav.*, **25**, p. 145004.

[125] Bojowald, M. and T. Strobl (2003) "Poisson geometry in constrained systems," *Rev. Math. Phys.*, **15**, pp. 663–703.

[126] Torre, C. G. (1999) "Midisuperspace models of canonical quantum gravity," *Int. J. Theor. Phys.*, **38**, pp. 1081–1102.

[127] Anderson, I. M., M. E. Fels, and C. G. Torre (1999) "Group invariant solutions without transversality and the principle of symmetric criticality," math-ph/9910014.

[128] Calcagni, G., S. Gielen, and D. Oriti (2012) "Group field cosmology: a cosmological field theory of quantum geometry," *Class. Quant. Grav.*, **29**, p. 105005.

[129] Gielen, S., D. Oriti, and L. Sindoni (2013) "Cosmology from Group Field Theory Formalism for Quantum Gravity," *Phys. Rev. Lett.*, **111**(3), p. 031301.

[130] Gielen, Steffen and Oriti, Daniele and Sindoni, Lorenzo (2014) "Homogeneous cosmologies as group field theory condensates," *JHEP*, **06**, p. 013.

[131] Gielen, S. and D. Oriti (2014) "Quantum cosmology from quantum gravity condensates: cosmological variables and lattice-refined dynamics," *New J. Phys.*, **16**(12), p. 123004.

[132] Gielen, S. (2015) "Perturbing a quantum gravity condensate," *Phys. Rev.*, **D91**(4), p. 043526.

[133] Calcagni, G. (2014) "Loop quantum cosmology from group field theory," *Phys. Rev.*, **D90**(6), p. 064047.

[134] de Cesare, M., A. G. A. Pithis, and M. Sakellariadou (2016) "Cosmological implications of interacting Group Field Theory models: cyclic Universe and accelerated expansion," *Phys. Rev.*, **D94**(6), p. 064051.

[135] Pithis, A. G. A., M. Sakellariadou, and P. Tomov (2016) "Impact of nonlinear effective interactions on group field theory quantum gravity condensates," *Phys. Rev.*, **D94**(6), p. 064056.

[136] Bojowald, M., A. L. Chinchilli, C. C. Dantas, M. Jaffe, and D. Simpson (2012) "Non-linear (loop) quantum cosmology," *Phys. Rev.*, **D86**, p. 124027.

[137] Waldmann, O. (2001) "Spin dynamics of finite antiferromagnetic Heisenberg spin rings," *Phys. Rev. B*, **65**, p. 024424.

[138] Wilson-Ewing, E. (2012) "Holonomy Corrections in the Effective Equations for Scalar Mode Perturbations in Loop Quantum Cosmology," *Class. Quant. Grav.*, **29**, p. 085005.

[139] Salopek, D. S. and J. R. Bond (1990) "Nonlinear evolution of long-wavelength metric fluctuations in inflationary models," *Phys. Rev. D*, **42**, pp. 3936–3962.

[140] Wands, D., K. A. Malik, D. H. Lyth, and A. R. Liddle (2000) "A New approach to the evolution of cosmological perturbations on large scales," *Phys. Rev.*, **D62**, p. 043527.

[141] Bertschinger, E. (2006) "On the Growth of Perturbations as a Test of Dark Energy," *Astrophys. J.*, **648**, pp. 797–806, astro-ph/0604485.

[142] Bonner, J. C. and M. E. Fisher (1964) "Linear Magnetic Chains with Anisotropic Coupling," *Phys. Rev.*, **135**, pp. A640–A658.

[143] Karbach, M. and K. H. Mutter (1995) "The antiferromagnetic spin- 1/2 -XXZ model on rings with an odd number of sites," *Journal of Physics A: Mathematical and General*, **28**(16), p. 4469.
URL http://stacks.iop.org/0305-4470/28/i=16/a=007

[144] Machens, A., N. P. Konstantinidis, O. Waldmann, I. Schneider, and S. Eggert (2013) "Even-odd effect in short antiferromagnetic Heisenberg chains," *Phys. Rev. B*, **87**, p. 144409.

[145] Bojowald, M. (2015) "Quantum cosmology: a review," *Rept. Prog. Phys.*, **78**, p. 023901.

[146] Bojowald, S. B. S. A. T. A., M. (2009) "Effective Constraints for Quantum Systems," *Rev. Math. Phys.*, **21**, pp. 111–154.

[147] Bojowald, M. and A. Tsobanjan (2009) "Effective Constraints for Relativistic Quantum Systems," *Phys. Rev.*, **D80**, p. 125008.

[148] Bernu, B., C. Lhuillier, and L. Pierre (1992) "Signature of Néel order in exact spectra of quantum antiferromagnets on finite lattices," *Phys. Rev. Lett.*, **69**, pp. 2590–2593.

[149] Bernu, B., P. Lecheminant, C. Lhuillier, and L. Pierre (1994) "Exact spectra, spin susceptibilities, and order parameter of the quantum Heisenberg antiferromagnet on the triangular lattice," *Phys. Rev. B*, **50**, pp. 10048–10062.

[150] Guth, A. H. (1981) "The Inflationary Universe: A Possible Solution to the Horizon and Flatness Problems," *Phys. Rev.*, **D23**, pp. 347–356.

[151] Linde, A. D. (1982) "A New Inflationary Universe Scenario: A Possible Solution of the Horizon, Flatness, Homogeneity, Isotropy and Primordial Monopole Problems," *Phys. Lett.*, **B108**, pp. 389–393.

[152] Albrecht, A. and P. J. Steinhardt (1982) "Cosmology for Grand Unified Theories with Radiatively Induced Symmetry Breaking," *Phys. Rev. Lett.*, **48**, pp. 1220–1223.

[153] Starobinsky, A. A. (1982) "Dynamics of Phase Transition in the New Inflationary Universe Scenario and Generation of Perturbations," *Phys. Lett.*, **B117**, pp. 175–178.

[154] Hawking, S. W. (1982) "The Development of Irregularities in a Single Bubble Inflationary Universe," *Phys. Lett.*, **B115**, p. 295.

[155] Guth, A. H. and S. Y. Pi (1982) "Fluctuations in the New Inflationary Universe," *Phys. Rev. Lett.*, **49**, pp. 1110–1113.

[156] Mukhanov, V. (2005) *Physical Foundations of Cosmology*, Cambridge Univ. Press, Cambridge.

[157] Einstein, A. (1916) "The Foundation of the General Theory of Relativity," *Annalen der Physik*.

[158] Bardeen, P. J. S., J. M. and M. S. Turner (1983) "Spontaneous Creation of Almost Scale - Free Density Perturbations in an Inflationary Universe," *Phys. Rev.*, **D28**, p. 679.

[159] Bardeen, J. M. (1980) "Gauge Invariant Cosmological Perturbations," *Phys. Rev.*, **D22**, pp. 1882–1905.

[160] Dodelson, S. (2003) *Modern Cosmology*, Academic Press.

[161] Lyth, D. and A. Liddle (2009) *The Primordial Density Perturbation: Cosmology, Inflation and the Origin of Structure*, Cambridge University Press.

[162] Baumann, D. (2009) "TASI Lectures on Inflation," .

[163] Birkhoff, G. D. (1931) "Proof of the ergodic theorem," *Proc. Natl. Acad. Sci.*, **17**, pp. 656–660.

[164] Lim, E. A. (2012) *Advanced Cosmology : Primordial non-Gaussianities, lectures given to the Cambridge DAMTP Math Tripos 2012 Advanced Cosmology Class*.

[165] Bartolo, N., S. Matarrese, M. Peloso, and A. Ricciardone (2013) "Anisotropic power spectrum and bispectrum in the $f(\phi)F^2$ mechanism," *Phys. Rev.*, **D87**(2), p. 023504.

[166] Nelson, E. and S. Shandera (2013) "Statistical Naturalness and Non-Gaussianity in a Finite Universe," *Physical Review Letters*, **110**(13), 131301.

[167] Nurmi, S., C. T. Byrnes, and G. Tasinato (2013) "A non-Gaussian landscape," *JCAP*, **1306**, p. 004.

[168] LoVerde, M., E. Nelson, and S. Shandera (2013) "Non-Gaussian Mode Coupling and the Statistical Cosmological Principle," *JCAP*, **1306**, p. 024.

[169] Thorsrud, M., D. F. Mota, and F. R. Urban (2014) "Local Observables in a Landscape of Infrared Gauge Modes," *Phys. Lett.*, **B733**, pp. 140–143.

[170] LoVerde, M. (2014) "Super cosmic variance from mode-coupling: A worked example," *Phys. Rev.*, **D89**(2), p. 023505.

[171] Thorsrud, M., F. R. Urban, and D. F. Mota (2014) "Statistics of Anisotropies in Inflation with Spectator Vector Fields," *JCAP*, **1404**, p. 010.

[172] Byrnes, C. T., S. Nurmi, G. Tasinato, and D. Wands (2013) "Implications of the Planck bispectrum constraints for the primordial trispectrum," *EPL*, **103**(1), p. 19001.

[173] Bramante, J., J. Kumar, E. Nelson, and S. Shandera (2013) "Cosmic Variance of the Spectral Index from Mode Coupling," *JCAP*, **1311**, p. 021.

[174] Adhikari, S., S. Shandera, and A. L. Erickcek (2016) "Large-scale anomalies in the cosmic microwave background as signatures of non-Gaussianity," *Phys. Rev.*, **D93**(2), p. 023524.

[175] Bonga, B., S. Brahma, A.-S. Deutsch, and S. Shandera (2016) "Cosmic variance in inflation with two light scalars," *JCAP*, **1605**(05), p. 018.

[176] Ade, P. A. R. et al. (2016) "Planck 2015 results. XVI. Isotropy and statistics of the CMB," *Astron. Astrophys.*, **594**, p. A16.

[177] Ade, P. A. R. and others (2016) "Planck 2015 results. XVII. Constraints on primordial non-Gaussianity," *Astron. Astrophys.*, **594**, p. A17.

[178] Leistedt, B., H. V. Peiris, and N. Roth (2014) "Constraints on Primordial Non-Gaussianity from 800?000 Photometric Quasars," *Phys. Rev. Lett.*, **113**(22), p. 221301.

[179] Creminelli, P. and M. Zaldarriaga (2004) "Single field consistency relation for the 3-point function," *JCAP*, **0410**, p. 006.

[180] Dalal, N., O. Dore, D. Huterer, and A. Shirokov (2008) "The imprints of primordial non-gaussianities on large-scale structure: scale dependent bias and abundance of virialized objects," *Phys. Rev.*, **D77**, p. 123514.

[181] Chiang, C.-T., C. Wagner, F. Schmidt, and E. Komatsu (2014) "Position-dependent power spectrum of the large-scale structure: a novel method to measure the squeezed-limit bispectrum," *JCAP*, **1405**, p. 048.

[182] Maldacena, J. M. (2003) "Non-Gaussian features of primordial fluctuations in single field inflationary models," *JHEP*, **05**, p. 013.

[183] Cheung, C., A. L. Fitzpatrick, J. Kaplan, and L. Senatore (2008) "On the consistency relation of the 3-point function in single field inflation," *JCAP*, **0802**, p. 021.

[184] Senatore, L. and M. Zaldarriaga (2012) "A note on the consistency condition of primordial fluctuations," *jcap*, **8**, 001, 1203.6884.

[185] Assassi, V., D. Baumann, and D. Green (2012) "On Soft Limits of Inflationary Correlation Functions," *JCAP*, **1211**, p. 047.

[186] Goldberger, W. D., L. Hui, and A. Nicolis (2013) "One-particle-irreducible consistency relations for cosmological perturbations," *Phys. Rev.*, **D87**(10), p. 103520.

[187] Hinterbichler, K., L. Hui, and J. Khoury (2014) "An Infinite Set of Ward Identities for Adiabatic Modes in Cosmology," *JCAP*, **1401**, p. 039.

[188] Joyce, A., J. Khoury, and M. Simonovi? (2015) "Multiple Soft Limits of Cosmological Correlation Functions," *JCAP*, **1501**(01), p. 012.

[189] Mirbabayi, M. and M. Zaldarriaga (2015) "Double Soft Limits of Cosmological Correlations," *JCAP*, **1503**(03), p. 025.

[190] Senatore, L., K. M. Smith, and M. Zaldarriaga (2010) "Non-Gaussianities in Single Field Inflation and their Optimal Limits from the WMAP 5-year Data," *JCAP*, **1001**, p. 028.

[191] Scoccimarro, R., L. Hui, M. Manera, and K. C. Chan (2012) "Large-scale Bias and Efficient Generation of Initial Conditions for Non-Local Primordial Non-Gaussianity," *Phys. Rev.*, **D85**, p. 083002.

[192] Ade, P. A. R. et al. (2014) "Planck 2013 Results. XXIV. Constraints on primordial non-Gaussianity," *Astron. Astrophys.*, **571**, p. A24.

[193] Byrnes, C. T., M. Sasaki, and D. Wands (2006) "The primordial trispectrum from inflation," *Phys. Rev.*, **D74**, p. 123519.

[194] Smith, K. M., M. Loverde, and M. Zaldarriaga (2011) "Universal Bound on N-Point Correlations from Inflation," *Physical Review Letters*, **107**(19), 191301, 1108.1805.

[195] Feng, C., A. Cooray, J. Smidt, J. O'Bryan, B. Keating, and D. Regan (2015) "Planck Trispectrum Constraints on Primordial Non-Gaussianity at Cubic Order," *Phys. Rev.*, **D92**(4), p. 043509.

[196] Dai, L., E. Pajer, and F. Schmidt (2015) "Conformal Fermi Coordinates," *JCAP*, **1511**(11), p. 043.

[197] Dai, Liang and Pajer, Enrico and Schmidt, Fabian (2015) "On Separate Universes," *JCAP*, **1510**(10), p. 059.

[198] Young, S. and C. T. Byrnes (2015) "Long-short wavelength mode coupling tightens primordial black hole constraints," *Phys. Rev.*, **D91**(8), p. 083521.

[199] Linde, A. D. and V. F. Mukhanov (1997) "Nongaussian isocurvature perturbations from inflation," *Phys. Rev.*, **D56**, pp. R535–R539.

[200] Moroi, T. and T. Takahashi (2001) "Effects of cosmological moduli fields on cosmic microwave background," *Phys. Lett.*, **B522**, pp. 215–221.

[201] Lyth, D. H. and D. Wands (2002) "Generating the curvature perturbation without an inflaton," *Phys. Lett.*, **B524**, pp. 5–14.

[202] Enqvist, K. and M. S. Sloth (2002) "Adiabatic CMB perturbations in pre - big bang string cosmology," *Nucl. Phys.*, **B626**, pp. 395–409.

[203] Dvali, G., A. Gruzinov, and M. Zaldarriaga (2004) "A new mechanism for generating density perturbations from inflation," *Phys. Rev.*, **D69**, p. 023505.

[204] Zaldarriaga, M. (2004) "Non-Gaussianities in models with a varying inflaton decay rate," *Phys. Rev.*, **D69**, p. 043508.

[205] Chen, X. and Y. Wang (2010) "Quasi-Single Field Inflation and Non-Gaussianities," *JCAP*, **1004**, p. 027.

[206] Byun, J. and R. Bean (2013) "Non-Gaussian Shape Recognition," *JCAP*, **1309**, p. 026.

[207] Fergusson, J. R. and E. P. S. Shellard (2009) "The shape of primordial non-Gaussianity and the CMB bispectrum," *Phys. Rev.*, **D80**, p. 043510.

[208] Meerburg, P. D. (2010) "Oscillations in the primordial bispectrum: Mode expansion," *prd*, **82**(6), 063517, 1006.2771.

[209] Byun, J., N. Agarwal, R. Bean, and R. Holman (2015) "Looking for non-Gaussianity in all the right places: A new basis for nonseparable bispectra," *Phys. Rev.*, **D91**(12), p. 123518.

[210] Behbahani, S. R., M. Mirbabayi, L. Senatore, and K. M. Smith (2014) "New natural shapes of non-Gaussianity from high-derivative interactions and their optimal limits from WMAP 9-year data," *JCAP*, **1411**(11), p. 035.

[211] Byun, J. and R. Bean (2015) "Non-Gaussian Shape Discrimination with Spectroscopic Galaxy Surveys," *JCAP*, **1503**(03), p. 019.

[212] Raccanelli, A., M. Shiraishi, N. Bartolo, D. Bertacca, M. Liguori, S. Matarrese, R. P. Norris, and D. Parkinson (2017) "Future Constraints on Angle-Dependent Non-Gaussianity from Large Radio Surveys," *Phys. Dark Univ.*, **15**, pp. 35–46.

[213] Cheung, C., P. Creminelli, A. L. Fitzpatrick, J. Kaplan, and L. Senatore (2008) "The Effective Field Theory of Inflation," *JHEP*, **03**, p. 014.

[214] Creminelli, P., G. D'Amico, M. Musso, J. Norena, and E. Trincherini (2011) "Galilean symmetry in the effective theory of inflation: new shapes of non-Gaussianity," *JCAP*, **1102**, p. 006.

[215] Babich, D., P. Creminelli, and M. Zaldarriaga (2004) "The Shape of non-Gaussianities," *JCAP*, **0408**, p. 009.

[216] Nielsen, M. A. and I. L. Chuang (2000) *Quantum computation and quantum information*, Cambridge University Press, Cambridge, New York, 2010 : 10th anniversary ed.
URL http://opac.inria.fr/record=b1135621

[217] Livine, E. R. and D. R. Terno (2006) "Reconstructing quantum geometry from quantum information: Area renormalisation, coarse-graining and entanglement on spin networks," gr-qc/0603008.

[218] Bojowald, M. and S. Brahma (2014) "Canonical derivation of effective potentials," 1411.3636.

[219] Freidel, L. and E. R. Livine (2010) "The Fine Structure of SU(2) Intertwiners from U(N) Representations," *J. Math. Phys.*, **51**, p. 082502, 0911.3553.

Vita

Bekir Baytas

Bekir Baytas was born in Istanbul, Turkey on April 18, 1986. He obtained his Bachelor degree in physics from Bosphorus University, Istanbul in June 2012. He joined the Ph.D. program at Pennsylvania State University in August 2012. He has been doing his research under the supervision of Sarah Shandera since 2014. His publications include:

- Baytaş, B., A. Kesavan, E. Nelson, S. Park, and S. Shandera (2015) Nonlocal bispectra from super cosmic variance, Phys. Rev., D 91
- Baytaş, B. and S. Shandera (2016) Space of non-Gaussian fields with single-clock bispectra, Phys. Rev., D 94
- Baytaş, B. and M. Bojowald (2017) Minisuperspace models of discrete systems, Phys. Rev., D 95
- Baytaş, B., E. Bianchi, and N. Yokomizo (2018) Gluing polyhedra with entanglement in loop quantum gravity, arXiv:1805.05856 [gr-qc]